Multispectral optics in complex media: theory and application to dense microalgal media in a context of mass cultivation monitoring

S. Bellini

To cite this version:

S. Bellini. Multispectral optics in complex media: theory and application to dense microalgal media in a context of mass cultivation monitoring. Environmental Sciences. Doctorat en génie des procédés, 2014. English. NNT : . tel-02600846

HAL Id: tel-02600846
https://hal.inrae.fr/tel-02600846
Submitted on 16 May 2020

Collège Doctoral
du Languedoc-Roussillon

THÈSE
Pour obtenir le grade de
Docteur

Délivré par **MONTPELLIER SUPAGRO**

Préparée au sein de l'école doctorale **SP-SA**
Et de l'unité de recherche **UMR ITAP**

Spécialité: **Génie des procédés**

Présentée par **Sarah Bellini**

Multispectral optics in complex media: theory and application to dense microalgal media in a context of mass cultivation monitoring

Soutenue le 18/11/2014 devant le jury composé de

M. Jack Legrand	PR	Université de Nantes	Rapporteur
M. Claude Amra	DR1	CNRS	Rapporteur
M. Jean-Philippe Steyer	DR	INRA	Examinateur
M. Fabrice Béline	DR	IRSTEA	Examinateur
M. Eric Fouilland	CR	CNRS	Examinateur
M. Jean-Louis Meyzonnette	Expert		Examinateur
M. Jean-Michel Roger	DR	IRSTEA	Directeur
M. Ryad Bendoula	CR	IRSTEA	Encadrant

Montpellier SupAgro

Qu'on avance ou qu'on recule,
l'important c'est de continuer à pédaler.
— Un humble cycliste

Aux miens, sans qui la vie n'aurait pas de sens…

Acknowledgements

Je tiens tout d'abord à exprimer ma reconnaissance aux membres de mon jury, qui m'ont fait l'honneur d'accepter de considérer avec attention mes travaux de recherches, et notamment le présent manuscrit. Je suis très touchée de leur considération et espère de tout coeur être à la hauteur de leurs attentes.

Cette thèse est l'aboutissement de trois années passées au sein de l'équipe Capteurs Optiques de l'UMR ITAP de l'IRSTEA. Je remercie les personnes qui m'ont ainsi donné l'opportunité de mener à bien ce travail de recherche dans des conditions agréables et sérieuses, notamment le professeur Tewfik Sari directeur d'ITAP, Alexia Gobrecht chef de l'équipe, Jean-Michel Roger mon directeur, ainsi que tous les membres de l'équipe. Merci à mon collègue doctorant Xavier Hadoux pour son aide en informatique, surtout dans la dernière étape de la rédaction.

Je tiens à adresser des remerciements tous particuliers à mon encadrant, Ryad Bendoula, qui est à l'origine du projet de thèse, et qui s'est beaucoup investi à tous les stades de son déroulement. Grand merci à Michèle Egea, Elodie Borg et Danièle Hoarau qui ont toujours été là pour rendre possibles mes déplacements, achats de matériel ou participations à des conférences. Leur soutien et leur compétences ont été plus que précieux pendant ces trois années. Merci aussi à David Bastidon grâce à qui le dispositif a double spheres a put être monté, et à Daniel Moura, qui a interfacé le spectromètre. Je suis également extrêmement reconnaissante aux chercheurs de talent avec qui j'ai eu la chance d'avoir des collaborations enrichissantes au cours de mes recherches. Au LBE de Narbonne, je pense en particulier à Eric Latrille, Jean-Philippe Steyer et Bruno Sialve. Un merci tout spécial également à Enrica Uggetti et Violette Turon qui ont eut la gentillesse de me faire profiter de leurs compétences en biochimie et qui m'ont prêté un peu de leur culture d'algues. Je remercie chaleureusement toute l'équipe d'ECOSYM de l'UM2 pour les échanges stimulants que nous avons eu lors de notre campagne de mesure commune. Merci à Eric Fouilland, Emilie LeFloc'h, Francesca Vidussi, Sebastien Mas et Claire Carré d'avoir partagé avec moi leur expertise et leur temps, aussi bien pour mener à bien les analyses de la campagne que pour en valoriser les résultats. Merci aussi à Cyrille Przybila de l'IFREMER pour son enthousiasme vis-à-vis de mes recherches et pour sa participation sans faille à la campagne de mesure sur la prairie en bassin extérieur. J'adresse aussi des remerciements à Olivier Bernard de l'INRIA qui a suivi mon travail avec attention. Je tiens aussi à remercier Hubert et Charlotte du LOV pour leurs encouragements et leurs conseils précieux en matière d'algue. Ils font aussi partie de la brillante équipe orgnaisatrice de la conférence YAS 2014 à laquelle j'ai eu l'honneur de présenter mes travaux: je les remercie également pour cette oportunité. Je dois énormément au professeur Meyzonnette, d'abord pour son enseignement en photométrie durant mes études d'ingénieur à l'Institut d'Optique

Graduate School, et surtout pour avoir accepté d'apporter ses conseils plus qu'experts à mon travail. Il nous a ainsi fait l'honneur de plusieurs visites malgré son emploi du temps chargé, ce dont je suis extrêmement touchée.

D'un point de vue plus personnel, je ne saurai assez remercier Ben pour son soutien sans faille, ses brillants conseils d'ingénieur opticien et son aide salutaire en programmation. Sans son aide cette thèse ne serait que la moitié d'elle-même. Je dis aussi merci à mes parents et à ma famille, qui n'ont jamais cessé de m'encourager et de me soutenir. Enfin, je ne peux achever ces remerciements sans une dédicace speciale à mes deux chiens, Zlato et Mosca, dont la bonne humeur permanente a littéralement illuminé l'austère période de la rédaction. Plus de gens devraient avoir la chance de travailler avec leurs chiens à leurs côtés.

Les Matelles, le 21/09/2014 S.B.

Contents

List of Figures

List of Tables

Introduction

Contents

0.1 General aims of this work: operational issue

Autotrophic microalgae are single cell photosynthetic organisms that have been present in oceans and fresh waters for more than three and a half billion years. From the ambient carbon dioxide and the absorption of light energy at different wavelengths, photosynthesis makes them possible to produce biomass. Microalgae can be classified into numerous and various species according to their physical and chemical properties such as the pigment composition, the chemical nature of the storage materials coming from photosynthesis or the photosynthetic membranes organization. They show a high inter-species variability regarding the cell shape, size (with diameter from 0.5 to 160 μm) [52] and chemical composition. Microalgal cells have a division cycle as short as a few hours, which is a serious advantage for a fast biomass production. Due to those characteristics, autotrophic microalgae are seen today as a promising source of biomass for various applications such as high-value chemicals extraction [32], animal and human food [20, 17], aquaculture [41, 37] or biochemistry. They have also been identified as a major source of energy, via biogas or biofuel production [12, 11]. High rate algal pounds are also investigated for environment cleaning, for wastewaters decontamination [37], factory smokes treatment [6], carbon dioxide fixation [14] and heavy metal biosorption [27]. Consequently, the global mass production of microalgae has largely increased over the last decade [12].

Cultivation systems have been implemented in order to optimize the growth and harvesting of the algal cells. Algae are grown either in open culture systems (open pounds) or closed systems (photobioreactors) [54]. Those systems are designed to allow the control of the water quality, temperature and pH, nutrients availability, illumination, dissolved carbon dioxide rate and agitation of the culture medium which are crucial factors influencing the growth. In order to adapt the cultivation conditions at best, it is necessary to have real-time information about the state of the culture. For that purpose, the cultivation systems are equipped with different commercial probes and controllers: submersible CO_2 probes, gaseous infrared carbon dioxide analyzers, pH-controllers, temperature controllers and light probes [2]. However further optimization of the cultivation process would imply to monitor the physiological state of the algal cells themselves, i.e. cell number, mass and size, photopigment composition and quantity, lipids, proteins and carbohydrate quantities inside the cells. In practice, the analysis of the algal cells is implemented via several standard methods that can be hard to implement on-line [42, 48]. Cell number and size can be estimated with optical microscopy [2], flow cytometry [24], particle counters [8]. The biomass is usually determined by dry weight measurements [2] or in correlation with the turbidity of the algal medium, which can be estimated with devices such as nephelometers [6]. The pigment quantity and composition are usually determined with High-Performance Liquid Chromatography (HPLC) methods [58]. Fluorimetery [23] can also be implemented to give an estimate of the chlorophyll a (Chla) content [22]. Many of those techniques require sample preparation such as filtering, dilution or chemical extraction, which complicates in particular on-line implementation [42, 48]. New measurement techniques for the characterization of the algal cells state inside the culture medium are needed.

This work aims in particular at proposing a solution to this operational issue by investigating the potential of vibrationnal spectrometry for the characterization of microalgal cells inside dense cultivation media. Spectrometry designates the spectral analysis methods allowing to characterize the composition and structure of matter [4]. It is based on the quantitative and qualitative analysis of the spectra originating in the interaction of matter with various incoming radiations such as visible light (VIS), ultraviolet (UV), infrared (IR) and near infrared (NIR), X rays, microwaves or electrons. In this work in particular, VIS-NIR spectrometry was considered. Our approach was justified by two main reasons: on the one hand, VIS-NIR spectrometry has been proved to be a powerful diagnosis tool in various domains such as agri-food sciences [56], pharmaceutical industry [34] or even bioprocess and cell cultivation monitoring [13, 3]. One of the major advantages of spectrometry is that the measurements are non-destructive, can be performed with minimum or no sample preparation and with easy-to-operate instruments presenting a high signal-to-noise ratio: this makes it a first choice process analytical technology (PAT) [34]. On the other hand, previous studies demonstrated that the spectral properties of microalgal cells in the VIS-NIR domain depend heavily on the chemical characteristics [38, 10] (mainly nature and concentration of pigments) and physical characteristics [10, 57, 1, 15, 38, 45, 29, 28, 30] of the cells (size, shape, density of the cells). Retrieving the bulk optical properties of dense phytoplankton media on the VIS-NIR spectral range thus seems to show great potential for the advanced diagnosis in micro-algae cultivation processes [10, 31, 16]. In this thesis we thus aim at investigating a method to extract information of the physical and chemical characteristics of algal cells contained in a dense algal culture medium from spectral measurements implemented directly on the sample medium. In the next paragraph we describe more thouroughly the scientific issues addressed in this work.

0.2 Scientific issues at stakes

0.2.1 Spectral measurements and interpretation of the spectra in turbid media

The first scientific issue adressed is spectrometry in very dense, turbid media. The high particle densities have been shown to highly complicate the standard spectrometry methods, historically developed for diluted media and based on the applicability of Beer law [19]. Both the measurements method and setup implemented [43, 50] and the theoretical interpretation [46, 33] of the spectra measured are more complex in dense media. In this paragraph we first detail the exact medium under study, which determines the general framework of our work. We then expose the measurements and interpretation difficulties arising when considering dense media.

Description of the cultivated algal medium under study

In this work the particular object under study are dense cultivated microalgal medium. This prime definition allows a certain degree of freedom, since quite different media have been tested all along the three years of this study. We have worked with samples coming from various cultivation systems, from open cultivation pounds to photobioreactors and batches, and composed of various strains, single and multi-species. This diversity first originates in the opportunities we have had to meet and collaborate with various research units. Our particular example illustrates in a certain extent the diversity of microalgae world, which leads to multiple applications, from aquaculture to green chemistry and energy production, involves a lot of application-specific technologies and protocols and uses all the biodiversity encountered in the phytoplankton order.

Nevertheless a more detailed generic description can be given, which defines the physical orders of magnitude considered.

A cultivated microalgal medium is generally composed of various classes of elements: the algal cells themselves, bacterial cells, dissolved nutrients and detrital elements that can sometimes agglomerate. It can be said that in some cases, and in particular for culture media that are exposed to contamination, some zooplanktonic cells can be encountered. They usually feed with microalgal cells, and everything is done to limit their number to negligible in a culture. That is why they were not taken into account here.

A priori information can be given concerning the absorption and scattering properties of the different elements.

Table 1 gives orders of magnitude of the physical characteristics and abundance of the various elements composing a culture medium.

Table 1: Descriptive orders of magnitude of the elements composing a cultivated algal medium.

Element	Size (m)	Abundance	Absorption	Scattering
Algal cell	$0.5 - 160.10^{-6}$	$> 10^6 cell.L^-1$	Presence of photopigments	Yes
Bacterial cell	1.10^{-6}	$> 10^6 cell.L^-1$	No pigments	Yes
Dissolved nutrients	$<< 1.10^{-6}$	-	No pigments	-
Detrital elements	$1 - 50.10^{-6}$	-	No pigments	-

An algal culture medium can thus be described as particles of various size, suspended inside an aqueous medium in which there can be some dissolved elements. Table 1 shows that the majority of the particles of an algal medium are in the order of the micron or of tens of microns. The particle density inside the medium can be qualified as high. For the algal media that we have encountered in the frame of our work, the volume occupied by particles was estimated to vary between 0.1% and 1.4% of the total volume in the algal suspension. Following the definition of Ishimaru [25], this means that we are in the case of turbid suspensions.

Our thesis aims at proposing a first spectral approach of the dense cultivated microalgal media. That is why as a first step, we chose to start considering a simplified medium where only the algal cells were taken into account. This assumption appeared to be justified for the practical cases of the cultures that we used in our experimental works, where the non-algal particles were found to remain negligible.

Implications for the optical properties of the considered algal media

A photon incident on a particle medium such as the considered algal medium can have different behaviors: it can be absorbed, scattered or can cross throughout the sample without any interaction with matter. Absorption means that the photon is transferred to matter in another form of energy (generally heat). Scattering is the reradiation of the photon by particles in a direction of space different from its incident direction. In the case of high particle densities, such as those encountered in a cultivated algal medium, multiple scattering can occur: in that case, the scattered photon has a significant chance to undergo several sucessive scattering phenomena all along its path throughout the medium. Historically, the spectrometric methods have been developed for diluted media for which the scattering phenomena remain negligible. In that case the basic measurement is the radiation attenuation through the sample. The validity of Beer law [19] is assumed, which gives a logarithmic rule between the concentration of the analyte investigated and the transmission of the sample. However this approach fails when scattering phenomena become significant [35, 46, 50]. In that case, both the measurement setups and the theoretical interpretations become inadapted. Empirical preprocessing methods have been developed in order to correct the influence of the scattering phenomena on the measured spectra, such as the multiplicative scatter correction (MSC), the extended multiplicative signal correction (EMSC) [35], standard normal variate (SNV) and derivates [53, 47]. However those corrections methods are sometimes not realistic as the scattering phenomena are roughly approximated without any physical meaning. That is why several works [50, 51] have aimed at modelling the scattering phenomena by using rigorous physical formulations of light propagation inside a complex medium such as the radiative transport equation (RTE) [25]. Our work belongs to the same preoccupation of bringing more physical meaning to standard spectrometric methods. However we propose to carefully analyse the measurement setup itself instead of using preprocessing methods on spectra not carefully measured. This operationnal aspect is developed in Chapter 1 of this thesis called "How to measure the reflectance and transmittance properties of a dense particle medium?". In Chapter 2, the theoretical interpretation of the spectra measured on the sample suspension in terms of intrinsic optical properties is investigated, as we adress the question "How to describe the intrinsic optical properties of a dense medium made of random particles from the measurement of its reflectance and transmittance properties?".

0.2.2 Modelling the links between the chemical and physical characteristics of one cell and its optical properties

The second scientific issue adressed in this thesis is modelling the influence of the physiological state of algal cells on their spectral properties. Many previous studies have investigated the interpretation of the absorption and scattering spectra measured on diluted algal samples [15, 57, 9, 18, 49, 6, 26, 48]. The absorption properties in particular have been the most studied, as they are historically the most measured: indeed, most of available litterature belongs to oceanography where the algal suspensions considered are highly diluted, which limits the scattering phenomena. The absorption coefficient has thus been shown to be a nonlinear function of the intra-cellular pigment concentration [22], the absorption properties of the pigments [10] and cell size [44, 48, 15]. These properties of the cells are also known to modulate the shape of the algal cell suspensions absorption spectra in the visible domain with an effect commonly known as the flattening effect (sometimes called the packaging effect or particle effect) [21, 28]. Some studies [18, 10] have also investigated the scattering and extinction spectra of diluted algal suspensions. They have been shown to be mostly influenced by cell size and density inside the suspensions [18, 10].

However to the state of our knowledge, no explicit relation has been formulated between on the one hand the optical properties of the cells, and on the other hand their physical and chemical characteristics . Some theoretical formulations of the absortion coefficient values can be implemented by approximating algal cells by homogeneous absorbing spheres and using Mie theory and the anomalous diffraction approximation (ADA) [36, 55]. However they require to know the complex refractive index of the cells, which is not easily measured [31] and also depends on the cell physical and chemical characteristics [7]. This points out the fondamental issue that arises when attempting to formulate the link between the physical and chemical characteristics of one algal cell and its spectral properties. We will see in Chapter 3 that an implicit modelling can be implemented to adress this problem, formulated as "How to describe the optical properties of a single algal cell from its physical and chemical characteristics?".

0.2.3 Linking the different scales: from the individual cell to the spectral measurements

The third main issue approached in this thesis is a consequence of the previous ones, and is adressed in Chapter 4 called "How to link the individual cell chemical and physical properties to the bulk spectral properties measured on a dense algal medium?". Solutions to organize the whole theory developed on the one hand at the scale of a bulk dense algal medium and on the other hand at the scale of one individual cell are investigated and tested. Finally, figure 1 summarizes the thesis proposal.

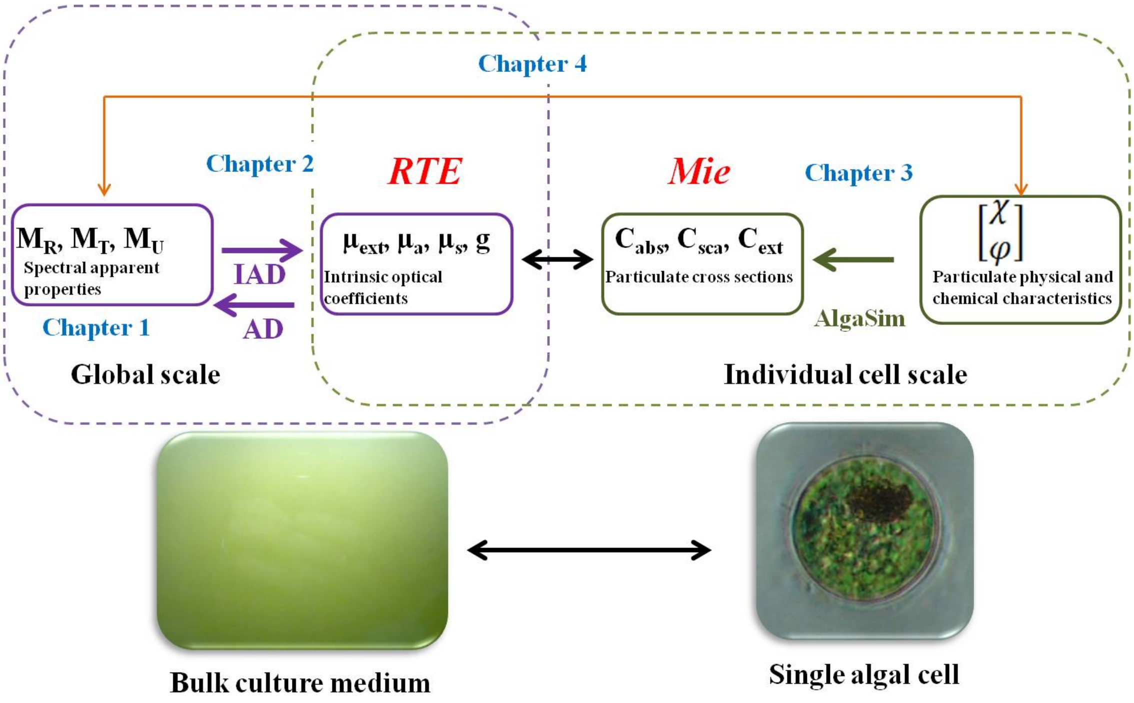

Figure 1: Flow-chart of the thesis proposal. Chapter 1: "How to measure the reflectance and transmittance properties of a dense particle medium?" Chapter 2: "How to describe the intrinsic optical properties of a dense medium made of random particles from the measurement of its reflectance and transmittance properties?" Chapter 3: "How to describe the optical properties of a single algal cell from its physical and chemical characteristics?" Chapter 4: "How to link the individual cell chemical and physical properties to the bulk spectral properties measured on a dense algal medium?"

In the framework of this thesis we have differentiated the intrinsic optical properties of the bulk medium made of random particles, designated as the linear optical coefficients (μ_{abs}, μ_{sca} and μ_{ext}), from the optical properties of the constitutive particles themselves, designated as the optical cross sections (C_{abs}, C_{sca} and C_{ext}). This distinction has been made in order to clarify the approach developed in the entire thesis, and to build awarness of the limits between the different scales of description. We will see in this thesis that switching from one scale to another is rarely trivial and must be handled carefully. We thus aimed at making the understanding easier by using a different vocabulary for each situation. In Chapter 1 we will define what can be called the apparent spectral properties of a bulk medium, designated as its reflectance and transmittance properties (M_R, M_T, M_U). In Chapter 2 we will make the links between the reflectance and transmittance properties of a bulk medium, and its intrinsic linear optical coefficients. The optical cross sections of the individual algal particles themselves will be investigated in Chapter 3, and in particular the influence of the physiological state of the algal cells on its optical properties. Finally, the links between the scale of the bulk medium and the scale of the individual algal cells will be done in Chapter 4.

0.3 Originality of the approach and application prospects

To the state of our knowledge, the available litterature investigating the optical properties of microalgae only deals with diluted algal media, presenting optical thickness below 0.3: in that case the scattering phenomena are considered as negligible. Our study is among the only ones that adress the issue of optics in dense, non-diluted algal media. Our work thus differentiates from the previous studies concerning ocean optics [10, 39, 40] and from the studies aiming at retrieving the radiation characteristics of given microalgae species selected for their industrial use [31, 7, 6, 26].

The novelty of the approach proposed by this thesis also relies on the classical spectrometric methods implemented to give a physical interpretation of the spectra shape, which has never been applied to algal media. This novelty could be pointed out while the thesis was conducted, in particular with a first published article in the journal Applied Spectroscopy [5]. The NIR 2013 conference (http://www.icnirs2013.org/) was also a great opportunity to perform an oral presentation of the approach of our work.

Last but not least, our study also shows the potential of an original operational method to retrieve the algal cell size, density and pigment composition from only one spectrometric measurement on the non-prepared algal medium directly extracted from the cultivation system. The first results obtained have been enthusiastically considered by the microalgae and bioprocess communities in the context of two oral presentations, in particular the Young Alganeers symposium 2014 (http://yas2014.sciencesconf.org/) and the Journée de l'Ecole Doctorale 2014 at Montpellier Supagro for which the first conference prize was awarded. This may point out the operationnal interest of the work accomplished in this thesis which offers great prospects for the implementation of an on-line measurement system adapted to the constraints of mass cultivation monitoring.

Bibliography

[1] E. Aas. Influence of shape and structure on light scattering by marine particles. Technical report, University of Oslo, 1984.

[2] R. A. Anderson. *Algal culturing techniques.* R.A. Anderson, 2005.

[3] S.A. Arnold, J. Crowley, N. Woods, L.M. Harvey, and B. McNeil. In-situ near infrared spectroscopy to monitor key analytes in mammalian cell cultivation. *Biotechnology and bioengineering*, 84, 2003.

[4] J.L. Basdevant, X. Bataille, P. Fleury, P. Kohl, and J. Robert. *Dictionnaire de physique et de chimie.* Nathan, 2004.

[5] S. Bellini, R. Bendoula, E. Latrille, and J.M. Roger. Potential of a spectroscopic measurement method using adding-doubling to retrieve the bulk optical properties of dense microalgal media. *Applied spectroscopy*, 68(10), 2014.

[6] H. Berberoglu, P.S. Gomez, and L. Pilon. Radiation characteristics of botryococcus braunii, chlorococcum littorale, and chlorella sp. used for co2 fixation and biofuel production. *Journal of Quantitative Spectroscopy and Radiative Transfer*, 110(17), 2009.

[7] H. Berberoglu and L. Pilon. Experimental measurements of the radiation characteristics of anabaena variabilis atcc 29413-u rhodobacter sphaeroides atcc 49419. *International Journal of Hydrogen Energy*, 32, 2007.

[8] O. Bernard, G. Malara, and A. Sciandra. The effects of a controlled fluctuating nutrient environment on continuous cultures of phytoplankton monitored by a computer. *Journal of experimental marine biology and ecology*, 197(2), 1996.

[9] A. Bricaud, A. L. Bédhomme, and A. Morel. Optical properties of diverse phytoplanktonic species: experimental results and theoretical interpretation. *Journal of plankton research*, 10(5), 1988.

[10] A. Bricaud, A. Morel, and L. Prieur. Optical efficiency factors of some phytoplankters. *Journal of limnology and oceanography*, 1983.

[11] J.S. Burlew. Algal culture from laboratory to pilot plant. *Aquatic Living Resources*, 23(2), 1953.

[12] J. P. Cadoret and O. Bernard. La production de biocarburant lipidique avec des microalgues: promesses et défis. *Société de biologie*, 202(3), 2008.

[13] A. Cervera and N. Petersen. Application of near-infrared spectroscopy for monitoring and control of cell culture and fermentation. *Biotechnology Progress*, 25, 2009.

[14] S.R. Chae, E.J. Hwang, and H.S. Shin. Single cell protein production of euglena gracilis and carbon dioxide fixation in an innovative photobioreactor. *Bioresource technology*, 97, 2006.

[15] A. M. Ciotti, M. R. Lewis, and J. J. Cullen. Assessment of the relationships between dominant cell size in natural phytoplankton communities and the spectral shape of the absorption coefficient. *Journal of limnology and oceanography*, 47, 2002.

[16] J-F. Cornet and J. Albiol. Modeling photoheterotrophic growth kinetics of rhodospirillum rubrum in rectangular photobioreactors. *Biotechnology progress*, 16(2), 2000.

[17] V. Dallaire, P. Lessard, G. Vanderberg, and J. de la Noüe. Effect of algal incorporation on growth, survival and carcass composition of rainbow trout (oncorhynchus mykiss) fry. *Bioresource technology*, 98, 2007.

[18] R. J. Davies-Colley, R. D. Pridmore, and J. E. Hewitt. Optical properties of some freshwater phytoplanktonic algae. *Hydrobiologia*, 1986.

[19] V.P. Dick. Applicability limits of beer's law for dispersion media with a high concentration of particles. *Applied optics*, 37(21), 1998.

[20] L. Dufossé, P. Galaup, A. Yaron, S. Malis Arad, P. Blanc, K. N. Chidambara Murthy, and G. A. Ravishankar. Microorganisms and microalgae as sources of pigments for food use: a scientific oddity or an industrial reality? *Trends in food science and technology*, 16, 2005.

[21] L. N. M. Duysens. Flattening of the absorption spectrum of suspensions, as compared to that of solutions. *Biochimica and Biophysica acta*, (19), 1956.

[22] E. Le Floc'h, G. Malara, and A. Sciandra. An automatic device for in vivo absorption spectra acquisition and chlorophyll estimation in phytoplankton cultures. *Journal of Applied Phycology*, 14, 2002.

[23] J. Gregor, R. Geris, B. Marsalek, J. Hetesa, and P. Marvan. In situ quantification of phytoplankton in reservoirs using a submersible spectrofluorometer. *Hydrobiologia*, 548, 2005.

[24] P. Hyka, S. Lickova, P. Pribyl, K. Melzoch, and K. Kovar. Flow cytometry for the development of biotechnological process with microalgae. *Biotechnology advances*, 2012.

[25] A. Ishimaru. *Wave propagation and scattering in random media.* IEEE press: New York, 1997.

[26] R. Kandilian, E. Lee, and L. Pilon. Radiation and optical properties of nannochloropsis oculata grown under different irradiances and spectra. *Bioresource Technology*, 2013.

[27] S. Karthikeyan, R. Balasubramanian, and C.S.P. Iyer. Evaluation of the marine algae ulva fasciata and sargassum sp. for the biosorption of cu(ii) from aqueous solutions. *Bioresource technology*, 98, 2007.

[28] J. T. O. Kirk. A theoretical analysis of the contribution of algal cells to the attenuation of light within natural waters. 1. general treatment of suspensions of pigmented cells. *New phytologist*, 75, 1975.

[29] J. T. O. Kirk. A theoretical analysis of the contribution of algal cells to the attenuation of light within natural waters. ii. spherical cells. *New phytologist*, 75, 1975.

[30] J. T. O. Kirk. A theoretical analysis of the contribution of algal cells to the attenuation of light within natural waters. iii. cylinfrical and spheroidal cells. *New phytologist*, 77, 1976.

[31] E. Lee, R. L. Heng, and L. Pilon. Spectral optical properties of selected photosynthetic microalgae producing biofuels. *Journal of Quantitative Spectroscopy and Radiative Transfer*, 114, 2013.

[32] R.T. Lorenz and G.R. Cysewski. Commercial potential for haematococcus microalgae as a natural source of astaxanthin. *TIBTECH*, 18, 2000.

[33] B. Lu, S.P. Morgan, J.A. Crowe, and I.M. Stockford. Comparison of methods for reducing the effects of scattering in spectrophotometry. *Applied spectroscopy*, 60(10), 2006.

[34] J. Luypaert, D.L. Massart, and Y. Vander Heyden. Near-infrared spectroscopy applications in pharmaceutical analysis. *Talenta*, 72(3), 2007.

[35] H. Martens, J. Pram Nielsen, and S. Balling Engelsen. Light scattering ans light absorbance separated by extended multiplicative signal correction. application to near-infrared transmission analysis of powder mixture. *Analytical Chemistry*, 75(3), February 2003.

[36] G. Mie. Beitrage zur optik trüber medien, speziell kolloidaler metallösungen. *Annalen der physik*, 25(3), 1908.

[37] I. Mladineo, I. Bocina, C. Przybyla, J. Fievet, and J-P. Blancheton. Fish growth and health aspects of sea bass (dicentrarchus labrax) reared in standard vs. high rate algal pond recirculation systems. *Aquatic Living Resources*, 23(2), 2010.

[38] A. Morel and A. Bricaud. Theoretical results concerning light absorption in a discrete medium, and application to specific absorption of phytoplankton. *Deep sea research*, 28, 1981.

[39] A. Morel and A. Bricaud. Theoretical results concerning the optics of phytoplankton, with special reference to remote sensing applications. *Oceanography from space*, 1981.

[40] J. L. Mueller. *The influence of phytoplankton on ocean color spectra.* PhD thesis, Oregon state university, 1973.

[41] A. Muller-Feuga. The role of microalgae in aquaculture: situation and trends. *Journal of applied phycology*, 12, 2000.

[42] A. Nair, S. Sathyendranath, T. Platt, J. Morales, V. Stuart, M. Forget, E. Devred, and H. Bouman. Remote sensing phytoplankton functional types. *Remote sensing of environment*, 112, 2008.

[43] J. W. Pickering, C. J. M. Moes, H. J. C. M. Sterenborg, S. A. Prahl, and M. J. C. van Gemert. Two integrating spheres with an intervening scattering sample. *Journal of Optical society of America*, 9(4), 1992.

[44] T. Platt and A.D. Jassby. The relationship between photosynthesis and light for natural assemblages of coastal marine phytoplankton. *Journal of Phycology*, 12, 1976.

[45] A. Quirantes and S. Bernard. Light scattering by marine algae: two-layer spherical and non-spherical models. *Journal of Quantitative Spectroscopy and Radiative Transfer*, 89, 2004.

[46] M.M. Reis, P.H.H. Araújo, C. Sayer, and R. Giudici. Spectroscopic on-line monitoring of reactions in dispersed medium: Chemometric challenges. *Analytical and Chemical acta*, 595(1-2), 2007.

[47] A. Rinnan, F. van den Berg, and S.B. Engelsen. Review of the most common pre-processing techniques for near-infrared spectra. *Trends in analytical chemistry*, 28(10), 2009.

[48] S. Roy, S. Sathyendranath, and T. Platt. Retrieval of phytoplankton size from bio-optical measurements: theory and applications. *Journal of the royal society Interface*, 8, 2011.

[49] S. Sathyendranath, L. Lazzara, and L. Prieur. Variations in the spectral values of specific absorption of phytoplankton. *Limnology and Oceanography*, 32(2), 1987.

[50] R. Steponavicius and S. N. Thennadil. Extraction of chemical information of suspensions using radiative transfer theory to remove multiple scattering effects: application to a model two-component system. *Analytical Chemistry*, 18, 2009.

[51] R. Steponavicius and S. N. Thennadil. Extraction of chemical information of suspensions using radiative transfer theory to remove multiple scattering effects: application to a model multicomponent system. *American Chemical Society*, 83, 2011.

[52] D. Stramski, E. Boss, D. Bogucki, and K.J. Voss. The role of seawater constituents in light backscattering in the ocean. *Progress in Oceanography*, 61, 2004.

[53] S. N. Thennadil and E. B. Martin. Empirical preprocessing methods and their impact on nir calibrations: a simulation study. *Journal of chemometrics*, 19, 2005.

[54] C. U. Ugwu, H. Aoyagi, and H. Uchiyama. Photobioreactors for mass cultivation of algae. *Bioresource Technology*, 99, 2008.

[55] H. C. van de Hulst. *Light scattering by small particles.* Wiley, 1957.

[56] P. Williams and K. Norris. *Near-Infrared Technology in the Agricultural and Food Industries.* American association of cereal chemists, Saint Paul, Minnesota, 2001.

[57] J. R. V. Zaneveld and J. C. Kitchen. The variation in the inherent optical properties of phytoplankton near an absorption peak as determined by various models of cell structure. *Journal of geophysical research*, 100, 1995.

[58] M. Zapata, F. Rodriguez, and J. Garrido. Separation of chlorophylls and carotenoids from marine phytoplankton: A new hplc method using a reversed phase c-8 column and pyridine-containing mobile phases. *Marine ecology progress series*, 195, 2000.

Chapter 1

How to measure the reflectance and transmittance properties of a dense particle medium?

Contents

In this first Chapter, the operational means to make a rigorous measurement of the apparent spectral quantities characterizing a bulk, dense particle medium are investigated.

We first define precisely what we call the apparent spectral quantities all along this thesis, namely the reflectance and transmittance. We then review briefly the main existing practical measurement techniques developed in various reasearch domains to determine those apparent properties. Finally, we present the principle of a setup, using two intergrating spheres, which was found particularly adapted for the practical case of this thesis, i.e. dense algal supensions. Indeed, the integrating spheres are optical devices collecting light over large solid angles, which makes it possible to measure signals with a high signal to noise ratio, especially in the case of highly absorbing and scattering samples. We detail in particular the different technical key points to take into account when mounting such a practical setup, propose a technical solution and test it on phantom suspensions of polystyrene microspheres.

1.1 Glossary

Table 1.1: Glossary of the physical quantities used in this chapter

Designation	Definition	Units
Φ	Optical radiation rate, optical power	W
L	Radiance: flux density per unit solid angle and per unit projected area	$W.m^{-2}.sr^{-1}$
E	Irradiance. Density of incident flux per unit area of receiving surface	$W.m^{-2}$
$p(\vec{u_i}, \vec{u})$	Phase function. Fraction of incident light flux incident along the direction $\vec{u_i}$ reradiated in the direction $\vec{u}$	$-$
g	Anisotropy factor. Mean of the cosine of the angle between the vectors $\vec{u}$ and $\vec{u_i}$	$-$
c	Particle concentration in a liquid suspension	particlesm^{-3}
I	Electric output signal from the photodetector proportional to the incident light flux upon it	V

1.2 Theory: general definitions

In this section we first give general notions about light interaction with matter, and introduce the phenomena of light absorption and scattering. We then define the notions of reflectance and transmittance, and review the main techniques developed for their practical measurement.

1.2.1 Interaction of light with a sample: absorption and scattering phenomena

Interaction of light with matter can be explained by describing light as an electromagnetic wave. The complete theory is fully adressed eslewhere [3, 31, 16], yet we found interesting to introduce briefly the basic principles in this first paragraph.

Matter is composed of discrete electric charges, i.e. electrons and protons. When reached by an incident electromagnetic wave, they are set in oscillatory motion by the electric field of the incoming light. Accelerated electric charges then radiate energy in all directions: this phenomenon is known as the secondary radiation, also called the *scattered* radiation:

$$scattering = excitation + reradiation.$$

The reradiated wave may have the same frequency as the incident wave (elastic scattering), otherwise we talk about inelastic scattering (Brillouin and Raman scattering for example). In the framework of this thesis, only the elastic scattering was significant enough to be considered. The excited elementary charges can convert a part of the incident electromagnetic energy into other forms, e.g. thermal energy. This phenomenon is called *absorption*. Absorption and scattering are thus related to the same basic excitation phenomenon.

The wavelength of the incident light provides the physical scale that determines if a given structure can be considered as optically homogeneous or not. When the atomic or molecular heterogeneities are small compared to λ the medium is considered as optically homogeneous. On the contrary, when the heterogeneities of the medium belong to dimensions greater or of the same order of magnitude than the incident radiation wavelength, the medium is defined as optically heterogeneous, or complex [3].

For a given point of observation, the scattered field observed for a whole particle is the superimposition of all the wavelets scattered by the elementary dipoles forming the particle. What determines the scattered field observed at one point is the phase difference of those wavelets, which varies according to the direction of scattering. That is why the bigger (and the more distorted) the particle compared with the wavelength, the greater the difference between the wavelets phase and the higher peaks and valleys in the scattering pattern. On the contrary scattering does not vary significantly with the direction for small particles.

This description implies basic ideas that must be kept in mind when dealing with absorption and scattering of light by matter:

- absorption and scattering properties of a material are expressions of its instrinsic chemical and physical structure.
- absorption and scattering depend on the frequency of the incident light.
- absorption and scattering are intrinsically interdependent for a given material.

- heterogeneous bulk media are composed of obstacles of different materials for which scattering and absorption phenomena occur: the resulting bulk absorption and scattering are a combination of the specific effects of each obstacle.

For a real heterogeneous medium, it can be convenient to characterize light propagation from a stastistical point of view, by considering what happens to a large amount of photons in terms of their probability to be absorbed or scattered. From this stastistical point of view come the notions of linear optical properties, as it will be presented thoroughly in Chapter 2 of this thesis.

Along its way throughout a sample material, a photon can undergo different events, as summarized by figure 1.1. A photon incident with a direction $\vec{u_i}$ on a medium can be absorbed by the medium (a), scattered only once such that its transport direction is modified (b), scattered more than once (c), or it can be regularly transmitted (d): in that case nothing happens to it and it follows its genuine transport direction.

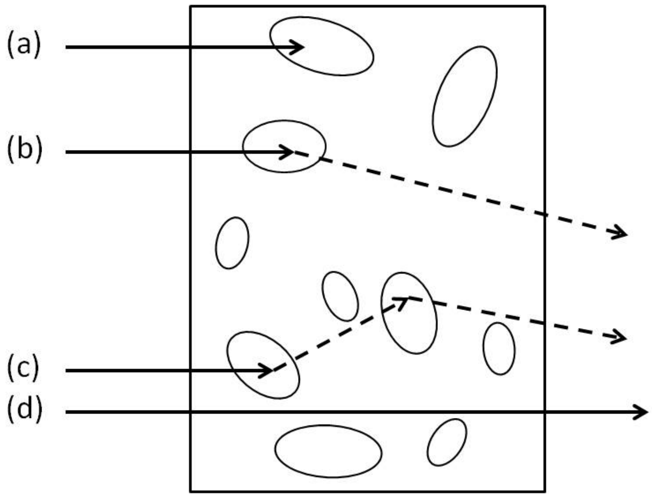

Figure 1.1: Illustration of the different interactions between an incident photon and a heterogenous medium: (a) Absorption,(b) Single scattering, (c) Multiple scattering,(d) Regular transmission.

Absorption and scattering are thus the basic principles giving a physical description of the interaction of light with matter. However they characterize the intrinsic properties of a material, and are not trivial to measure. In spectrometry, the actual properties that can be measured are the apparent optical properties of a given sample, as it will be presented in the next paragraph.

1.2.2 Measuring the apparent optical properties of a sample in VIS-NIR spectroscopy : definitions

It is usual to characterize the apparent radiometric properties of a medium illuminated by a monochromatic light flux incident with the angle θ by using the notions of reflectance and transmittance [20]. Let us consider a surface dividing space into two half-spaces and representing the limit between two media of different refractive indices, for example air and the sample medium, as shown on figure 1.2. Please note that, unless otherwise indicated, we consider a geometry with the asumption of rotational symetry for the next definition sections. On figure 1.2 in particular, an infinitely thin slab of a semi-infinite medium is considered.

Reflectance

The reflected flux $\Phi_R(\lambda, \theta)$ is the flux that is sent by the medium back into the half space containing the incident light beam $\Phi_i(\lambda, \theta)$. It is the sum of the backscattered flux reflected in the same direction θ than the incident beam, the specularly reflected flux and the diffusely reflected flux. The total reflectance $M_R(\lambda, \theta)$ is the dimensionless ratio of the total reflected flux $\Phi_R(\lambda, \theta)$ and the incident flux $\Phi_i(\lambda, \theta)$, and can be expressed as:

$$M_R(\lambda, \theta) = \frac{\Phi_R(\lambda, \theta)}{\Phi_i(\lambda, \theta)} \tag{1.1}$$

Transmittance

The transmitted flux $\Phi_T(\lambda, \theta)$ is the flux that goes across the medium and reaches the other half-space. It is the sum of the regular transmitted flux, in the same direction than the incident beam, and of the diffusely transmitted flux in all the other directions. As for the reflectance, the total transmittance $M_T(\lambda, \theta)$ can be expressed as the dimensionless ratio of the transmitted flux and the incident flux $\Phi_i(\lambda, \theta)$:

$$M_T(\lambda, \theta) = \frac{\Phi_T(\lambda, \theta)}{\Phi_i(\lambda, \theta)} \tag{1.2}$$

In practice, the regular transmittance $M_U(\lambda, \theta)$ is used: it is defined as the ratio between the regularly transmitted flux and the incident flux $\Phi_i(\lambda, \theta)$.

$$M_U(\lambda, \theta) = \frac{\Phi_{T,regular}(\lambda, \theta)}{\Phi_i(\lambda, \theta)} \tag{1.3}$$

Absorptance

A portion of the incident light can also be absorbed during its way throughout the medium. The ratio of the absorbed light flux over the incident flux defines the absorptance. It is expressed from the reflectance and the transmittance such that:

$$A(\lambda,\theta) = 1 - M_R(\lambda,\theta) - M_T(\lambda,\theta) \tag{1.4}$$

Geometric descriptors of reflected and transmitted light: BRDF, BTDF, phase function, anisotropy factor

Reflectance and transmittance indicate the portion of incoming light being respectively reflected and transmitted by the medium, within two half spaces delimited by the surface of the medium. However they do not give information about the angular distribution of the reflected and transmitted light in space. The fundamental geometric descriptor of reflectance is the Bidirectional Reflectance Distribution Function (BRDF) in sr^{-1}, defined as the differential element of reflected radiance dL_r in a specified direction, per unit differential element of incident irradiance $dE_{\lambda,i}$ also in a specified direction [1]:

$$BRDF(\lambda,\theta_i,\psi_i,\theta_r,\psi_r) = \frac{dL_{\lambda,r}(\lambda,\theta_i,\psi_i,\theta_r,\psi_r,E_{\lambda,i})}{dE_{\lambda,i}(\lambda,\theta_i,\psi_i)} \tag{1.5}$$

The polar angle θ is measured from the surface normal and the azimuth angle ψ is measured from an arbitrary reference in the surface plane , most often the plane containing the incident beam . The subscripts i and r refer to the incident and reflected beams, respectively. Equation (6.1) gives the most general definition of reflectance. However, by integrating over varying solid angles, Nicodemus et al. [21] defined nine goniometric reflectances, and by extension nine goniometric reflectance factors. To avoid confusion, it is thus necessary to explicit which definition of reflectance is used in a particular context or study.

Similarly, the angular distribution of the flux transmitted by a medium can be described by the Bidirectional Transmittance Distribution Function (BTDF) defined as [1]:

$$BTDF(\lambda,\theta_i,\psi_i) = \frac{dL_{\lambda,t}(\lambda,\theta_t,\psi_t,E_{\lambda,i})}{dL_{\lambda,i}(\lambda,\theta_i,\psi_i)d\Omega_i} = \frac{dL_{\lambda,t}(\lambda,\theta_t,\psi_t,E_{\lambda,i})}{dE_{\lambda,i}(\lambda,\theta_i,\psi_i)} \tag{1.6}$$

Similarly, the polar angle θ is measured from the surface normal and the azimuth angle ψ is measured from an arbitrary reference in the surface plane , most often the plane containing the incident beam . The subscripts i and t refer to the incident and transmitted beams, respectively.

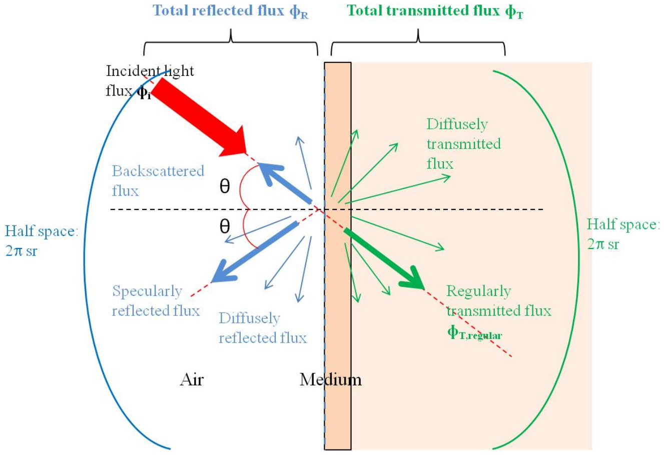

Figure 1.2: Illustration of the reflected and transmitted flux by an illuminated surface [20]

Another way to describe the angular distribution of the reradiated light by a scattering medium is using the notion of phase function p [4]. For a medium illuminated by an incident light beam along direction $\vec{u_i}$, the phase function $p(\vec{u}, \vec{u_i})$ gives the fraction of the incident flux that is sent in the direction $\vec{u}$, as shown in figure 1.3. The phase function is normalised such that:

$$\int p(\vec{u}, \vec{u_i}) d\Omega = 4\pi \tag{1.7}$$

It is usual to define the anisotropy factor g which is the mean of the cosine of the angle between the vectors $\vec{u}$ and $\vec{u_i}$ [4]:

$$g = \frac{1}{4\pi} \int_{4\pi} \vec{u}.\vec{u_i} p(\vec{u}, \vec{u_i}) d\Omega \tag{1.8}$$

For most dense media [11], the phase function p can be satisfyingly approximate by the Henyey Greenstein function giving its expression as a function of the anisotopy factor g and the angle θ:

$$p = \frac{1}{4\pi} \frac{1 - g^2}{(1 + g^2 - 2g\cos(\theta))^{\frac{3}{2}}}; \tag{1.9}$$

All along this thesis, we will use the terms reflectance, transmittance and regular transmittance to refer to the definitions given in the previous paragraph by relations (6.1) to (6.3). Note in particular that in our definition, we consider the light flux reflected and transmitted within two half-spaces of 2π sr.

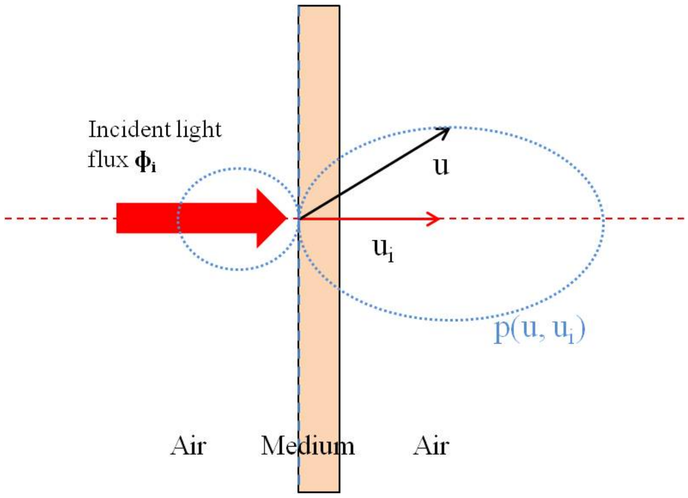

Figure 1.3: Geometry used to define the phase function p

1.2.3 Measuring the optical properties of a sample in VIS-NIR spectroscopy: short technical review

Now that the reflectance and transmittance spectral quantities have been defined, we will now investigate how they can be measured in practice. VIS-NIR spectroscopy particularity is to deal with a wide range of research domains and applications. The panel of samples encountered is thus nearly unlimited, from very diluted and clear samples (gases, diluted liquid solutions) to the most turbid ones (agrifood products, biological tissues, dense liquid suspensions) [27, 9, 24]. That is why various techniques have been developped to measure the reflectance and transmittance characteristics of the sample medium, depending of its general optical nature. In this section we will review some of the most classically implemented setups.

Measurement of the transmittance

A basic architecture for the direct measurement of the regular transmittance, commonly described in litterature [32, 33, 35, 24] is shown on figure 1.4. The incident light beam is collimated. Two aperture stops are placed in the setup: one immediately behind the sample holder, and the other in front of the detector aligned with the incident beam axis. The detector is placed "at infinity" from the sample (generally at distances above one meter), in order to reduce the quantity of scattered photons detected. Some works propose to replace the system pinhole+detector by an integrating sphere placed far from the sample [34].

The direct measurement of the regular photons may be awkward, especially for optically thick, scattering samples [24]. In that case the regular photons are few in number, resulting in a poor signal to noise ratio. Lock-in detection may be implemented in order to enhance

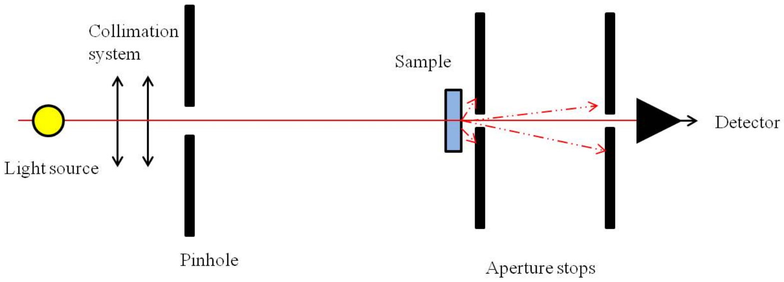

Figure 1.4: Experimental setup for regular transmittance measurements.

the signal to noise ratio: the incident light beam flux is thus modulated by a chopper at a given frequency $F_{chopper}$. The photodiode signal is fed into a lock-in amplifier tracking the frequency $F_{chopper}$ [32].

The measurement of the regular transmittance can also be achieved by differential method [26]. By measuring first the total transmittance, and second the diffuse transmittance it is possible to retrieve the regular component of the total transmittance by substracting the diffuse one. This can be implemented in particular with integrating spheres setups, as shown in figure 1.5. An integrating sphere is an optical device aiming at integrating radiant flux: in practice it is a solid sphere equipped with various entry ports, which inner wall is highly reflective. The principle of the integrating sphere is to collect the photons coming from various directions. It will be more thouroughly described in section 1.3.2 of the present chapter. One major advantage of the differential technique is the higher signal to noise ratio that can be obtained, as the total transmitted and diffuse transmitted signals are generally higher than the regular transmitted signal: this is all the more significant that the sample is optically complex. The integrating sphere setups are commonly used, especially in the VIS-NIR spectral domain where the highly reflective inner coating is easy to manufacture (generally with barium sulfate BaSO4).

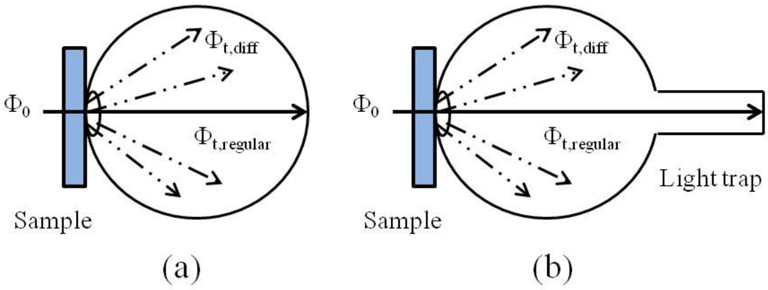

Figure 1.5: Configurations for the measurement of total (a) and diffuse (b) transmittance using an integrating sphere.

Commercial spectrophotometers are also widely used to measure the transmittance properties of a sample [30, 8, 2, 18, 27]. Conventional spectrophotometers are of the double-beam configuration [1], as shown in figure 1.6. The output is the ratio of the signal from the sample beam to the signal from the reference beam. The experimentator thus must ensure that the only difference between the two beams is the unknown quantity investigated. For liquid suspensions and gas in particular, this means that the same amount of solute or carrier gas must be put in the reference cell and in the sample cell. Some technical factors limit the performance of the double-beam intruments, and limit the ultimate uncertainties to the order of 0.1 percent: the beam geometry in particular is critical. Most intruments present a converging beam in the sample space. If the optical path is not the same for the two beams this may introduce a systematic error. Another limit may originate from stray light coming from the monochromator, especially for models equiped with only one monochromator. Those stray radiations can introduce trouble when measuring samples that are highly absorbing in a spectral region and transmitting in another one. Another architecture that may be encountered is the single beam spectrophotometer, with the principle shown on figure 1.7. In that case the operational method is to make the measurement with and without the sample, ensuring that the geometry of the beam remains the same during the operations.

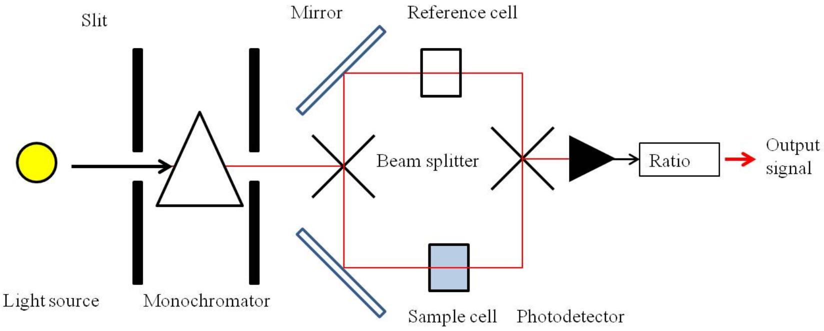

Figure 1.6: Schematic of the dual-beam spectrophotometer configuration.

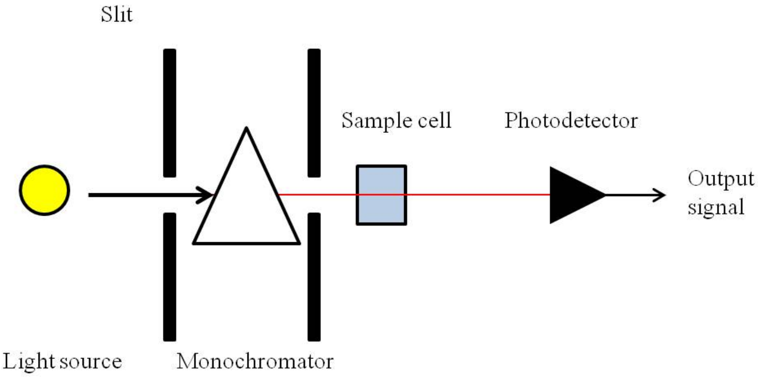

Figure 1.7: Schematic of the single-beam spectrophotometer configuration.

Many designs can be implemented to achieve the best performance of conventional spectrophotometers. A double monochromator may be used to reduce stray light and efficient collimating systems may be implemented in order to avoid beam geometry problems. The use of commercial spectrophotometers can be practical in routine, for repetitive and numerous characterization of samples. However it can be noted that the particular architecture of one instrument may be extremely specific: it is a fact that in the case of conventional spectrophotometers in the basic "transmittance" configuration, a certain amount of diffusely transmitted photons is measured, depending on the beam geometry, detectors, dimensions of the slits. As a consequence it can be expected that the transmittance measured for the same sample with two different instruments can be different. This may introduce trouble especially for calibration and model transfer, from one particular instrument to another.

When measuring diffuse transmittance, extra materials may be added to the basic designs to perform beam integration that reduces the effects of non-uniform detectors and beam shifts: among them, the integrating sphere is the most commonly employed.

Measurement of the reflectance

Simple reflectometers for the measurement of specular reflectance

The basic architecture for the absolute measurement of the specular reflectance was proposed by Strong [29, 28], and is shown on figure 1.8.

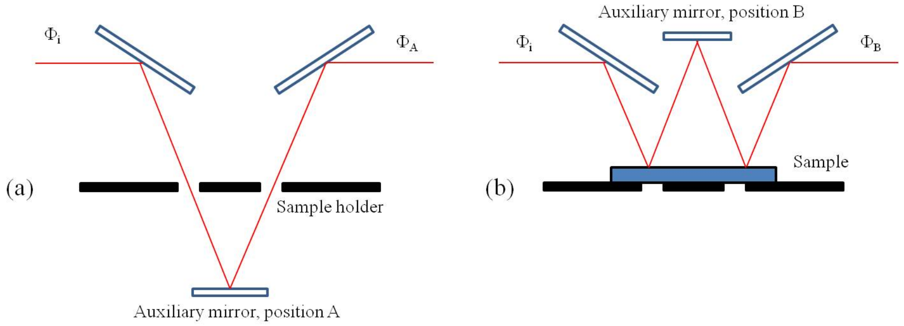

Figure 1.8: Basic architecture of the Strong V-W reflectometer. Measurement of the input light flux is made in configuration (a). The flux of the light specularly reflected twice by the sample is measured in configuration (b). The square of the specular reflectance of the sample is thus expressed by the ratio $\frac{\Phi_B}{\Phi_A}$.

Numerous improvements have been made on this basic design [5]. Conventional spectrophotometers usually propose such devices that can be adapted in the intrument.

Goniophotometric measurement of reflectance

Numerous procedures and instruments have been developped for goniophotometry. Measurements are made at several angles from normal (usually 20°, 30°, 45°, 60°, 75°, 85° and beyond) what makes it possible to characterize the BRDF of the sample material. Figure 1.9 shows an example of a gonioreflectometer setup [15]. Reflected light is probed on a defined polar angle range by the detector placed on a turntable. The flux of the incident light is measured when the detector is in the direction of the incident beam: in that case the sample is translated out of the axis of the incident beam. The incident angle can also be adjusted by rotating the sample, placed on another turntable coaxial with that rotating the detector. A beam splitter makes it possible to probe the incident light to correct the source unstabilities.

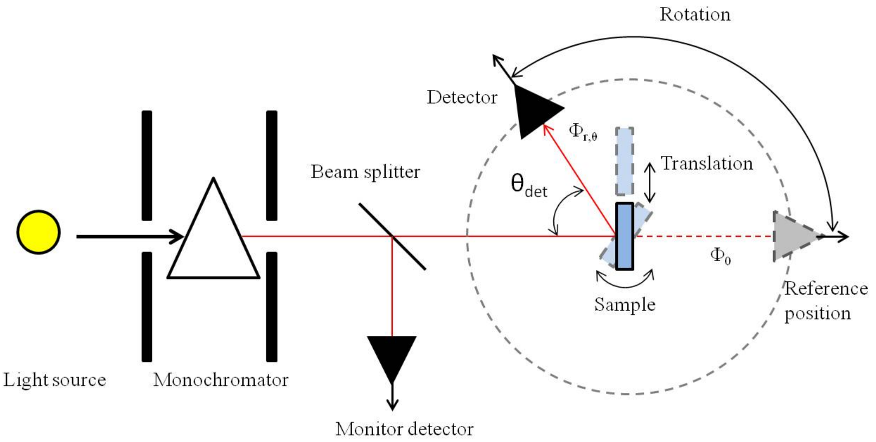

Figure 1.9: Example of a goniophotometer for the measurement of a sample BRDF.

Angular integration of goniophotometric measurements makes it possible to obtain the diffuse reflectance of the sample. However the gold method for measuring the diffuse reflectance, and particularly in the VIS-NIR spectral range, is surely the integrating sphere setup [17, 13].

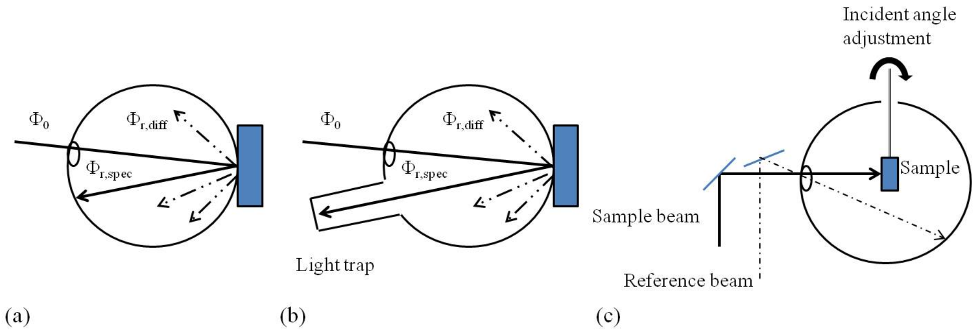

Figure 1.10: Integrating sphere setups for reflectance measurements. (a) Measurement of total reflectance (diffuse + specular), (b) diffuse reflectance only, (c) reflectance with a varying incident angle.

Numerous research works [6, 25] have proposed different instruments, methods and procedures using the integrating sphere for the measurement of the reflectance. Figure 1.10 shows some of them. Some configurations make it possible to measure both the specular and the diffuse reflectance figure 1.10 (a). As shown in figure 1.10 (b), the specular reflectance can also be excluded from the measurement by using a light trap. By placing the sample at the center of the sphere, the incidence angle can also be varied 1.10 (c).

All the presented architectures can be implemented to modern conventional spectrophotometers.

Measurement of reflectance and transmittance with the Double Integrating Sphere (DIS) setup

All the integrating sphere setups previously presented can be combined for the measurement of both transmittance and reflectance in a derivative measurement configuration called the double-integrating sphere setup [35]. As shown on figure 1.11, the sample is thus sandwiched between the reflectance and transmittance spheres, and illuminated by an incident beam. Reflected signal is collected by the reflectance sphere, while transmitted signal is measured in the transmittance sphere. The DIS setup has been proved to be a reference measurement technique, investigated in particular in biomedical optics [22, 23], and for highly scattering media such as organic tissues [35].

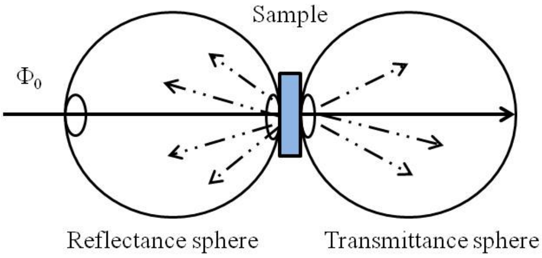

Figure 1.11: Configuration of the Double Integrating Sphere (DIS) setup for the reflectance and transmittance measurements.

In this thesis, the DIS setup was chosen as the measurement technique for the reflectance and transmittance measurements. The details of the setup implemented are given in the section 1.3 of the present chapter.

Measurement of the absorptance

In most cases, the absorptance is not directly measured, but is retrieved from reflectance and transmittance measurements [14]. If the experimentator makes sure that all the total transmittance and all the total reflectance have been measured, the absorptance can be inferred with relation (1.4).

However it can be mentionned that some devices have been developped for a direct measurement of absorptance. A technique particularly suited for liquid samples with low absorption properties, called the integrating cavity, was proposed by Elterman [10] and Fry [12]. A diffuse light field is set up within a cavity with highly reflective inner walls and filled with the sample. As the incident light field is already completly diffuse, the scattering properties of the sample do not intervene, and the device makes it possible to measure only the absorption properties. Moreover, due to multiple reflections on the cavity reflective walls, the photons undergo long light path, which makes it possible to enhance the absorption pheneomena and detect low absorption properties. As already said this technique only suits to very diluted solutions, which makes it unadapted to the practical case of the dense algal suspensions studied in this thesis.

1.3 Material and Method

As defined in the Introduction of this thesis, the practical material under study for us is dense algal suspensions. That is why it was necessary to choose measurement methods that were adapted to dense media. The DIS appeared to be a natural choice, as it had been proved to be particularly adapted to biological, complex materials [22, 23, 35]. In this section we thus present the example of the DIS setup developed by our research unit for the optical characterization of turbid media. The general design is given and the material used is detailled. The technical choices made are then explained one by one regarding the theoretical performance of the whole setup.

1.3.1 The Double Integrating Sphere (DIS) setup: general overview

The DIS setup was developed to measure simultaneously the total transmittance, total reflectance and regular transmittance of an optically complex sample. It was designed to be a complete and consistent characterization bench with no need of extra material for the regular transmittance measurement as it is the case for other works [27]. Figure 6.2 and 6.3 show the general geometry and dimensions of the setup.

The sample is sandwiched between the two collection spheres and stuck to the sample ports: it is directly illuminated by the incident light beam. Light is provided by a light source which is tilted with an angle θ from the optical axis such that the specularly reflected signal hits the inner surface of the reflectance sphere. It is then possible to collect the diffusely reflected and specularly reflected signals in the reflectance sphere. The backscattered signal however is not collected and escapes from the enter port. In practice, θ remained small (below 8°). In our work we chose to neglect the influence of this tilt in the setup, and did not throuroughly model its consequences. As a first step, in the rest of our work we made as if we were in a case of normal incidence.

The transmittance sphere is equipped with a special removable ligth trap, aligned with the direction of the incident light beam. In practice, the light trap is a hole in the sphere wall that can be either opened or closed: in the first case, the regularly transmitted signal escapes from the sphere, whereas in the second, everything happens as if the sphere was complete. With an opened light trap it is then possible to collect only the diffusely transmitted signal in the transmittance sphere. When the light trap is closed, both the diffusely transmitted and regularly transmitted signals are measured.
The detection of the flux level inside the sphere is achieved by photodetectors placed right

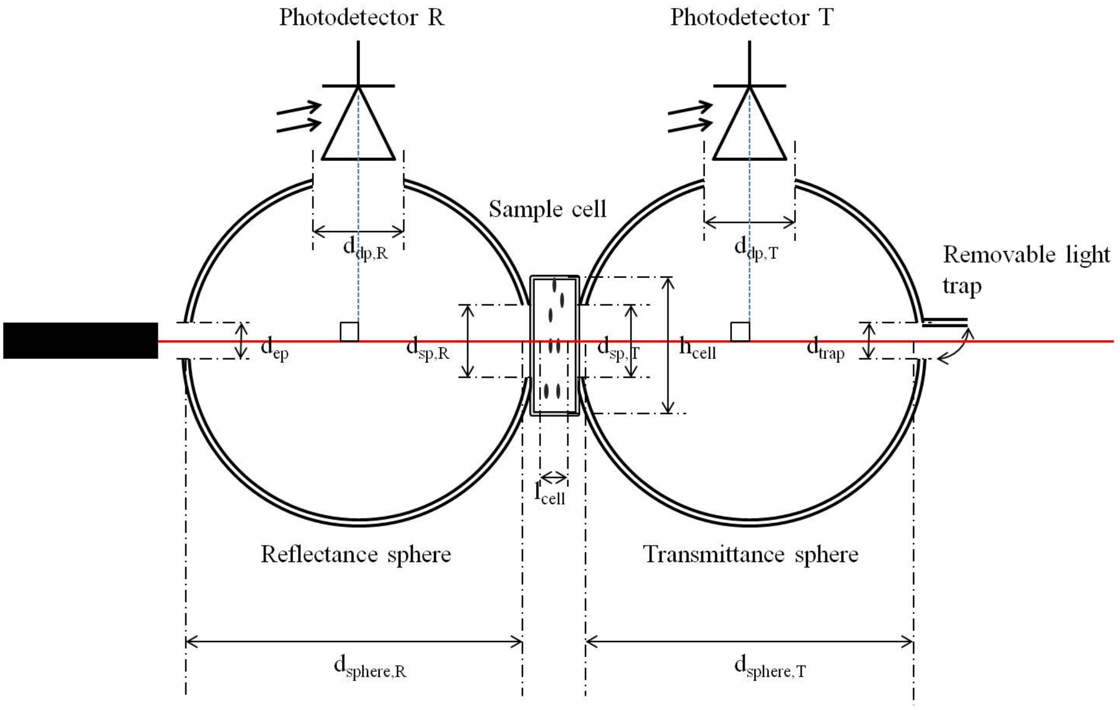

Figure 1.12: Side view of the double integrating sphere setup

at the detection ports of the spheres. Table 1.2 sums up the dimensions of the the DIS setup. Table 1.3 shows the reference of the material that was purchased for the setup.
In the following sections we will detail the points that we have identified as critical in order to choose adequately the dimensions and the configuration of the DIS setup.

Table 1.2: Designation and values of the dimensions of the DIS setup

Designation	Definition	Dimensions (mm)
$d_{sphere,R}$	inner diameter of the reflectance sphere	83.82
$d_{sphere,T}$	inner diameter of the transmittance sphere	83.82
d_{ep}	diameter of the entry port of the reflectance sphere	10
$d_{dp,R}$	diameter of the detection port of the reflectance sphere	25.4
$d_{dp,T}$	diameter of the detection port of the transmittance sphere	25.4
$d_{sp,R}$	diameter of the sample port of the reflectance sphere	25.4
$d_{sp,T}$	diameter of the sample port of the transmittance sphere	25.4
d_{trap}	diameter of the light trap of the transmittance sphere	10
l_{cell}	length of the sample cell	variable
h_{cell}	heigth of the sample cell	variable
w_{cell}	width of the sample cell	variable
θ	angle of the incident light beam with the optical axis	8°

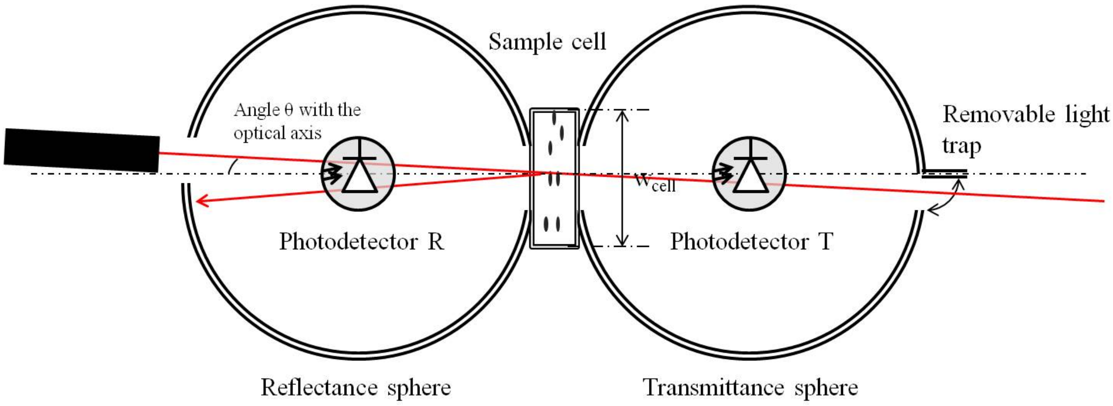

Figure 1.13: Upper view of the double integrating sphere setup

Table 1.3: Reference of the material used for the DIS setup

Designation	Reference
Reflectance integration sphere	3P-GPS-033-SL (Labsphere) modified
Transmittance integration sphere	3P-GPS-033-SL (Labsphere) modified
Photodetectors	PDA100A (Thorlabs)

1.3.2 Technical keypoints

The integrating spheres: Theory

A complete description of the integrating sphere theroy and application can be found elsewhere [17, 13, 19]. In this section we will provide key relationships making it possible to understand the basic principles of an integrating sphere.

For a plane diffuse surface illuminated by a input light beam of area A with a input flux Φ_i, the flux density per unit solid angle and per unit area, called the radiance L is given by the relationsphip:

$$L = \frac{\Phi_i \rho}{\pi A} \tag{1.10}$$

Where ρ is the reflectance of the surface.

An integrating sphere is an optical device aiming at integrating spatially a radiant flux. The sphere inner surface is highly diffusive, which makes that light incident on it undergoes sucessive, multiple reflections. Consequently, for an input flux Φ_i, the total flux incident on the sphere surface Φ_{tot} is expressed by:

Table 1.4: Example of the general purpose integrating spheres range of Labsphere

Designation	Interior diameter (mm)	ports diameter (mm)
3P-GPS-010-SL	24.5	6.35
3P-GPS-020-SL	50.8	12.7
3P-GPS-033-SL	83.82	25.4
3P-GPS-053-SL	134.6	25.4

$$\Phi_{tot} = \frac{\Phi_i \rho (1-f)}{1-\rho(1-f)} \tag{1.11}$$

Where ρ is the reflectance of the sphere walls, Φ_i is the input flux and f is the port fraction defined as $f = (\sum A_i)/A_s$ with i the number of open ports of the sphere. Equation (1.11) means that the flux incident upon the sphere surface is enhanced compared to the actual input flux. This modifies equation (1.10) such that the radiance of the sphere surface can be expressed as a function of the incident flux and of the sphere properties as:

$$L_s = \frac{\Phi_i}{\pi A_s} * \frac{\rho}{1-\rho(1-f)} \tag{1.12}$$

Where A_s is the area of the inner sphere surface in m^2.

The integrating spheres: Practical choice of the sphere dimensions

To choose adequately the dimensions of the sphere, one must make a compromise depending on the purpose of the setup. The general purpose spheres range proposed by Labsphere (http://www.labsphere.com) can be taken as a practical example. Table 1.4 shows the characteristics of the commercially available models. In this section we will present the key points to consider to choose a sphere model fitting the application needs. On the one hand, we will see that the sphere gain can be optimized by choosing the sphere diameters and port dimensions. Second, we will note that the actual solid angles collected by the spheres are also influenced by the dimensions of the sphere ports, and also plays a crucial role in the DIS performance. Making a compromize between the sphere gain and the collection solid angles thus appears to be necessary.

The integrating spheres: Optimizing the sphere gain

Equation (1.12) can be divided in two terms: the first term decreases when the sphere area increases. This means that for a given total port area, the inner radiance of the sphere decreases when the sphere area increases, as shown on figure 1.14. The second term of the right side of equation (1.12) is usually called the sphere multiplier M, accounting for the increase of radiance coming from the multiple reflections inside the sphere:

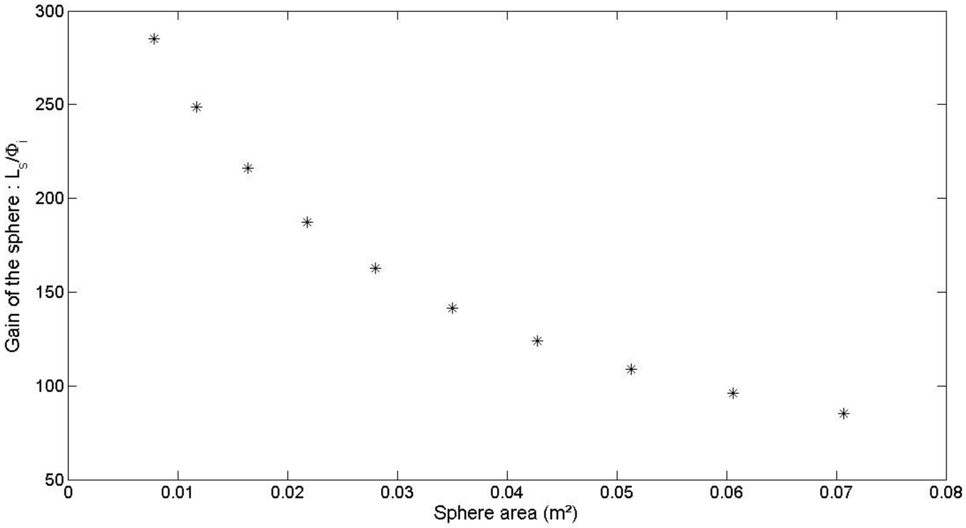

Figure 1.14: Evolution of the sphere gain as a function of the sphere inner area for a fixed total port area (here $79mm^2$)

$$M = \frac{\rho}{1-\rho(1-f)} \tag{1.13}$$

Figure 1.15 shows the influence of the port fraction f and of the reflectance of the sphere wall ρ on the value of M. As expected, M increases with the reflectance of the sphere, but it is also important to note that the decrease of the port fraction f dramatically increases the sphere multiplier. Following that rule, in theory f must be taken as low as possible, what can be made by taking the smallest ports as possible. One practical rule is that most integrating spheres have $f < 0.05$ with the largest port dimension $< 1/3$ of the sphere diameter.

This means that the highest gain $\frac{L_s}{\Phi_i}$ will be obtained with the smallest spheres and the smallest sample ports. This is indeed illustrated by table 1.5, which compares the fraction $\frac{L_s}{\Phi_i}$ obtained for the same input flux Φ_i for the four commercially available sphere models.

The integrating spheres: Optimizing the sphere collection solid angle in the case of an external sample

In the DIS configuration which is considered for this thesis application, and which is presented in figures 6.2 and 6.3, the sample is placed outside of the spheres: as a consequence, one has to study carefully the actual solid angle that is collected with the sphere setup. According to the definition of the reflectance and transmittance given in section 1.2.2, the spheres should ideally collect the light in a half-space of 2π sr to measure the total reflected

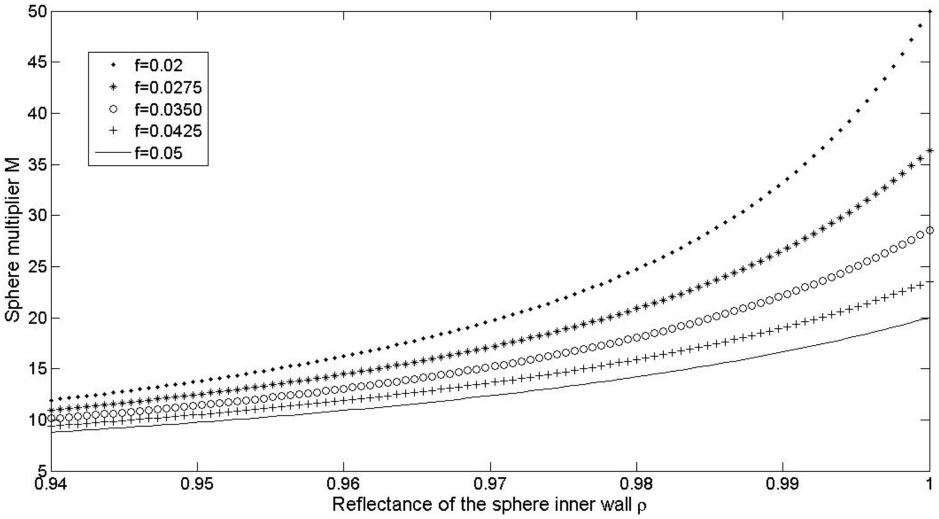

Figure 1.15: Evolution of the sphere multiplier M as a function of the sphere reflectance ρ and of the port fraction f

Table 1.5: Sphere gain $\frac{L_s}{\Phi_i}$ for the different sphere models, for the same input flux Φ_i. The case of integrating spheres with two open ports was considered, with the respective dimensions of the different sphere models.

Designation	$\frac{L_s}{\Phi_i}$ $(m^{-2}sr^{-1})$
3P-GPS-010-SL	3040
3P-GPS-020-SL	760
3P-GPS-033-SL	217
3P-GPS-053-SL	146

and total transmitted signals.

Figure 1.16 illustrates the geometry of the problem: the sample is placed right at the sample port of the sphere. In a first approximation we can consider the problem as rotationally symmetrical and we will only take into account the vertical plane (OXY) containing the optical axis. In that plane, the point P is described by its coordinates (x, y) according to the orthonormed system (OXY). The width of the sphere walls and the diameter of the sample port are respectively designated by w_{sphere} and d_{sp}. Light coming from point P directly enters the sphere with the angle α: the corresponding solid angle Ω is then deduced using the relationship $\Omega = 2\pi(1 - cos(\frac{\alpha}{2}))$. The light coming from point P that hits the sphere ledges, represented by dotted arrows on figure 1.16 must also be taken into account: indeed, as the sphere ledges are coated with highly reflective spectralon, we can consider they act nearly as a light guide inside the sphere. In a first approximation it was considered that 90% of the light reaching the sphere ledges was collected. Figure 1.17 shows the solid angle seen by the sphere for various positions of point P and for different sample ports diameters, for a fixed wall width ($5mm$ here).

The cases of the commercially available sphere models shown in table 1.4 were compared: as shown on figure 1.17, decreasing the sample port dramatically decreases the solid angle with which light is actually collected by the sphere. This effect is all the more important as the point P is far from the sphere and from the optical axis. For highly scattering samples, this effect is critical and strongly affects the actual incident flux Φ_i that enters the sphere. Figure 1.18 shows the fraction of the incident flux Φ_i coming upon the sample at the point P that actually enters the sphere for different values of the anisotropy factor g. For this example, the point P is situated 5mm at the front of the sphere sample port. Figure 1.18 illustrates that the larger sample port, the higher portion of the incident flux on the sample is collected, this rule being all the more critical that the sample is highly scattering, ie the anisotropy factor g is close to 0.

Maximizing the sample port diameter is then necessary to collect the maximum flux coming from the sample, in particular when it is highly scattering.

The integrating spheres: Making a compromise

As illustrated by the previous primary investigation, it seems that a compromise must be made to choose the sphere dimensions with on the one hand the optimization of the sphere gain, and on the other hand the optimization of the collection angle. For the case of this thesis, and as presented in section 1.3.1, the spheres needed for the DIS setup were collection spheres. Moreover, the setup aimed at being used for samples that might be highly scattering: given the previous discussions the sample ports thus had to be chosen sufficiently large. In order to maintain a sufficient gain in the sphere the sphere diameter should also be chosen as a compromise between a high enough sphere multiplier M and

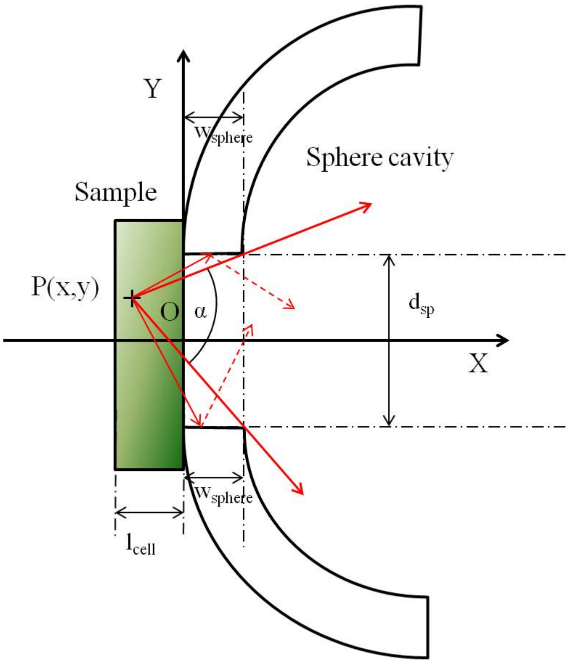

Figure 1.16: Calculation of the solid angle seen by the sphere: geometry of the problem

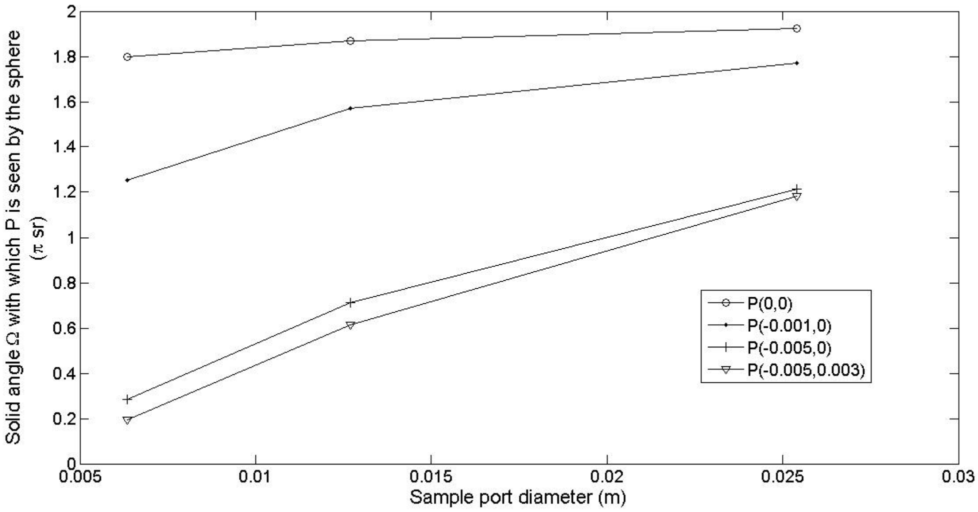

Figure 1.17: Solid angle Ω under which the point P is seen by the sphere for different sample port diameters and various positions of P

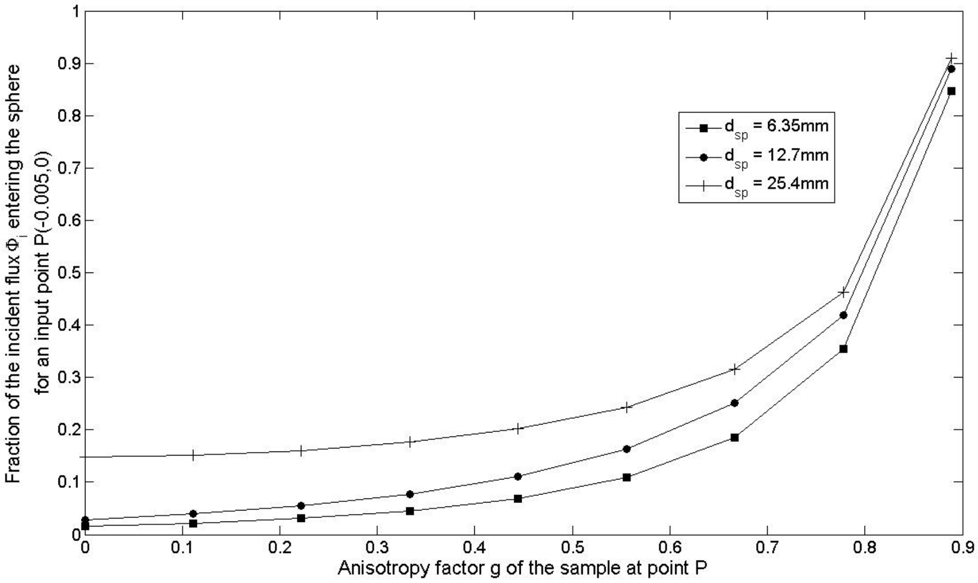

Figure 1.18: Fraction of the incident flux Φ_i on the point $P(-0.005, 0)$ on the sample actually entering the sphere for various values of the sample port diameter d_{sp} and various anisotropy factor g

and limited sphere inner area. The sphere model 3P-GPS-033-SL proposed by Labsphere was judged to be a satisfying compromise, presenting a large sample port diameter and a sensible sphere gain, which may assure high enough signal levels.

The commercial spheres were modified by us on several points: the diameter of entry port of the reflectance sphere was reduced to $10mm$. A 10mm-light trap was drilled in the back of the transmittance sphere. The final fraction port of the reflectance sphere and of the transmittance sphere with an opened light trap is thus 0.0463. The transmittance sphere with a closed light trap presents a port fraction of 0.0427. The resulting characteristics of the spheres used in the DIS setup are shown in table 1.6.

Table 1.6: Characteristics of the spheres used in the DIS setup.

Designation	Open port diameter (mm)	port fraction f	$\frac{L_s}{\Phi_i}$
Reflectance sphere	Entry port : 10, Sample and detector ports: 25.4	0.0463	206.4
Transmittance sphere open trap	Sample and detector ports: 25.4, Light trap: 10	0.0463	206.4
Transmittance sphere closed trap	Sample and detector ports: 25.4	0.0427	217.4

The detection system

The integrating spheres are not the only critical point of the DIS. Another major element of the setup is also the detection system. The detectors geometry must be taken consistently regarding the dimensions of the spheres that have been fixed. For flux collectors, the detector field of view must be greater than the source field of view. In the case where the source to be measured is an integrating sphere as presented in figure 1.19, the total flux Φ_{det} incident on the detector active area is thus expressed as:

$$\Phi_{det} = L_s A_{det} \Omega_{det} \tag{1.14}$$

Where L_s is the sphere inner radiance in $Wm^{-2}sr^{-1}$, A_{det} is the detector active area in m^2 and Ω_{det} in sr is the projected solid angle seen by the detector such that $\Omega_{det} = \pi sin^2(\frac{\alpha_{det}}{2})$.

Expression (1.14) illustrates that the larger the detector active area A_{det} and the greater Ω_{det}, the higher detected flux Φ_{det}. To maximize the flux actually detected, the dectectors must thus be taken with the largest active area as possible and placed as close as possible to the sphere detection port. Note also that having large detection ports enhances the solid angle scanned by the detector, which concurs with the previous remarks about the sphere port dimension.

The order of magnitude of the influence of light losses due to the injection in the detection system can be illustrated by taking two example cases. Let us first consider a practical case where a $100mm^2$-active area, amplified, switchable-gain, silicon detector from Thorlabs (PDA100A) is chosen. This model can be interesting in particular because it is designed for detection over all the visible range [400-1100nm]. If the detector is placed right at the detector port of the sphere, following equation (1.14), the theoretical ratio $\frac{\Phi_{det}}{L_s}$ should be:

$$\frac{\Phi_{det}}{L_s} = A_{det} \pi sin^2(\frac{\alpha_{det}}{2}) = \pi * 0.01 * sin^2(\frac{\pi}{2}) = 3.10^{-4}$$

In practice, the detector actual detection angle is generally limited, due in particular to reflexions at the edges of the silicon active area. To take this limitation into account, we estimated that a correction factor of 0.5 could be applied in a first approximation to give a more realistic prediction:

$$\frac{\Phi_{det}}{L_s} = 0.5 * \pi * 0.01 * sin^2(\frac{\pi}{2}) = 1,5.10^{-4} \tag{1.15}$$

One should be particularly aware of the significance of the signal loss due to the injection in the detector: the value of $\frac{\Phi_{det}}{L_s}$ obtained with the PDA100A may seem particularly small, even if the detector was chosen among the biggest ones commecially available. The loss

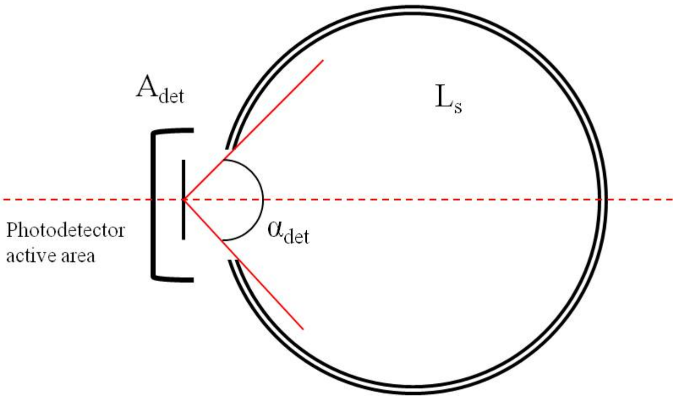

Figure 1.19: Configuration in the case of the detection of the sphere radiance by a flux collector

would be even more effective if we imagine a second example case where a $1mm$-core, 0.22-NA, classically used fiber was chosen: in that case, the ratio $\frac{\Phi_{det}}{L_s}$ dramatically decreases.

$$\frac{\Phi_{det}}{L_s} = \pi^2 * 0.005^2 * 0.22^2 = 1.2.10^{-5}$$

This example shows that a common pitfall would be to neglect the light injection in the detection chain, what would dramatically reduce the signal level of the entire setup, losing all what could have been gained by correctly choosing the integrating sphere dimensions.

The incident light beam

Other key points influencing the setup performance are the characteristics of the illumination, and in particular the diameter of the incident light beam. Indeed, as seen in section 1.3.2, the farther the observed point P from the center of the disc plane formed by the sphere sample port, the smaller the solid angle actually collected by the sphere. This means that light coming from regions of the sample that are too far away from the center of the sample port may not be actually detected. This constraints the direction and diameter of the incident light beam: in the planes of the sample ports of both the transmittance and reflectance spheres, the beam must be centered at best with respect to the port edges, and taken as small as possible compared to the port dimensions. As shown in figure 6.3, the input beam direction must also respect a tilt with respect to the normal direction to the sample surface, in order to keep the specular reflected signal inside of the reflectance sphere. Finally, the input beam must be aligned with the light trap at the back of the transmittance sphere. In the case of the DIS setup presented in this study, the light trap was designed specially to be tilted from the normal to the sample plane with the same angle θ than the input beam, what made the whole alignment possible.

The sample

Finally, even if the DIS setup aims at being used for any media, the way the sample is presented to the measurement system must also be defined with care as it influences significantly the measurements. The size of the sample in particular is a critical point. Due to the limited solid angle collected by the spheres imposed by the dimensions of the sample ports, complex variability in the measurement of the reflected and transmitted signals may appear for different sample size. Figure 1.20 shows that in the case of the presented DIS setup, the collected solid angle is highly dependent on the position of the observed point P, and in particular on the position x. This means that for thick samples, the successive vertical planes are not seen in the same way by the sphere, which may introduce unexpected effects on the measurements. In practice those effects might be limited by choosing a sample as thin as possible. For liquid samples, this implies that the thickness of the glass or quartz cell containing the liquid must be chosen small enough. In practice the commercially available cell dimensions are usually constrained. It is possible to order specially designed quartz cells, even if this solution remains expensive. Unfortunately in this thesis we did not order special quartz cells and used common Hellma models.

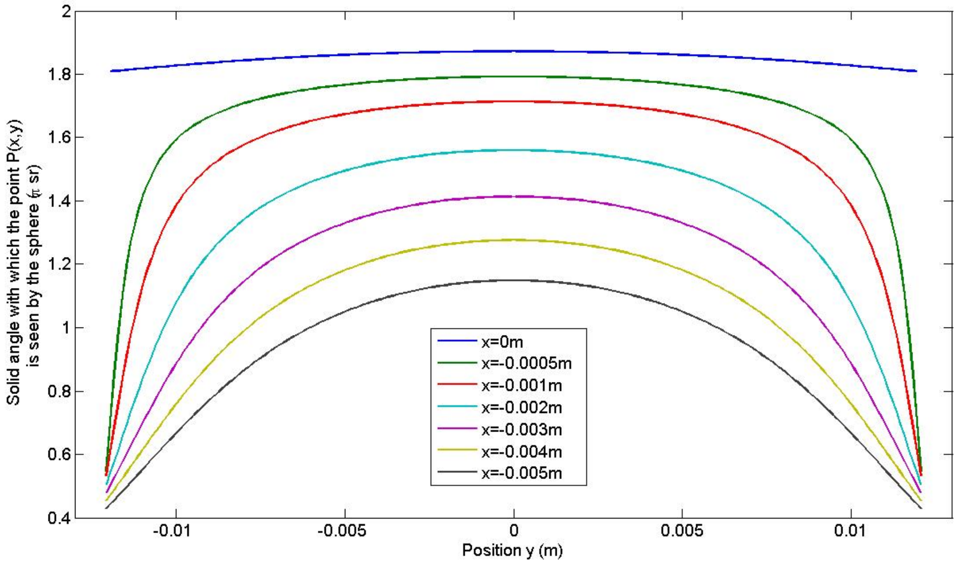

Figure 1.20: Solid angle under which the point P sees the sphere as a fonction of its coordinates (x, y), in the case of the presented DIS setup.

The previous practical investigation illustrates the influence of the different elements of the DIS on the measurement performance. The dimensions of the spheres must be chosen carefully by making a compromise between the sphere gain and the collection solid angles. The injection in the detection system must also be taken into account, as well as the dimension and position of the incident light beam, and the position of the sample under test. Once the material hes been properly defined, a justified method must also be implemented to make suitable measurements. The next section thus describes the measurement protocol developed and implemented during this thesis.

1.3.3 Description of the measurement protocol

Measurement configurations and signals

In this section we detail the measurements implemented with the DIS: the exact configuration of the setup as well as the signals measured are described step by step.

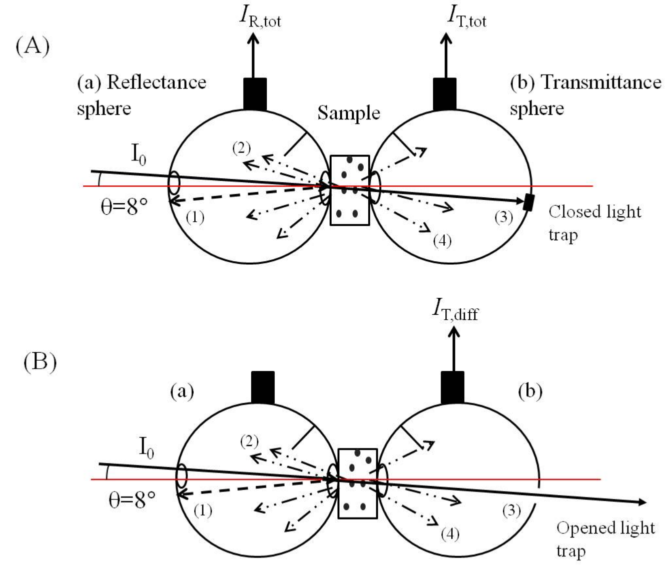

Figure 1.21: (A) Experimental measurements of the totally reflected $I_{R,tot}$ and totally transmitted $I_{T,tot}$ signals. (B) Experimental measurement of the diffusely transmitted light $I_{T,diff}$.

Measurement of the totally reflected, totally transmitted and diffusely transmitted signals

Figure 1.21 shows the experimental configurations implemented on the DIS setup when measuring the totally reflected and totally transmitted light (A), and when measuring the diffusely transmitted light (B).

The sample was sandwiched between the two spheres. In configuration (A), the light trap in the transmittance sphere (b) was closed. In the reflectance sphere (a), the specularly reflected light (1) and the diffusely reflected light (2) were thus collected. Note that the backscattered light was not collected and escaped throughout the enter port, and was thus not taken into account in the signal designated as $I_{R,tot}$. In the transmittance sphere

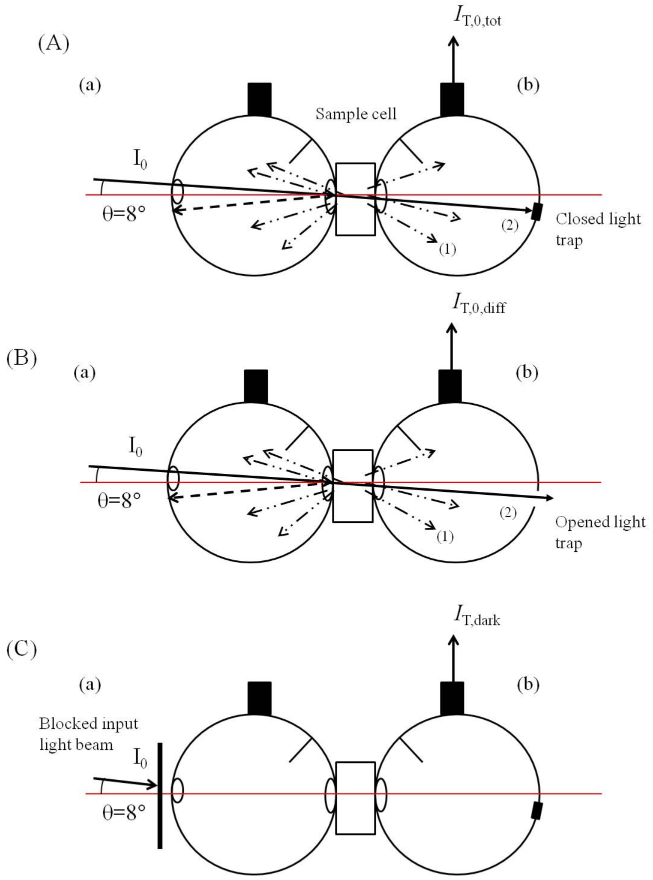

Figure 1.22: (A) Experimental measurement of the input totally transmitted $I_{T,0,tot}$ signal. (B) Experimental measurement of the input diffusely transmitted light $I_{T,0,diff}$. (C) Experimental measurement of the dark signal $I_{T,dark}$ in the transmittance sphere.

(b), the regularly transmitted (3) and diffusely transmitted (4) signals were collected, and their addition was designated as $I_{T,tot}$. In configuration (B) the light trap was opened. This time, the regularly transmitted signal (3) escaped from the transmittance sphere (b). Only the diffusely transmitted signal (4) was thus collected in the sphere, and designated as $I_{T,diff}$.

Measurement of the incoming light and of the dark signals in the reflectance and transmittance spheres

Figure 1.22 shows the experimental configurations implemented on the DIS setup when measuring the input light and the dark signal in the transmittance sphere (b).

The sample was removed from the setup. For aqueous liquid samples, the medium was replaced by distilled water and the cell was put in the same position in which the measurements were implemented with the sample. This condition was found necessary in

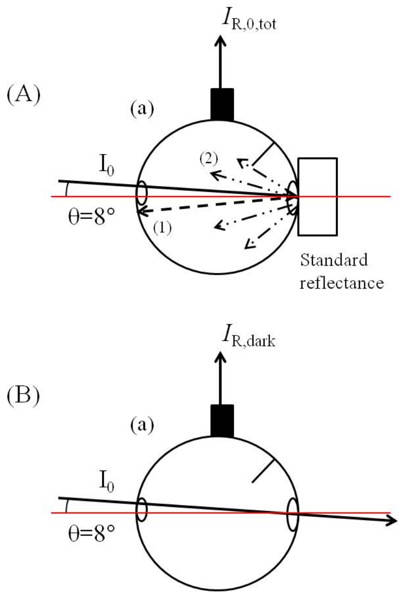

Figure 1.23: (A) Experimental measurement of the input totally reflected $I_{R,0,tot}$ signal. (B) Experimental measurement of the dark signal $I_{R,dark}$ in the reflectance sphere.

order to take into account the influence of the reflections of light within the sample cell, and to reproduce at best the refractive indices difference between air, the sample cell and the medium. Configuration (A) shows the measurement of the input totally transmitted signal $I_{T,0,tot}$ when the light trap was closed in the transmittance sphere. In configuration (B) the light trap was opened and only the input diffusely transmitted light (1) was measured and designated as $I_{T,0,diff}$. When the input light beam was blocked as shown in configuration (C), the dark signal $I_{T,dark}$ was measured. In the dark experiment room where the measurements were made, it was found experimentally no difference bewteen dark signals measured with opened or closed light trap, what indicated that no significant parasite light entered throughout the light trap.

Figure 1.23 shows the experimental configurations implemented on the DIS setup when measuring the input light and the dark signal in the reflectance sphere (a).

In configuration (A), the sample port of the reflectance sphere was filled with a highly reflective, standard reflectance. The specular reflected light (1) and the diffusely reflected light (2) were then collected in the sphere. The standard reflectance used in this study was a spectralon (LabSphere) with a spectral reflectivity r_{std} close to 0.98 on the spectral domain considered. The values of r_{std} were provided by the manufacturer. In configuration (B) the sample port was opened such that the incident light beam directly escaped throughout the sphere. Parasite light remaining in the sphere was then measured and designated as $I_{R,dark}$.

Implementation of the signals corrections

As explained previously, the successive measurement configurations implemented in order to measure the raw signals made that the sphere ports were not always in the same state (opened or closed) for all the configurations. This induced differences in the sphere gains at each measurement. A correction must be implemented in order to compensate those gain differences. This was made in this study by normalizing all the raw signals measured relatively to the configuration where the sphere gain was the highest.

Table 1.7: Sphere theoretical port fraction and gain for each measurement configuration of the raw signals in sphere R, for a completely reflective sample.

Raw signal measured	port fraction f	$G_{th} = \frac{L_s}{\Phi_i}$
$I_{R,tot}$	0.024	325
$I_{R,0,tot}$	0.027	325
$I_{R,dark}$	0.046	217

Table 1.8: Sphere theoretical port fraction and gain for each measurement configuration of the raw signals in sphere T, for a completely transmittive sample.

Raw signal measured	port fraction f	$G_{th} = \frac{L_s}{\Phi_i}$
$I_{T,tot}$	0.023	332
$I_{T,diff}$	0.024	325
$I_{T,0,tot}$	0.0451	225
$I_{T,0,diff}$	0.0496	211
$I_{T,dark}$	0.0496	225

Tables 1.7 and 1.8 summarize the value of the port fraction and of the sphere gain that would be obtained in each measurement configuration respectively if the sample was theoretically completely reflective (table 1.7) and completely transmittive (table 1.8). When the sample was placed at the sample port, the port was considered as closed, which also implies that the sample was large enough for totally filling the sample port. If the sample had been smaller than the sample port, some light could have escaped throughout the gaps between the edges of the sample and the edges of the sample port, which would have needed some extra corrections.

Table 1.7 and 1.8 show that the maximum sphere theoretical gain $G_{th,max}$ corresponds to the configuration of the measurement of the totally transmitted signal $I_{T,tot}$, with only the enter port opened in the transmittance sphere. In this study we chose to compensate the sphere gain difference by multiplying the raw signal measured in a sphere of theoretical gain G_{th} by a factor corresponding to the ratio $\alpha = \frac{G_{th,max}}{G_{th}}$. The corrected values $I^*_{R,tot}$, $I^*_{R,0,tot}$, $I^*_{R,dark}$, $I^*_{T,diff}$, $I^*_{T,0,tot}$, $I^*_{T,0,diff}$ and $I^*_{T,dark}$ were thus obtained.

Calculation of the normalized reflectance M_R, normalized transmittance M_T and normalized regular transmittance M_U

Following the definition of reflectance and of transmittance given prévisously in section 1.2.2 of the present Chapter, the normalized reflectance M_R, normalized transmittance M_T and normalized regular transmittance M_U are obtained from the corrected measured signals such that:

$$M_R = r_{std} \frac{I^*_{R,tot} - I^*_{R,dark}}{I^*_{R,0,tot} - I^*_{R,dark}} \tag{1.16}$$

$$M_T = \frac{I_{T,tot} - I^*_{T,dark}}{I^*_{T,0,tot} - I^*_{T,dark}} \tag{1.17}$$

$$M_U = \frac{I_{T,tot} - I^*_{T,diff} + I^*_{T,0,diff} - I^*_{T,dark}}{I^*_{T,0,tot} - I^*_{T,dark}} \tag{1.18}$$

Where r_{std} is the reflectivity of the standard reflectance used for the measurement of $I_R, 0, tot$.

The spectral quantities defined by relations (1.16) to (1.18), measured and corrected according to the protocol described in this section were used throughout this thesis to characterize the apparent spectral properties of a sample. In the following Chapters we chose for simplicity not to mention all the steps of the measurement protocol implemented, in particular the correction of the signals. Nevertheless it has to be noted that the complete protocol as described in this section was followed for each of our experiments.

1.4 Results and discussion: validation with microsphere phantoms

In this section we describe the primary results obtained on phantom solutions of dyed polystyrene microspheres with various particle densities when measuring their total reflectance M_R, total transmittance M_T and regular transmittance M_U with the measurement setup and protocol previously described. As a first step, those measurements were performed at one single wavelength (632.8 nm). This study was implemented as a first test of the DIS configuration.

1.4.1 Experimental design

The DIS setup was tested on known phantom solutions of polystyrene microspheres. 14 phantom solutions of colored polystyrene microspheres were obtained by successive dilutions of a stock standard solution with an initial particle concentration of $1,055.10^{18}$ particles/m^3 (Red Carboxylate-modified Polystyrene reagent microspheres from Thermo Scientific), in distilled water. The microspheres were certified by the manufacturer to have a $0.41 \mu m$ diameter.

The spheres described in the previous section 1.3.1 were used. Illumination was provided by a Helium-Neon gas laser (HNL008 from Thorlabs) at 632.8 nm. The incident beam diameter on the sample was estimated to be 0.5 mm. The detection system was composed of two $100mm^2$-active area, amplified, switchable-gain, silicon detector from Thorlabs (PDA100A), put right at each of the detection ports of the reflectance, and transmittance spheres.

Measurements of $I_{R,tot}$, $I_{R,0,tot}$, $I_{R,dark}$, $I_{T,tot}$, $I_{T,diff}$, $I_{T,0,tot}$, $I_{T,0,diff}$ and $I_{T,dark}$ were performed on the DIS setup with the protocol described previously. Three replicates of each signal were acquired and averaged. The measurements were carried out on each sample separately, with sample solutions put respectively in a 2mm, 4mm and 5mm-wide quartz sample cell (Hellma).

1.4.2 Total fraction of the incident light collected

Figure 1.24 shows the fraction of the incident light respectively reflected (M_R), transmitted (M_T) and regularly transmitted (M_U) by the samples put in a 5mm-sample cell, as a function of the particle concentration c. The total measured light, expressed by the quantity $M_R + M_T$, and the diffusely transmitted light expressed by $M_T - M_U$ are also represented.

The total fraction of the incident light that is actually detected in the DIS setup is represented by the quantity $M_R + M_T$: it should be noted first that the quantity $M_R + M_T$ never equals 1 even for low concentrations. Two main phenomena can explain why a fraction of the incident light can disapear, and is finally never collected in the setup. First, light can be absorbed by the sample medium, and transformed into another form of energy within the matter itself. Second, some light can physically escape from the DIS setup, and leak at the edges of the sample cell [7].

The light leaks result mainly from the fact that the solid angles seen by the spheres are actually smaller than the ideal 2π sr. As explained previously, this effect is all the more important that the sample cell is wide.

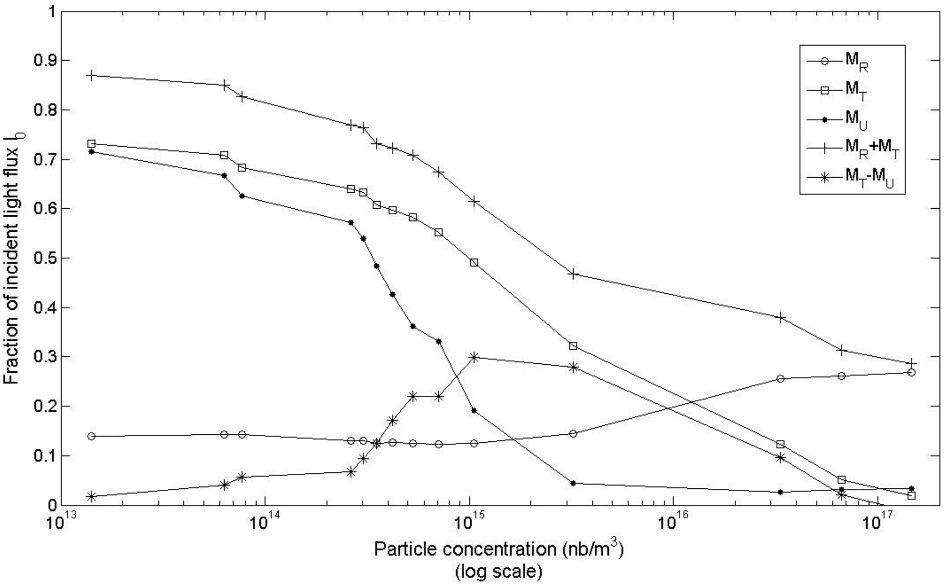

Figure 1.24: Fraction of the incident light I_0 respectively reflected (M_R), transmitted (M_T) and regularly transmitted (M_U) by the samples put in a 5mm-sample cell, as a function of the particle concentration. The quantity $M_R + M_T$ expresses the total fraction of I_0 that was measured with the DIS setup. $M_T - M_U$ is the fraction of I_0 that was diffusely transmitted by the sample

1.4.3 General variations of the reflected and transmitted light: distinction of the scattering regimes

Three main regimes can be observed as a function of the particle concentration.
At low particle concentration, i.e. c below $c_{lim,singlescatt} = 10^{14}$ particles/m^3, most of the incident light is transmitted by the sample, which is indicated by M_T values close to 1, varying above 0.7 . More precisely, it can be seen that most of the transmitted light is actually regularly transmitted, as M_U values are high whereas the diffusely transmitted signal remains very low. Similarly, the fraction of the incident light that is collected by the reflectance sphere remains small, around 0.15. This is explained by the fact that the scattering phenomena are limited at low particle concentrations: we are in the case of a quasi non-scattering regime.

For higher particle concentrations, with c between 10^{14} and $c_{lim,multiscatt} = 7.10^{14}$ particles/m^3, M_T values decrease quickly when c increases, from around 0.65 to less than 0.6. More precisely, the regularly transmitted light M_U descreases dramatically with increasing c, meanwhile the diffusely transmitted light $M_T - M_U$ increases. This indicates that the scattering phenomena are getting more and more important: as most of the transmitted light is still regularly transmitted, we could say that we are in the case of a single scattering regime.

Table 1.9: Summary of the quantities used to describe the light variations.

Designation	Definition
$c_{lim,singlescatt}$	limit particle concentration above which the single scattering regime is reached
$c_{lim,multiscatt}$	limit particle concentration above which the multi scattering regime is reached
$c_{lim,abs}$	limit particle concentration above which scattering dominates absorption

For very concentrated samples, with c above $c_{lim,multiscatt}$ particles/m^3, M_T values keep decreasing with increasing c. This time, most of the transmitted signal is actually diffusely transmitted, and the regularly transmitted light becomes negligible. The reflected light increases quickly with increasing c : finally, most of the detected light is collected in the reflectance sphere, meanwhile the transmitted signal becomes close to 0. We have reached a multi-scattering regime.

It can be seen that the variations of M_R are not monotonic with respect to the particle concentration. Indeed, for low concentrations, the reflected light decreases with increasing c. On the contrary, above a limit concentration $c_{lim,abs}$ the trend reverses and the reflected light increases with c. This can be explained by a competition between the absorption and scattering phenomena: at low concentrations, below $c_{lim,abs} = 7.10^{14}$, absorption is the dominant phenomenon: the portion of absorbed light is higher than the portion of light that is scattered back in the reflectance sphere. Since absorption increases with increasing particle concentrations, the resulting M_R decreases with c. However in the multi-scattering regime, the scattering phenomena dominate: the portion of light scattered in the reflectance sphere overcomes the portion of absorbed light. Since scattering increases with increasing concentrations, the resulting M_R increase with c.

1.4.4 Influence of the sample cell width on M_R, M_T and M_U

The M_R, M_T, M_U, $M_R + M_T$ and $M_T - M_U$ measured with the other sample cells, respectively 2mm and 4mm-wide are shown in appendix A for general information. What has to be noted is that the same absorption and scattering regimes can be observed than with the previously presented 5mm-sample cell, however the limit concentrations $c_{lim,singlescatt}$, $c_{lim,multiscatt}$ and $c_{lim,abs}$ depend on the sample thickness. Table 1.10 presents the limit concentrations for each regimes for each sample cell size. The thicker the cell, the smaller $c_{lim,singlescatt}$ and $c_{lim,multiscatt}$ and the higher $c_{lim,abs}$. This is explained by the fact that increasing the sample cell width increases the actual optical thickness of the sample. For a given particle concentration, the sample put in the larger cell is optically thicker, what increases both the effects of scattering and absorption. The stronger absorption, the higher $c_{lim,abs}$, the higher scattering, the lower $c_{lim,singlescatt}$ and $c_{lim,multiscatt}$ what explains the observed results.

Figure 1.25 compares the reflected (a), transmitted (b) and regularly transmitted (c) light measured at different particle concentrations for the three sample cell size. Note that

Table 1.10: Comparison of the values of the limit concentrations (in particles $/m^3$) for the different sample cell size.

Designation	2mm-sample cell	4mm-sample cell	5mm-sample cell
$c_{lim,singlescatt}$	3.10^{14}	2.10^{14}	1.10^{14}
$c_{lim,multiscatt}$	2.10^{15}	1.10^{15}	5.10^{14}
$c_{lim,abs}$	3.10^{14}	4.10^{14}	7.10^{14}

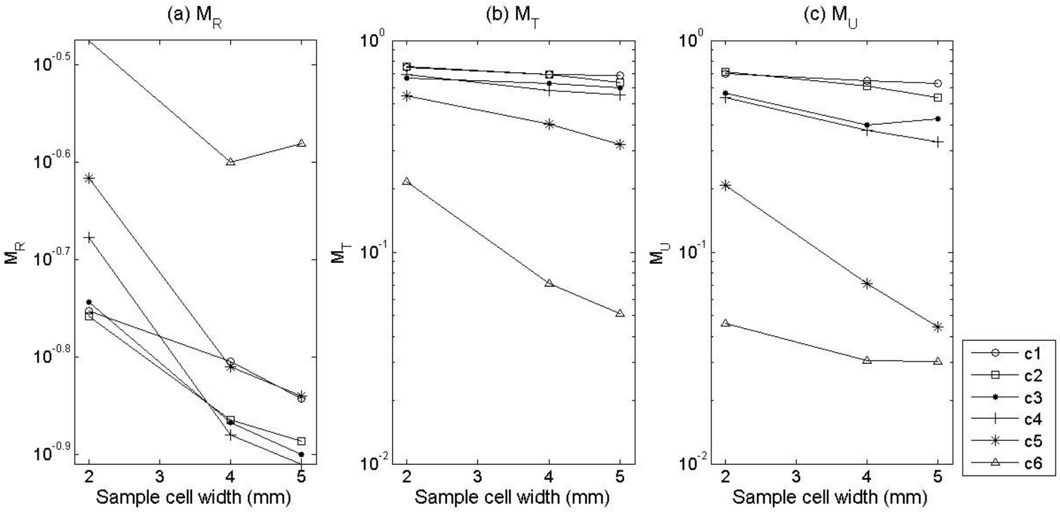

Figure 1.25: (a) Reflected (M_R), (b) transmitted (M_T) and (c) regularly transmitted (M_U) light measured at different particle concentrations for the three sample cell size, namely 2mm, 4mm and 5mm wide. The particle concentrations are expressed in particles$/m^3$ such that $c1 = 7, 7.10^{13}, c2 = 3.10^{14}, c3 = 4, 2.10^{14}, c4 = 7.10^{14}, c5 = 3, 2.10^{15}, c6 = 6, 6.10^{16}$.

the ordinate axis is in logarithmic scale

On figure 1.25 (a) it can be seen that the more concentrate the sample, the less linear the relation between the M_R values and the sample cell width. This is surely an effect of the competition between absorption and scattering previously described: at low concentrations, the thicker the sample, the more absorbing and the less reflected light detected. When concentration increases, the scattering phenomena become more and more important: this time, the thicker the sample, the more scattering and the more important the reflected light detected: at the highest concentration $c6$ in particular, it can be observed that the reflected light is more important with the 5mm-sample cell than with the 4mm-wide one.

Figure 1.25 (b) shows that M_T decreases with increasing sample cell size in a quasi-linear way. Indeed, contrary to reflected light, transmitted light (diffuse plus regular) is only influenced by the absorption phenomena, as the diffusely transmitted light is supposed to be measured. The results are thus in accordance with Beer law.

In theory, the regularly transmitted light depends on both the absorption and scattering phenomena according to a logarithmic law. Figure 1.25 (c) shows that the results obtained follow this expected trend for most particle concentrations. However there are some discrepancies for $c3$ and $c6$. For $c3$ the discrepancies should probably be imputed to experimental errors. For $c6$, the effect might be due to a lower signal to noise ratio in the measurement of the regularly transmitted light at very concentrate samples.

1.5 Conclusion

In this Chapter, the notion of spectral transmittance and reflectance as they will be used throughout this thesis were defined. Spectral reflectance and transmittance are apparent spectral quantities that can be measured with various setups, depending on the nature of the sample under study and on the application domain. In practice, M_R, M_T, and M_U depend first on the intrinsic optical properties of the sample itself, but also on the definition of the experimental conditions and protocol that are implemented for their measurements (in particular with the proper definition of the solid angles considered). For complex media such as complex organic samples, the Double-Integrating Sphere setup (DIS) is a practical solution commonly implemented [22, 23, 35]. Two integrating spheres are thus used in order to collect the light respectively reflected and transmitted by the sample illuminated by an incident light beam. Collecting light in a wide solid angle makes it possible to have more signal, especially for highly scattering and absorbing samples. That is why in our case of dense algal suspensions, the DIS was thought to be particularly adapted and was chosen as a measurement setup. In practice, technical key points must be carefully analyzed when designing a DIS setup. Indeed, photometrical considerations constrain the sphere dimensions, the detection system, the characteristics of the illumination beam and of the sample itself. In this Chapter we discussed the critical technical points and proposed a model DIS setup for the application needs of our study. This DIS setup was tested as a first step on phantom solutions of polystyrene microspheres at one single wavelength (632.8 nm). This primary test allowed to observe the evolution of M_R, M_T and M_U as functions of the particulate concentration and of the sample thickness.

Bibliography

[1] M. Bass, editor. *Handbook of Optics, Third Edition Volume II: Design, Fabrication and Testing, Sources and Detectors, Radiometry and Photometry.* McGraw-Hill, Inc. New York, 1995.

[2] H. Berberoglu and L. Pilon. Experimental measurements of the radiation characteristics of anabaena variabilis atcc 29413-u rhodobacter sphaeroides atcc 49419. *International Journal of Hydrogen Energy*, 32, 2007.

[3] C. F. Bohren and D. R. Huffman. *Absorption and scattering of light by small particules.* Wiley-VCH, 2008.

[4] R. Carminati. Optique des milieux complexes. cours de 3ème année, Institut d'Optique Graduate School, 2009.

[5] C. Castellini, G. Emiliani, E. Masetti, P. Poggi, and P.P. Polato. Characterization and calibration of a variable-angle absolute reflectometer. *Applied Optics*, 29(4), 1990.

[6] F.J.J. Clarke and J.A. Compton. Correction methods for integrating sphere measurement of hemispherical reflectance. *Color Research and Application*, 11, 1986.

[7] G. de Vries, J. F. Beek, G. W. Lucassen, and M. J. C. van Gemert. The effects of light losses in double integrating spheres on optical properties estimation. *IEEE journal of selected topics in quantum electronics*, 5(4), 1999.

[8] E. Dzhongova, C. R. Harwood, and S. N. Thennadil. Changes in the absorption and scattering properties in the near-infrared region during the growth of bacillus subtilis in liquid culture. *Applied Spectroscopy*, 63(1), 2009.

[9] E. Dzhongova, C. R. Harwood, and S. N. Thennadil. Effects of sample thickness on the extracted near-infrared bulk optical properties of bacillus subtilis in liquid culture. *Applied Spectroscopy*, 65, 2011.

[10] P. Elterman. Integrating cavity spectroscopy. *Applied Optics*, 9, 1970.

[11] S. T. Flock, B. C. Wilson, and M. S. Patterson. Total attenuation coefficients and scattering phase functions of tissues and phantom materials at 633nm. *Medical physics*, 14, 1987.

[12] E.S. Fry, G.W. Kattawar, and R.M. Pope. Integrating cavity absorption meter. *Applied Optics*, 31, 1992.

[13] D.G. Goebel. Generalized integrating sphere theory. *Applied Optics*, 6, 1967.

[14] L. Hansenn. Integrating-sphere system and method for absolute measurement of transmittance, reflectance and absorptance of specular samples. *Applied Optics*, 40(19), 2001.

[15] S. Holopainen, F. Manoocheri, S. Nevas, and E. Ikonen. Effect of light scattering from source optics in goniometric diffuse reflectance measurements. *Metrologia*, 44(3), 2007.

[16] A. Ishimaru. Wave propagation and scattering in random media. *IEEE press: New York*, 1997.

[17] J.A.J. Jacquez and H.F. Kuppenheim. Theory of the integrating sphere. *Optical Society of America*, 45, 1955.

[18] R. Kandilian, E. Lee, and L. Pilon. Radiation and optical properties of nannochloropsis oculata grown under different irradiances and spectra. *Bioresource Technology*, 2013.

[19] Labsphere. *Integrating sphere theory and applications.*

[20] J-L. Meyzonnette. Radiometry and detection systems. Institut d'Optique Graduate School courses, 2009.

[21] F.E. Nicodemus, J.C. Richmond, and J.J. Hsia. Geometrical considerations and nomenclature for reflectance. NBS Monograph 160, 1977.

[22] J. W. Pickering, C. J. M. Moes, H. J. C. M. Sterenborg, S. A. Prahl, and M. J. C. van Gemert. Two integrating spheres with an intervening scattering sample. *Journal of Optical society of America*, 9(4), 1992.

[23] J. W. Pickering, S. A. Prahl, N. van Wieringen, J. F. Beek, H. J. C. M. Sterenborg, and M. J. C. van Gemert. Double-integrating-sphere system for measuring the optical properties of tissue. *Applied optics*, 32(4), 1993.

[24] S. A. Prahl. *Optical-Thermal Response of Laser Irradiated Tissue*. 1995.

[25] W. Richter and W. Erb. Accurate diffuse reflectance measurements in the ir spectral range. *Applied Optics*, 26, 1987.

[26] A. Roos. Interpretation of integrating sphere signal output for nonideal transmitting samples. *Applied Optics*, 30, 1991.

[27] W. Saeys, M. A. Velazco-Roa, S. N. Thennadil, H. Ramon, and B. M. Nicolaï. Optical properties of apple skin and flesh in the wavelength range from 350 to 2200nm. *Applied Optics*, 47(7), 2008.

[28] J. Strong. *Procedures in experimental physics*. Prentice-Hall, 1938.

[29] J. Strong. *Procedures in applied optics*. Dekker, NY, 1989.

[30] S. Tassan and G.M. Ferrari. A sensitivity analysis of the.

[31] H. C. van de Hulst. *Light scattering by small particles*. Wiley, 1957.

[32] H.J. van Staveren, C.J.M. Moes, J. van Marle, and S.A. Prahl. Light scattering in intralipid-10% in the wavelength range of 400-1100nm. *Applied Optics*, 30(31), 1991.

[33] I. V. Yaroslavsky, A. N. Yaroslavsky, T. Goldbach, and H. J. Schwarzmaier. Inverse hybrid technique for determining the optical properties of turbid media from integrating-sphere measurements. *Applied optics*, 35, 1996.

[34] B.G. Yust, D.K. Sardar, and A. Tsin. A comparison of methods for determining optical properties of thin samples. In *Optical Interactions with Tissues and Cells XXI*, volume 7562. SPIE, 2010.

[35] E. Zamora-Rojas, B. Aernouts, A. Garrido-Varo, D. Perez-Marin, J. E. Guerrero-Ginel, and W. Saeys. Double integrating sphere measurements for estimating optical properties of pig subcutaneous adipose tissue. *Innovative Food Science and Emerging Technologies*, 2013.

Chapter 2

How to describe the intrinsic optical properties of a dense medium made of random particles from the measurement of its reflectance and transmittance properties?

Contents

In Chapter 1 the spectral reflectance and transmittance properties of a sample were defined: they represent apparent properties of a sample medium that depend on the experimental measurement setup, as well as properties that intrinsically characterize the sample medium itself. In Chapter 1 a practical measurement setup, using double-integrating spheres, and a complete measurement protocol were also defined. In this Chapter 2 we aim at investigating more specifically the intrinsic spectral properties of a dense sample medium. We are interested in particular in how to switch from the apparent spectrophotometric quantities such as reflectance and transmittance to optical properties characterizing the dense, bulk sample medium considered. We will see that any medium made of random particles can indeed be described by its intrinsic optical linear coefficients indicating how light propagates inside of it. We will see that those coefficients work with the Radiative Transport Equation (RTE), which is one of the paradigms that can be used to formulate the physical phenomena occuring when light propagates inside a medium. The RTE is the theoretical mechanism that links quantities such as reflectance and transmittance to the inherent optical properties of a medium. However solving the RTE is not trivial, especially for the general case of dense media where multi-scattering occurs. Solving the RTE in that case requires implementing an approximation method. In this work we chose to present a numerical approximation of the RTE called Adding-Doubling (AD), and its inverse problem Inverse-Adding-Doubling (IAD), based on a matrix formulation of the reflectance and transmittance for a sample seen as a juxtaposition of thin layers. In this work, by applying the inverse method on real algal samples, we propose to retrieve the bulk optical coefficients from reflectance and transmittance measurements implemented with a DIS setup with a configuration similar to the one presented in Chapter 1. We will see that the Inverse-Adding-Doubling method allowed us to retrieve the bulk linear absorption and scattering coefficients of the four algal samples tested over the [300-1020nm] spectral range.

The major advantage of the method is that it is fast. The major drawback is that the convergence of the algorithm can be critically influenced by experimental errors in the measurement of the reflectance and transmittance, and in particular because of light losses in the DIS setup. In the case of this study, the DIS setup needed to be mobile, which constrained its dimensions and imposed to use a mobile small spectrometer. This thus lead to quantitative errors in the estimation of the coefficients. Nevertheless, our preliminary results show that the linear optical coefficients retrieved included information about the chemical and physical composition of the samples. This is a promising finding which justifies our approach: future work could be achieved to solve the optical measurements problems by implementing a DIS with adapted dimensions and detection system, as presented in Chapter 1.

2.1 Theory: modelling the intrinsic optical properties of a bulk medium made of random particles

In this first section we present the quantities that can be defined in order to describe the intrinsic optical properties of a medium made of random particles, namely the linear absorption, scattering and extinction coefficients. Those coefficients are defined in the frame of a theory of light propagation inside a medium called the radiative transport theory, which is based in particular on the radiative transport equation (RTE). After explaining the RTE formalism, we will see that it is not easily solvable in the general case of a dense particulate medium, and that it is necessary to implement an approximation method. We will review briefly the main approximation methods, and describe more thouroughly the one that has been implemented in this thesis, named the Adding-Doubling (AD) method.

2.1.1 Historical development

Historically, two distinct theories have been developed to describe the propagation of light throughout dense distrubutions of particles in which multiple scattering phenomena occur [16]: one may be called the analytical theory and the other the transport theory.

Analytical theory, also called multiple scattering theory, starts with the basic differential equations such as the Maxwell equations or the wave equation [2]. The scattering and absorption properties of the particles are then introduced, which makes it possible to obtain appropriate differential or integral equations for the statistical quantities such as variance and correlation functions [16]. Within this approach, all the multiple scattering, diffraction and interference effects can be included in principle. However in practice it is impossible to obtain an operable formulation including completely all those effects. That is why various theories, based on approximations of the analytical equations have been developed, each being useful and limited to a given range of parameters. Among them one may cite the Twersky's theory [38], the diagram method and the Dyson and Bethe-Salpeter equations [11].

The transport theory has been heuristically developed [5, 36, 34, 21]. It directly deals with the transport of energy throughout a medium containing particles: it is the same formulation than heat transfer for example. Transport equation does not rely on the wave equation, which means that it does not fundamentally includes the wave nature of light. It is thus assumed that there is no correlation between fields, which implies that the addition of powers rather than the addition of fields holds. However transport theory can adequately describe the propagation of light within a medium containing particles provided that the optical characteristics of those particles are derived this time from the wave equation [16].

In Chapter 3 we will detail how to retrieve the optical characteristics of particles properly by using Maxwell equations.

In this work we chose to use the framework of the transport theory in order to describe light propagation within a bulk medium made of particles, and therefore to characterize the bulk optical properties of this medium.

2.1.2 Light transfer: the radiative transport theory

Linear absorption, scattering and extinction coefficients, albedo and optical thickness of a medium

The optical properties of a bulk medium are usually formulated in terms of linear absorption, scattering and extinction coefficients respectively designated as μ_{abs}, μ_{sca} and μ_{ext}, and expressed in m^{-1} [22]. They represent the fraction of the incident light flux that is respectively absorbed, scattered and attenuated by the medium per unit length. That is why those quantities can be understood as "statistical", as they represent phenomena occuring at the scale of a unit length inside the medium. The effects of thousands of photons and particles are then contained in those linear coefficients. Figure 6.4 shows the configuration considered: the input light flux $\Phi_i(\lambda, z)$ comes upon a volume medium of length l with a direction z. The flux $\Phi_{abs}(\lambda, z)$ is absorbed by the volume medium. The flux that is scattered by the medium is designated as $\Phi_{sca}(\lambda, z)$. The flux that is transmitted regularly by the volume medium in the direction z is designated as $\Phi_{T,regular}(\lambda, z)$

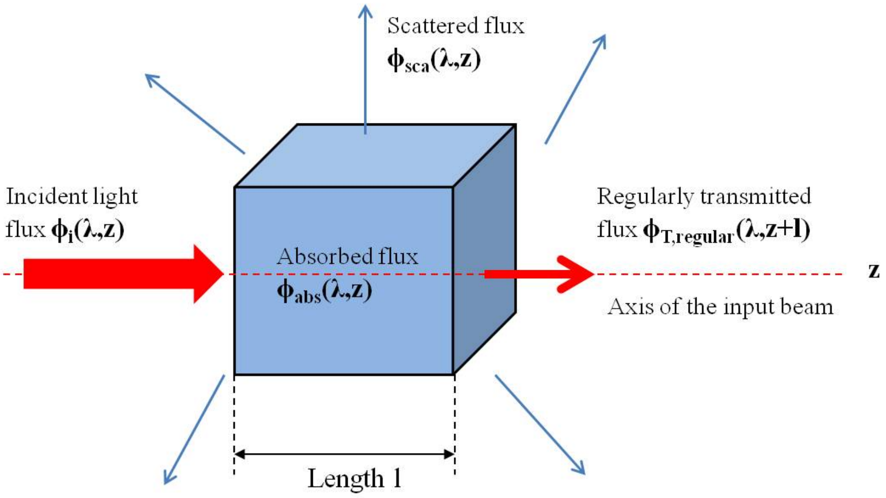

Figure 2.1: Scheme of the interaction of an incident light flux with a volume of bulk medium [22].

The linear absorption (μ_{abs}), scattering (μ_{sca}) and extinction (μ_{ext}) coefficients are defined such that:

$$\mu_{abs} = \frac{\Phi_{abs}(\lambda, z)}{l\Phi_i(\lambda, z)} \tag{2.1}$$

$$\mu_{sca} = \frac{\Phi_{sca}(\lambda, z)}{l\Phi_i(\lambda, z)} \tag{2.2}$$

$$\mu_{ext} = \mu_{abs} + \mu_{sca} \tag{2.3}$$

If μ_{abs}, μ_{sca} and μ_{ext} do not depend upon position, the medium is homogeneous. On the contrary, if the linear coefficients vary with the position within the medium, it is said to be inhomogeneous. As defined in Chapter 1, the anisotropy factor g expresses the geometrical properties of the medium. The reduced scattering coefficient μ'_{sca} is also commonly used, and defined such that:

$$\mu'_{sca} = \mu_{sca}(1 - g) \tag{2.4}$$

Some other properties can be defined from the linear coefficients [16], and are commonly used to describe the optical properties of a bulk medium of width l: the albedo a and the optical thickness τ. They are expressed such that:

$$a = \frac{\mu_{sca}}{\mu_{sca} + \mu_{abs}} \tag{2.5}$$

$$\tau = (\mu_{sca} + \mu_{abs})l \tag{2.6}$$

The radiative transport equation (RTE)

In this section we give and explain the differential equation describing the variation of the radiance in a medium containing random particles [16], called the radiative transport equation (RTE). The RTE is the exact expression linking the variation of radiance inside a medium containing random particles to the linear optical properties of this medium μ_{abs}, μ_{sca} and g as defined above. As explained in chapter 1, the variation of radiance can be expressed in terms of reflectance and transmittance. Consequently, the RTE allows to link the linear optical properties of a sample to its apparent reflectance and transmittance properties.

If we consider a wave energy at a point r in a radom medium, the spectral radiance $L(r, \vec{u})$ defined for a given direction $\vec{u}$ of space as shown in figure 2.2 can be expressed such that:

$$L(r, \vec{u}) = \frac{dP}{cos(\theta)dad\omega d\nu} \tag{2.7}$$

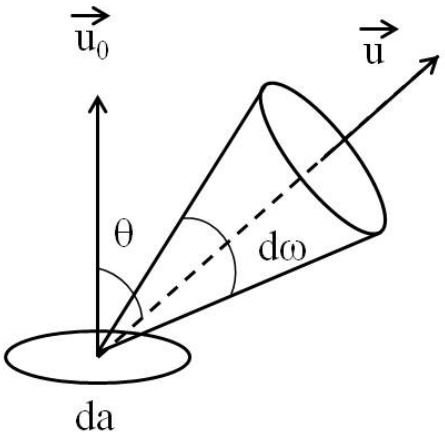

Figure 2.2: Configuration considered for equation (2.7).

With dP the amount of power flowing within a solid angle $d\omega$ through an elementary area da oriented in a direction of unit vector $\vec{u_0}$ in a frequency interval $(\nu, \nu + d\nu)$. Spectral radiance $L(r, \vec{u})$ is thus the density of radiated flux per unit solid angle and projected area per frequency, and is expressed in $W.m^{-2}sr^{-1}Hz^{-1}$.

Let us now consider a cylindrical elementary volume of particle medium with unit cross section and length ds as shown on figure 2.3. The medium is characterized by its linear absorption, scattering and extinction coefficients μ_{abs}, μ_{sca} and μ_{ext}, as presented above.

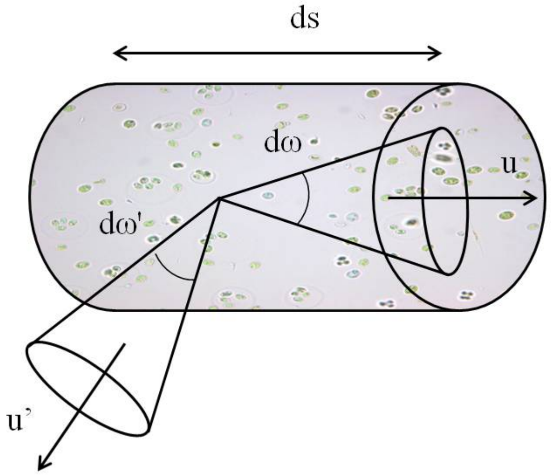

Figure 2.3: Configuration considered for equation (6.10).

If we describe the change of spectral radiance $dL(r, \vec{u})$ in the direction $\vec{u}$ within this cylindrical elementary volume, we must first take into account the loss due to the absorption and scattering phenomena occurring along path length ds. The decrease of spectral radiance in the elementary volume is thus expressed as:

$$dL(r,\vec{u}) = -ds(\mu_{abs} + \mu_{sca})L(r,\vec{u}) = -ds\mu_{ext}L(r,\vec{u})$$

In the same time, the radiance $L(r,\vec{u})$ inside the considered elementary volume increases because a portion of the radiance $L(r,\vec{u'})$ incident on this volume from other directions $\vec{u'}$ is scattered back into the direction $\vec{u}$ and adds to $L(r,\vec{u})$. This contribution can be expressed [16] using the phase function $p(\vec{u'},\vec{u})$ as defined in Chapter 1:

$$dL(r,\vec{u}) = \frac{\mu_{sca}}{4\pi}\int_{4\pi} dsp(\vec{u'},\vec{u})L(r,\vec{u'})d\omega'$$

The spectral radiance may also increase due to emission of light from within the volume of path length ds. If we denote by $\varepsilon(r,\vec{u})$ the power radiation per unit volume per unit solid angle per frequency in the direction $\vec{u}$, the resulting increase of the spectral radiance is given by:

$$dL(r,\vec{u}) = ds\varepsilon(r,\vec{u})$$

Adding all those contributions we obtain the radiative transport equation (RTE) [16] defined as:

$$\frac{dL(r,\vec{u})}{ds} = -\mu_{ext}L(r,\vec{u}) + \frac{\mu_{sca}}{4\pi}\int_{4\pi} p(\vec{u'},\vec{u})L(r,\vec{u'})d\omega' + \varepsilon(r,\vec{u}) \tag{2.8}$$

Exact solutions of the radiative transport equation can be obtained only for a limited few cases, such as the parallel-plane problem and the isotropic scattering problem [16]. However, in the majority of the practical cases the RTE cannot be solved exactly. In the next section we quickly review some methods that have been developed in order to numerically solve or approximate the RTE solution.

2.1.3 Short review: solving or appromixating the radiative transport equation (RTE)

Exact solutions of equation (6.10) have been obtained only for a limited few cases [16]. Among them, one can cite in particular the parallel-plane problems and isotropic scattering problems [16] for example. However in most practical cases, the RTE cannot be solved exactly. Given $\mu_a(\lambda), \mu_s(\lambda)$ and p of the analysed medium, several methods have been developed [28] to solve equation (6.10):

- approximation: some simplified formulations of equation (6.10) can be implemented for a few particular physical cases, for very diluted and very dense scatterers distributions. For tenuous distributions of scatterers (optical thickness $\tau \leq 0.4$ and albedo

$a \leq 0.9$) Ishimaru [16] obtained the first order multiple scattering solutions. For very dense distributions, with the volume occupied by the particles much greater than 1% of the total volume, the diffusion approximation can be used [26]. In the case of this study, the algal media considered showed optical thickness τ much higher than 0.4, but their volume density was estimated to remain below 1%, which excluded the possibility to use those approximate solutions. Phenomenological approximations can also be implemented, with multiple flux models and among them Kubelka-Munk [18]. Multiple-flux methods describe light in terms of a finite number of reflected and transmitted flux: the model is too simple to accurately describe complex samples [28].

- numerical resolution: discrete ordinate [16] and adding-doubling [33]. In that case, the principle is to formulate the RTE in a numerical formulation that allows approximate calculation of the solution. In the case of discrete ordinates, the RTE is discretized by considering a set of discrete directions according to a Gauss-Legendre quadrature [37]. Adding-Doubling [30] method discretizes the RTE by modelling the propagation medium as a set of infinitely thin slabs.

- numerical simulation: Monte-Carlo method [32] [12]. Monte-Carlo simulation method uses a stochastic approach to model the physical phenomenon of light propagation: it is based on the computation of the paths of a large amount of photons propagating in the particulate medium.

- hybrid methods[41]. Hybrid methods can be implemented, by associating two or more numerical methods and approximations.

Discrete ordinates, Adding-doubling and Monte Carlo methods give similar results to calculate M_R and M_T for a sample with no hypothesis on its optical properties. That is why in our case we chose to implement one of these methods to solve the RTE. In particular, the Adding-Doubling (AD) method [30] was elected, as it was the method that was practically the easiest to invert.

2.2 Material and method: solving the radiative transport equation with the Adding-Doubling method

The AD method was introduced by van de Hulst [39] to solve the radiative transport equation in a slab geometry. It makes it possible to describe the total reflectance, total transmittance and regular transmittance properties M_R, M_T and M_U of a sample from its optical properties, namely the albedo a, the optical thickness τ and the anisotropy factor g. The inverse problem, consisting in retrieving the intrinsic optical properties from the reflectance and transmittance of the sample can thus be adressed by applying the IAD method, as summarized by figure 2.4.

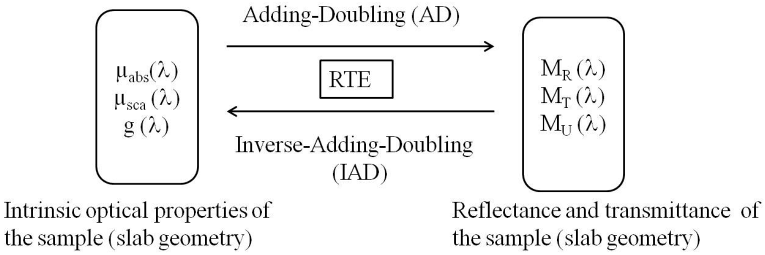

Figure 2.4: Block diagram showing the principle of Adding-Doubling and Inverse-Adding-Doubling method to numerically solve the RTE.

In this section we describe the general theory of the Adding-Doubling calculations and we detail in particular the running of the program implemented by Scott Prahl [31] and made available on the website http://omlc.ogi.edu/software/.

2.2.1 Geometry of the problem, reflectance and transmittance matrices

The method is adapted to solve equation (6.10) in a case of a slab geometry, in any situation with no restriction on the ratio between scattering and absorption, no restriction on the scattering anisotropy and it includes reflection at the boundaries of the sample. However a reduced set of assumptions specifies the validity scope of the method: the problem is supposed to be no time-dependent, with a geometry consisting of uniform layers of finite thickness and infinite extent in the direction parallel to the surface. The scattering and absorption are supposed to be uniform on one particular layer. The illumination is supposed to be uniform as well, by collimated or diffuse incident light. On figure 2.5, the slab geometry considered to describe the case of an algal sample put in a quartz cell is shown: it corresponds to the representation made within the scope of the AD method [30].

For each infinitely thin uniform layer of width dl, the reflection and transmission properties are described in terms of reflectance and transmittance matrices, respectively denoted as $\mathbf{R}$ and $\mathbf{T}$. This matrix form is the key point of the Adding-Doubling method, as it allows to make the computations of the radiative transport equation solution with a classical personal computer.

For a normally incident beam, the idea is to discretise the two half spaces on both sides of the infinitely thin slab by taking into account a reduced number of solid angles ν, called the quadrature angles.

As shown on figure 2.6, if we consider two solid angles ν and ν', the reflection function $R(\nu, \nu')$ can be defined as the radiance reflected by the slab in direction ν' for light conically incident from the ν direction [39]. The reflection function is normalized to an incident diffuse flux π, which means that it is the ratio of the actual reflection function of the slab to the reflection function of an ideal white Lambertian surface. The transmission function $T(\nu, \nu')$ is defined similarly. For instance, if a vector of four solid angles $[\nu_1, \nu_2, \nu_3, \nu_4]$ is

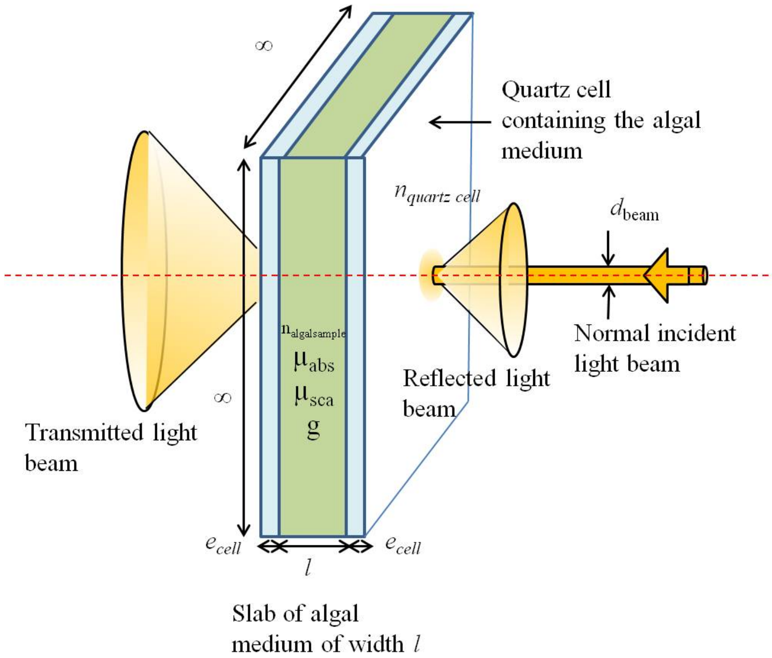

Figure 2.5: Description of the geometry of the problem in the Adding-Doubling method in the case of a collimated incident beam.

chosen to describe a whole half space, the reflectance matrix **R** can be defined such that:

$$\mathbf{R} = \begin{vmatrix} R(\nu_1,\nu_1) & R(\nu_2,\nu_1) & R(\nu_3,\nu_1) & R(\nu_4,\nu_1) \\ R(\nu_1,\nu_2) & R(\nu_2,\nu_2) & R(\nu_3,\nu_2) & R(\nu_4,\nu_2) \\ R(\nu_1,\nu_3) & R(\nu_2,\nu_3) & R(\nu_3,\nu_3) & R(\nu_4,\nu_3) \\ R(\nu_1,\nu_4) & R(\nu_2,\nu_4) & R(\nu_3,\nu_4) & R(\nu_4,\nu_4) \end{vmatrix} \tag{2.9}$$

The equivalent definition can be given for the transmittance matrix **T**.

2.2.2 Principles of the Adding process

The reflectance and transmittance matrices **R** and **T** can be used to define matrix relations for adding layers. If we consider an infinitely thin unit layer (01) as described in figure 2.7, we denote as L_0^+ the radiance incident on side 0 in the downward direction and L_1^- the radiance incident on side 1 in the upward direction. Similarly, L_0^- designates the radiance exiting from the side 0 in the upward direction, and L_1^+ the radiance exiting from the side 1 in the downward direction. The downward radiance from side 1, L_1^+, is thus the sum of the transmitted incident radiance from side 0 and the reflected radiance from side 1. With T^{01} and R^{10} respectively the transmittance matrix for light incident on side 0 and moving towards side 1, and the reflectance matrix for light coming upon side 1 towards side 0, L_1^+ can be expressed by [30]:

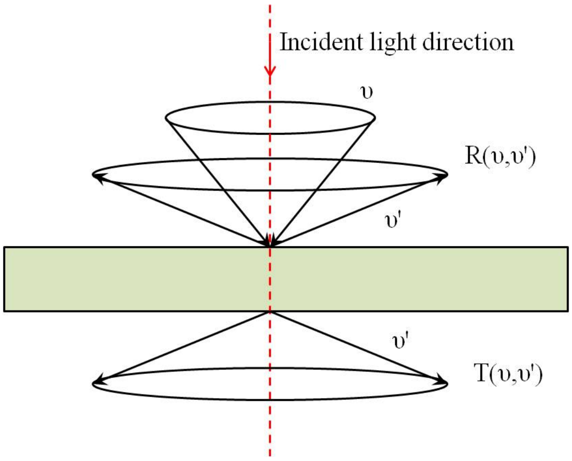

Figure 2.6: Description of the geometry of the problem in the Adding-Doubling method in the case of a collimated incident beam.

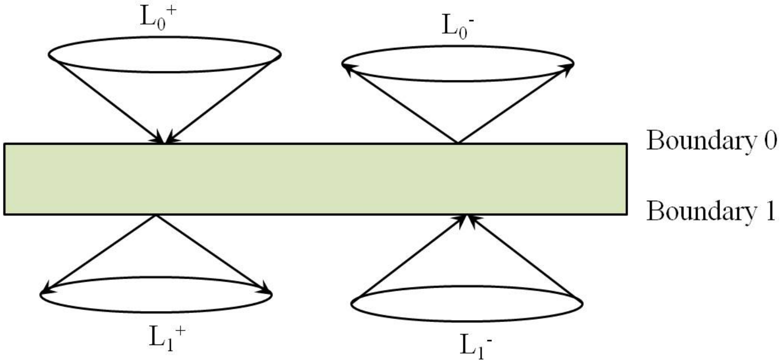

Figure 2.7: Nomenclature for the derivation of the adding-doubling equations. A minus sign indicates upward travelling light and a plus sign downward directed light.

$$L_1^+ = T^{01}L_0^+ + R^{10}L_1^- \tag{2.10}$$

Similarlry, the upward radiance from side 0 is the transmitted radiance from side 1 and the reflected radiance from side 0 such that:

$$L_0^- = R^{01}L_0^+ + T^{10}L_1^- \tag{2.11}$$

If we now consider another unit layer with sides 1 and 2, similar expressions can be obtained:

$$L_2^+ = T^{12}L_1^+ + R^{21}L_2^- \tag{2.12}$$

$$L_1^- = R^{12} L_1^+ + T^{21} L_2^- \tag{2.13}$$

By adding layers (01) and (12) a combined, thicker layer (02) is obtained. We can express the radiance for the layer (02):

$$L_2^+ = T^{02} L_0^+ + R^{20} L_2^- \tag{2.14}$$

$$L_0^- = R^{02} L_0^+ + T^{20} L_2^- \tag{2.15}$$

The idea is thus to express the reflectance and transmittance matrices $\mathbf{R}^{02}$ and $\mathbf{T}^{20}$ of the combined layer (02) from the reflectance and transmittance matrices of the individual unit layers (01) and (12). For this pourpose, L_1^+ and L_1^- must be expressed as functions of L_0^{+-} and L_2^{+-}. By left multiplying equation (2.10) by $\mathbf{R}^{12}$ and adding it to equation 2.13, we can obtain the expression for L_1^-:

$$L_1^- = (E - R^{12} R^{10})^{-1} (R^{12} T^{01} L_0^+ + T^{21} L_2^-) \tag{2.16}$$

Where E designates the identity matrix. Expression (2.16) gives the upward radiance at the interface between the two layers. An expression for the downward radiance can be obtained by left multiplying equation (2.13) by $\mathbf{R}^{12}$ and adding it to equation (2.10):

$$L_1^+ = (E - R^{10} R^{12})^{-1} (T^{01} L_0^+ + R^{10} T^{21} L_2^-) \tag{2.17}$$

By substituting equation (2.17) into equation (2.12) we find:

$$L_2^+ = [T^{12} (E - R^{10} R^{12})^{-1} T^{01}] L_0^+ + [T^{12} (E - R^{10} R^{12})^{-1} R^{10} T^{21} + R^{21}] L_2^- \tag{2.18}$$

Comparing with equation (2.14) makes it possible to find:

$$T^{02} = T^{12} (E - R^{10} R^{12})^{-1} T^{01} \tag{2.19}$$

$$R^{20} = T^{12} (E - R^{10} R^{12})^{-1} R^{10} T^{21} + R^{21} \tag{2.20}$$

Similarly, equation (2.16) can be substituted into equation (2.11) to obtain:

$$T^{20} = T^{10} (E - R^{12} R^{10})^{-1} T^{21} \tag{2.21}$$

$$R^{02} = T^{10}(E - R^{12}R^{10})^{-1}R^{12}T^{01} + R^{01} \tag{2.22}$$

Equations (2.19) to (2.22) [30] define the reflectance and transmittance matrices for a combined layer from the ones of each unit layer. By iterating the process, using these expressions makes it possible to express the reflectance and transmittance of an arbitrary layered sample. The equations given above are entirely appropriate if the direct beam corresponds to one of the quadrature angles. If not, the equations are more complex, as separate terms for primary and scattered light must be added [7, 13]. This situation will not be more thouroughly described here.

Those equations describe what is called the Adding process. The Doubling process relies on the exact same principle, but this time it is considered that the two successive unit layers have similar absorption and scattering properties, as they are made of the same material.

2.2.3 Implementation of the computations for the forward method

In practice, the AD method is implemented by the following successive steps:

- Choosing the quadrature angles
- Generating the starting layer
- Generating the boundary layers
- Doubling the starting layer until the desired thickness is reached
- Adding the boundary layers
- Deducing the reflectance and transmittance of the entire sample

The complete description of those steps can be found in [30], and will not be detailed here. The quadrature scheme is determined by means of three different methods, Gaussian, Lobatto and Radau [5, 23, 14] depending on the boundary conditions. Starting the AD method requires knowing the reflectance and transmittance properties of an initial, infinitely thin slab. For that purpose, the diamond initialization method [40] is employed: it makes it possible to discretise equation (6.10) and to calculate the reflectance and transmittance matrices of the infinitely thin initial layer. The boundary layers are generated in order to include the boundary conditions of the problem in the transport calculation. The reflectance and transmittance matrices of those boundary layers are defined using the Fresnel coefficients [15]. The Doubling and Adding processes are implemented following the principles described previously.

2.2.4 Implementation of the computations for the inverse method

The inverse problem is the retrieval of the intrinsic optical coefficients from measurements describing light variations in space: it can be solved with Inverse-Adding-Doubling (IAD).

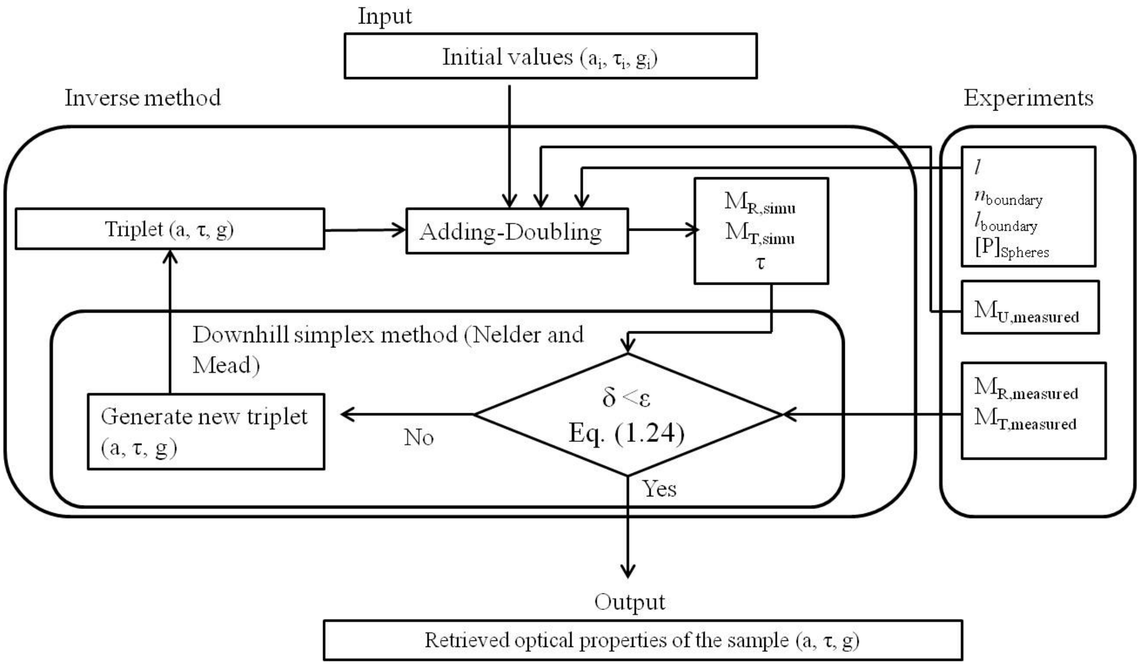

Figure 2.8: Block diagram showing the principle of the Inverse-Adding-Doubling method in the case of three measurements (M_R, M_T and M_U).

The radiance throughout the sample can be characterized by measuring the reflectance and transmittance characteristics of a sample of known width l with a dedicated double integrating sphere setup, as shown in Chapter 1. Several configurations may be considered depending on the setup. A first case may be that three quantities, normalized total reflectance M_R, normalized total transmittance M_T and normalized regular transmittance M_U are measured. This can be achieved for samples with optical thickness low enough to allow measuring the regular transmittance with a satisfying signal-to-noise ratio. Another case may be that the regular transmittance could not be measured: only two measurements, M_R and M_T are available.

In the case of three measurements, it is assumed that the unscattered reflection from each surface is equal to the Fresnel reflection for light normally incident on the sample [30]. From this assumption comes a direct expression for the regular transmittance as a function of the optical thickness τ and the reflection factors r_{s1} and r_{s2} of the front and back surfaces of the slab (including the internal reflection in a glass slide if it is present):

$$M_U = \frac{(1 - r_{s1})(1 - r_{s2}e^{-\tau})}{1 - r_{s1}r_{s2}e^{-2\tau}} \tag{2.23}$$

This simplifies the problem, as once the optical thickness is determined, only the albedo a and the anisotropy factor g need to be retrieved. In that case, the Inverse-Adding-Doubling program outputs are the linear absorption and scattering coefficients μ_{abs} and μ_{sca} as well as the anisotropy factor g.

If only M_R and M_T could be measured, only two optical parameters can be retrieved. A value for the anisotropy factor g is thus assumed, and the phase function p is calculated using the Henyey-Greenstein function [9]. The albedo a and optical thinckness τ are thus retrieved based upon the assumed value of g. In that case, the IAD program outputs are the absorption coefficient μ_{abs} and the reduced scattering coefficient μ'_{sca} as defined by equation (6.9).

The principle of the inverse algorithm (assuming here that three measurements are available) is shown on figure 4.4. From a triplet (a,τ,g), and the experimental conditions considered, i.e. thickness of the sample l_{sample}, optical index of the boudary layers $n_{boundary}$, width of the boundary $l_{boundary}$, parameters (geometry and reflectivity) of the integrating spheres used $[P]_{Spheres}$, the forward Adding-Doubling code is used to generate simulated total reflectance, total transmittance and collimated transmittance $M_{R,simu}$, $M_{T,simu}$ and $M_{U,simu}$ respectively. A metric δ is thus used to estimate the error between the simulated reflectance and transmittance values and the ones actually measured, $M_{R,simu}$ and $M_{T,simu}$. This metric is defined such that:

$$\delta(a,\tau,g) = \frac{|M_{R,simu} - M_{R,measured}|}{(M_{R,measured} + 10^{-6})} + \frac{|M_{T,simu} - M_{T,measured}|}{(M_{T,measured} + 10^{-6})} \tag{2.24}$$

Note that the factor 10^{-6} is included to prevent division by zero when the reflectance or transmittance is zero. δ is thus minimized by a minimization algorithm based on the downhill simplex method of Nelder and Mead [27], until reaching the convergence limit defined by the value ϵ.

An initial triplet (a_i, τ_i, g_i) must be generated in a first time in order to initialize the convergence process. This step remains crucial, as it affects both the rapidity and the accuracy of the convergence. In the IAD method, the choice was made to generate the initial values as crude fits of the reflectance and transmittance values, as explained in [33].

It has to be noted that the method includes the corrections of the integrating sphere effects on the measured reflectance and transmittance values: the measured M_R, M_T and M_U values can thus be directly used without conversion.

2.2.5 Practical use of the Adding-Doubling and Inverse-Adding-Doubling programs from Scott Prahl

This section summarizes the practical steps to implement as a user of the AD and IAD programs of Scott Prahl.

Adding-Doubling

In practice, the entry parameters of the Adding-Doubling program must be provided to the computation program as a text file with a number of lines corresponding to the number of wavelengths desired. The input parameters are the following: [31]

- value of the albedo a
- value of the optical thickness τ
- value of the anisotropy factor g
- value of the index of refraction of the boundary layer $n_{boundary}$. In the practical case of a liquid sample put in a glass or quartz cell for example, this corresponds to the refraction index of the cell.
- number of quadrature points q

Each line of the input text file is a set of entry values corresponding to a given wavelength. Consequently, the input text file requires as many lines as the number of wavelength desired. The output text file gives for each wavelength four output values:

- the reflectance for normal incident light $M_{R,n}$
- the reflectance for diffuse incident light $M_{R,d}$
- the transmittance for normal incident light $M_{T,n}$
- the transmittance for diffuse incident light $M_{T,d}$

Inverse-Adding-Doubling

For the IAD program, the following entry parameters are required in the input text file:[31]

- value of the wavelength λ
- value of the total reflectance M_R
- value of the total transmittance M_T
- value of the regular transmittance M_U (if measured)
- value of the index of refraction of the medium, $n_{algalsample}$ in the case of an algal medium for example
- value of the index of refraction of the cell containing the sample medium n_{cell}
- thickness of the sample slab l

- thickness of the boundary layer $e_{boundary}$
- input beam diameter d_{beam}
- value of the standard reflectance r_{std} used for the reflectance and transmittance measurements
- number of integrating spheres used for the measurements
- dimensions of the reflectance sphere (inner diameter, diameters of the sphere ports)
- reflectivity inside the reflectance sphere
- dimensions of the transmittance sphere (inner diameter, diameters of the sphere ports)
- reflectivity inside the transmittance sphere

The output text file gives for each wavelength three output values:

- the estimated linear absorption coefficient μ_{abs}
- the estimated linear reduced scattering coefficient μ'_{sca}
- the estimated anisotropy factor g (in the case of three measurements)

The IAD program accuracy has been tested [30]: it was estimated that using only four quadrature angles, the IAD method generates optical properties (μ_{abs}, μ_{sca},g) that are accurate to 2-3% for most reflectance and transmittance values. Higher accuracy can be achieved using more quadrature points but requires increased computation time. By perturbing the reflectance and transmittance values and re-solving for the optical properties, the same authors [30] showed that the linear optical coefficients retrieved are significantly affected by variations in M_R and M_T: 1% variation of M_R and M_T thus result in errors of 0.4% for μ_{sca}, 17% for μ_{abs} and 0.4% for g. The sensitivity of the IAD to the input values of M_R and M_T is surely a delicate issue and the most important drawback of the method. In our work, and as shown in the next section which describes the application of the IAD method on real algal samples, we have faced this difficulty. We have thus found that experimental errors in the reflectance and transmittance could have significant impacts on the quantitative determination of the linear coefficients, especially for the μ_{abs}. This is fully explained in the next section.

2.3 Application to algal culture media

In this section we thus present the work we have achieved to determine the potential of using Adding-Doubling to retrieve the bulk optical properties of dense microalgal samples from the measurement of their total reflectance and total transmittance with a DIS. This part of our work in particular has been published [3]. Total transmittance and total reflectance measurements were performed over the 380-1020nm range on dense algal samples with a double integrating sphere setup. The bulk absorption and scattering coefficients were thus extracted over the 380-1020nm range by inverting the radiative transfer theory using IAD computations. Meanwhile, the complete characterization of the algal samples (pigment composition, cell number and size) was implemented by standard methods. The experimental results are presented and discussed: the configuration of the optical setup remains a critical point. Due to the sensitivity of the IAD convergence to errors in the input values of M_R and M_T, it was observed that the light losses inside the DIS setup can cause some quantitative errors in the estimation of the linear optical coefficients. However the qualitative analysis of the linear coefficient spectra obtained revealed that they seem to depend highly on the sample chemical and physical composition. This is a promising result that justifies the principle of the approach implemented in this work.

2.3.1 Experimental design

Four mixed populations of Scenedesmus and Chlorella were grown in four distinct external ponds numbered S1, S2, S3 and S4, at Laboratoire de Biotechnologie de l'Environnement (LBE), Narbonne (INRA France). Illumination was provided by the sun and no specific temperature regulation was applied. Mixing and bubbling were carried out with a pump system. Nutrients were provided by regular inputs of fertilizer (ANTYS®8, Fertil France). Samples were taken at 3 p.m. from each pond and entirely characterized using standard methods in the shortest time possible in order to minimize the impacts caused by a change in the algal culture environment. In the meantime the spectroscopic measurements of M_R and M_T were performed on each sample.

2.3.2 Measurement of total reflectance and total transmittance spectra

Optical setup

A double integrating sphere setup was used for the measurement of the total reflectance M_R and total transmittance M_T of the algal samples. To fill the experimental requirements, and in particular the need to make the measurements on the site of the cultivation ponds, a mobile setup needed to be specifically implemented for the campaign. It was based on the same configuration as the setup presented in Chapter 1, but smaller spheres, and a mobile small spectrometer were employed: the transmittance sphere used in particular was not equipped with a light trap and consequently, no measurement of the regular transmittance M_U was implemented. Figure 2.9 shows the general configuration of the setup.

The measurement protocol detailed in Chapter 1 was followed to retrieve the normalized total reflectance M_R and normalized total transmittance M_T for each sample.

Ten measurements were collected for each sample, what made it possible to limit the

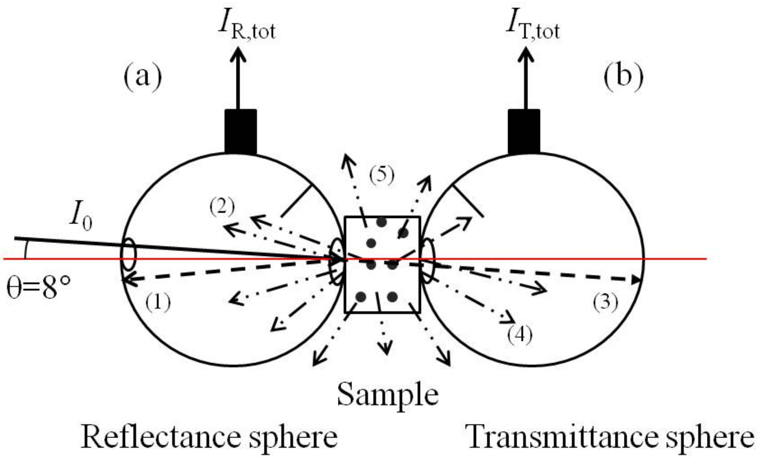

Figure 2.9: Description of the adding-doubling measurement setup implemented for the measurement campaign. The reflectance sphere (a) collects the total reflected signal $I_{R,tot}$ including both regulary reflected (1) and diffusely reflected (2) light. The total transmitted signal $I_{T,tot}$, including regularly transmitted (3) and diffusely transmitted (4) light, is collected in the transmittance sphere (b). Due to the thickness of the sample and to the finite solid angle actually collected by the spheres, a certain amount of light (5) is lost outside of the setup.

effects of the experimental conditions. The measurements were conducted using 30mm-diameter reflectance and transmittance spheres (AvaSphere-30, Avantes) fibered with 1mm-core low OH optical fibers (Ocean Optics). Illumination was provided by a tungsten halogen light source (HL - 2000, Ocean Optics) and the spectral acquisition was carried out using a spectrometer (MMS1, Zeiss). The temperature fluctuations of the light source were limited by turning on the lamp at least one hour before beginning the measurements: this lapse of time was observed to be sufficient for the light source to be as stable as possible. The integration time varied between 4000 and 6500 ms depending on the signal measured. Liquid samples were put in quartz cells (100-QS, Hellma) with a 10 mm-optical thickness and maintained between the two spheres thanks to a customized cell holder fitted to the bench dimensions. The measurements were made in the spectral region between 380 and 1020 nm with 10 nm resolution intervals and 3 nm step intervals.

As explained in Chapter 1, the double integrating sphere configuration forced the positionning of the sample cell outside of the spheres, reducing the actual solid angle collected. The effect was all the more important that the small dimensions of the spheres imposed a reduced sample port diameter. A significant amount of light ((5) on figure 2.9) could thus leak in directions that were not detected by the spheres, at the edges of the sample cell and at the sphere ports. In order to limit those effects, the sample cell thickness, the sample cell position, the incident light beam size upon the sample were adapted at best. In the case of this study, the solid angle detected by one sphere was estimated to reach approximately 1.7 π sr.

Determination of the errors in the spectroscopic measurement procedure

In order to test the influence of the experimental errors on the results of the IAD computations, it was necessary to implement a method to quantify and represent those experimental errors. This was done in practice by using classical techniques encountered in data processing and chemometrics. The idea was to generate high dimensions databases of plausibly measured M_R and M_T, and to test the running of the IAD program on those databases. It should thus be possible to estimate the variability of the resulting μ_{abs} and μ'_{sca} coefficients retrieved. The first step was thus to generate large databases of M_R and M_T corresponding to plausible measurements. In practice this could have been made by repeating the measurements dozens of time with the measurement setup for each sample. However, the algal medium is a biological material evolving rapidely in time. This was thus not possible to make the measurements in practice, and a virtual solution had to be implemented. The idea was to model the spectral behaviour of the experimental errors, and to extrapolate from this plausible measurements. In practice, ten measurements of M_R and M_T were implemented with the measurement setup for one algal sample. From those ten measurements, the analysis of the experimental variability was performed, by means of a Principal Component Analysis (PCA). It was thus possible to generate a hundred noise spectra for M_R measurements and M_T measurements. Those noise spectra were added to an averaged M_R, and an averaged M_T spectra in order to simulate one hundred measurements replicates on the same sample. This procedure is explained in the following paragraph.

Ten measurements of M_T spectra were conducted on the same algal sample and put in a matrix **X** with dimension 10 x p where p is the number of wavelengths:

$$\mathbf{X}_{10\times p}$$

X was analyzed by means of a Principal Component Analysis (PCA) [20] which made it possible to approximate it by the matrix $\hat{\mathbf{X}}$ such that:

$$\hat{\mathbf{X}} = \mathbf{S}_{10\times k} \times \mathbf{L}_{k\times p}$$

Where **S** and **L** are respectively the matrices of the scores and of the loadings, and k the number of loadings. The loadings obtained were the eigenvectors describing a new linear vector space where M_T spectra were represented by the values of their scores, which were their coordinates in that space. The advantage of the vector space found with PCA was that it had a smaller dimension than the original space of description of the Ttot spectra and was thus easier to analyze. One hundred noise spectra were then simulated by randomly choosing the values of the scores, and put in the matrix **N**:

$$\mathbf{N}_{100\times p} = N_{100\times k}(0,1) \times (\mathbf{G}_S)_k \times \mathbf{L}_{k\times p}$$

Where *N(0,1)* is a normal law centered on zero with standard deviation 1 and $\mathbf{G}_S$ the diagonal matrix of the scores standard deviation values. Those simulated noise spectra were added to an averaged M_T spectrum in order to simulate a hundred replicates of total transmittance measurements on the same sample.

$$\mathbf{M}_{M_{Ttot,100\times p}} = \mathbf{M}_{Taveraged,100\times p} + \mathbf{N}_{100\times p}$$

The spectral standard deviation of the set of M_T spectra stored in $\mathbf{M}_{M_{Ttot}}$ was then calculated and used to characterize the errors on the measurement procedure of M_T. The same method was applied to estimate the error on the total reflectance measurement, and the matrix $\mathbf{M}_{M_{Rtot}}$ of one hundred simulated M_R spectra was calculated. This procedure was conducted for the four algal samples: for each sample the $\mathbf{M}_{M_{Ttot}}$ and $\mathbf{M}_{M_{Rtot}}$ matrices were obtained.

Computation of absorption and reduced scattering spectral coefficients

Inverse-adding-doubling computations were performed on the measured spectra of M_R and M_T using the software developed by Prahl and run with MatLab (R2012b version). As explained previously, the computations were made by only using M_R and M_T and approximating the phase function p with the empirical Henyey-Greenstein phase function [9]. The real part of the refractive index of the cell slab was set as 1.46 according to manufacturer data and considered as constant over the spectral region studied. The real part of the refractive index of the sample solutions was measured at 598 nm using an Abbe refractometer (NAR-1T, Atago) and assumed to be constant as well over the visible spectral range, and set as $n_{algalsample}$=1.334. According to the measurements published by Lee et al. [19], the anisotropy factor g was fixed to 0.98 throughout the [380-1020nm] spectral domain.

2.3.3 Propagation of the measurement procedure errors in the IAD computation

For each sample, the impact of the measurement errors on the IAD results was estimated by calculating the absorption and scattering coefficient spectra of one hundred possible doublets of M_R and M_T, taken in the generated matrices $\mathbf{M}_{M_{Rtot}}$ and $\mathbf{M}_{M_{Ttot}}$. Those doublets were built by randomly associating a vector M_T of the matrix $\mathbf{M}_{M_{Ttot}}$ to a M_R coming from $\mathbf{M}_{M_{Rtot}}$. For each sample, one hundred spectra of possible absorption coefficient and one hundred spectra of possible reduced scattering coefficient were obtained. It was thus possible to estimate the variation of the μ_{abs} and μ'_{sca} spectra originating from the errors in the measurements. The mean value and the standard deviation of μ_{abs} and μ'_{sca} spectra were calculated.

2.3.4 Measurement of cell number and size

Cell number and size of each sample were determined by mean of a Z2 Coulter Counter (Beckman Coulter): samples were diluted in isotonic solution by a factor of 1/200 and the counting was carried out on a 0.5mL volume aliquot. The particle volume was represented in terms of equivalent spherical diameter (ESD) [17], i.e. the diameter of the sphere having the same volume as the particle of interest. By summing the volumes occupied by the cells of increasing size, the total biovolume of the sample was obtained (figure 2.10). The size distribution was calculated by normalizing by the total biovolume (figure 2.11). Microscopic observations and counting were conducted concurrently using a BX40 phase-contrast microscope (BX40, Olympus) and Toma counting cells.

2.3.5 Measurement of Chlorophyll concentrations

Chlorophyll a (Chl a) and chlorophyll b (Chl b) contents of the algal samples were determined through pigment extraction and colorimetric measurements. Solutions containing 2×10^6 cells were obtained after centrifugation (19000 × g, 10min). 1mL of acetone was added and mixed by vortexing. The volume solution was completed at 2mL with acetone and mixed again. The sample was then put in ultrasound tub for 60min and centrifuged (19000 × g, 8 min). Absorption coefficient of the obtained supernatant at 664nm and 647nm was then measured using a Shimadzu spectrophotometer, and correction was applied by subtracting acetone absorption. The pigment concentrations [Chl a] and [Chl b] were calculated using the spectrophotometric equations of Porra et al. [29]

The intracellular pigment concentration c_i was computed according to Bricaud et al. definition [4]:

$$c_i(Chl) = [Chl](\frac{N\pi d^3}{6V})^{-1} \tag{2.25}$$

Where N/V is the cell number density in the medium, d the mean cell diameter (m) and [Chl] the concentration of chlorophyll in the extraction (g.m^{-3}).

2.4 Results and discussion

2.4.1 Sample characteristics

Sample composition

Microscopic observations revealed that the main mesoscopic constituents of the samples were microalgal cells: no significant amount of detrital particles was observed, and no particular bacterial population was detected, which was confirmed by the granulometric results indicating no significant amount of small particles ($< 3\mu$m). In a first approach, the samples were thus considered to be exclusively composed of algal cells and water. The impact of dissolved nutrients was also judged negligible in the framework of this study.

Cell size distribution

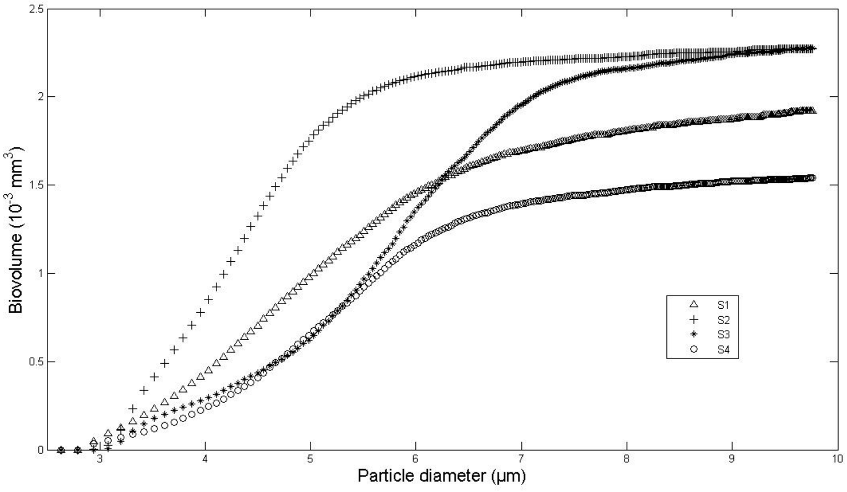

Figure 2.10: Integrated biovolume of particles with size below the diameter in abscissa.

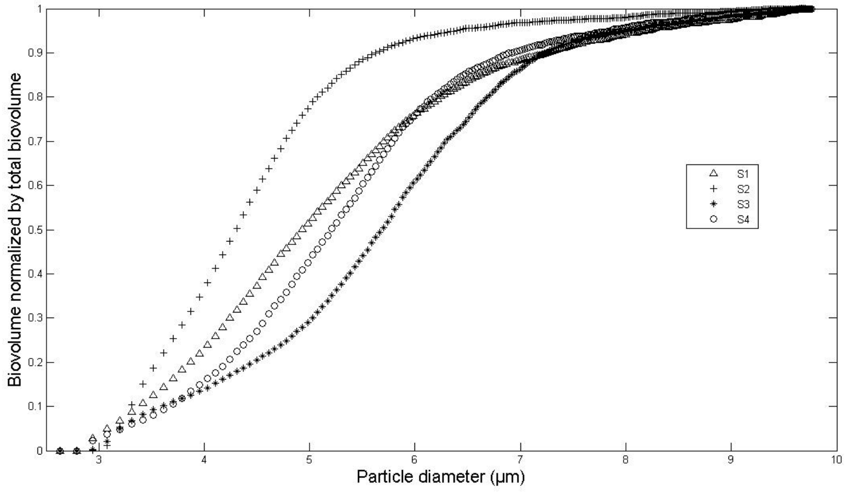

Figure 2.11: Percentage of biovolume occupied by particles of size below the diameter in abscissa.

On the ordinate axis, figure 2.10 shows the total biovolume in mm^3 taken up by algal cells whose diameters are inferior to the value given on the abscissa axis. Cell diameters are distributed over a range from 3μm to 10μm. Total biovolume is read for x = 10μm. Sample S4 biovolume is the smallest. S2 and S3 present the same total biovolume. Figure 2.11 shows the same results but this time the biovolume is normalized by the total biovolume: this makes it possible to directly compare the size distribution profiles of the cells in the different sample algal suspensions. Consequently we observe that S3 biovolume is mainly made up of big cells, whereas S2 biovolume principaly consists of small cells. This indicates that two pairs of samples can be clearly differentiated: the pair 1-4 with samples having similar size distribution profiles but significantly different total biovolumes, and the pair 2-3 with samples presenting considerably distinct size distribution profiles but similar total biovolumes.

Chlorophyll concentrations

Table 2.1 shows the intracellular pigment concentrations measured for Chl a, Chl b and the total pigment concentration, approximated as the sum of the two chlorophylls. The four sample algal populations are distinctly pigmented: the intracellular total chlorophyll concentration for S4 is 6 times that of S1 and S3 and reaches the value of $12.2 \pm 0.6 \times 10^3$ g.Chl.m^{-3}. S1 and S3 present intracellular total pigment rates that are comparable. However Chl a proportion is much higher in S1 (74% of total pigment) than in S3 (64% of total pigment). S2 has the lowest concentration in chlorophyll with an intracellular total pigment concentration that is half those of S1 and S3, for a value of $1.03 \pm 0.05 \times 10^3$ g.Chl.m^{-3}.

Table 2.1: Information measured by standard methods on the algal cultures studied

Sample	mean cell diameter (ESD) (μm)	cell density in the medium (m^{-3})	$c_i(Chla)$ (mg *Chla*.m^{-3})	$c_i(Chlb)$ (mg *Chlb*.m^{-3})	$c_i(Chl_{tot})$ (mg *Chla*+*b*.m^{-3})
S1	4.3 ± 0.4	$1.5 \pm 0.2 \times 10^{13}$	$1.73 \pm 0.09 \times 10^3$	$0.62 \pm 0.09 \times 10^3$	$2.3 \pm 0.1 \times 10^3$
S2	4.0 ± 0.4	$2.4 \pm 0.2 \times 10^{13}$	$0.80 \pm 0.04 \times 10^3$	$0.25 \pm 0.01 \times 10^3$	$1.03 \pm 0.05 \times 10^3$
S3	4.6 ± 0.4	$1.4 \pm 0.1 \times 10^{13}$	$1.33 \pm 0.07 \times 10^3$	$0.75 \pm 0.04 \times 10^3$	$2.1 \pm 0.1 \times 10^3$
S4	4.5 ± 0.4	$1.1 \pm 0.1 \times 10^{13}$	$9.4 \pm 0.5 \times 10^3$	$3.00 \pm 0.2 \times 10^3$	$12.2 \pm 0.6 \times 10^3$

2.4.2 Raw reflectance and transmittance spectra

Total transmittance and total reflectance

Figure 2.12 (a) shows the raw total reflectance spectra measured for the four samples. The error bars are set to plus or minus twice the standard deviation.

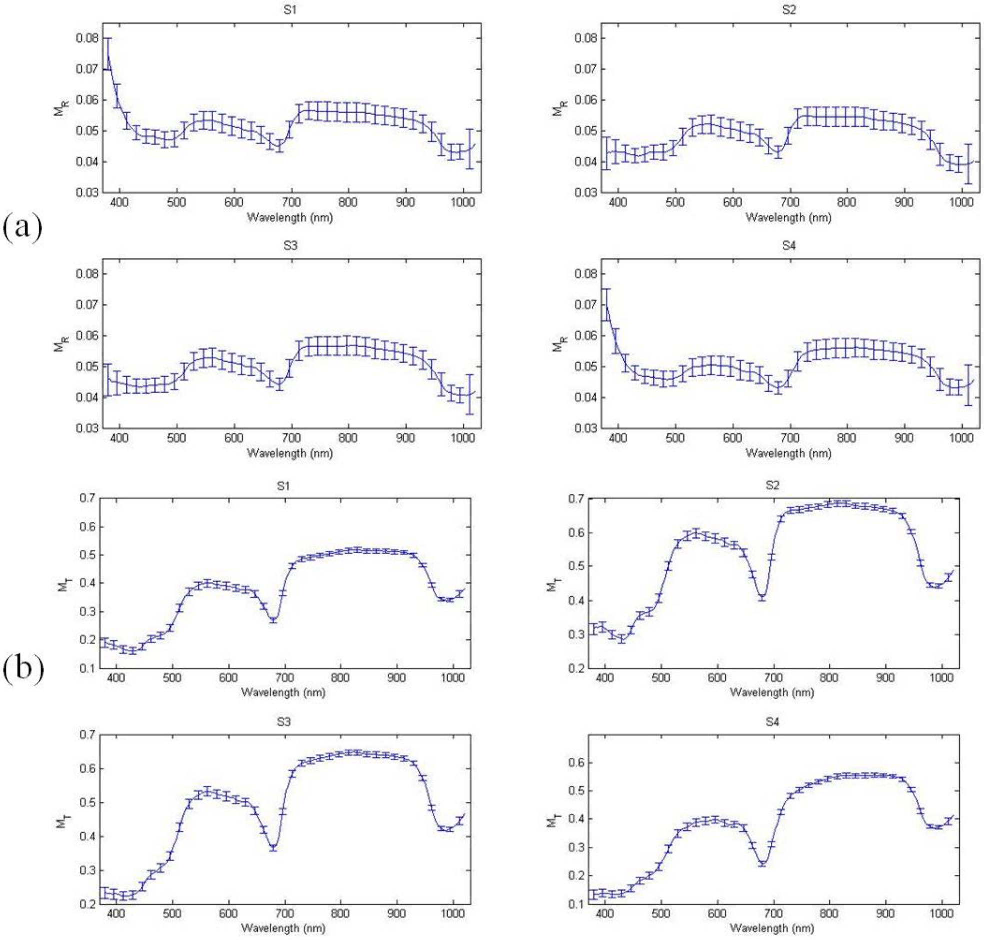

Figure 2.12: Raw total reflectance spectra M_R (a) and raw total transmittance spectra M_T (b) measured for the four samples. The error bars are set to $\pm 2\sigma$, with σ the standard deviation.

For the four samples, the measurements were made with a relative error that does not exceed 6% of the value on the [400-950 nm] spectral range. As expected, the uncertainty grows at the upper and lower limits of the detection range of the spectrometer, reaching up to 20% at 1020 nm and 10% at 380 nm. The position of the sample cell, the fluctuations in time of the light source and the noise of the spectrometer at the limits of its detection bands were identified as the major experimental factors introducing variation in the measurements. It had been observed that the angular position of the sample significantly influenced the signals measured, and particularly the regular reflected signal. This explained why a small angular deviation of the cell would dramatically change the amount of total reflected light collected in the sphere. Therefore, special care was taken in positioning the sample cell at each replicate to limit the impact of the cell position.

M_R spectra consistently illustrate the chemical composition of the samples: they show three major spectral regions where the reflected signal is lower: the [400-550 nm], [650-700 nm] and [900-1020 nm] bands. This originates from the significant absorption phenomena occurring at these wavelengths, due to the presence of pigments ([400-550 nm] and [650-700 nm] bands) and water ([900-1020 nm] band) in the samples.

Figure 2.12 (b) shows the raw total transmittance spectra. As previously the error bars show plus or minus twice the standard deviation. The measurements of M_T were conducted with a relative error lower than 4% throughout the [400-1000 nm] spectral domain. As for M_R, the limitation of the spectrometer introduces higher uncertainty for the lower wavelengths. M_T measurements appear to be less sensitive to the experimental conditions than M_R measurements. This is explained by the fact that the Signal to Noise Ratio (SNR) is higher for the M_T than for M_R due to higher levels. Moreover, the transmitted signal collected is less dependent on the angular cell position than M_R.

M_T spectra show the same absorption bands as observed for M_R.

Figure 2.13 (a) shows the fraction of incident light that has not been collected in the double-sphere setup: it is expressed as $1-(M_R+M_T)$. It can be seen that less than 100% of the incident light is actually detected by the measurement system, which originates from expected absorption phenomena inside the sample as well as supplementary, unwanted light losses depending of the configuration of the optical setup.

A qualitative analysis of the shape of the spectra makes it possible to identify three major effects, as shown by figure 2.13 (b): a baseline, a decreasing trend with increasing wavelength and absorption peaks.

The baseline indicates that a portion of incident light has been lost in a way that does not depend on the wavelength. Those losses may originate from the geometrical configuration of the measurement setup and the thickness of the sample as previously discussed in Chapter 1.

The linear decreasing trend with increasing wavelength may represent light losses due to scattering phenomena, that are expected to be wavelength dependent and higher at lower wavelengths. A linear approximation of the four different spectra shows that the slope is the highest for sample S4. In decreasing order come S3, S1 and S2. Finally, a significant amount of light is absorbed within the sample with a particular spectral pattern depending on the chemical absorbers. The three majors absorption bands previously identified are also clearly visible on the spectra.

Eight main absorption peaks can thus be identified, and are presented in table 2.2.

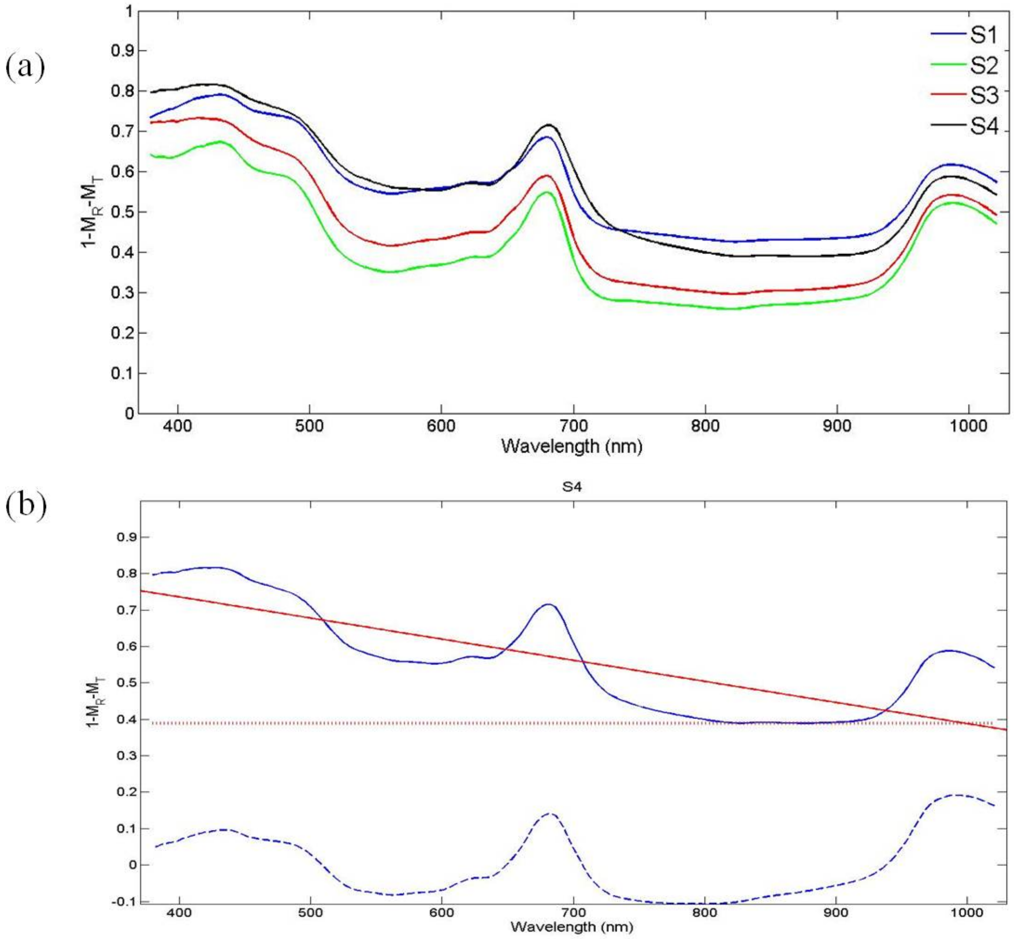

Figure 2.13: (a) Fraction of incident light that has not been collected in the double sphere setup. (b) The three major effects visible on the loss spectrum (blue line): a baseline (dotted red line), a decreasing trend with increasing wavelength (red line), and absorption peaks (dotted blue line)

Table 2.2: Maxima of absorption identified on the absorption spectra and the corresponding μ_a values for each sample

Peak	Wavelength (nm)	Absorbing species	$\mu_a (mm^{-1})$			
			S1	S2	S3	S4
1	416 ± 2	Chla	0.097 ± 0.009	0.084 ± 0.008	0.092 ± 0.008	0.11 ± 0.01
2	492 ± 2	Chlb	0.080 ± 0.008	0.062 ± 0.007	0.067 ± 0.008	0.086 ± 0.008
3	546 ± 2		0.038 ± 0.007	0.032 ± 0.008	0.030 ± 0.006	0.047 ± 0.007
4	590 ± 2	Chla-Chlc, carotenoids	0.039 ± 0.008	0.034 ± 0.009	0.032 ± 0.008	0.044 ± 0.008
5	619 ± 2	Chla	0.045 ± 0.008	0.038 ± 0.008	0.036 ± 0.008	0.049 ± 0.008
6	682 ± 2	Chla	0.075 ± 0.007	0.061 ± 0.006	0.062 ± 0.006	0.088 ± 0.007
7	842 ± 2		0.023 ± 0.007	-	0.022 ± 0.007	0.022 ± 0.007
8	971 ± 2	Water	0.064 ± 0.008	-	0.061 ± 0.008	0.060 ± 0.008

They are consistent with many studies on microalgal pigments reported in Aguirre-Gomez et al. [1]. Peaks 1, 4, 5 and 6 (Table 2.2) correspond to in vivo absorption by Chl a. Peak 2 is clearly attributable to Chl b. The 590 nm peak could be attributed to Chl a-Chl c or to carotenoid-like pigments. Peak 8 corresponds to absorption by water. The values of the peaks may be linked to the quantity of absorbers inside the samples. If we compare the values of the spectra of the different samples at Chla main absorption peaks (1 and 6), it seems that sample S4 is the most concentrated in Chla and sample S2 is the least pigmented. It is difficult to conclude something about S3 and S1 as their relative position does not remain the same at peak 1 and 6. At 492 nm the values of the peaks may indicate the Chlb level of the samples: here again, S4 is clearly more pigmented than S2, S1 and S3, while S2 is the least pigmented. S1 and S3 seem to have quite similar Chlb levels. Those results are consistent with the pigment concentrations measured and shown in table 2.1.

2.4.3 Absorption and reduced scattering coefficient spectra

Convergence of the IAD algorithm

Figure 2.14 shows the absorption (a) and reduced scattering (b) coefficient spectra obtained after IAD computations. The mean absorption and reduced scattering spectra were computed for the samples throughout the spectral range [380-1020 nm]. The error bars represent plus or minus twice the standard deviation obtained by repeating one hundred times the IAD computations as explained previously.

It has to be noted that convergence of the IAD program appears to be erroneous for sample S2 beyond $\lambda = 700$nm since the reduced scattering coefficient obtained is null. This indicates that the results computed with the IAD in the case of this study must be handled critically. In particular, the effect of the unwanted light losses in the measurement setup described previously (figure 2.9, (5)) has to be taken into consideration. The study of de Vries et al. [8] showed that in the case of samples with low absorption and high scattering coefficients, those unwanted light losses may be interpreted by the IAD algorithm as absorption phenomena inside the sample rather than losses in the outside world, which would lead to an overestimation of the absorption coefficient. The quantitative values of the μ_{abs} and μ'_{sca} computed with IAD may then be dependent on the optical setup with which the measurements were conducted. It can also be conjectured that the results obtained with a given optical setup for two objects with different ranges of optical characteristics (distinct order of magnitude for the optical thickness and albedo) could not be compared.

Absorption

From figure 2.14 (a) it can be seen that the relative estimation error on the μ_{abs} values computed largely depend on the wavelength. It is quite high throughout the spectrum (more than 6% and up to 17% at 750nm) except on the main absorption bands (the [400-

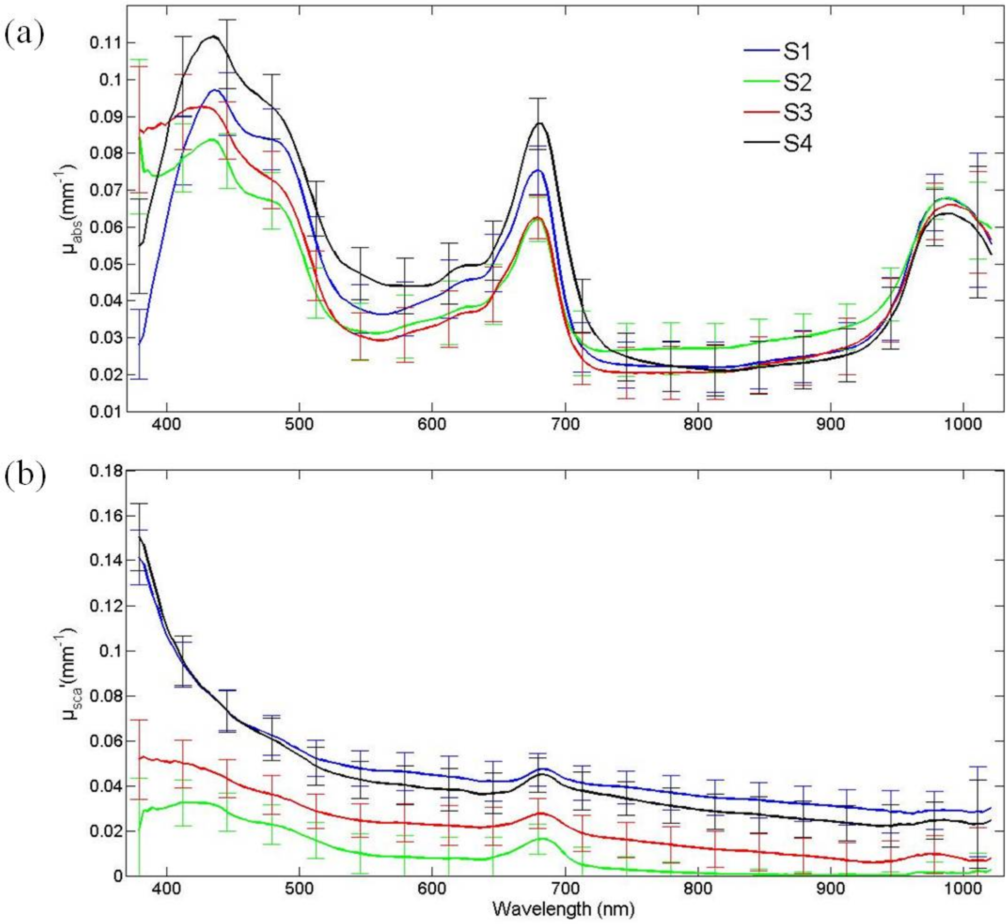

Figure 2.14: Absorption (a) and reduced scattering spectra (b) obtained for the four algal samples in the [380-1020 nm] range. The error bars represent ±2σ with σ the standard deviation of the values at each wavelength.

550nm], [650-700nm] and [900-1000nm] bands) where it is as low as 4%. This is probably explained by the fact that the absorption coefficient is much higher on those spectral domains, what significantly reduces the relative error. As what was observed on M_R and M_T spectra (figure 2.12), absorption spectra are mainly shaped by the absorption of the photosynthetic pigments.

For two samples, the overlap of the error bars indicate that their μ_{abs} values at that wavelength cannot be considered as different. From this it appears that the μ_{abs} spectra of the four samples are quite similar throughout the considered spectral domain, except on the [380-550nm] and [650-710nm] bands where they can be distinct. It can be observed in particular that the four μ_{abs} spectra are completely overlapping on the [900-1000nm] band corresponding to the absorption of water. This is not surprising, as the water volume was significantly higher than the algal volume in the four samples. The comparison of μ_{abs} values at peaks 1 and 6 can be done. μ_{abs} (S1) and μ_{abs}(S2) are distinct at peaks 1 and

6 with the following order: μ_{abs} (S1)> μ_{abs}(S2). μ_{abs} (S1) and μ_{abs}(S3) are overlapping at peak 1 and are different at peak 6 where μ_{abs} (S1)> μ_{abs}(S3). It is the same thing for S1 and S4, overlapping at peak 1 but distinct at peak 6 with μ_{abs} (S4)> μ_{abs}(S1). μ_{abs}(S2) and μ_{abs}(S3) are very similar and cannot be distinguished. Again these observations are consistent with the pigments measurements given in table 2.1. The information of relative Chla quantity in the samples appears to be more represented by peak 6. For Chlb at peak 2 we can only conclude that μ_{abs}(S1)>μ_{abs}(S2) and that μ_{abs}(S4)> μ_{abs}(S2) ; μ_{abs}(S4)>μ_{abs}(S3). S1 and S4, S1 and S3 and S2 and S3 are not distinct at 492nm. This gives a first idea of the results found by the pigment measurement (table 2.1).

While remaining critical concerning the μ_{abs} absolute values computed for the four algal samples in this study, it can be reported still that they seem to be consistent with the results that can be found in literature. This may indicate that the errors of estimation of the μ_{abs} introduced by the IAD process remain reasonable relatively to the actual value of the absorption coefficient. In order to take into account the dependency of absorption on the physical structure of the algal population, the dimensionless efficiency factors Q_{abs} ,Q_{sca} and Q_{ext} are usually considered [4]. They are the ratio between the energies that are respectively absorbed, scattered and attenuated within the medium and the input energy. For a suspension of microalgal cells, a simple relation exists between μ_i and Q_i [4] :

$$Q_{i,cell} = \frac{\mu_{i,cell} V}{\Sigma N_{cell}} \tag{2.26}$$

Where Σ is the geometrical cross section of one cell, N_{cell} the number of cells of uniform size in a volume V , and i= abs, sca or ext. Here $\mu_{i,cell}$ is the bulk optical coefficient of one cell. If the algal cells are approximated as spheres the value for Σ can be easily deduced from the cell diameter d: $\Sigma = \pi d^2/4$. As the efficiency factors take into account the influence of cell size and density in the medium, it is more relevant to use them instead of bulk absorption coefficient μ_{abs} in order to compare distinct measurements of the absorption properties of various algal polydispersions. Table 2.3, adapted from the article of Sathyendranath et al. [35] compares the efficiency factors for absorption obtained in this study with those obtained by other previous studies. Table 2.3 shows that the efficiency factors computed from the measurements on the four samples of this study are consistent with the literature regarding their order of magnitude and their dependency upon the characteristics of the algal population. Fluctuations of the Q_{abs} values observed can be both intra and inter species and originate from difference in the relative amount of pigments in the algal cells as well as from variation in the cell density and size between two samples.

Table 2.3: Comparison of the characteristics of the measured samples to other research works, adapted from [35]

		Age	Pigment concentration ($mg.m^{-3}$)					No. cells	mean diam.	Q_{abs}	
Sample	Alga	(day)	Chla	Chlb	Pheopigments	Chlc	Carotenoids	($10^{10} \times m^{-3}$)	(μm)	(440nm)	(737nm)
S1	*Scenedesmus + Chlorella*	-	1730 ± 90	620 ± 30	-	-	-	$1.5 \pm 0.2 \times 10^3$	4.3 ± 0.4	0.4 ± 0.1	0.11 ± 0.04
S2	*Scenedesmus + Chlorella*	-	800 ± 40	250 ± 10	-	-	-	$2.4 \pm 0.2 \times 10^3$	4.0 ± 0.4	0.27 ± 0.07	-
S3	*Scenedesmus + Chlorella*	-	1330 ± 70	750 ± 40	-	-	-	$1.4 \pm 0.1 \times 10^3$	4.6 ± 0.4	0.4 ± 0.1	0.09 ± 0.04
S4	*Scenedesmus + Chlorella*	-	9350 ± 470	3000 ± 150	-	-	-	$1.01 \pm 0.1 \times 10^3$	4.5 ± 0.4	0.7 ± 0.1	0.15 ± 0.05
5	*Platymonas suecica*	3	138	42.3	5.1	0	114	26	5.8	0.671	0.080
6	*Platymonas suecica*	7	245	131	46.5	0	261	49	5.6	0.837	0.103
7	*Dunaliella marina*	7	225	88.8	27.2	0	219	16	8.5	0.979	0.197
8	*Tetraselmis maculata*	-	467	231	0	0	435	90	8.5	0.465	0.079
9	*Platymonas sp.*	-	624	298	25.3	0	662	207	6.8	0.472	0.102
10	*Hymenomonas elongata*	7	247	0	23.6	49.1	233	5.8	13.4	0.7653	0.080
11	*Hymenomonas elongata*	9	384	0	7.5	79	333	8.1	13.5	0.693	0.021
12	*Hymenomonas elongata*	14	781	0	10.3	166	640	17	14	0.618	0.034
13	*Hymenomonas elongata*	17	1019	0	22.7	300	769	23	15.1	0.507	0.034
14	*Chaetoceros protuberans*	1	172	0	14.9	95.6	73.4	7.5	9.5	0.941	0.090

Reduced scattering coefficients

The mean reduced scattering coefficient spectra have been obtained for the four samples and are shown in figure 2.14 (b). The relative error is higher throughout the spectral domain than it was for μ_{abs} spectra. It increases with increasing wavelengths, and varies from 5% at 380nm to 17% at 920nm for S4. This trend is explained because the μ'_{sca} values decrease with increasing wavelengths. The relative error for S2 grows dramatically beyond 700nm and exceeds 50%. This is surely due to convergence failure of the IAD computation for sample S2 at higher wavelengths, meaning this part of the spectrum should not be taken into account for S2. The four reduced scattering coefficient spectra are more dissimilar the one from the other than what was observed for μ_{abs} spectra: there is less overlap of the spectra throughout the spectral domain considered. Although S2 and S3 show very similar μ_{abs} spectra, their μ'_{sca} spectra seem more distinct the one from the other. On the contrary, S1 and S4 spectra are very similar. However they are distinct from S2 and S3 spectra. This seems to be explained by the granulometric properties of the samples, and more particularly by the size distribution of the algal cells. Unlike what could have been expected, the total quantity of biomass inside the sample does not appear to be influential on the reduced scattering coefficient in the case of this study: indeed figure 2.10 shows that S1 and S4 have different total biovolumes but their μ'_{sca} spectra are similar. However, the size distribution of the algal cells is the same for those two samples, as shown in figure 2.11. On the contrary, S2 and S3 biovolumes are the same but the size distributions of the cells are dissimilar: in that case it is observed that the μ'_{sca} spectra of S2 and S3 are quite distinct. From this analysis it seems that the size distribution of the algal cells inside the sample is very influential on the values of μ'_{sca} spectra.

From figure 2.14 (b) the general shape of μ'_{sca} spectra can be described: firstly, they are a decreasing function of wavelength and secondly, they show pronounced enhancements in the vicinity of the absorption bands. Unlike what is usually thought in analytical spectroscopy, those peaks in the reduced scattering spectra appear not to be erroneous: they are actually expected, and consistent with the Lorentz-Mie [24] theory and Ketteler-Helmholtz's theory of anomalous dispersion [39]. If the algal cells are considered as homogeneous spheres whose refractive index is close to that of the surrounding medium (here water), their efficiency factors throughout the visible spectrum depend upon the optical size parameter ρ, defined as [4, 39]:

$$\rho = \frac{2\pi d}{\lambda} \times (n-1) \tag{2.27}$$

Where d is the cell diameter, n the real part of the cell complex refractive index relative to water defined as $m = n + in'$ and λ the wavelength in the surrounding medium. For absorbing particles, the efficiency factors are given [39, 25] by:

$$Q_{sca} = Q_{ext} - Q_{abs} \tag{2.28}$$

$$\begin{gathered}Q_{ext} = 2 - 4e^{-\rho tan(\frac{n'}{n-1})}[\frac{cos(\frac{n'}{n-1})}{\rho}.sin(\rho - (\frac{n'}{n-1}))+ \\ (\frac{cos(\frac{n'}{n-1})}{\rho})^2.cos(\rho - 2(\frac{n'}{n-1})]+ \\ 4(\frac{cos(\frac{n'}{n-1})}{\rho})^2.cos(2(\frac{n'}{n-1}))\end{gathered} \tag{2.29}$$

$$Q_{abs} = 1 + [e^{-2\rho tan(\frac{n'}{n-1})}.(2\rho tan(\frac{n'}{n-1}) + 1) - 1]/2\rho^2(tan(\frac{n'}{n-1}))^2 \tag{2.30}$$

Bricaud et al. [4] computed the variations of the efficiency factors for simulated algal suspensions. They observed different patterns depending on the value of ρ with respect to the values ρ_m corresponding to the first maximum in $Q_{ext}(\rho)$:

- If ρ is lower than ρ_m throughout the spectrum Q_{ext} increases with ρ i.e. with decreasing λ
- If the range of variation of ρ includes ρ_m, Q_{ext} has a maximum inside the spectrum
- If ρ remains close but higher than ρ_m, Q_{ext} decreases with increasing ρ, i.e. with decreasing λ
- For high values of ρ, Q_{ext} is almost constant on the spectrum.

Q_{sca} variations (and consequently those of μ_{sca}) follow the same patterns given the relationship between Q_{sca} and Q_{ext} as shown by equation (2.28). Bricaud et al [4] computed that ρ_m ranges between 2 and 4 and depends on the size distribution law in the case of algal suspensions. Q_{abs}, Q_{sca} and Q_{ext} variations according to ρ were computed in the case of our samples using equations (2.30), (2.28) and (2.29). The example of sample S1 at $\lambda = 440nm$ is presented on figure 2.15. Values of the relative complexe refractive index at $\lambda = 440nm$ was taken according to our measurements: $n = 1.015$ and $n' = 0.004$. We computed that the value of ρ_m in the case of our samples varies slightly around 4. The computation of ρ for the four samples presented on figure 2.16 shows that throughout the ranged spectrum, the values of ρ remain lower than ρ_m, which is consistent with the shape of measured μ'_{sca} spectra.

Over the [380-1100nm] range we computed that ρ ranged between extreme values of 0.5 and 1.8 with slight differences between the samples. This shows the observed decrease of μ'_{sca} as a function of increasing λ is consistent with the predictions given by the Lorentz-Mie theory [24], [39].

The influence of an absorption band upon scattering properties has been well described by the same authors in [25]. By simulating the variations of Q_{sca} in the vicinity of an absorption line (occurring at $\lambda = 675nm$) for various values of ρ they show different phenomena may occur depending on the value of ρ:

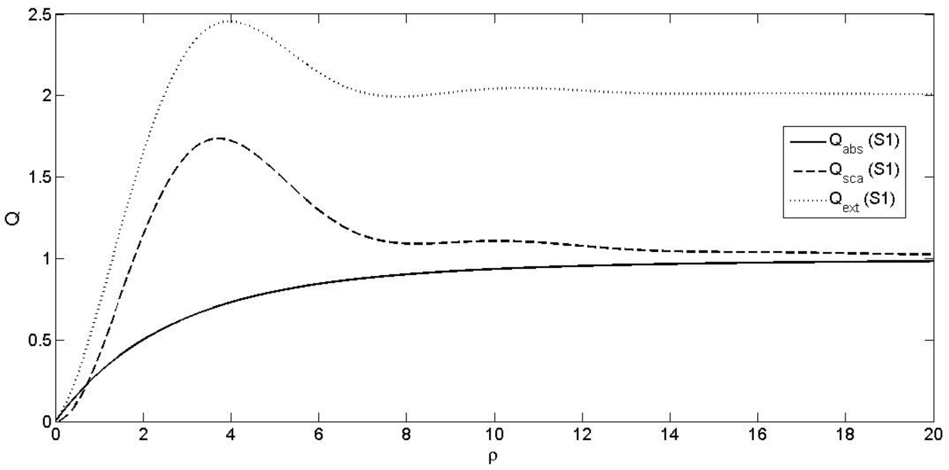

Figure 2.15: Theoretical variations of the efficiency factors Q_a, Q_s and Q_{ext} with optical size parameter ρ in the case of the algal suspension S1

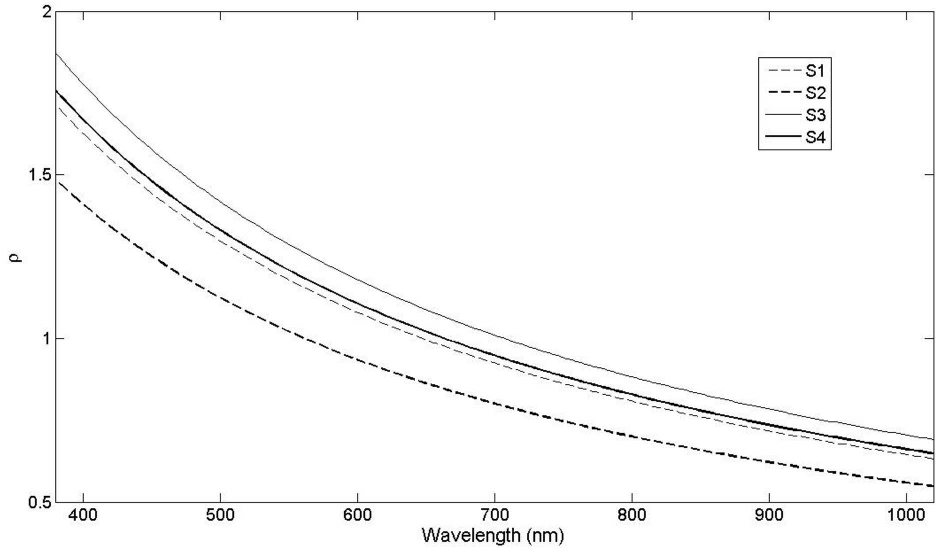

Figure 2.16: Factor ρ calculated for the four samples, according to the definition of Bricaud et al. [4].

- For $\rho < 2$ or 3 the scattering coefficient is enhanced inside and slightly beyond the absorption band, resulting in peaks that may shift slightly towards upper wavelengths compared to the absorption bands.
- For $\rho > 3$ the scattering coefficient is reduced inside the absorption line, what leads to variations of Q_{sca} opposite to those of Q_{abs}.

In our case, figure 2.16 shows that ρ remains below to two on the considered spectrum, which explains the peaks observed on the reduced scattering spectra measured (figure 2.14 (b)) in the vicinity of the absorption bands identified in table 2.2.

2.4.4 Conclusion

This study reports the results obtained while testing the Adding-Doubling method on the [380-1020nm] spectral range for four non-diluted algal samples extracted from real cultivation ponds. The spectra of absorption and reduced scattering coefficients were computed with Inverse-Adding-Doubling algorithm from total reflectance and total transmittance measurements conducted with a double integrating sphere setup. Several critical points have been encountered, first to optimize the configuration of the optical setup, and second in the convergence of the IAD algorithm from experimental, imperfect measurements of M_R and M_T. Because the sample cell was positioned outside of the spheres in the double integrating sphere setup, it was impossible in practice to avoid light losses at the sphere ports and at the edges of the sample cell. Those losses can be limited at best by adapting carefully the optical setup dimensions. In the case of this study however, the optical setup required to be mobile which constrained some dimensions and the detection system, and the light losses remained significant. Light losses within the setup may introduce errors in the IAD algorithm convergence and the estimation of the absorption and reduced scattering coefficient absolute values might be erroneous and dependent on the setup with which the optical measurements were conducted [30, 8]. In the case of this study however, it was possible to analyze the absorption and reduced coefficient spectra obtained by keeping in mind this difficulty. The absorption coefficient spectra computed represent qualitatively the difference in pigmentation between the four algal samples. It is also consistent with values found in litterature [35]. This seems to indicate that despite the uncertainty due to experimental errors, our method shows quantitative results at least comparable with litterature. As for the reduced scattering coefficient, it appears to include information on the size distribution of the algal cells. It seems to vary significantly with the granulometric properties of the microalgal samples. This conclusion is consistent with other works [6, 10]. Moreover its spectral patterns were shown to be consistent with the trends expected using Mie theory predictions. Our preliminary study thus proved that the linear optical coefficients of real dense algal samples could be adequately estimated by solving the RTE with the IAD method, provided that the measurements of the reflectance and the transmittance properties are implemented with care. Using a DIS setup adapted to reduce the light losses and enhance the signal to noise ratio at best as presented in Chapter 1 could surely adress the optical measurement setup issues.

2.5 Conclusion

In this Chapter we precised the links between on the one hand the apparent spectral properties measured on a bulk particulate medium, namely its reflectance and transmittance (total and regular), and on the other hand the instrinsic spectral properties characterizing this medium, i.e. the linear absorption, scattering and extinction coefficients. We saw that the radiative transport equation made it possible to model the apparent light behaviour in the sample medium from the knowledge of its intrinsic properties, and its geometry. The RTE formulation in the general case of dense particle media with volume occupation between 0.1 and 1% cannot be simplified with an approximation theory such as simple scattering model or the diffusion approximation [16]. It is thus necessary to solve it. As no explicit analytical solution can be found, the solution must be numerically found. This can be done in particular with the Adding-Doubling method and its inverse problem the Inverse Adding-Doubling method, making it possible to numerically solve the RTE for a sample described as made of infinitely thin homogeneous slabs [30]. We applied the IAD to real dense algal samples in order to test the retrieval of the intrinsic linear absorption and scattering properties from the measurements of M_R and M_T implemented with a Double Integrating Sphere setup. Our first results showed that the obtained linear spectral coefficients seem to be qualitatively and quantitatively in accordance with the observations commonly described in litterature. We also noted the significant influence of the experimental errors that can be made when measuring M_R and M_T on the quantitative values of the retrieved intrinsic properties on certain spectral ranges. The light losses in the DIS setup in particular can introduce significant misestimations of the linear coefficients. This operational issue has to be kept in mind, and illustrates how important it is to pay the greatest attention to the measurement setup. In the next Chapter, we will this time go deeper in the algal medium scale and investigate the optical properties of the constitutive particles themselves. In particular we will concentrate on the dense algal medium which is the practical case investigated in this thesis. More precisely, we will propose a description of the algal cell spectral characteristics as functions of their physical and chemical characteristics.

Bibliography

[1] R. Aguirre-Gomez, S. R. Boxall, and A. R. Weeks. Identification of algal pigments using high order derivatives. *IEEE*, 1995.

[2] Y.N. Barabanenkov, Y.A. Kravstov, S.M. Rytov, and V.I. Tatarski. Status of the theory of propagation of waves in a randomly inhomogeneous medium. *Soviet Physics Uspekhi*, 13, 1971.

[3] S. Bellini, R. Bendoula, E. Latrille, and J.M. Roger. Potential of a spectroscopic measurement method using adding-doubling to retrieve the bulk optical properties of dense microalgal media. *Applied spectroscopy*, 68(10), 2014.

[4] A. Bricaud, A. Morel, and L. Prieur. Optical efficiency factors of some phytoplankters. *Journal of limnology and oceanography*, 1983.

[5] S. Chandrasekhar. *Radiative transfer.* Oxford University Press, London, 1950.

[6] A. M. Ciotti, M. R. Lewis, and J. J. Cullen. Assessment of the relationships between dominant cell size in natural phytoplankton communities and the spectral shape of the absorption coefficient. *Journal of limnology and oceanography*, 47, 2002.

[7] H.C. Van de Hulst. *Multiple light scattering*, volume 1. Academic Press, New York, 1980.

[8] G. de Vries, J. F. Beek, G. W. Lucassen, and M. J. C. van Gemert. The effects of light losses in double integrating spheres on optical properties estimation. *IEEE journal of selected topics in quantum electronics*, 5(4), 1999.

[9] S. T. Flock, B. C. Wilson, and M. S. Patterson. Total attenuation coefficients and scattering phase functions of tissues and phantom materials at 633nm. *Medical physics*, 14, 1987.

[10] C. Frankovitch, O. Reich, and H.G. Löhmannsröben. Investigation of microalgae with photon density waves. *Proceedings SPIE 6761, Optics for Natural Resources, Agriculture, and Foods II*, 2007.

[11] V. Frisch. *Wave propagation in random media, in Probabilistic methods in applied mathematics.* Academic Press, New York, 1968.

[12] R. A. Groenhuis, H. A. Ferwerda, and J. J. Ten Bosch. Scattering and absorption of turbid materials determined from refection measurements: 1: Theory. *Applied optics*, 22, 1983.

[13] J.E. Hansen and L.D. Travis. Light scattering in planetary atmospheres. *Space scienc reviews*, 16, 1974.

[14] F.B. Hildebrand. *Introduction to numerical analysis.* Dover publications, New York, 1974.

[15] A. Ishimaru. *Electromagnetic wave propagation, radiation, and scattering.* Prentice-Hall, Inc, 1991.

[16] A. Ishimaru. *Wave propagation and scattering in random media.* IEEE press: New York, 1997.

[17] B.R. Jennings and K. Parslow. Particle size measurement: The equivalent spherical diameter. *Proceedings of the Royal Society of London, Series A*, 419, 1988.

[18] P. Kubelka and F. Z. Munk. Ein beitrag zur optik der farbanstriche. *Zeits. f. techn. Physik*, 1931.

[19] E. Lee, R. L. Heng, and L. Pilon. Spectral optical properties of selected photosynthetic microalgae producing biofuels. *Journal of Quantitative Spectroscopy and Radiative Transfer*, 114, 2013.

[20] H. Martens and T. Naes. *Multivariate Calibration.* Wiley, 1989.

[21] D.H. Menzel, editor. *Selected papers on the transfer of radiations.* Dover, New York, 1966.

[22] J-L. Meyzonnette. Radiometry and detection systems. Institut d'Optique Graduate School courses, 2009.

[23] H.H. Michels. Abscissas and weight coefficients for lobatto quadrature. *Mathematical computations*, 17, 1963.

[24] G. Mie. Beitrage zur optik trüber medien, speziell kolloidaler metallösungen. *Annalen der physik*, 25(3), 1908.

[25] A. Morel and A. Bricaud. Theoretical results concerning the optics of phytoplankton, with special reference to remote sensing applications. *Oceanography from space*, 1981.

[26] P.M. Morse and H. Feshbach. *Methods of theoretical physics.* McGraw-Hill, New York, 1953.

[27] J.A. Nelder and R. Mead. A simplex method for function minimization. *Computer journal*, 7, 1965.

[28] B. Philips-Invernizzi, D. Dupont, and C. Cazé. Bibliographical review for reflectance of diffusing media. *Optical Engineering*, 40(6), 2001.

[29] R. J. Porra, W. A. Thompson, and P. E. Kriedemann. Determination of accurate exctinction coefficients and simultaneous equations for assaying chlorophylls a and b extracted with four different solvents: verification of the concentration of chlorophyll standards by atomic absorption spectroscopy. *Biochimica and Biophysica acta*, (975), 1989.

[30] S. A. Prahl. *Optical-Thermal Response of Laser Irradiated Tissue.* 1995.

[31] S. A. Prahl. *Everything I think you should know about Inverse Adding-Doubling.* Oregon Medical Laser Center, 2011.

[32] S. A. Prahl, M. Keijzer, S. L. Jacques, and A. J. Welch. A monte carlo model of light propagation in tissue. *SPIE Proceedings of dosimetry of laser radiation in medicine and biology*, IS5, 1989.

[33] S. A. Prahl, M. J. C. van Gemert, and A. J. Welch. Determining the optical properties of turbid media using adding-doubling method. *Applied optics*, 32(4), 1993.

[34] R. W. Preisendorfer. *Radiative transfer on discrete spaces.* Oxford University Press, London and New York, 1965.

[35] S. Sathyendranath, L. Lazzara, and L. Prieur. Variations in the spectral values of specific absorption of phytoplankton. *Limnology and Oceanography*, 32(2), 1987.

[36] V.V. Soblev. *A treatise on radiative transfer.* Van Nostrand-Reinhold, Princeton, New Jersey, 1963.

[37] S.T. Thynell. Discrete-ordinates method in radiative heat transfer. *International Journal of Engineering Science*, 36, 1998.

[38] V. Twersky. On propagation in random media of discrete scatterers. *Proceedings of the american mathematical society*, 16, 1964.

[39] H. C. van de Hulst. *Light scattering by small particles.* Wiley, 1957.

[40] W. J. Wiscombe. On initialization, error and flux conservation in the doubling method. *Journal of Quantitative Spectroscopy and Radiative Transfer*, 16, 1976.

[41] I. V. Yaroslavsky, A. N. Yaroslavsky, T. Goldbach, and H. J. Schwarzmaier. Inverse hybrid technique for determining the optical properties of turbid media from integrating-sphere measurements. *Applied optics*, 35, 1996.

Chapter 3

How to describe the optical properties of a single algal cell from its physical and chemical characteristics?

Contents

In the previous Chapter, the intrinsic linear spectral properties of a dense medium made of random particles were investigated, with a special attention to the means of linking them to the apparent reflectance and transmittance. We saw that the RTE is a rigorous formulation of the behaviour of light in a medium defined by its intrinsic optical quantities and its geometry. It can be solved in particular with the Adding-Doubling method, and its inverse problem the Inverse Adding-Doubling method. The work implemented in Chapter 2 showed that, subject to careful experimental measurements of the reflectance and transmittance, the IAD method seemed to be adapted in the case of the particle media under study, i.e. dense cultivated algal media. We will now go deeper in the scale of the dense algal media under study, and investigate what happens at the scale of a single algal cell. In particular, this chapter aims at investigating the links between the chemical and physical characteristics of one single algal cell and its individual optical properties. We will see that the notion of optical cross sections has been defined in order to characterize the optical behavior for one single particle; they are strongly influenced by the particle size, shape and composition. The exact description of light interaction with a particle defined by its geometrical structure and chemical composition is provided by Maxwell equations. However in practice, no formulation can be found to describe all the complexity of the problem: approximations can be done in defined frameworks in order to provide solutions specific to a limited range of particle size, shape and refractive index. Among them, the Mie theory is the exact solution of the Maxwell equations to describe light interaction with a spherical particle of size larger or comparable to the incident wavelength. It has been extended to more complex structures such as multilayered spheres. In this work, we concentrated on the practical case of dense algal media and investigated the use of extended Mie theory in order to describe the optical cross sections of a single algal cell described by its physical and chemical parameters. We implemented a model of an algal cell seen as a spherical particle composed of successive layers of organic materials, based on the litterature describing the microalgae physiology. By performing Mie calculations on this model cell, the corresponding optical cross sections could be deduced over the [400-750 nm] spectral range. In particular, a program called *AlgaSim* was developed to implement this method. In this chapter we detailed the implementation of *AlgaSim*, and we tested its ability to adequately simulate the optical cross sections of real algal cells. We also investigated our model by generating large databases of different individual algal cells and their corresponding cross section spectra. Those databases were analysed by principal composant analysis (PCA) in order to retrieve the influence of the cell physical and chemical characteristics on the simulated cross section spectra shape, magnitude and patterns.

3.1 Theory: modelling the optical properties of a single cell

In this section we present the quantities describing the optical properties of a single particle, as well as the paradigms used to model their dependency on the rough characteristics of the particle (size and refractive index). We then investigate more thouroughly the particular case of the algal cells.

3.1.1 Definitions

The notion of optical cross sections is used in order to describe the optical properties of a single particle which size is smaller than the incident light beam. As already presented in the general definition given in chapter 1, and illustrated by figure 3.1, light incident upon a particle can be either absorbed or scattered.

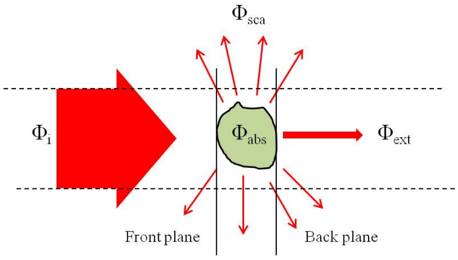

Figure 3.1: Scheme of the interaction of light with a particle

The scattering cross section of the particle C_{sca} in m^2 can be defined as the ratio of Φ_{sca}, the total power scattered in whole space by the particle, and the incident particle irradiance at front plane E_i [34]:

$$C_{sca} = \frac{\Phi_{sca}}{E_i} \tag{3.1}$$

Similarly, the absorption cross section C_{abs} in m^2 of the particle is defined as the ratio of the total power absorbed by the particle and the incident particle irradiance at front plane E_i such that [34]:

$$C_{abs} = \frac{\Phi_{abs}}{E_i} \tag{3.2}$$

It is also usual to describe the extinction of light in the direction of the incident radiation. In the direction of the input beam, the power that was transferred to the particle was either scattered in another direction, or absorbed. From this comes the relation between the cross sections [34]:

$$C_{ext} = C_{sca} + C_{abs} \tag{3.3}$$

This relation expresses in particular the energy conservation in a process of light scattering.

The notion of optical efficiency can also be used in order to decribe the optical properties of a particle. If Σ in m^2 is the geometrical cross section of the particle seen in the incidence direction, the scattering, absorption and extinction efficiency factors are defined respectively such that:

$$Q_{sca} = \frac{C_{sca}}{\Sigma} \tag{3.4}$$

$$Q_{abs} = \frac{C_{abs}}{\Sigma} \tag{3.5}$$

$$Q_{ext} = \frac{C_{ext}}{\Sigma} \tag{3.6}$$

Note that the efficiency factors are dimensionless.

As for a bulk medium, the geometrical repartition of the reradiated power by the particle can be described by the phase function p and the anisotropy factor g, defined in Chapter 1.

Optical regimes

The interaction of light with particles is strongly dependent on several parameters [16]. First of them is the size parameter x, defined as the ratio of the particle radius R to the wavelength λ within the medium with real refractive index n_m:

$$x = 2\pi \frac{Rn_m}{\lambda} \tag{3.7}$$

Another important parameter characterizing the interaction of light with the particle is the ratio of the speed of light within the particle to that in the host medium. It can be evaluated by calculating the quantities: $|m_{medium} - m_{particle}|$ and $|n_{medium} - n_{particle}|$, with m and n the imaginary and real part of the refractive index of the medium and particle respectiveley. In the case of algal cells, $|m_{water} - m_{algalcell}| \approx |n_{water} - n_{algalcell}| \ll 1$, what means that algal particles refractive index is close to that of water: they can be considered as optically "soft" [37, 29].

Last important parameter is the phase shift parameter ρ, accounting for the shift in phase between the wave travelling within the particle and the wave travelling in the embedding medium. It is a function of the size parameter x and of the real part of the refractive index n of the particle:

$$\rho = 2x(n - 1) \tag{3.8}$$

Those parameters are used to delineate rough optical regimes for which analytical approximations applying to the case of soft particles have been derived from the Maxwell equations, which rigorously describe light behaviour when encountering a particle.

Particles much smaller than the wavelength : the Rayleigh region

If $x \ll 1, \rho \ll 1$ and $D \ll \lambda$, we are in the case of the Rayleigh regime. The particle cross sections can be defined directly from the particle volume V and the refractive index of the particle $n_{particle} + im_{particle}$:

$$\begin{aligned} C_{ext} &= \frac{k^2 V^2 |\frac{m^2_{particle}}{m^2_{medium}} - 1|^2}{6\pi} && (3.9) \\ C_{abs} &= \frac{4\pi k V}{\lambda} && (3.10) \\ C_{scat} &= C_{ext} - C_{abs} && (3.11) \end{aligned}$$

Where $k = 2\pi/\lambda$ is the wave number. This solution is thus shape independent.

Particles of size much larger than the wavelength: the geometric optics

When $x \gg 1, \rho \gg 100$ and $R \gg \lambda$ the geometric optic domain is reached. In this optical region, scattering is largely dominated by diffraction. Light behaviour can be described by Snell-Descartes laws of refraction.

Particles of size comparable to or larger than the wavelength: the Rayleigh-Gans-Debye and the van de Hulst region

Scattering by soft particles in this region is dominated by diffraction, although contributions from reflections and refraction have to be taken into account. For homogeneous spherical particles, Mie theory [35] gives the exact solution of Maxwell's equations in form of a series expansion: it makes it possible to retrieve the optical cross sections given the particle refractive index and diameter. Aden and Kerker [4] derived the extension of Mie theory to the case of a concentrically coated sphere, and Kerker [23] generalized that result to scattering by a concentrically stratified sphere having an arbitrary number of layers. For other shapes, there is no equivalent converging solution covering all the relevant size range. However analytical solutions such as the T-matrix method [36] can be applied on defined particle-size ranges.

3.1.2 Modelling the optical properties of algal cells: a short review

As already presented in the Introduction, many studies have investigated how to model the algal cell optical properties as functions of their characteristics. However it appeared that the influence of the algal cell physical and chemical characteristics on their optical properties was not linear, and could not be adequately formulated by explicit analytical relations. That is why more complex, implicit models have been investigated. In the VIS-NIR spectral range, single algal cell sizes are in majority comparable to or larger than the wavelength, that is why the optical models developed for algal cells are derived mainly from simple and extended Mie theory, even if some corrections have been applied to take into account the non-spherical cases.

Algal cells as homogeneous spheres

The simple Mie theory have been applied to model the optical properties of algal cells since the 1970s, and more particularly in optical oceanography [13]. Algal cells are thus modeled as homogeneous spheres of given refractive index and diameter. Mie theory is widely used to model the inherent optical properties of aquatic particles in oceanography [48]. It is also inverted to retrieve the optical properties of algal cells from spectral measurements [10], [47]: the refractive index of the algal cells in particular is investigated in many recent studies aiming at optimizing the photobioreactors design, and light supplying in the context of mass cultivation [22, 42, 28].

The anomalous diffraction approximation (ADA) [49] is often used coupled to Mie theory in order to give an analytical formulation of the optical efficiency factors [10, 42]. In that case, the efficiency factors of optically "soft" spherical particles can be expressed as functions of the complex refractive index of the particle and of the surrounding medium.

Algal cells as multilayered spheres

Real-life algal cells are known to present many heterogeneities due to the presence of complex internal structures [43, 2], such as silicate, cellulose or calcite coatings, absorbing chloroplasts, nucleus, mitochondria or gas vacuoles. In order to take into account those internal heterogeneities, the solution of Kerker [23] has been investigated to model the algal cells [39, 27, 43]. In that case, the cells are modeled as a two or more layer sphere, each layer representing an organic material: the outer layer generally mimes the membrane, and an inner, absorbing core represents the pigmented chloroplasts.

Algal cells as non-spherical particles

The assumption of sphericity is obviously a rough simplification, as real algal cells can present shapes that significantly deviate from the spherical. The influence of shape has been demonstrated to be particularly important on the backscattering properties [1, 43]. That is why non-spherical models have been investigated: solution for spheroids of arbitrary orientation was obtained by Asano and Yamamoto [6], but was limited to particles of size parameter below 30. One can cite the Paramonov approximation method that makes it possible to obtain the attenuation, absorption and scattering of optically soft spheroids [45]. For the determination of the light scattering properties of non-spherical particles, the T-matrix method [51] is considered as a reference method as it is the exact solution of Maxwell's equation [43]. It can also include the added complexity of layered body [41]. In practice, the T-matrix method requires long-time calculations, which explains why it is not more systematically implemented in research works, and was not tested in the present thesis.

Comparison of the different models

Quirantes et al. [43] compared the light scattering and absorption of algal cells modeled with the T-matrix method to the results obtained with simpler models, such as homogeneous (Mie) and coated (Aden-Kerker) models coupled with the anomalous diffraction approximation (ADA). They tested different cell structures (homogeneous or coated cells) and shapes (spheres and spheroids). Their work showed that absorption was poorly influenced by the cell geometry and shape, depending mainly on the particle size and refractive index. Their conclusions thus confirmed previous published results [1, 27]. They also demonstrated that scattering properties (scattering efficiency) remained correctly approximated by the spherical case if the algal cell shape was not to different from a sphere: in particular, Aas [1] found that the scattering cross sections by thin disks or long cylinders were different from those of equal-volume spheres with a ratio 0.76 when the length:diameter ratio reaches 10. The backscattering properties were shown to be more significantly affected by cell shape. The work of Quirantes et al. [43] justified the use of Aden-Kreker coated sphere model as a good approximation for the modelling of scattering, extinction and absorption coefficients for phytoplankton cells presenting geometry that does not differ too much from a sphere. Kitchen et al. [27] performed theoretical scattering and absorption coefficient computations on a model consisting of three concentric spheres, using extended Mie theory. They observed that including the internal structure in the model produced more realistic extinction coefficient spectra and volume scattering functions than a simplistic homogeneous model. Another advantage of the multilayered sphere model is that there is no need to estimate the complex refractive index of one entire algal cell, which is awkward. Indeed, only the refractive index of the successive layers, seen as raw materials, need to be defined. In practice, the resulting refractive index of the entire algal cell is not known, but taken into account in the Mie calculations. Based on those results, and aware of the quasi-spherical shape hypothesis implied, we have chosen to implement the Aden-Kreker coated sphere model in this study in order to simulate the optical properties of real algal cells. The next section details how we have implemented the multi-layered sphere modelling of the algal cells in practice: we developed in particular a simulation program called *AlgaSim*.

3.2 Description of *AlgaSim*

For this thesis, a simulation program named *AlgaSim* was developed and run with MatLab (R2009a) in order to model a single algal cell described by its chemical and physical parameters, and to simulate its spectral absorption (C_{abs}), scattering (C_{sca}) and extinction (C_{ext}) cross sections. In the following paragraphs we detail the multi-layered sphere model used to describe an algal cell. We then describe the operations implemented by the program, first to determine the physical structure, and then to retrieve the refractive index of each layer from input data about the physiological state of the cell.

3.2.1 Description of the three-layer model

Individual algal cells were modeled according to the description shown on figure 3.2. They are designed as a sphere composed of three concentric layers of different materials representing the main organic substances encountered in the organelles of an algal cell. According to litterature, the major constituents of a micro algal cell are water, proteins, carbohydrates and fats [2, 12]. Even if the photopigments content is small, they can be considered as the only significantly absorbing specie of the cell [39, 2] and are responsible for the major part of its absorption properties.

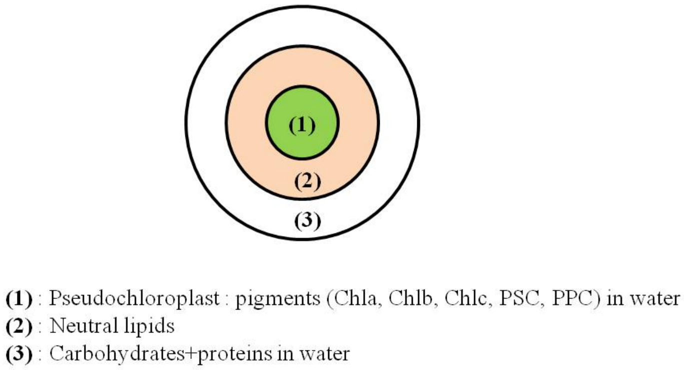

Figure 3.2: Structure of the virtual algal cell modeled as a sphere composed of successive concentric layers of organic materials.

In a real cell, the photopigments are embedded inside the chloroplasts and are not evenly distributed. This discrete distribution of the absorbing specie within the surrounding medium has been well described by Kirk [24] and is highly influential with the light absorption and scattering properties that can be effectively observed. It generates phenomena known as the packaging effect which results in the "flattening" of the absorption spectrum compared to what could be expected if the pigments were simply homogeneously dissolved within the cell. This justifies the choice we made to mime the embedding of the absorbing species within compartmentalized organelles by reproducing a multi-layered structure. The successive non-absorbing layers of carbohydrates-proteins and fat were implemented in order to model the internal structure of an algal cell in an accurate way from the light interaction point of view. The outer layer was considered to be a mixture of carbohydrates and proteins with a non-negligible amount of water. The pigmented part of the cell was thus modeled by a colored layered, called pseudo-chloroplast with reference to Mueller's work [39], composed of dissolved photopigments inside water. Following the work of Bidigare et al. [8], we chose to take into account chlorophyll a (Chla), chlorophyll b (Chlb), chlorophyll c1+2 (Chlc), photosynthetic carotenoids (PSC) and photoprotective carotenoids (PPC), which constitute the major algal pigments groups that can be found in microalgae. The successive order of the layers has been chosen with a concern to remain as plausible as possible, within the limitation imposed by the simplicity of our model compared to a real phytoplankton cell organization: the carbohydrate-proteins and lipidic layers represent a membrane-like structure, while the pigmented pseudochloroplast is embedded in a core layer. It has to be noted that in a first approximation, we considered that the lipid layer represented the neutral lipids that would be stored by the cells in a stress situation. The neutral lipids are currently particularly studied as they have been identified as a possible source of biofuels [54].

3.2.2 Overview of the computational method implemented

The *AlgaSim* simulation program was implemented and run with MatLab (R2009a). Figure 3.3 illustrates the main steps of the program computations. *AlgaSim* program models the algal cell from the biochemical input parameters characterizing its state: it calculates for each layer the size parameter x_l and the complex refractive index N_l. Those parameters are then used by the Mie calculation program *Scattnlay*, developed by Peña et al. [40], which computes the optical efficiencies Q_{abs}, Q_{sca} and Q_{ext} of the algal cell. The corresponding optical cross sections C_{abs}, C_{sca} and C_{ext} of the cell are deduced from the optical effciencies with relations (3.4) to (3.6). It has to be noted that the calculation of C_{abs}, C_{sca} and C_{ext} is repeated for each wavelength λ.

Table 3.1 precises the variable and fixed input parameters that can be ajusted in *AlgaSim*. The program was implemented with a view to remaining as flexible as possible for the definition of the physical and chemical characteristics of the cells. This was done in particular in order to simulate a wide range of different algal cells.

Table 3.1: List of the input parameters for *AlgaSim*.

	Variables	
R_{cell}	Total radius of the cell	μm
M_{dry}	Total dry mass of the cell	pg
p_{fat}	Massic proportion of lipids	% of cell dry mass
p_{carbo}	Massic proportion of carbohydrates	% of cell dry mass
p_{prot}	Massic proportion of proteins	% of cell dry mass
$p_{pig,tot}$	Massic proportion of pigments	% of cell dry mass
$Chla$	Massic proportion of Chla	% of total pigment mass
$Chlb$	Massic proportion of Chlb	% of total pigment mass
$Chlc$	Massic proportion of Chlc	% of total pigment mass
PSC	Massic proportion of PSC	% of total pigment mass
PPC	Massic proportion of PPC	% of total pigment mass
	Fixed data	
ρ_{fat}	Specific gravity of lipids	-
ρ_{carbo}	Specific gravity of carbohydrates	-
ρ_{prot}	Specific gravity of proteins	-
$\rho_{pig,i}$	Specific gravity of pigment i	-
$a^*_{pig,i,Bidigare}$	Specific absorption coefficient of pigment i as measured by Bidigare et al. [8]	m^2mg^{-1}
n_{carbo}	Real refractive index of carbohydrates	-
n_{prot}	Real refractive index of proteins	-
n_m	Real refractive index of the host medium (here water)	-

Table 3.2: List of the output parameters for *AlgaSim*.

C_{abs}	Absorption cross section of the cell	m^2
C_{sca}	Scattering cross section of the cell	m^2
C_{ext}	Extinction cross section of the cell	m^2

Table 3.3: List of the input parameters for *Scattnlay*.

x_l	Size parameter of the l^{th} layer	-
N'_l	Relative refractive index of the l^{th} layer	-

Table 3.4: List of the output parameters for *Scattnlay*.

Q_{abs}	Absorption efficiency of the cell	-
Q_{sca}	Scattering efficiency of the cell	-
Q_{ext}	Extinction efficiency of the cell	-

In the next sections we will described each successive step. Section 3.2.3 describes the method implemented to determine the physical structure of the cell. Section 3.2.4 details how the refractive indices of each layer were calculated. Section 3.2.5 gives information about the *Scattnlay* program achieving the calculation of the scattering properties of the modelled multi-layer algal cell.

3.2.3 Modelling the physical structure of the cell

With a view to simplification and ease of use, the parameters needed to generate the cell structure have been reduced to minimum, as shown on figure 3.4.

Finally, only the cell total radius R_{cell} and dry mass $M_{dry,cell}$ and the massic percentage p_{fat} and specific gravity ρ_{fat} of lipids are required to generate a cell. The total cell volume $Vol_{cell,tot}$ is calculated from the radius R_{cell} with the following relation:

$$Vol_{cell} = \frac{4}{3}\pi R_{cell}^3$$

The volumic proportion of the pseudo-chloroplast layer has been fixed to 85% corresponding to the proportion of water generally observed in algal cells[2]. The volume Vol_1 of the core layer is thus determined as:

$$Vol_1 = 0.85 \times Vol_{cell}$$

The neutral lipids layer volume is deduced from the massic percentage p_{fat} and specific gravity ρ_{fat} such that:

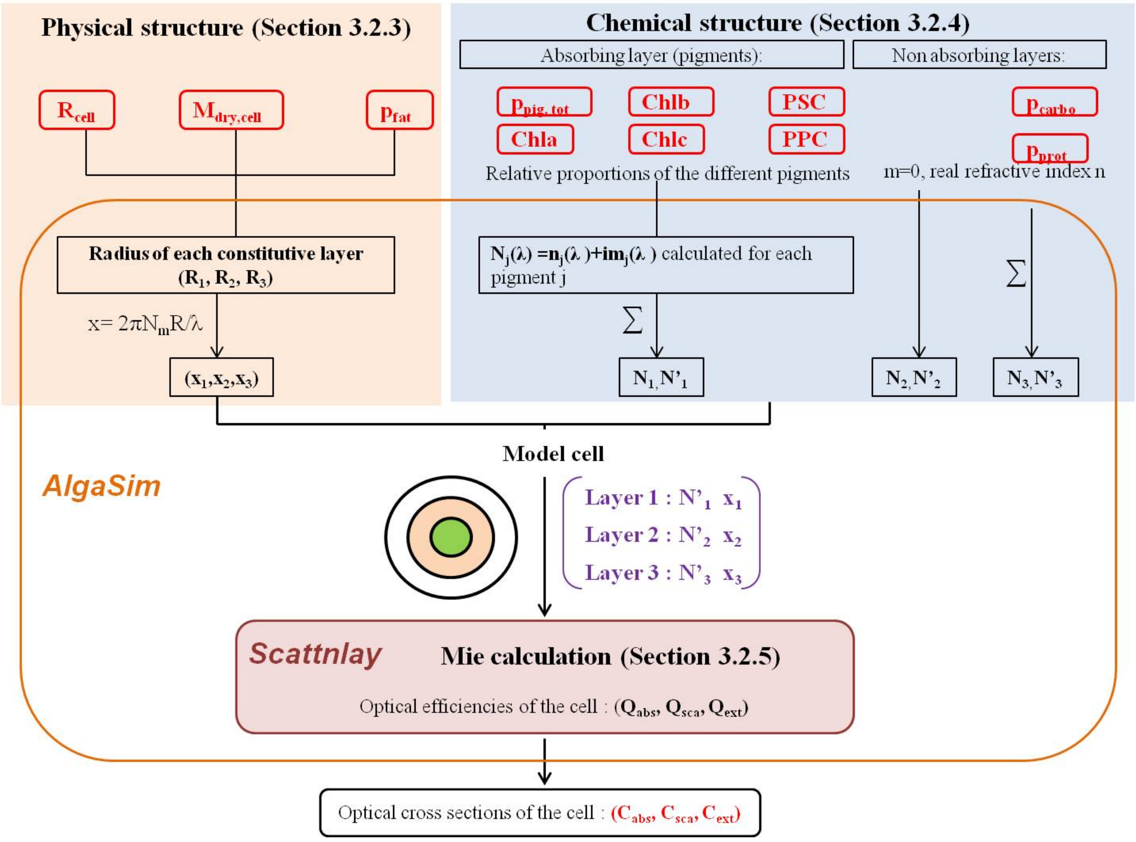

Figure 3.3: Overview of the *AlgaSim* program structure. Note that only the variable input parameters are represented.

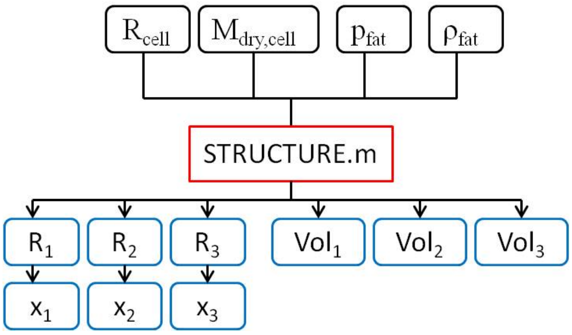

Figure 3.4: Simplified flow chart: generation of the cell structure.

$$Vol_2 = \frac{M_{dry,cell} \times p_{fat}}{\rho_{fat}}$$

The final proteins-carbohydrate layer volume is thus deduced from the above:

$$Vol_3 = V_{cell,tot} - Vol_1 - Vol_2$$

If the resulting volume is null or of negative value, an error message is displayed.

Once the successive volumes have been determined, the radius r_l of the l^{th} layer (see figure 3.5) can be deduced such that:

$$r_{l+1} = \sqrt[3]{\frac{3}{4\pi} V_{l+1} + r_l^3}$$

From the values computed for the radius of each layer r_l, the real refractive index n_m of the host medium (here water) and the wavelength of the incident wave in vacuum λ, the parameter x_l is deduced such that:

$$x_l = 2\pi n_m \frac{r_l}{\lambda} \tag{3.12}$$

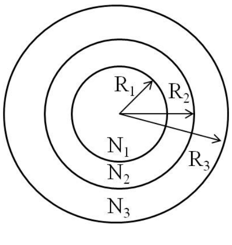

Figure 3.5: Principle of the generation of each layer.

These computations make it possible to give the size parameter x of each layer, which determines the physical structure of the model cell.

3.2.4 Modelling the chemical structure of the cell

Once the physical parameter x is determined, it is necessary to compute the refractive index N for each layer. For this purpose, two methods are implemented if the layer is absorbing or not. In the following paragraphs we first detail the calculation of the real refractive index of the non-absorbing layers (layer 2 and 3). Second, we explain the computation of the complex refractive index of the absorbing pseudo-chloroplast layer. For this purpose we used in particular the Kramers-Kronig relations [30].

Calculation of the refractive indices of the non-absorbing layers (layers 2 and 3)

The refractive indices of the non-absorbing layers were considered as real [39], which means that the imaginary part m_2 and m_3 of N_2 and N_3 are null. The spectral index of lipids, carbohydrate and proteins were obtained on the web. As layer 2 is considered as made of pure lipids, the real refractive index N_2 of the neutral lipid layer corresponds to that of the pure material. However, layer 3 is a mixture of carbohydrate, proteins and water. The resulting real refractive index N_3 of the layer must thus be calculated according to the equation of Gladstone and Dale [18]:

$$N_3 = \frac{Vol_{carbo}}{Vol_3} n_{carbo} + \frac{Vol_{prot}}{Vol_3} n_{prot} + \frac{Vol_3 - Vol_{prot} - Vol_{carbo}}{Vol_3} n_{water} \tag{3.13}$$

With n_{water} the refractive index of water, and Vol_{carbo} and Vol_{prot} the occupied volumes by carbohydrates and proteins respectively, expressed from the massic proportions p_{carbo} and p_{prot}, the total cell dry mass $M_{dry,cell}$ and the specific gravities ρ_{carbo} and ρ_{prot} such that:

$$Vol_{carbo} = \frac{p_{carbo} \times M_{dry,cell}}{\rho_{carbo}}$$

$$Vol_{prot} = \frac{p_{prot} \times M_{dry,cell}}{\rho_{prot}}$$

From the values of N_2 and N_3, the relative refractive indices N'_2 and N'_3 are calculated following the relation:

$$N'_l = \frac{N_l}{n_m} \tag{3.14}$$

Where n_m and N_l are the refractive index of the medium outside the particle (here water) and of its l^{th} component respectively.

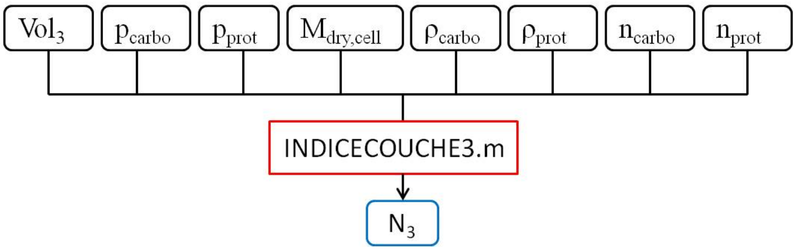

Figure 3.6: Simplified flow chart: calculation of the refractive index of the outer layer.

Calculation of the refractive index of the absorbing layer

The absorbing layer containing the photopigments requires some extra considerations. Following the principle of Mueller [39], the pigmented layer is supposed to be composed of the cell photopigments dissolved inside water: the pseudochloroplast volume is thus mainly determined by the water content of the cell. The resulting complex refractive index $N_1 = n_1 + im_1$ of the layer must be calculated from the complex refractive index of all the pure photopigments, which are present in various proportions. To the state of our knowledge, there is no available database giving directly the *in vivo* values of the complex refractive index of the main algal photopigments on the VIS-NIR spectral range. However, reference measurements of the pigments specific absorption coefficients a_j^* of the *in vivo* main phytoplanktonic photopigments on the [400-750 nm] spectral range were performed by Bidigare at al. [8]. Those data were used to retrieve the imaginary part of the refractive index of the photopigments. The real part of the refractive index was thus deduced from the imaginary part thanks to the Kramers-Kronig relations [30].

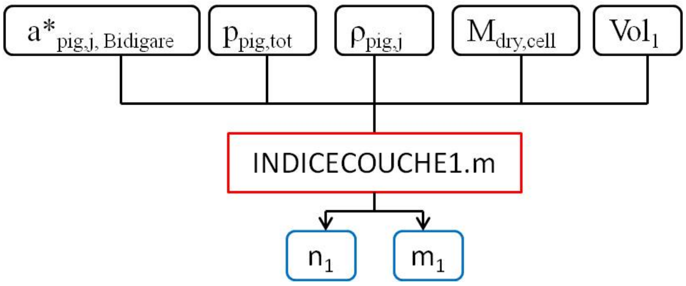

Figure 3.7: Simplified flow chart: calculation of the complex refractive index $N_1 = n_1 + im_1$ of the pseudo-chloroplast layer. $a*_{pig,j,Bidigare}$ is the specific absorption coefficient of pigment j as measured by Bidigare et al. [8].

Kramers-Kronig equations

A more complete definition of the complex refractive index of a medium has been provided in appendix B. In this part we only give the formulation of the Kramers-Kronig equations linking the real and imaginary parts of the refractive index of a medium. The Kramers-Kronig relations formulate the fundamental interdependence of the in-phase and the out-of-phase responses of a material to a sinusoidal time-varying external perturbation, such as incident light. The real and imaginary parts of the complex refractive index, denoted as n and m respectively, are thus connected by the following relations:

$$n(\omega) - n(\omega_\infty) = \frac{2}{\pi} P \int_0^\infty \frac{\omega' m(\omega')}{\omega'^2 - \omega^2} d\omega' \tag{3.15}$$

$$m(\omega) = \frac{-2\omega}{\pi} P \int_0^\infty \frac{n(\omega' - 1)}{\omega'^2 - \omega^2} d\omega' \tag{3.16}$$

Where ω is the pulsation of the electromagnetic field, directly linked to the wavelength λ and the celerity c by the simple relation: $\omega = 2\pi c/\lambda$. $n(\omega_\infty)$ is the real part of the refractive index at a frequency where the absorption m is negligible. P stands for the Cauchy principal value which makes it possible to assign values to the integral despite the singularities of the integrand. The complete establishment of the Kramers-Kronig (K-K) relations from Maxwell constitutive laws can be found in [30].

The Kramers-Kronig relations rigorously describe the relations between the real and imaginary parts of the refractive index, by formulating the fundamental interdependency of those two quantities. However, our work could be considered as original by taking them into account. Indeed, especially in the field of applied spectroscopy, the Kramers-Kronig relations are often ignored. It is thus common to see research works where the real and imaginary parts of the refractive index are assumed to be unconnected. This assumption erases the effects due to the interdependency of n and m, in particular in the spectral domain of the strong absorption bands. From this originate absorption and scattering models where the two quantities seem to be spectrally independent. This might unfortunately introduce confusion in the research community, by propagating inaccurate representation of the absorption and scattering spectra, in particular by suggesting that the latter does not show "humps" in the vicinity of high absorption bands.

Application to the calculation of the refractive index of the photopigments

The complex refractive index of each pure pigment was deduced from the reference measurements of the pigments absorption coefficients given in [8]. After chemical extraction and separation of the photopigments present in samples of marine phytoplanktonic waters, Bidigare et al. performed a spectrometric measurement of the absorption coefficients of each *ex vivo* pigment. From those measurements, the *in vivo* specific aborption spectra a_j^*, expressed in $m^2.mg^{-1}$, were generated by taking into account the wavelength shifts between *ex vivo* and *in vivo* pigments. For simplicity, pigments were classified into five major groups: Chla (Chlorophyll a equivalents, including chlorophyll a, divinyl chlorophyll a, chlorophyllide a and chlorophyll a'), Chlb (Chlorophyll b), Chlc (Chlorophyll c equivalents, including chlorophylls c_{1+2}, chlorophyll c_3 and Mg 2,4-D), PSC (photosynthetically active carotenoids including fucoxanthin, peridinin and prasinoxanthin) and PPS (photoprotectant carotenoids, including diadinoxanthin, alloxanthin, zeaxanthin and β,β-carotene). From a_j^* the imaginary part m_j of the complex refractive index of pigment j present in the core layer with a concentration c_j can be obtained thanks to the following relation [28]:

$$m_j(\lambda) = \frac{\lambda a_j^*(\lambda)}{4\pi} c_j \tag{3.17}$$

With c_j the concentration of pigment j expressed in $mg.m^{-3}$ such that:

$$c_j = \frac{\%pig_j \times p_{pig,tot} \times M_{dry,cell}}{Vol_1}$$

With $\%pig_j$ the massic proportion of pigment j compared to the total pigment dry mass, $p_{pig,tot}$ the massic proportion of total pigment compared to the cell dry mass $M_{dry,cell}$, and Vol_1 the volume of the pseudochloroplast layer. The real part n_j of the refractive index of the pigments can thus be obtained from m_j with relation (3.15), by setting the values $n(\omega_\infty)$ to the values given in [2], and presented in table 3.5. Figure 3.8 shows the imaginary part m and the real part n of the refractive index of each pure photopigments derived from the reference measurements of Bidigare et al., for an theoretical example where the concentrations of each pigment is set to $1.10^7 mg.m^{-3}$.

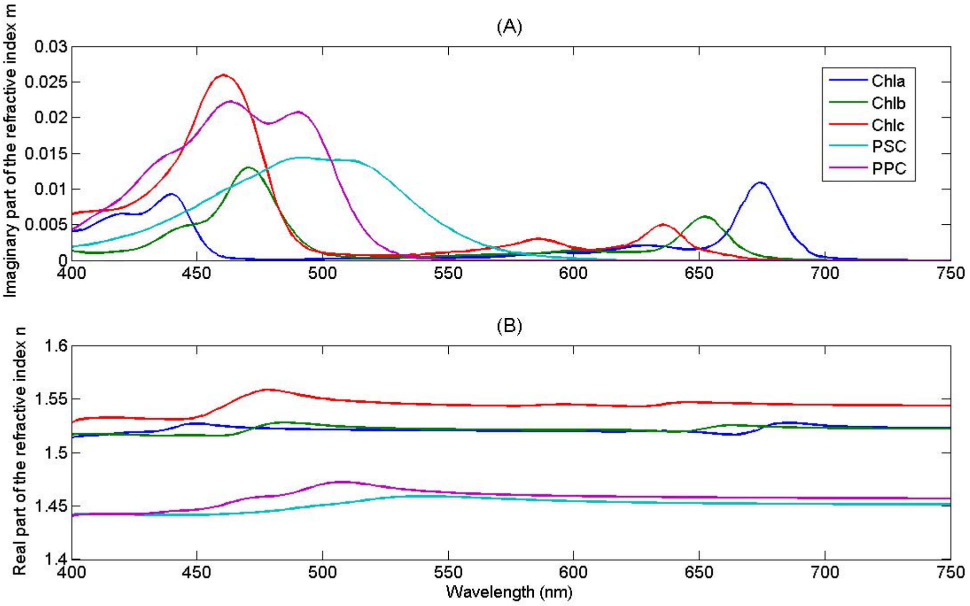

Figure 3.8: Imaginary (A) and real (B) part of the refractive index of each pure photopigment derived from the specific absorption coefficients a_j^* from [8], for a pigment concentration $c_j = 1.10^7 mg.m^{-3}$ inside the chloroplast.

The total resulting complex refractive index N_1 of the total layer is then calculated with the following method: the total imaginary part m_1 is calculated as the sum of the imaginary parts m_j of all the pigments:

$$m_1 = \sum_{j=1}^{5} m_j \tag{3.18}$$

Please note that in equation (3.18), the m_j are not weighted by the pigment concentration c_j because the influence of the quantity c_j has already been included in the very definition of m_j, as shown by equation (3.17). This choice was made on purpose. Our approach was motivated by the fact that it seemed physically meaningless to express the absorption of a substance without any idea about the actual quantity that was considered. In our sense, and in our modelling, the refractive index of a quantity c_1 of a given pigment is not the same as the one of a quantity $2 \times c_1$ of the same pigment. This point may surely be discussed and may depend on the exact definition given to the refractive idex of a substance. Nevertheless, we noted that our approach made it possible to obtain refractive indices showing the expected orders of magnitude regarding litterature, which validated our method.

The real part n_1 is then retrieved from m_1 by using equation (3.15) and by setting the value of $n_1(\omega_\infty)$ such that:

$$n_1(\omega_\infty) = \sum_{j=1}^{5} \frac{c_j}{\rho_j} n_j(\omega_\infty) \tag{3.19}$$

Where ρ_j is the density of pigment j in $mg.m^{-3}$, taken from [2], and presented in table 3.5.

The relative refractive index N_1' of the absorbing layer is then deduced from $N_1 = n_1 + im_1$ thanks to equation (3.14).

Table 3.5: Real refractive index and density of the different pure photopigments [2].

Pigment	Refractive index $n(\omega_\infty)$ @ 589 nm	Density ($10^9 mg.m^{-3}$)
Chla	1,520	1.11
Chlb	1,520	1.13
Chlc	1,540	1.31
PSC	1,448	1.06
PPC	1,453	1

3.2.5 Mie calculation for the determination of the scattering properties of a multi-layer sphere: the *Scattnlay* program

Once the size parameter x and the refractive index N of each layer have been determined, the Mie calculations can be implemented.

Overview of the Mie equations for the multilayered sphere

In this section we give some details about the mathematical formulation of Aden-Kerker for the determination of the scattering properties of an example three layer sphere [39]. The aim of this section is to illustrate briefly the kind of equations on which relies the use of Mie theory formulated for a multilayered sphere. In this thesis the Mie equations were only used as a practical tools.

Following Kerker formulation [23], at each j^{th} wavelength, the extinction and scattering cross sections of the particle may be expressed directly from the coefficients a_{nj} and b_{nj}, called the Mie coefficients:

$$C_{ext,j} = \frac{2}{x_3^2}\sum_{n=1}^{\infty}(2n+1)[Re(a_{nj}+b_{nj})] \tag{3.20}$$

$$C_{sca,j} = \frac{2}{x_3^2}\sum_{n=1}^{\infty}(2n+1)[|a_{nj}|^2+|b_{nj}|^2] \tag{3.21}$$

The absorption cross section can then be derived using relation (6.13). Equations (3.20) and (3.21) are equally applicable to homogeneous and concentrically stratified spheres. The two cases differ on the computation of Mie coefficients a_{nj} and b_{nj}. For the case of a three-layered sphere, a_{nj} and b_{nj} are functions of the particle layer outer radii (r_1, r_2, r_3) and refractive indices $N_{l,j} = n_{lj} + im_{lj}$, with $l = 1, 2, 3$, such that:

$$a_{nj} = \frac{|A|_{nj}}{|B|_{nj}} \tag{3.22}$$

$$b_{nj} = \frac{|C|_{nj}}{|D|_{nj}} \tag{3.23}$$

The determinants $|A|_{nj}, |B|_{nj}, |C|_{nj}$ and $|D|_{nj}$ are defined such that:

$$|A|_{nj} = \left| \begin{array}{cccccc} \psi_n'(kN_1r_1) & \psi_n'(kN_2r_1) & \chi_n'(kN_2r_1) & 0 & 0 & 0 \\ N_1\psi_n(kN_1r_1) & N_2\psi_n(kN_2r_1) & N_2\chi_n(kN_2r_1) & 0 & 0 & 0 \\ 0 & \psi_n'(kN_2r_2) & \chi_n'(kN_2r_2) & \psi_n'(kN_3r_2) & \chi_n'(kN_3r_2) & 0 \\ 0 & N_2\psi_n(kN_2r_2) & N_2\chi_n(kN_2r_2) & N_3\psi_n(kN_3r_3) & N_3\chi_n(kN_3r_2) & 0 \\ 0 & 0 & 0 & \psi_n'(kN_3r_3) & \chi_n'(kN_3r_3) & \psi_n'(kr_3) \\ 0 & 0 & 0 & N_3\psi_n(kN_3r_3) & N_3\chi_n(kN_3r_3) & \psi_n(kr_3) \end{array} \right|_j \tag{3.24}$$

Where k is the propagation constant of the medium containing the cell.

$|B|_{nj}$ is obtained by substituting $\zeta_n'(r_3)$ for $\psi_n'(r_3)$ and $\zeta_n(r_3)$ for $\psi_n(r_3)$ in expression (3.24). $|C|_{nj}$ is obtained by raising the refractive indices N_l, $l = 1, 2, 3$ one row from what they are in expression (3.24). $|D|_{nj}$ is obtained by substituting $\zeta_n'(r_3)$ for $\psi_n'(r_3)$ and $\zeta_n(r_3)$ for $\psi_n(r_3)$ in the expression of $|C|_{np}$.

The functions ψ_n and χ_n are the Ricatti-Bessel functions defined as [3]:

$$\psi_n(kNr) = (\frac{1}{2}\pi kNr)^{(1/2)} J_{n+\frac{1}{2}}(kNr) \tag{3.25}$$

$$\chi_n(kNr) = (\frac{1}{2}\pi kNr)^{(1/2)} N_{n+\frac{1}{2}}(kNr) \tag{3.26}$$

Where $J_{n+\frac{1}{2}}$ and $N_{n+\frac{1}{2}}$ are the half integral order Bessel and Neumann functions respectively. The Hankel functions ζ_n are such that:

$$\zeta_n(kNr) = \psi_n(kNr) + i\chi_n(kNr) \tag{3.27}$$

Primes stand for differentiation with respect to the argument.

Choosing a computational algorithm for light scattering by a multilayered sphere

In practice, the implementation of the calculation of the Mie coefficients a_{np} and b_{np} may be achieved by a computational algorithm. However, solving equations (3.22) and (3.23) is not a trivial issue as numerical problems may arise. It is a complex subject that has been investigated by many works [50, 7, 31, 52, 20]. The problem is within the scope of computer science, and several ready-to-use programs are made publicly available for application use. Nevertheless care must be taken in choosing the algorithm among the available ones, as it appears that they generally have very limited operation ranges. The expression of the Mie coefficients involves several numerical difficulties which make most existing algorithms inapplicable to several cases [40], being limited in the possible particle size range, number of layers or values of the refractive indices.

In this work we chose to use the algorithm developed by Peña et al. [40], using the formulation proposed by Yang [53], and working with the program named *Scattnlay*. The input parameters required are the size parameter x_l and the relative refractive index N'_l of each layer as defined respectively by equation (3.12) and (3.14). The algorithm was proved to be accurate for a wide range of size parameters and high refractive indices.

In our case, the *Scattnlay* program was integrated within the general *AlgaSim* program: as already explained, the parameters x_l and N'_l were calculated for each layer by the *AlgaSim* program, depending on the description of the model algal cell as explained in the previous sections, and were given as input parameters to the *Scattnlay* program which calculates the corresponding absorption, scattering and extinction efficiencies Q_{abs}, Q_{sca} and Q_{ext}.

From the optical efficiencies, the optical cross sections C_i were deduced by *AlgaSim* by using equations (3.4) to (3.6) and by taking $\Sigma = \pi R_{cell}^2$.

3.2.6 Preliminary validation: comparison to litterature

Some test simulations have been implemented to make a primary validation of the *AlgaSim* program. Those first tests aimed at checking the program running, and if the simulated cross section spectra presented the expected shape and order of magnitude. Available litterature reporting optical cross section spectra for single algal cells remain quite limited. Spectra measured on algal media can be found, however they may not be directly comparable to *AlgaSim* simulations because of several points: the first problem is that a few works present a thourough characterization of the measured cells (size and quantitative chemical composition) that would be necessary to properly simulate the spectra with *AlgaSim*. Generally, the characterization of the measured algal material is made by determining the size of the cells with optical microscopy sometimes coupled with image analysis [22, 28], but the chemical composition is rarely reported, if ever measured. Another issue is that the measurement of the optical properties is achieved not for a single algal cell, but for a bulk algal media containing thousands of different cells. This means that the litteratue data and the ones simulated with *AlgaSim* do not represent the same scale of description, as implied in the approach of this thesis. We will see in Chapter 4 how to switch from those different scales, however it is beyond the scope of the present Chapter. That is why we chose here to compare with Mueller's work, which seemed to be the more comparable to our situation.

.

Comparison to Mueller simulation of a single cell [39]

Mueller's work [39] was found to be an interesting reference as it gives cross section spectra simulated for a single algal cell of known size and pigment composition. Mueller developed his own simulation programm also based on a three-layer sphere model and Aden-Kerker theory. However, contrary to *AlgaSim* his model did not allow to change the physical and chemical states of the model algal cells: those characteristics were fixed. More precisely, Mueller did not link the size parameter x and the refractive index N of the successive layers to meaningful quantities such as the pigment composition and quantity and the massic proportions of organic materials. He chose to implement mean plausible values of x and N taken from litterature without any intention to go further in the physiological meaning beyond them. That is why our *AlgaSim* program differs from Mueller's model, as it was designed on the contrary to investigate the influence of the physiology of the cells on their spectral properties.

The example case of the 5-μm radius algal cell presented in [39] was reproduced with *AlgaSim*. The cell size and pigment composition were taken as described in [39]. The proportions of carbohydrate, proteins and lipids, as not stated in Mueller's model, were set to classically observed values (cf section 3.3.1 for more details). The absorption, scattering and extinction cross section spectra were obtained with *AlgaSim* on the [400-750 nm] spectral range, and are shown in figure 3.9. Figure 3.9 should thus be compared to figure 4.6. from [39] (p 125), that is reproduced on figure 3.10 here.

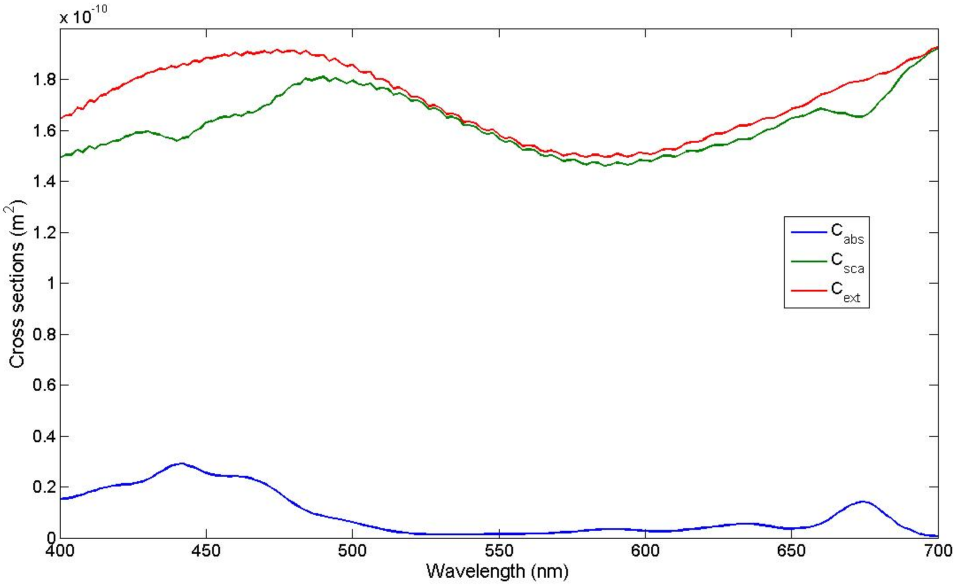

Figure 3.9: Spectra of absorption, scattering and extinction cross sections for a single three-layered algal cell of 5 μm outer radius, with a pigment composition similar to the one taken by Mueller [39].

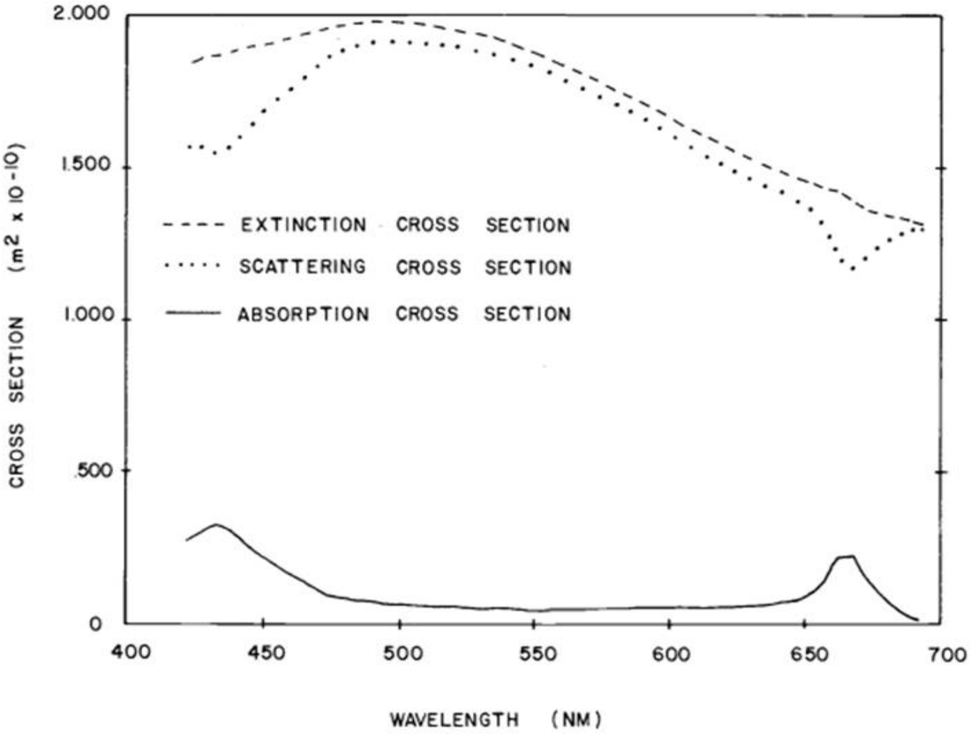

Figure 3.10: Spectra of absorption, scattering and extinction cross sections for a single three-layered algal cell of 5 μm outer radius by Mueller [39].

The absorption cross section spectrum obtained with *AlgaSim* shows values that vary between 0 and around 3.10^{-11} m^2 over the [400-700 nm] spectral range. The scattering and extinction cross sections present higher values, ranging between $1,5.10^{-10}$ and $1,9.10^{-10}$ m^2 over the considered spectral range. Those orders of magnitude notably concur with the ones presented by Mueller.

The absorption cross section spectrum presents absorption peaks in the [400-480 nm] and [650-690 nm] ranges that match those observed in [39]. Figure 3.9 shows that scattering cross section spectrum presents dips in the spectral regions of the abovementioned main absorption bands, as well as a general wave shape with high values around 500 nm, decreasing for the upper wavelengths until increasing again above 600 nm. The extinction cross section spectrum has the same general shape than the scattering cross section spectrum, but the dips in the absorption bands have disappeared.

The dip shapes in the main absorption bands on the scattering sepctrum are also clearly visible on Mueller's work. The general shape of the scattering cross section spectrum also matches, except the final increase around 600 nm that is not shown on Mueller's spectrum. As what can be observed in our simulated spectra, the extinction spectrum is very similar in shape to the scattering spectrum but does not present the dip shapes in the absorption bands.

Conclusion on the preliminary test of *AlgaSim*

This first comparison of the optical cross section spectra simulated with *AlgaSim* for one single algal cell to the results of Mueller validates the general running of the program, and shows that the results present good agreement with Mueller's. The quantitative values obtained completely concur with Mueller's findings. The general shape of the absorption cross section spectrum also seems to match. The general shapes of the scattering and extinction cross sections appear to be similar as well, except at wavelength above 600 nm where our simulations increase while Mueller's decrease with increasing wavelength. However we can observe the same absorption-band patterns on the scattering spectrum on both simulations. This seems to confirm in a first time that the simulations obtained with *AlgaSim* are as good as other reference models developed elsewhere.

Now that the general running of the *AlgaSim* program had been proved, we wanted to investigate more thouroughly the very physiological meaning of the simulated cross sections spectra. That is why we implemented another test of *AlgaSim*: by simulating and analysing large databases of optical cross sections spectra, the dependency of the spectra shapes on the physical and chemical characteristics of the algal cell has been studied, and compared to what has been reported in litterature. The next sections thus describes the method implemented, as well as the results obtained.

3.3 Study of the impact of the cell characteristics on the simulated spectra

The *AlgaSim* program was tested by applying a data analysis method to simulated databases of spectra of algal cells of known chemical and physical characteristics. This work aimed first at comparing the results found with *AlgaSim* to the trends expected considering litterature, and second at giving preliminary keys for the interpretation of the simulated spectra, atempting to link the general shape of the spectra to rough conclusions about the algal cells states.

3.3.1 Method

Variation of the physical and chemical parameters: generation of spectral databases

As explained above and summed up by table 3.1, the composition of the simulated algal cell can be varied with *AlgaSim* by adjusting 11 main different parameters. In this preliminary investigation we chose to variate a reduced set of parameters in order to limit the size of the databases and the time needed for data processing. The cell size and dry weight, the pigment composition (total pigment quantity and relative proportions of each pigment group) and the proportion of lipids were finally kept as variables, since their influence on the optical properties were expected to be significant [15, 1, 27, 11]. The proportions of carbohydrates and proteins however were set to fixed values. In order to remain in the case of plausible, living algal cells, care must be taken in fixing the values of the descriptive parameters.

The reign of microalgae is very wide and includes species that have extremely different physical characteristics. Hence the algal cell diameter can vary from 0,5 μm to values as high as 160 μm [46]. A classification of phytoplanktonic cells has been proposed in particular by Ciotti et al. [15]: picoplankton for the algal cells with diameters between 0,5 and 2 μm, ultraplankton between 2 and 5 μm, nanoplankton between 5 and 20 μm and microplankton for diameters above 20 μm. However we found that most of the previous works and experiments aiming at analysing the optical properties of algal cells dealt with species which diameter size ranged between 1 and 20 μm [44, 9, 28, 22, 39]. In order to remain in comparable conditions and in a first step, we thus decided to simulate algal cells with a diameter belonging to that reduced range.

The range of variation of the cell dry weight was determined from the work of Brown et al. [12] on the determination of the biochemical composition of several algal species commonly encountered in mariculture: we thus chose to consider dry weights between 5 and 50 pg/cell.

According to Aas [2], the massic proportion of total pigments generally varies from about 1 to 10% of the cell dry weight. The proportions of the different pigment groups were expressed relatively to the total pigment dry weight. The ranges of variation were chosen based on the observations reported in [8], and are summarized in table 3.6.

For algal cells grown in normal conditions, the total neutral lipids proportion generally varies from 8.5 to about 20% of total dry weight [12]. However in some applications such as biofuels production [14], reaching up to 50% of the dry weight has been evoked as a possible goal, even if this seems very ambitious given the current state of the art. In order to investigate whether such a high neutral lipids composition could affect the optical properties of the algal cells, we decided to take an extrapolated range for the proportion of lipids, between 1 to 50% of the cell dry weight.

As far as the fixed values taken for the proportion of carbohydrates and proteins are concerned, they were respectively set to 25% and 30% of the dry mass according to the orders of magnitude cited by Aas [2].

Table 3.6: Variation ranges of the algal cell parameters considered in this study.

Parameter	R_{cell}	$M_{dry,cell}$	p_{fat}	p_{carbo}	p_{prot}	$p_{pig,tot}$	Chla	Chlb	Chlc	PSC	PPC
Range	[0.5-10]	[5-50]	[1-50]	25	30	[5-10]	[10-80]	[5-25]	[1-10]	[0-80]	[1-10]
Unit	μm	pg	% of dry weight				% of total pigment dry weight				

Two databases, $Data_1$ and $Data_2$ were generated by discretely varying the parameters within the chosen variation ranges. Table 3.7 and table 3.8 sum up the values that were taken for each database. Database 1 was generated in order to investigate the influence of the rough structure of the cell. That is why the different cell material proportions were varied. However the pigment detailed composition (relative proportions of each pigment group) was set to a fixed value.

Database 2 was implemented in order to analyse the influence of the change of pigment composition on the simulated spectra: this time, the total pigment proportion was fixed while the relative proportions of the pigment groups were varied. The proportion of PSC was deduced from the other pigment values such that:

$$PSC = 1 - (Chla + Chlb + Chlc + PPC)$$

Table 3.7: Values taken by the variable parameters for Database 1.

Parameter	R_{cell} (μm)	$M_{dry,cell}$ (pg)	p_{fat}	$p_{pig,tot}$
Values	0.5	5	5	5
	2	16.25	16.25	6.25
	3.5	27.5	27.5	7.5
	5	38.75	38.75	8.75
	6.5	50	50	10

Table 3.8: Values taken by the variable parameters for Database 2.

Parameter	R_{cell} (μm)	$M_{dry,cell}$ (pg)	p_{fat}	Chla	Chlb	Chlc	PPC
Values	1.7	10	1	10	5	1	1
	4.4	30	20	50	15	5	5
	6.5	60	50	80	10	5	5

For each database, all the combinations of the variating parameters were first generated. The impossible cases, corresponding to negative outer layer volume Vol_3 or total pigment proportion sum not equal to 100% were removed from this initial set. Finally, 420 plausible individuals were generated for database 1, and 1342 for database 2. Those possible combinations were thus given as input parameters to *AlgaSim*, and the extinction, absorption and scattering cross sections were simulated for each individual on the [400-750 nm] spectral range (176 wavelengths). The matrices $\mathbf{C}_{abs,data1}$, $\mathbf{C}_{sca,data1}$, $\mathbf{C}_{ext,data1}$ of dimensions [420×176] and $\mathbf{C}_{abs,data2}$, $\mathbf{C}_{sca,data2}$, $\mathbf{C}_{ext,data2}$ of dimensions [1342×176] were thus generated. The structure of those matrices is presented by figure 3.11. The simulated matrices present a high dimensionality which makes them hard to interprete as they are: a data processing technique is required, and we chose to apply the Principal Component Analysis.

Once the cross sections databases had been simulated, the idea was to analyze them. This was made in practice by implementing a Principal Component Analysis (PCA).

$$\begin{array}{cc} & \begin{array}{cccc} \lambda_1 & \lambda_2 & \dots & \lambda_{176} \end{array} \\ \begin{array}{c} \text{Cell n°1} \\ \text{Cell n°2} \\ \vdots \\ \text{Cell n°k} \end{array} & \begin{pmatrix} C_{1,1} & C_{1,2} & \dots & C_{1,176} \\ & & & \\ & & \vdots & \\ C_{k,1} & & \dots & C_{k,176} \end{pmatrix} \end{array}$$

Figure 3.11: Representation of the structure of the spectral cross sections matrices **C** simulated

Principal Component Analysis on the simulated spectral cross section matrices

Principal Component Analysis (PCA) is a multivariate data processing technique aiming at reducing the dimensionality of a data set consisting of a large number of interrelated variables, while retaining as much as possible of the variation present in the dataset [21, 32]. The basic idea is thus to transform the initial set of variables to a new one called the principal components (PCs) which are uncorrelated, and which are ordered so that the first few retain most of the variation present in all the original variables.

Let us consider that X is a vector of p random variables $(a_1, a_2, ...a_k, ...a_p)$ the correlations of which are of interest.

$$X = x_1 a_1 + x_2 a_2 + x_3 a_3 + ... + x_p a_p$$

Where x_k is the k^{th} coordinate of X in the basis $(a_1, a_2, ...a_k, ...a_p)$. PCA principle is to express X in another basis $(l_1, l_2, ...l_m)$ such that:

- $m \ll p$
- $\forall (i,j), l'_i l_j = 0$
- $\forall (i), l'_i l_i = 1$
- If Σ is the covariance matrix of the vector X, the vector l_k is such that $var[l'_k X] = l'_k \Sigma l_k = \lambda_k$, where λ_k is the k^{th} largest egeinvalue of Σ.

The vector X can thus be expressed in the new basis such that:

$$X = s_1 l_1 + s_2 l_2 + s_3 l_3 + ... + s_m l_m$$

The vectors l_k are called the loadings. The coordinates s_k of the vector X in the basis of the loadings are called the scores. The very structure of the loadings implies that most of variation of X is contained within the first loadings. That is why it is usual to study only the first few loadings, standing for at least 90% of the variance of the dataset X.

PCA was applied separately to the simulated spectral cross sections matrices, generated from database 1 ($C_{abs,data1}$, $C_{sca,data1}$, $C_{ext,data1}$) and generated from database 2 ($C_{abs,data2}$, $C_{sca,data2}$ and $C_{ext,data2}$). For each matrix, the loadings and the scores were determined. The correlation between the scores and the input parameters charaterizing the cells was thus calculated for each loading, in an atempt to link the observed variance to a physical or chemical information about the cell.

3.3.2 Results and discussion

In this section we present the results of the PCA applied on the absorption, scattering and extinction cross section spectra simulated from database 1 and database 2. The observations made for the scattering and extinction cross sections are similar for database 1 and database 2, that is why we chose to show only the figures obtained with database 1. However, it was found interesting to show the loadings obtained for the absorption cross section for both databases, as database 2 explores more precisely the influence of the pigment composition on the spectral shape.

PCA on the absorption cross section matrix $\mathbf{C}_{abs,data1}$

$99,85\%$ of the variance of $C_{abs,data1}$ is expressed by the first loading L_1. The three first loadings are kept as significant.

Loading 1 expressing a multiplicative effect

Figure 3.12 shows the first loading L_1 and the mean value $Mean(C_{abs})$ of the absorption cross section spectra. Please note that the spectra have no dimension and have been put to the same scale for clarity. It can be seen that the two spectra are very similar in absolute value: this means that the first loading expresses a multiplicative effect on the spectra, which implies that $99,85\%$ of the variance of C_{abs} is explained by a homothetic effect.

Table 3.9 shows the correlation between the cell parameters and the score S_1 associated to loading L_1. The closer to 1 the correlation between a parameter and the score S_1, the more influencial this parameter on the loading L_1.

Table 3.9: Correlation between the cell parameters and the score S_1 .

Parameter	R_{cell}	$M_{dry,cell}$	p_{fat}	$p_{pig,tot}$
Correlation with S_1	0.23	0.74	0.1	0.97

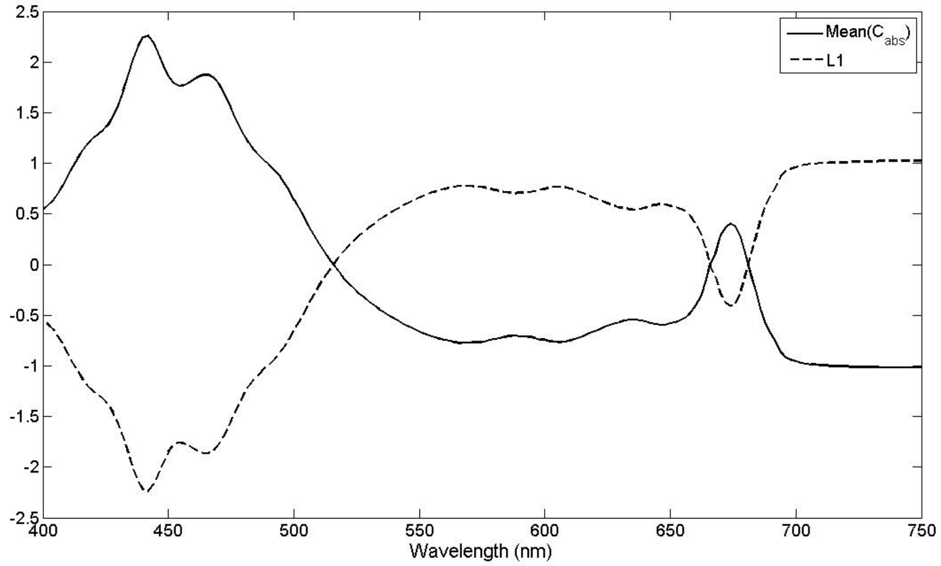

Figure 3.12: Loading L_1 and the mean value $Mean(C_{abs})$ of the absorption cross section spectra $\mathbf{C}_{abs,data1}$.

Table 3.9 shows that the first loading L_1 is highly correlated to the total pigment quantity in the cell. As it is a fraction of the total dry mass, we find also a good correlation with this parameter.
As expected, we observe that the total pigment quantity in the algal cell is the first parameter influencing the absorption spectrum. In particular, the pigment total quantity influences the general level (i.e. mean value) of the absorption spectrum.

Loading 2 expressing a balance between the main absorption peaks of Chla as well as a flattening of the absorption peak at 500 nm

Loading L_2 presents two humps with opposite signs respectively on the [410-480 nm] and [650-690 nm] ranges. This means that L_2 expresses an effect that modifies the peak height ratio between the two main absorption peaks of chlorophyll a. The negative hump on the [480-550 nm] indicates a flattening effect on the main absorption peak of Chla (at 420-480 nm).

Table 3.10: Correlation between the cell parameters and the score S_2 .

Parameter	R_{cell}	$M_{dry,cell}$	p_{fat}	$p_{pig,tot}$
Correlation with S_2	0.52	0.18	0.19	0.36

Table 3.10 shows that loading L_2 is mainly influenced by the size of the cell, and by the pigment proportion in a lesser extent. We are not surprised to find a strong correlation

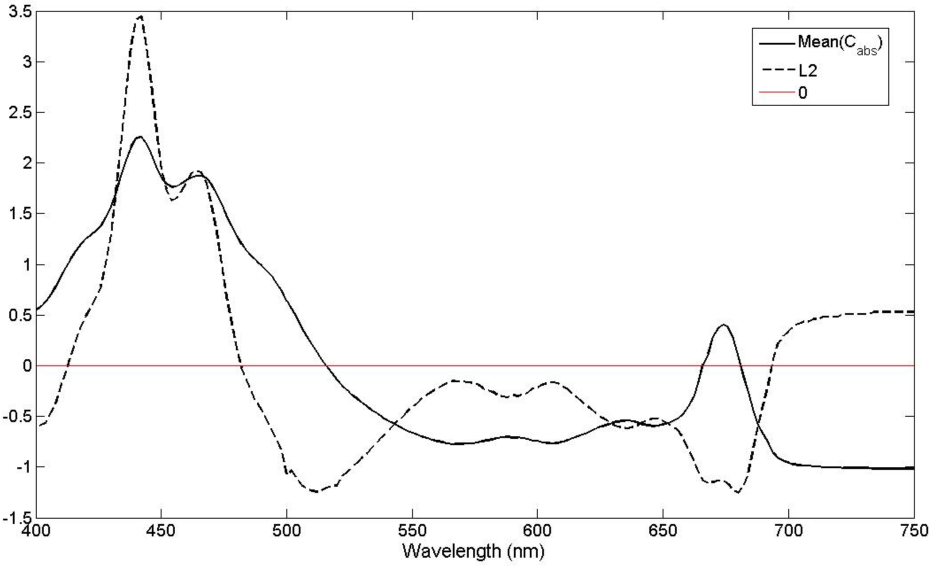

Figure 3.13: Loading L_2 and the mean value $Mean(C_{abs})$, for $\mathbf{C}_{abs,data1}$.

between the absorption spectra shapes and the size of the cell as it is in accordance with observations on real algal absorption spectra found in litterature.

Indeed, the two main effects illustrated by loading L_2 correspond to trends that have been observed on real measured spectra, and that have been designated as "package effect" [17, 38, 25, 24, 26].

The "package effect" has been first evoked by Duysens [17] in order to explain the difference in the absorption properties of suspensions compared to those of solutions. Suspension stands here for a medium composed of discrete absorbing particles with size comparable to or greater than the incident wavelength in a non-absorbing substrate, whereas solution describes an absorbing medium optically homogeneous. For an equal amount of pigments, a suspension presents an absorption spectrum flattened compared to that of a dissolved solution. This is due to the very physical structure of the medium, as a suspension is optically heterogeneous while a solution is homogenous. Scattering phenomena occuring in suspensions thus explain the flattening of the absorption peaks. The same phenomenon has been described in algal cells [38, 25, 24, 26]. As the absorbing pigments are embedded in chloroplasts, themselves contained in a complex structure made of organelles, scattering phenomena occur. The more scattering (i.e. the more complex the cell), the more flattened the absorption peaks. Consequently, the bigger the cell, the more scattering and the more flattened the absorption peaks, as observed with loading L_2.

Furthermore, Ciotti et al. [15] assessed the relationship between dominant cell size in algal media and the spectral shape of the absorption coefficient. Their observations completely confirm the trends illustrated by loading L_2: the bigger the cells, the more flattened the [400-500 nm] absorption peak and the higher the 680 nm absorption peak.

Another point to be noted is that loading L_2, expressing directly the influence of scattering phenomena on the shape of the absorption spectra shows that the scattering effects may not be adequately represented by multiplicative, linear effects, as it is assumed in classical preprocessing methods such as the multiplicative scatter correction (MSC) [33].

Loading 3 expressing deformations on the main absorption peaks of Chla

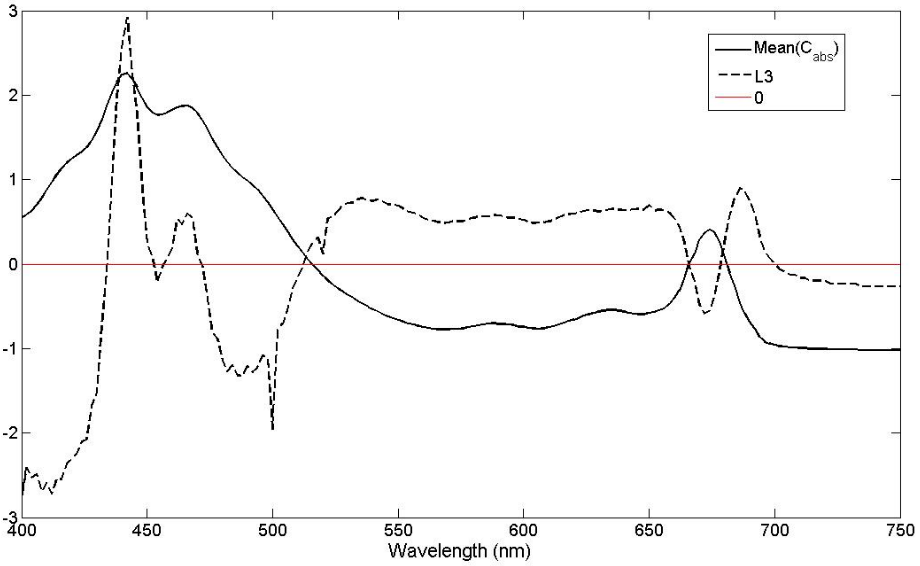

Figure 3.14: Loading L_3 and the mean value $Mean(C_{abs})$ for $\mathbf{C}_{abs,data1}$.

Loading L_3 presents humps at 450 and 480-500 nm that have opposite signs, which also express spread effects on the first absorption peak of Chla. At 680 nm, loading L_3 expresses a shift of the absorption peak towards higher wavelengths.

Table 3.11: Correlation between the cell parameters and the score S_3 .

Parameter	R_{cell}	$M_{dry,cell}$	p_{fat}	$p_{pig,tot}$
Correlation with S_3	0.18	0.08	0.06	0.20

Table 3.11 shows that the parameters influencial on loading L_3 are not easily identified, even if the cell size and pigment proportion remain the more correlated to score S_3. This probably illustrates less visible effects of the cell structure on the absorption spectra.

PCA on the absorption cross section matrix $C_{abs,data2}$

We now describe the analysis made on the simulated absorption cross section spectra obtained from database 2. The five first loadings are kept as significant, and explain 99.98% of the variance of matrix $C_{abs,data2}$.

Loading 1 expressing a balance between the two main absorption peaks at 450 and 680 nm

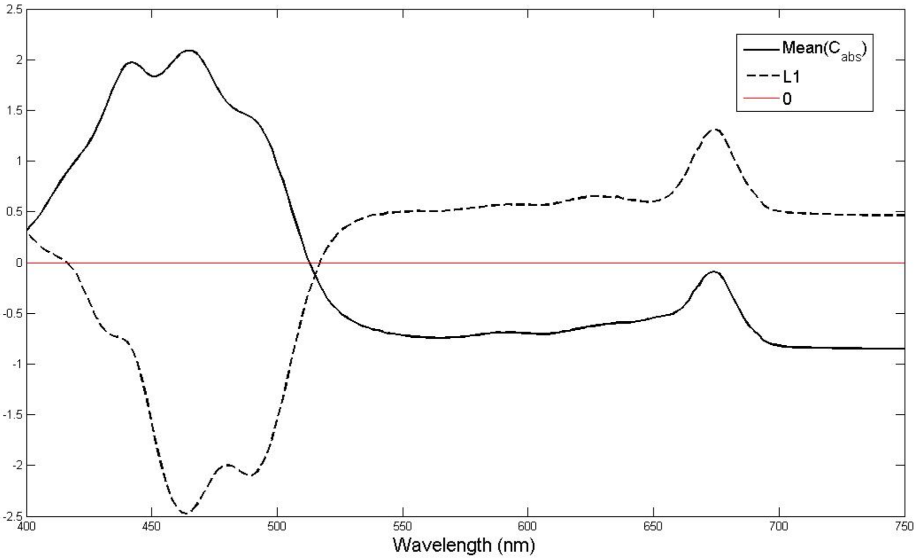

Figure 3.15: Loading L_1 and the mean value $Mean(C_{abs})$ for $C_{abs,data2}$.

Loading L_1 presents two humps of opposite signs centered on the two main absorption bands, repectively [450-550 nm] and 680 nm. L_1 thus expresses a balance between those two absorption peaks: depending on the score sign, when one is enhanced, the other decreases.

Table 3.12: Correlation between the cell parameters and the score S_1 .

Parameter	R_{cell}	$M_{dry,cell}$	p_{fat}	Chla	Chlb	Chlc	PPC
Correlation with S_1	0.43	0.03	0.17	0.8	0.02	0.05	0.03

Table 3.12 shows that loading L_1 is highly correlated to the proportion of Chla among the total pigments, and in a second order by the size of the cell.

Loading 2 expressing a flattening of the two main absorption peaks at 450 and 680 nm

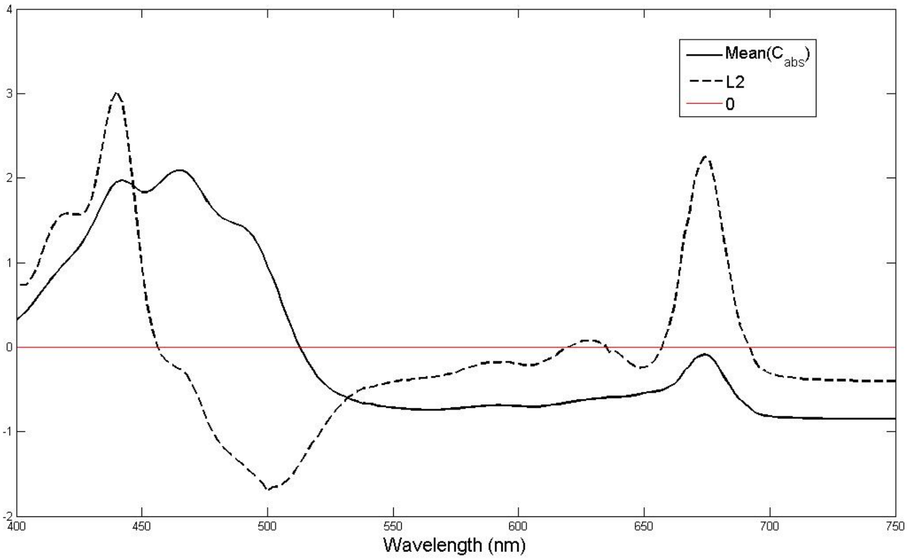

Figure 3.16: Loading L_2 and the mean value $Mean(C_{abs})$ for $C_{abs,data2}$.

Loading L_2 shows two humps of opposite signs on the [400-450 nm] and [450-550 nm] ranges, which expresses an effect of flattening of the first main absorption peak. The same effect occurs for the 680 nm absorption peak. We thus observe the same effects as for the second loading obtained for database 1.

Table 3.13: Correlation between the cell parameters and the score S_2 .

Parameter	R_{cell}	$M_{dry,cell}$	p_{fat}	Chla	Chlb	Chlc	PPC
Correlation with S_2	0.72	0.05	0.30	0.52	0.30	0.03	0.21

Table 3.13 illustrates that this loading is highly correlated to the cell size, and to a lesser extent by the quantity of pigments and lipids. We find again effect of flattening of the absorption peaks due to the package effect and the influence of cell size upon the absorption spectra.

Loading 3 expressing an asymmetry of two main absorption peaks

The same flattening effect on the 480 nm absorption peak can be seen, as well as a shift of the 680 nm absorption peak.

Table 3.14 illustrates that those effects on the absorption spectra shape are mainly influenced by the proportions of Chlb and Chlc.

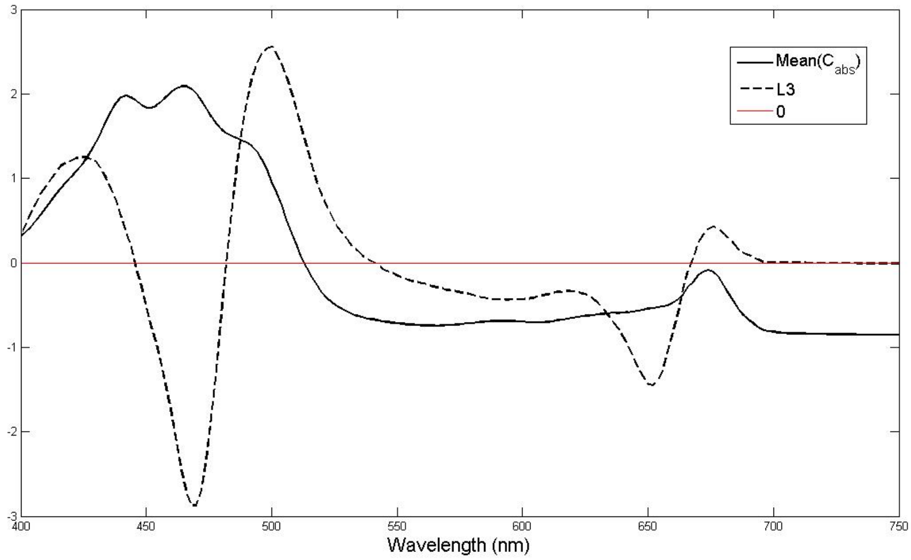

Figure 3.17: Loading L_3 and the mean value $Mean(C_{abs})$ for $C_{abs,data2}$.

Table 3.14: Correlation between the cell parameters and the score S_3 .

Parameter	R_{cell}	$M_{dry,cell}$	p_{fat}	Chla	Chlb	Chlc	PPC
Correlation with S_3	0.16	0.04	0.05	0.05	0.77	0.50	0.10

Loading 4 expressing the increase of the three secondary peaks on the [400-500 nm] range.

Loading L_4 expresses deformations of the main absorption peaks: on the [400-500 nm] range, the three humps express effects of increase or flattening of the three small secondary absorption peaks (at 430, 480 and 500 nm). The increase or decrease of the 680nm absorption peak balances this effect.

Table 3.15: Correlation between the cell parameters and the score S_4 .

Parameter	R_{cell}	$M_{dry,cell}$	p_{fat}	Chla	Chlb	Chlc	PPC
Correlation with S_4	0.19	0.04	0.08	0.02	0.13	0.04	0.95

Table 3.16 shows that loading L_4 is strongly linked to the relative proportion of carotenoids. It should be noted that due to the very structure of the database, the relative quantities of pigment of each group are correlated. This means that more pigment of one group implies less of another. This may explain why some effects on the absorption peaks seem to balance each other, such as what can be observed here.

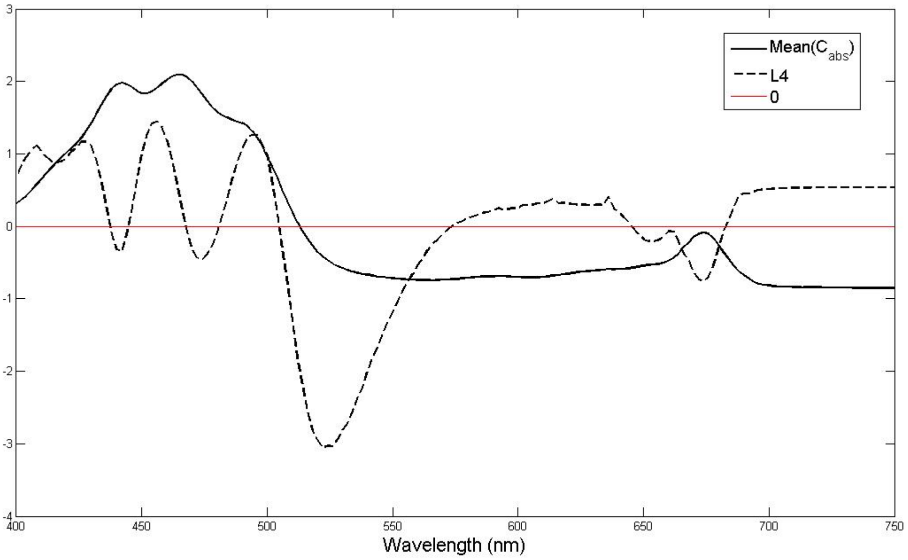

Figure 3.18: Loading L_4 and the mean value $Mean(C_{abs})$ for $C_{abs,data2}$.

Loading 5 expressing the increase of the 480nm and 680nm peaks.

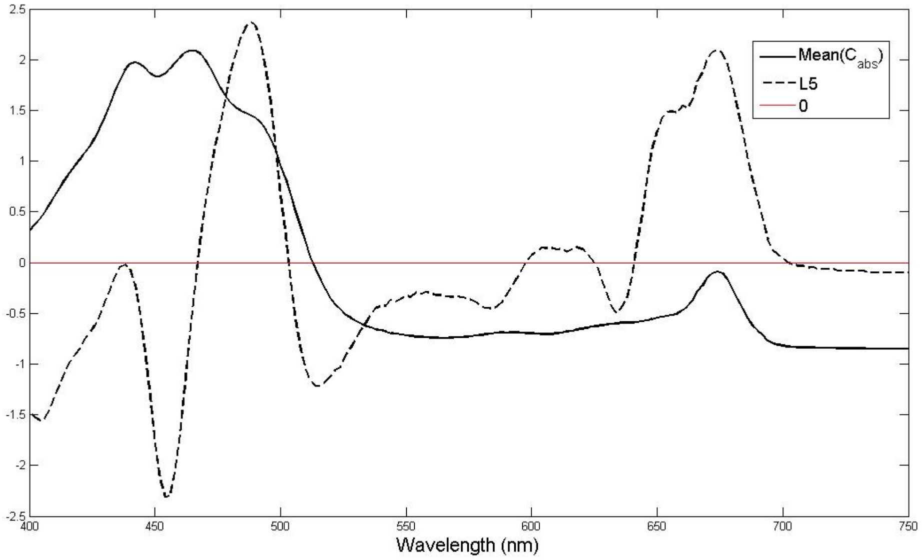

Figure 3.19: Loading L_5 and the mean value $Mean(C_{abs})$ for $C_{abs,data2}$.

We can observe a competitive effect between the increase of the 480 nm absorption peak and a decrease at lower wavelengths, and at 580 and 630 nm. The increase at 480 nm is also linked to an increase of the 680 nm absorption peak, spread towards 650 nm.

Table 3.16: Correlation between the cell parameters and the score S_5 .

Parameter	R_{cell}	$M_{dry,cell}$	p_{fat}	Chla	Chlb	Chlc	PPC
Correlation with S_5	0.06	0.001	0.02	0.13	0.30	0.75	0.09

We can see that loading L_5 is directly correlated to the Chlc proportion.

PCA on the scattering cross section matrix $C_{sca,data1}$ (similar results are obtained with $C_{sca,data2}$)

We now present the analysis of the scattering cross section spectra database 1: similar results (not shown here) were obtained with database 2. 99.98% of the variance of $C_{sca,data1}$ is expressed by considering the three first loadings. The three first loadings are thus kept as significant.

Loading 1 expressing a multiplicative effect

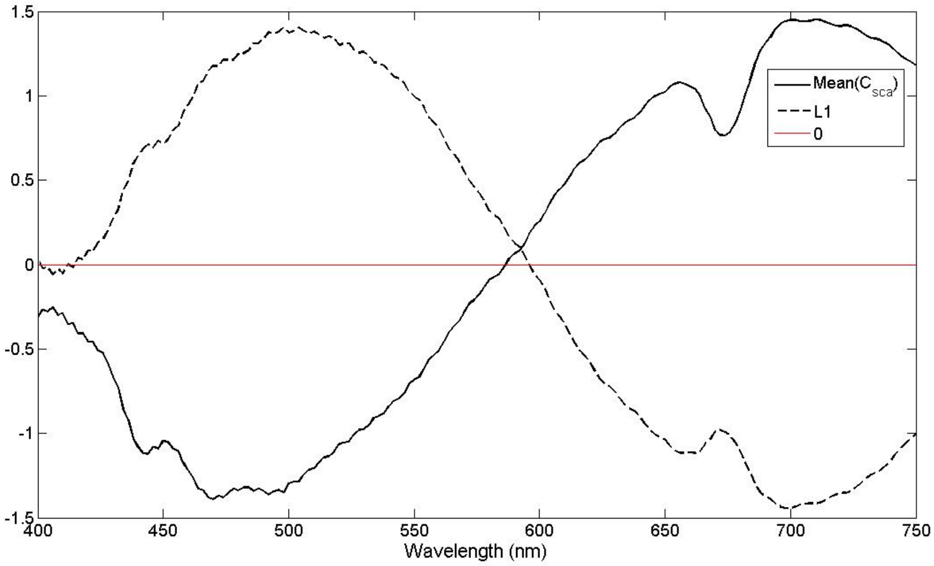

Figure 3.20: Loading L_1 and the mean value $Mean(C_{sca})$.

As for the absorption cross section, the first effect responsible for the variance of $C_{sca,data1}$ is a multiplicative effect: it can be seen on figure 3.20 that the shape of loading

L_1 is indeed very similar to the one of the mean value of the scattering cross section spectra $Mean(C_{sca})$.

Table 3.17: Correlation between the cell parameters and the score S_1 .

Parameter	R_{cell}	$M_{dry,cell}$	p_{fat}	$p_{pig,tot}$
Correlation with S_1	0.97	0.10	0.12	0.06

Table 3.17 shows that the first loading is strongly correlated to the total radius of the algal cell. This means that the mean value of the scattering spectra is directly linked to the cell size. This is in accordance with the common rule linking the scattering properties to the physical structure of the cells

Loading 2 expressing a flattening of the scattering cross section spectrum

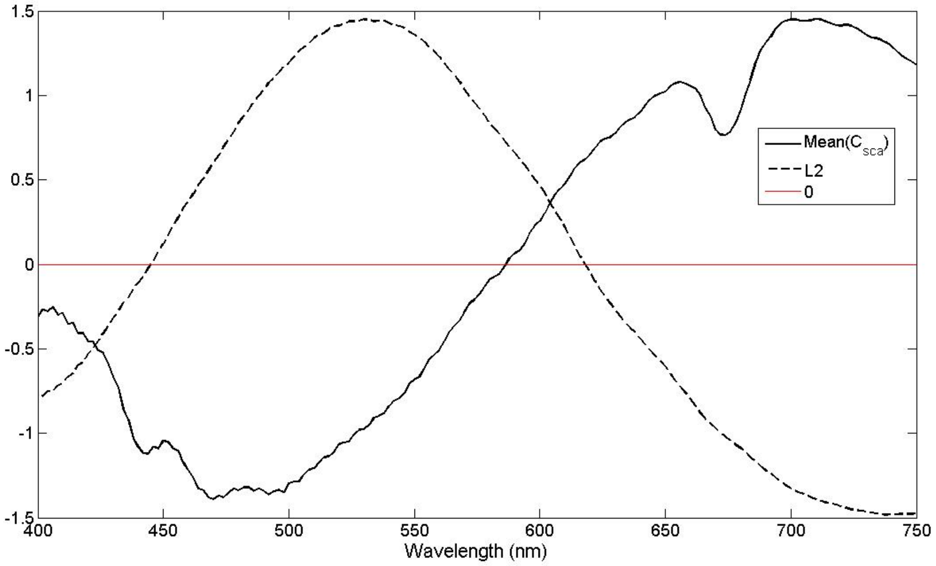

Figure 3.21: Loading L_2 and the mean value $Mean(C_{sca})$.

Loading L_2 presents three main humps of different signs, respectively on the [400-450 nm], [450-620 nm] and [620-750 nm] ranges. L_2 expresses a global flattening effect on the spectrum for a positive score value, or on the contrary an increase of the dip on the [450-620 nm] spectral range for a negative score value. Loading L_2 thus governs the general shape of the spectrum.

Table 3.18 shows that the cell size seems to be the more correlated to score S_2, even if the correlation remains weak.

Table 3.18: Correlation between the cell parameters and the score S_2 .

Parameter	R_{cell}	$M_{dry,cell}$	p_{fat}	$p_{pig,tot}$
Correlation with S_2	0.14	0.01	0.02	0.02

Loading 3 expressing the influence of absorption on the scattering spectrum

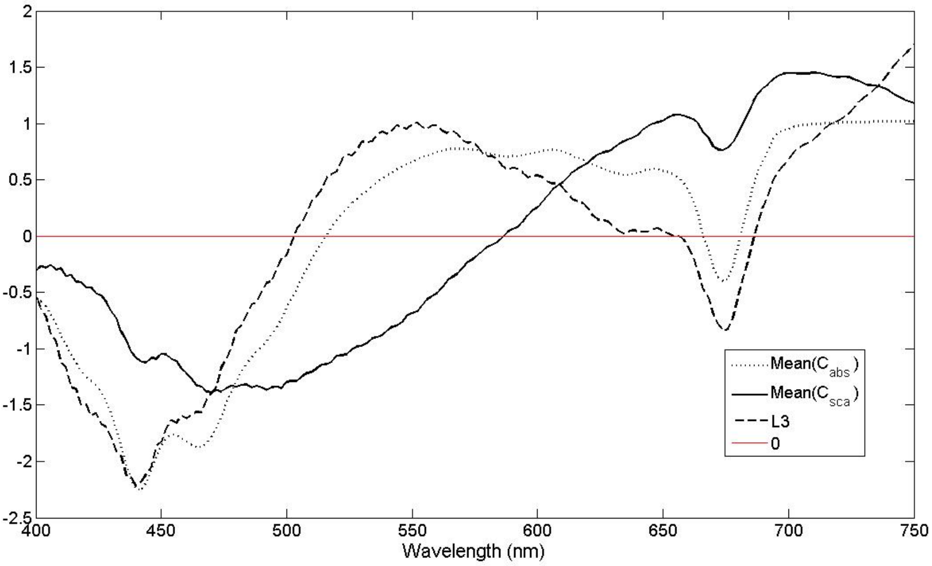

Figure 3.22: Loading L_3,mean value $Mean(C_{sca})$ and $Mean(C_{abs})$.

Loading L_3 presents a general shape that looks like the one of the absorption cross section spectra, as it can be seen by comparing to the $Mean(C_{abs})$ spectrum that has been shown on the same figure for more clarity. This means that loading L_3 expresses the emergence of humps or dips on the scattering spectrum at the wavelenghts corresponding to the main absorption peaks, in particular on the [400-500 nm] and [660-690 nm] ranges.

Table 3.19: Correlation between the cell parameters and the score S_3 .

Parameter	R_{cell}	$M_{dry,cell}$	p_{fat}	$p_{pig,tot}$
Correlation with S_3	0.50	0.48	0.13	0.70

Table 3.19 shows that loading L_3 is highly influenced by the pigment total proportion, and by the cell size in a lesser extent. This observation implies interesting prospects, as it means that information about the pigment composition and quantity could be extracted from scattering spectra. This idea is all the more interesting as it is rarely condidered, and could give an alternative way to determine chemical information in highly heterogeneous samples.

PCA on the extinction cross section matrix $C_{ext,data1}$ (similar results are obtained with $C_{ext,data2}$)

Loading 1 expressing a multiplicative effect

The case of the extinction cross section matrix $C_{ext,data1}$ is very similar to what has been observed above in section 3.3.2 for the scattering cross section matrix $C_{sca,data1}$. Three significant loadings can be kept: the first loading expresses a multiplicative effect, and the second loading expresses effects on the general shape of the spectrum such as for $C_{sca,data1}$. However what has to be noted is that loading L_3 is different, as it can be seen on figure 3.23.

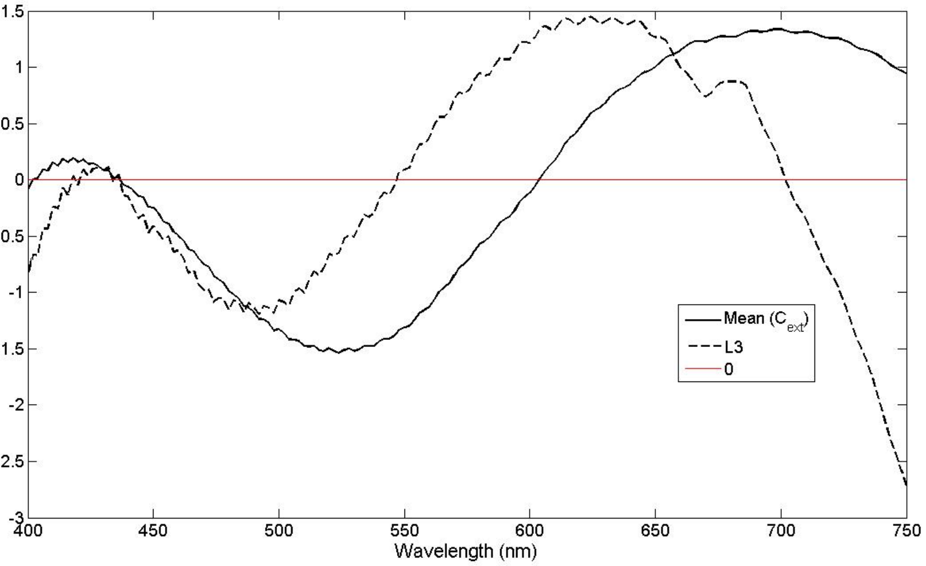

Figure 3.23: Loading L_3 and mean value $Mean(C_{ext})$.

This time loading L_3 does not present the absorption-like patterns as it was the case for the scattering cross section spectra. In the case of the extinction cross section, loading L_3 expresses an effect of flattening of the spectra around 550 nm.

Table 3.20: Correlation between the cell parameters and the score S_3 .

Parameter	R_{cell}	$M_{dry,cell}$	p_{fat}	$p_{pig,tot}$
Correlation with S_3	0.45	0.11	0.07	0.10

Contrary to what has been obtained for the scattering spectra, it can be seen that the chemical information seems to be lost in the extinction spectra: table 3.20 shows in particular that loading L_3 is not significantly correlated to the pigments. This effect has also been reported in available litterature [11] The extinction cross section is the sum of absorption and scattering cross sections. However, in the vicinity of the absorption bands, the scattering and absorption spectra present patterns that are usually symetrical for most algal media [11]. That is why those effects balance each other, resulting in a "smooth" extinction coefficient spectrum.

Conclusion on the PCA study

The PCA applied on the absorption cross sections spectra simulated from Database 1 shows that the first effect of variability between the individuals is a multiplicative effect, directly linked to the total pigment quantity. This result is completely intuitive and was expected. At the second and third orders come non-linear deformations of the spectra with flattening or enhancing of the main absorption peaks. The parameters influencing those effects are first the pigment total quantity, and second the total radius of the cell. The results obtained with the absorption spectra simulated from Database 2 show that the relative proportion of the different pigment groups is highly influencial on the shape of the absorption cross section spectra. The successive loadings make it possible to discriminate one by one the patterns of each pigment, that can be recognized on the spectra shape. This was also expected, as the absorption spectra are routinely used as a reference technique to retrieve the pigment qualitative composition of algal cells [5, 19]. As for Database 1, it is also clear that the physical structure of the cell (mainly the cell size) largely influences the shape of the absorption spectra, being responsible for flattening effects on the absorption peaks. This result concurs with observations made by other works [15, 38] on real algal media, and means that the three-layer sphere model implemented in *AlgaSim* adequately mimes the package effect occuring in real algal cells.

The study of the scattering spectra shows that the first effect of variability between individuals is also homothetic, depending mainly on the cell size. At the second order come effects governing the general shape of the spectra, that can be more or less flattened. At the third order are represented more acute patterns on the spectra, in particular in the vicinity of the main absorption bands. The first parameter influencing the scattering cross section spectra shape is the size of the cell, accounting for the expected dependency of the scattering properties on the physical structure. However, an important observation is that the pigments also influence in a significant way the spectra shape at the third order, which means that some information about the chemical composition of the algal cell could be extracted from a scattering spectrum.

The extinction cross section spectra have characteristics that are very similar to those of the scattering spectra. However at the third order the influence of the pigments seem to be erased, as absorption and scattering effects balance each other on the absorption bands. This is due to the fact that in some scattering regimes, concerning in particular most of the algal cells studied, the absorption and scattering spectra present patterns that are symetrical in the vicinity of the absorption bands [11].

The trends observed with this study are in accordance with litterature, giving a supplementary assessment of the capacity of *AlgaSim* to properly simulate optical properties of algal cells.

3.4 Conclusion

In this Chapter, the optical properties at the scale of one algal cell were investigated with a special attention to the influence of the cell physiological state on the optical properties. The modelling of a single algal cell was achieved by assimilating it to a three-layer sphere composed of different organic materials. The core layer was designed as a water layer with dissolved photopigments, miming the absorbing chloroplasts in a real cell. The intermediate and outer layers were taken as a lipid layer and a mixture of carbohydrates, proteins and water respectively, miming some organelles structures and membrane present in real cells. This modelling was inspired by previous works [39, 27, 43] that were proved to give satisfying approximation of the optical properties of algal cells [43], as long as the shape does not differ too much from the spherical. Despite the limitation imposed on the cell shape we found this modelling was interesting as a first approximation, as many commonly encountered cells in applied algal culture can be assimilated to spheres. Moreover, the spherical modelling of algal cells is a common approach, as the resolution of Maxwell's equations can thus be done thanks to Mie theory [35], and the solution of Aden-Kerker for multilayered spheres in particular [23], which gives exact expressions of the optical cross sections. The *AlgaSim* computation program was thus implemented in order to retrieve the absorption, scattering and extinction cross sections of a single algal cell described by its physical (size, width of each layer) and chemical (proportions of the different cell materials, nature and quantity of the pigments) characteristics. For each wavelength of the considered spectral range, the descriptive parameters of the cell are transformed by *AlgaSim* in terms of size parameters and refractive indices for each constitutive layer. They are taken as input parameters by the *Scattnlay* program developed by Peña et al. [40] which computes the corresponding Mie coefficients and optical efficiency factors by solving the Kerker equations. Finally, *AlgaSim* deduces the optical cross sections spectra from the ones of the optical efficiencies. The method was preliminarily tested by reproducing the case of a 5-μm algal cell with a determined pigment composition presented by Mueller in his PhD thesis [39]. The simulated optical cross section spectra obtained with *AlgaSim* show good qualitative and quantitative agreement with the ones of Mueller, which gives a primary, rough validation of our program. A more thourough investigation of *AlgaSim* validity was achieved by simulating and analysing large databases of optical cross section spectra. The databases were simulated by creating thousands of different individual cells with chemical and physical characteristics ranging between plausible values. A Principal Component Analysis (PCA) [21] was then applied to the databases of simulated spectra in order to determine the links between the spectra variations and the cell characteristics. The trends observed on the optical cross section spectra appear to be consistent with previous observations reported in litterature [15, 38]. The absorption spectra are influenced by the pigment composition and quantity as well as by the cell size, following Ciotti et al. findings [15]. The scattering spectra are mainly dependent on the size of the algal cell: an important observation though is that the scattering spectra also brings information about the chemical state of the cell, in particular about the pigments. This gives another validation of *AlgaSim* capacity to simulate adequately the optical properties of single algal cells by taking into account the influence of the cell physiology. The next logical step in the general thinking of this thesis was to explore the means to switch from the descriptive scale of one algal cell to the ones presented in Chapters 1 and 2, i.e. the apparent reflectance and transmittance and the intrinsic linear coefficients respectively. This issue is addressed by the following Chapter 4.

Bibliography

[1] E. Aas. Influence of shape and structure on light scattering by marine particles. Technical report, University of Oslo, 1984.

[2] E. Aas. Refractive index of phytoplankton derived from its metabolite composition. *Journal of Plankton Research*, 18(12), 1996.

[3] M. Abramowitz and I.A. Segun. *Handbook of mathematical functions.* Dover, New York, 1965.

[4] A.L. Aden and M. Kerker. Scattering of electromagnetic waves from two concentric spheres. *Journal of Applied Physics*, 22, 1951.

[5] R. Aguirre-Gomez, S. R. Boxall, and A. R. Weeks. Identification of algal pigments using high order derivatives. *IEEE*, 1995.

[6] S. Asano and G. Yamamoto. Light scattering by a spheroidal particle. *Applied Optics*, 14, 1975.

[7] R. Bhandari. Scattering coefficients for a multilayered sphere: analytic expressions and algorithms. *Applied Optics*, 24(13), 1985.

[8] R. R. Bidigare, M. E. Ondrusek, J. H. Morrow, and D. A. Kiefer. In vivo absorption properties of algal pigments. *SPIE*, 1302, 1990.

[9] A. Bricaud, A. L. Bédhomme, and A. Morel. Optical properties of diverse phytoplanktonic species: experimental results and theoretical interpretation. *Journal of plankton research*, 10(5), 1988.

[10] A. Bricaud and A. Morel. Light attenuation and scattering by phytoplanktonic cells: a theoretical modeling. *Applied optics*, 25(4), February 1986.

[11] A. Bricaud, A. Morel, and L. Prieur. Optical efficiency factors of some phytoplankters. *Journal of limnology and oceanography*, 1983.

[12] M. R. Brown and S. W. Jeffrey. Biochemical composition of microalgae from the green algal classes chlorophyceae and prasinophyceae. 1. amino acids, sugars and pigments. *Journal of experimental marine biology and ecology*, 161, 1992.

[13] O.B. Brown and H.R. Gordon. The size-refractive index distribution of clear coastal water particulates from light scattering. *Applied Optics*, 13, 1974.

[14] J. P. Cadoret and O. Bernard. La production de biocarburant lipidique avec des microalgues: promesses et défis. *Société de biologie*, 202(3), 2008.

[15] A. M. Ciotti, M. R. Lewis, and J. J. Cullen. Assessment of the relationships between dominant cell size in natural phytoplankton communities and the spectral shape of the absorption coefficient. *Journal of limnology and oceanography*, 47, 2002.

[16] W.R. Clavano, E. Boss, and L. Krap-Boss. Inherent optical properties of non-spherical marine-like particles - from theory to observation. *Oceanography and Marine Biology*, 45, 2007.

[17] L. N. M. Duysens. Flattening of the absorption spectrum of suspensions, as compared to that of solutions. *Biochimica and Biophysica acta*, (19), 1956.

[18] J.H. Gladstone and T.P. Dale. Researches on the refraction, dispersion and sensitiveness of liquids. *Philosophical Transactions of the Royal Society of London*, 153, 1863.

[19] N. Hoepffner and S. Sathyendranath. Effect of pigment composition on absorption properties of phytoplankton. *Marine Ecology Progress Series*, 73, 1991.

[20] B.R. Johnson. Light scattering by a multilayer sphere. *Applied Optics*, 35(18), 1996.

[21] I.T. Jolliffe. *Principal Component Analysis, second edition.* Springer, 2002.

[22] R. Kandilian, E. Lee, and L. Pilon. Radiation and optical properties of nannochloropsis oculata grown under different irradiances and spectra. *Bioresource Technology*, 2013.

[23] M. Kerker, editor. *Light scattering by non-spherical particles: theory, measurements and applications.* Academic press, New York, 1969.

[24] J. T. O. Kirk. A theoretical analysis of the contribution of algal cells to the attenuation of light within natural waters. 1. general treatment of suspensions of pigmented cells. *New phytologist*, 75, 1975.

[25] J. T. O. Kirk. A theoretical analysis of the contribution of algal cells to the attenuation of light within natural waters. ii. spherical cells. *New phytologist*, 75, 1975.

[26] J. T. O. Kirk. A theoretical analysis of the contribution of algal cells to the attenuation of light within natural waters. iii. cylinfrical and spheroidal cells. *New phytologist*, 77, 1976.

[27] J. C. Kitchen and J. R. V. Zaneveld. A three-layered sphere model of the optical properties of phytoplankton. *Journal of limnology and oceanography*, 37, 1992.

[28] E. Lee, R. L. Heng, and L. Pilon. Spectral optical properties of selected photosynthetic microalgae producing biofuels. *Journal of Quantitative Spectroscopy and Radiative Transfer*, 114, 2013.

[29] V.N. Lopatin and F.Y. Sidko. *Introduction to Optics of Suspended Cells.* Nauka, Novosibirsk, 1988.

[30] V. Lucarini, J. J. Saarinen, K. E. Peiponen, and E. M. Vartiainen. *KramersKronig Relations in Optical Materials Research.* Springer, 2005.

[31] D.W. Mackowski, R.A. Altenkirch, and M.P. Menguc. Internal absorption cross sections in a stratified sphere. *Applied Optics*, 29(10), 1990.

[32] H. Martens and T. Naes. *Multivariate Calibration.* Wiley, 1989.

[33] H. Martens, J. Pram Nielsen, and S. Balling Engelsen. Light scattering ans light absorbance separated by extended multiplicative signal correction. application to near-infrared transmission analysis of powder mixture. *Analytical Chemistry*, 75(3), February 2003.

[34] J-L. Meyzonnette. Radiometry and detection systems. Institut d'Optique Graduate School courses, 2009.

[35] G. Mie. Beitrage zur optik trüber medien, speziell kolloidaler metallösungen. *Annalen der physik*, 25(3), 1908.

[36] M.I. Mishchenko, J.W. Hoovenier, and L.D. Travis, editors. *Light scattering by non-spherical particles: theory, measurements and applications.* San Diego, California: Academic press, 2000.

[37] C.D. Mobley. *Light and Water: Radiative Transfer in Natural Waters.* Academic Press, New York, 1994.

[38] A. Morel and A. Bricaud. Theoretical results concerning light absorption in a discrete medium, and application to specific absorption of phytoplankton. *Deep sea research*, 28, 1981.

[39] J. L. Mueller. *The influence of phytoplankton on ocean color spectra.* PhD thesis, Oregon state university, 1973.

[40] O. Peña and U. Pal. Scattering of electromagnetic radiation by a multilayered sphere. *Computer Physics Communications*, 180, 2009.

[41] B. Peterson and S. Ström. T-matrix formulation of electromagnetic scattering from multilayered scatterers. *Physical Review D*, 10, 1974.

[42] L. Pottier, J. Pruvost, J. Deremetz, J. F. Cornet, J. Legrand, and C. G. Dussap. A fully predictive model for one-dimensional light attenuation by chlamydomonas reinhardtii in torus photobioreactor. *Wiley InterScience*, 2005.

[43] A. Quirantes and S. Bernard. Light scattering by marine algae: two-layer spherical and non-spherical models. *Journal of Quantitative Spectroscopy and Radiative Transfer*, 89, 2004.

[44] S. Sathyendranath, L. Lazzara, and L. Prieur. Variations in the spectral values of specific absorption of phytoplankton. *Limnology and Oceanography*, 32(2), 1987.

[45] N.V. Shepelevich, I.V. Prostakova, and V.N. Lopatin. Light scattering by optically soft randomly oriented spheroids. *Journal of Quantitative Spectroscopy and Radiative Transfer*, 70, 2001.

[46] D. Stramski, E. Boss, D. Bogucki, and K.J. Voss. The role of seawater constituents in light backscattering in the ocean. *Progress in Oceanography*, 61, 2004.

[47] D. Stramski, A. Morel, and A. Bricaud. Modeling the light attenuation and scattering by spherical phytoplanktonic cells: a retrieval of the bulk refractive index. *Applied Optics*, 27(19), 1988.

[48] D. Stramski, A. Morel, and A. Bricaud. Modeling the inherent optical properties of the ocean based on the detailed comparison of the planktonic community. *Applied Optics*, 40, 2001.

[49] H. C. van de Hulst. *Light scattering by small particles.* Wiley, 1957.

[50] J.R. Wait. Electromagnetic scattering from a radially inhomogeneous sphere. *Applied Scientific Research Section B*, 10(5-6), 1962.

[51] P.C. Waterman. Symmetry, unitarity, and geometry in electromagnetic scattering. *Physical Review D*, 3(4), 1971.

[52] Z.S. Wu and Y.P. Wang. Electromagnetic scattering for multilayered sphere: recursive algorithms. *Radio Science*, 26(6), 1991.

[53] W. Yang. Improved recursive algorithm for light scattering by a multilayered sphere. *Applied Optics*, 42(9), 2003.

[54] Y.Gong and M. Jiang. Biodiesel production with microalgae as feedstock: from strains to biodiesel. *Biotechnology letters*, 33(7), 2011.

Chapter 4

How to link the individual cell chemical and physical properties to the global spectral properties measured on a dense algal medium?

Contents

In Chapter 1 we investigated the technical means to measure spectral quantities characterizing a dense medium made of particles. We defined precisely what we call the spectral reflectance and the spectral transmittance of the bulk medium, and we described the ideal setup configuration to implement in order to measure adequately those quantities. Reflectance and transmittance belong to what could be called the "apparent optical properties" (AOPs), as a reference to the vocabulary used in oceanography [26]. They are global characteristics of the sample under study. They depend first on the experimental conditions in which the measurements are done [26]: size, width, refractive index of the quartz cell in which the aliquot is put, characteristics of the illumination beam (spectrum, power, beam diameter). They also depend on the intrinsic optical properties of the sample medium itself [26].

In Chapter 2 we saw that the instrinsic spectral properties of a medium could be represented by the linear absorption, scattering and extinction coefficients, μ_{abs}, μ_{sca} and μ_{ext}, and the anisotropy factor g. We saw that the rigorous relation between the intrinsic optical properties of a dense particulate medium and the global variations of light inside a defined aliquot of this medium could be described by the radiative transport equation (RTE) [17]. The RTE can be numerically solved with the Adding-Doubling (AD) and Inverse-Adding-Doubling (IAD) method in particular [33]: in chapter 2 we investigated the IAD to retrieve the intrinsic spectral properties of real algal samples from reflectance and transmittance measurements implemented with a double-integrating sphere setup (DIS). Despite some convergence problems due to experimental errors, as the ideal configuration of the DIS could not be implemented during this campaign, the method seemed to be promising and adapted to dense algal media.

In Chapter 3, the "microscopic" scale was considered. Quantities describing the optical properties of one single algal cell were defined: the absorption, scattering, extinction cross sections C_{abs}, C_{sca} and C_{ext} and the anisotropy factor g. We saw that the spectral properties of one algal cell were highly influenced by its structure and chemical composition [6, 10, 27, 34]. However the relations between the algal cell physical and chemical characteristics and its optical properties are nonlinear [15, 6, 31, 36, 10] which makes that no explicit formulation can be implemented. This problem is generally adressed by implementing a model of the algal cell which makes it possible to have an implicit representation of the links between the optical properties and the physical and chemical ones [41, 32, 28, 21, 34]. For the special needs of this thesis we developed in particular a three-layer sphere model of the algal cell for which the optical properties could be calculated thanks to the Kerker solution [20] of Mie theory [25]. A program called *AlgaSim* was implemented, and makes it possible to retrieve C_{abs}, C_{sca} and C_{ext} and g of one algal cell from parameters such as its total radius, pigment composition and concentration, neutral lipid, carbohydrate and protein contents. The first tests validated the program running, and a qualitative analysis of the simulations obtained showed that the model seemed to give results which concurr with previous observations made in litterature. To the state of our knowledge, our *AlgaSim* program is the first optical modelling program to explore that far the influence of the algal cell physiology on their spectral properties. It was designed on purpose, in order to make it flexible and able to simulate a wide range of different algal cells.

In the present Chapter 4, we aim at linking the microscopic scale and the global one. Our goal is to organize the paradigms and methods exposed in the previous chapters in order to link the apparent spectral properties measurable on a dense algal medium at the global scale to the physiological characteristics of the algal cells contained in it. We will thus use all the theoretical and practical tools described in the previous chapters to propose a complete method. The theoretical implementation of this complete method is tested on real algal samples of two different species. As a first step, we investigate the retrieving of physiological characteristics of algal cells from only the total transmittance measurements: our first results are very promising, and seem to validate the approach developed in this thesis.

At first, a theoretical section describes the principle of the complete method proposed here. Then we report how we applied it on real cultivated algal media. Finally, the results are shown and discussed.

4.1 Theory: description of the principle of the complete method

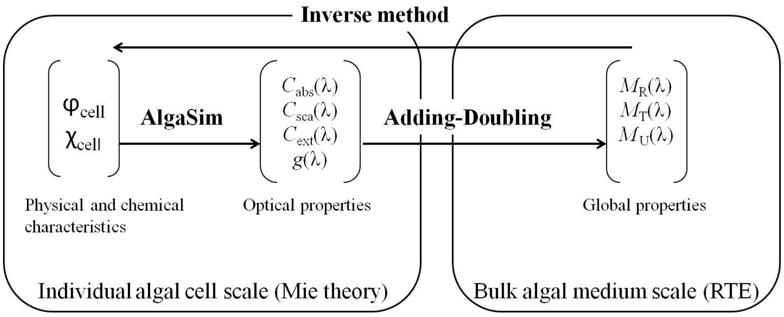

Figure 4.1: Block diagram illustrating the principle of the method implemented in this work to simulate the global reflectance and transmittance of an algal medium from the knowledge of the chemical and physical characteristics of the constitutive algal cells.

The principle of the approach is summarized by figure 4.1.

In the forward running, i.e. when starting from the microscopic physiological description of the algal cells to deduce the measurable reflectance and transmittance properties of a given aliquot of dense algal medium composed of those cells, the following steps are followed: at the individual cell scale, Mie theory [25], and in particular the solution of Kerker [20] was used. The cells are thus modeled as multilayered spheres of different organic materials and pigments, following the method thouroughly presented in Chapter 3. The solution of Kerker makes it possible to implicitly reproduce the influence of the cell structure and chemical composition on the optical properties of the cell by calculating the corresponding optical cross sections. As already shown in Chapter 3, the *AlgaSim* program was developed by us to implement both the building of the model algal cell from physiological quantities and the calculations of the optical cross sections by calling the Scattnlay program from Peña et al. [30]. From the calculated optical cross sections of one single cell, we will see in the next section that the linear optical coefficients intrinsic to the algal medium can be deduced. The Adding-Doubling method [33] is then implemented in order to solve the RTE [17], and retrieve the spectral reflectance and transmittance properties of a defined sample of algal medium containing the modeled algal cells.

The inverse method is the retrieving of the physiological characteristics of the algal cells from the measured global spectral properties of a given aliquot of medium. The inversion could be implemented step by step, i.e. applying Inverse-Adding-Doubling at first and inverting the *AlgaSim* program in a second step. However this solution was not chosen in this work . We decided to implement the inversion of the complete chain at once, as will be shown in the next sections.

Coupling Mie theory and Adding-Doubling is a principle that has already been tested in other domains, and in particular on phantom suspensions of polystyrene microspheres and toluene [39, 40]. In those cases the problem is simplified, as the microspheres are considered to be homogeneous and to present all the same size and properties.

However to the state of our knowledge our study is the first one where the method is applied on dense microalgal media. Some attempts have been made to link the apparent optical properties of some algal samples to information about the physiological state of the cells [15, 36, 10]. However, as explained in the introductory chapter of this thesis, all the works we investigated were dedicated to diluted algal media, which simplifies the measurements of the spectral intrinsic properties of the samples and makes it unnecessary to actually solve the RTE. Moreover, only a few physiological properties of the algal cells are investigated at once: the Chla and one accessory pigment content [15], the mean cell size [36, 10] for example. To the state of our knowledge our work is the first one aiming at retrieving a more complete set of physiological parameters from only one spectral measurement protocol.

4.1.1 Direct method: from the physiological parameters to the global spectral properties

The different steps implemented to retrieve the global spectral reflectance and transmittance of a given aliquot of algal medium from the description of the physiological characteristics of the constitutive algal cells are presented in figure 4.2.

(1) The individual cell model

The algal cells are described by their dry mass, total radius, massic proportions of neutral lipids, carbohydrates and proteins, total pigment quantity and relative composition. Those parameters are the inputs of the *AlgaSim* program, which gives in output the corresponding optical cross sections C_{abs}, C_{sca} and C_{ext} and the anisotropy factor g of one algal cell.

(2) The algal suspension: linking the individual cell cross sections to the intrinsic linear coefficients

It is necessary to model the algal suspension, composed of billion individual cells. Real algal media are composed of cells with various size and organic contents. The rigorous

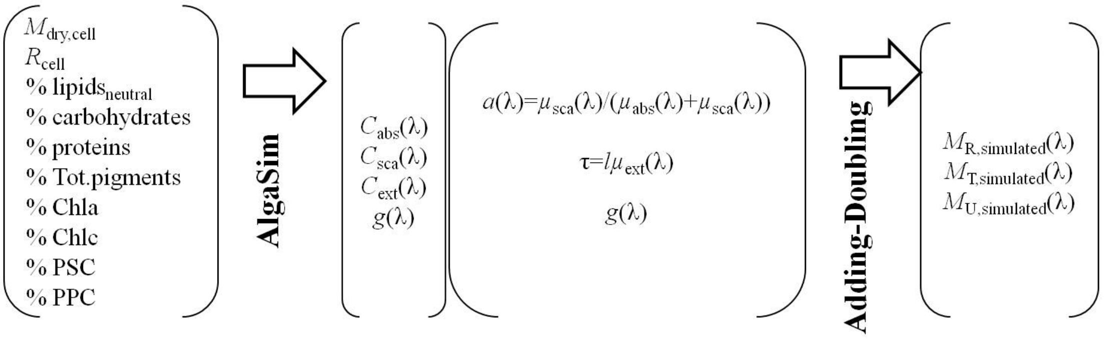

(1) Averaged measured physical and chemical data for one algal cell

(2) Simulated cross sections for one algal cell. Corresponding albedo and optical thickness of a slab aliquot of algal medium of width l and cell concentration N_{cell}

(3) Corresponding simulated reflectance, total transmittance and regular transmittance of the aliquot of algal medium

Figure 4.2: Block diagram of the procedure used to simulate the global reflectance and transmittance of a slab of algal medium of width l and cell concentration N_{cell}, with algal cells described by their chemical and physical characteristics.

means to deduce the optical properties of the global suspension from the ones of all the constitutive algal cells would be to sum the properties of each individual cell described by its own physical and chemical parameters. For example, if we consider an algal cell population such that each cell is described by three parameters (α, β, γ), the linear optical properties of the whole population would be expressed such that:

$$\mu_i = \int_{\alpha_{min}}^{\alpha_{max}} \int_{\beta_{min}}^{\beta_{max}} \int_{\gamma_{min}}^{\gamma_{max}} N(\alpha,\beta,\gamma) C_i(\alpha,\beta,\gamma) d\alpha d\beta d\gamma \tag{4.1}$$

With $i = abs, sca, ext$, $C_i(\alpha,\beta,\gamma)$ the cross section of a single cell of parameters α, β, γ, α_{max}, α_{min}, β_{max}, β_{min}, γ_{max}, γ_{min} respectively the maximum and mimimun value of the α, β and γ parameter encountered in the considered algal population and $N(\alpha,\beta,\gamma)$ the number of cells per unit volume of suspension having parameters respectively between α and $\alpha + d\alpha$, β and $\beta + d\beta$ and γ and $\gamma + d\gamma$. However in practice it is impossible to model individually each algal cell. The chemical and physical properties describing the algal cells are usually measured on a whole population, which means that they represent mean values. There results that it is only possible to know a mean dry mass, a mean pigment content and composition, and a mean organic content composition. Only the size measurements implemented with particle counters can give the histogram of the algal cell radius [19, 3, 23]. In that case it is thus possible to model the algal population considered as a polydispersion, and to calculate the linear optical coefficient such that:

$$\mu_i = \int_0^{\infty} N(r_{cell}) C_i(r_{cell}) dr_{cell} \tag{4.2}$$

With $i = abs, sca, ext$, $C_i(r_{cell})$ the cross section of a single cell of radius r_{cell} and $N(r_{cell})$ the number of cells per unit volume of suspension having a radius between r_{cell} and $r_{cell} + dr_{cell}$.

In the case where only one mean diameter can be measured for the whole algal suspension, it is usual to assume the case of a monodisperse suspension [27]: the algal cells are thus considered to be all the same size, corresponding to the mean size. This assumption simplifies the problem, and the intrinsic linear optical properties of the algal suspension with a cell concentration N_{cell} can be obtained such that [17]:

$$\mu_{abs} = N_{cell}.C_{abs} \tag{4.3}$$

$$\mu_{sca} = N_{cell}.C_{sca} \tag{4.4}$$

$$\mu_{ext} = N_{cell}.C_{ext} \tag{4.5}$$

The anisotropy factor g of the algal medium is the one of the constitutive algal cells. When considering a given aliquot of algal medium of cell concentration N_{cell}, and described as a slab of algal medium of width d and of infinite other dimensions, the albedo a and optical thickness τ on this particular aliquot can be described such that:

$$a = \frac{\mu_{sca}}{\mu_{ext}} \tag{4.6}$$

$$\tau = d.\mu_{ext} \tag{4.7}$$

(3) The algal medium aliquot under study

From the albedo a, the optical thickness τ and the anisotropy factor g, the Adding-Doubling method [33] makes it possible to solve the RTE and to retrieve the apparent reflectance and transmittance characteristics of an algal medium aliquot measured in certain experimental conditions: those experimental conditions must be described before running the Adding-Doubling program, by giving the size and refractive index of the quartz cell in which the algal medium aliquot is put and the characteristics of the incident light beam. It is thus possible to retrieve theoretical reflectance and transmittance characteristics $M_{R,simulated}$,$M_{T,simulated}$ and $M_{U,simulated}$.

Figure 4.3 illustrates the successive representations of the problem at each step of the implemented method. The individual cell scale, figure 4.3 (1), is described by the extended

Mie theory in terms of individual cross sections. Figure 4.3 (2): the intrinsic linear optical properties of a medium composed of those algal cells with a concentration N_{cell} are retrieved by adding the individual cell cross sections. This sum can be implemented in different ways according to the model of the algal suspension that is chosen, i.e. polydispersion or monodispersion. A given aliquot of this algal medium, put in a quartz cell of width l is then considered (figure 4.3 (3)): the Adding-Doubling method thus allows to retrieve the reflectance and transmittance properties of such a defined aliquot.

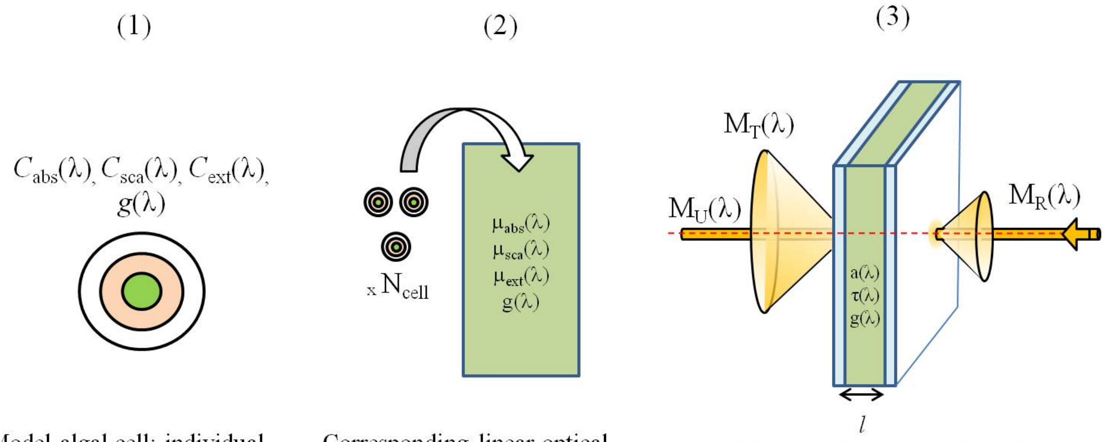

Model algal cell: individual cross sections.

Corresponding linear optical coefficients of the algal suspension with a cell concentration N_{cell}.

Slab of algal medium of width l: corresponding albedo a and optical thickness τ. Corresponding global reflectance and transmittance properties.

Figure 4.3: Representation of the problem at the different scales of description.

4.1.2 Inverse method: from the global spectral properties to the physiological parameters of the constitutive algal cells

The general principle of the inverse method used to retrieve the physical and chemical characteristics of the constitutive algal cells from the measured global reflectance and transmittance properties of a given aliquot of the algal medium is illustrated by figure 4.4.

The principle is to retrieve a set of parameters describing the algal cell characteristics, noted $[\varphi_{predicted}, \chi_{predicted}]$ on figure 4.4, which minimizes the error δ between the reflectance and transmittance spectra simulated and the measured ones, respectively designated as $[M_{R,simulated}, M_{T,simulated}, M_{U,simulated}]$ and $[M_{R,measured}, M_{T,measured}, M_{U,measured}]$ on figure 4.4. The *AlgaSim* program coupled with the Adding-doubling method is used in the forward model to simulate the spectra of the reflectance and transmittance $M_{R,simulated}$, $M_{T,simulated}$, $M_{U,simulated}$ corresponding to a slab of a particle medium made of algal cells described by an initial set of parameters $[\varphi, \chi]$. In some cases it can be necessary to give also some fixed imput parameters, in particular if it has been chosen to vary only a reduce number of physiological parameters and to fix others for time convergence issues.

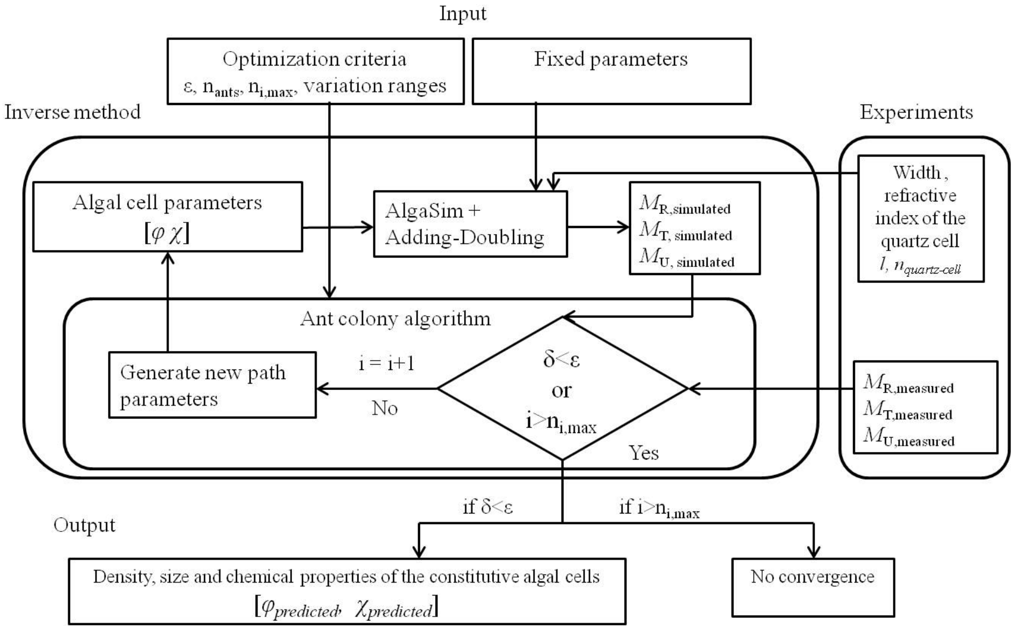

Figure 4.4: Principle of the procedure implemented to retrieve the algal cell density, mean size and chemical properties from the reflectance and transmittance spectra of a slab of algal medium of width l. δ is the error between the simulated and measured reflectance and transmittance spectra (equation (4.9)) and i the iteration number of the optimization algorithm.

The simulated reflectance and transmittance spectra are then compared to the measured ones by using the Spectral Angle Mapper (SAM) [22]. The SAM quantifies the spectral distance between two spectra by calculating the "angle" between the two spectra, treating them as vectors in a space with dimensionality equal to the number of wavelengths. For example, if a test vector $\vec{t}$ is compared to a reference vector $\vec{r}$, the SAM between them is expressed by [22]:

$$cos^{-1}(\frac{<\vec{t}|\vec{r}>}{||\vec{t}||.||\vec{r}||}) \tag{4.8}$$

More precisely, in this study we calculated the cosine of the SAM and compared it to the maximum value 1. An objective function δ was thus defined such that :

$$\delta = 1-\frac{<\mathbf{M}_{T,measured}|\mathbf{M}_{T,simulated}>}{||\mathbf{M}_{T,measured}||.||\mathbf{M}_{T,simulated}||}+1-\frac{<\mathbf{M}_{R,measured}|\mathbf{M}_{R,simulated}>}{||\mathbf{M}_{R,measured}||.||\mathbf{M}_{R,simulated}||}+1-\frac{<\mathbf{M}_{U,measured}|\mathbf{M}_{U,simulated}>}{||\mathbf{M}_{U,measured}||.||\mathbf{M}_{U,simulated}||} \tag{4.9}$$

Where $\mathbf{M}_{T,measured}$, $\mathbf{M}_{T,simulated}$ are the vectors of the spectral total transmittance respectively measured experimentally and simulated, $\mathbf{M}_{R,measured}$, $\mathbf{M}_{R,simulated}$ the vectors of the spectral total reflectance respectively measured experimentally and simulated and

$\mathbf{M}_{U,measured}$, $\mathbf{M}_{U,simulated}$ the vectors of the spectral regular transmittance respectively measured experimentally and simulated.

The goal is to minimize δ by varying the set of parameters describing the algal cells $[\varphi, \chi]$. For that purpose, several optimization algorithms can be used. In the context of this study in particular, the ant colony algorithm was considered [12]. The ant colony algorithm can find a global minimum of an objective function by miming the foraging behavior of some ant species that deposit pheromone on the ground in order to mark some favorable path that should be followed by other members of the colony. Ant colony optimization exploits a similar mechanism for solving optimization problems [12]. Each iteration i of the algorithm consists in two main steps: first, a given number n_{ants} of virtual ants are released in the possible variation space determined between specified ranges. Each ant has coordinates that correspond to a given set of entry parameters. Each ant deposits a quantity of pheromone Δph that depends on the quality of the solution obtained: the smallest the objective function δ, the higher Δph. Second, the pheromones are updated: the aim is to increase the pheromone values associated with good or promising solutions, and to decrease those that are associated with bad ones. Then another wave of ants is released: they will thus preferentially follow the paths that have the greatest amount of pheromones, which will make it possible to converge towards a minimum of the objective function by iteration process. The optimization session ends when the convergence criteria is reached, i.e. $\delta < \epsilon$ with ϵ the minimum error value desired, or if the maximum number of iterations has been done without convergence.

Implementing an optimization session thus requires to give the ranges of variation allowed for each variable, the number n_{ants} of virtual ants released at each iteration step i, the minimum error value ϵ desired for the convergence criteria as well as the maximum number of iterations $n_{i,max}$.

4.2 Application on real algal media: test of the complete method with total transmittance measurements

4.2.1 Description of the experiment: aims and technical choices

The complete method described above was tested in the context of a measurement campaign on two different monospecific algal cultures, *Isochrisys galbana* and *Phaeodactylum tricornutum*, grown in batch culture. Fresh samples were collected at day 7 (D7), day 14 (D14) and day 34 (D34) after the starting day of the culture. Standard reference measurement methods were performed on each sample in order to determine the chemical composition, the cell number, mean size and mean dry weight. Total reflectance $M_{R,measured}$, total transmittance $M_{T,measured}$ and regular transmittance $M_{U,measured}$ measurements were also implemented on the fresh, non-diluted samples over the [400-750 nm] spectral range.

Our goal was to test the complete method with the data collected during this campaign.

The first step would be to implement the direct method, i.e. simulate the reflectance and transmittance spectra from the physical and chemical data measured experimentally and given as entry parameters of *AlgaSim* and Adding-Doubling. By comparing the simulated spectra, to the spectra measured on the real algal samples it would be possible to discuss on the potential of the direct method. A second step would be to implement the inverse method, i.e. predict physical and chemical parameters characterizing the algal cells from the measured reflectance and transmittance spectra. Similarly, comparing the predicted values to the ones experimentally determined by standard methods would allow to discuss the potential of the inverse method.

However two main technical choices were made for the practical implementation of the tests of the direct and inverse method: the first one was using only the total transmittance M_T as a first step. The second choice was to test the inverse method while limiting the variable parameters to 7 instead of 11, which is the maximum number of descriptive parameters that can be given to *AlgaSim*.

The first technical choice was mainly justified by experimental constraints: the spectral measurements were implemented using a double integrating sphere setup (DIS), with dimensions of the spheres corresponding to the setup presented in Chapter 1. However the illumination and detection systems had to be adapted in order to make a measurement all over the [400-750nm] spectral range with the material possibly available at the time of the campaign. That is why a mercury-xenon arc lamp (67005, Newport) and a fibered spectrometer (MMS1, Zeiss) were used. This caused some measurement troubles, as that configuration required that the detection system was fibered with a $1mm$-core, 0.22-NA, optical fiber (Ocean Optics). The detector active area was thus very limited, which resulted in significant light losses due to poor injection in the detection system, as expected regarding Chapter 1. As a consequence the signals measured in the spheres were very low, in particular in the reflectance sphere, and in the transmittance sphere with an opened light trap. As a consequence, the total reflectance $M_{R,measured}$ and the regular transmittance $M_{U,measured}$ were only obtained with a low signal to noise ratio (SNR), respectively 6 and 25 at 576 nm, whereas the total transmittance measurements were measured with a SNR as high as 40 at 576 nm. Using poor measurements to test a theoretical method did not seem wise, that is why we decided to implement a first test by using only the total transmittance measurements $M_{T,measured}$. This would give a primary idea of the potential of the complete method applied to real algal samples.

Our second choice was to limit the variables in the inverse method. It was made for two main reasons: first, the primary tests of the *AlgaSim* program, presented in Chapter 3, had shown that no significant change in the simulated spectra could be directly attributed to the relative proportions of neutral lipids. As a first step, we thus fixed the massic proportions of neutral lipids, carbohydrates and proteins to plausible values commonly found in litterature as this was assumed to be without practical consequences on the running of the inverse method. Moreover, and this is the second reason justifying our choice, limiting the number of variables significantly reduces the convergence time of the optimization process, which was a precious practical advantage.

4.2.2 Material and method

Algal cultures

Two different monospecific batch cultures of *Isochrisys galbana clone T-iso* and *Phaeodactylum tricornutum* were tested. They were grown on Conway medium in 50L-polyethylene bags at 20°C under continuous irradiance provided by white fluorescent lights (average of 150 μmol photons.$m^{-2}.s^{-1}$) and under continuous aeration and homogeneization by bubbling filtrated air (0.2 μm). Three different stages of each of the 2 cultures were sampled, at day 7 (D7), day 14 (D14) and day 34 (D34) after the starting day of the culture.

Total biomass dry weight

For estimates of dry weight, triplicates aliquots of microalgal samples (15 to 50 mL depending on the algal density) were filtrated onto preweighed precombusted (450°C, 4h) glass fiber filters (Whatman GF/F 25 mm) under mild vacuum (<200 mbar). The filters were washed with ammonium formate solution (20 ml, 0.5 mol.L^{-1}) before being dried at 100 °C during at least 16 h [47].

Total carbohydrates

Triplicate sub-samples (15 to 50 mL depending on the algal density) were filtrated onto glass fiber filters (Whatman GF/F 25 mm) under mild vacuum (<200 mbar) for carbohydrates analysis. The filters were stored at -80°C (< 3 months) prior to analysis following the Dubois et al. [14] method modified by Brown et al. [8].

Total proteins

Triplicate sub-samples (15 to 50 mL depending on the algal density) were filtrated onto glass fiber filters (Whatman GF/F 25 mm) under mild vacuum (<200 mbar) for proteins analysis. The filters were stored at -80°C (< 3 months) prior to analysis following the Lowry et al. [24] modified by Packard et al. [29] and Dortch et al. [13].

Neutral lipids

Neutral lipids were quantified by fluorimetry with Nile red staining following the standard addition method of Bertozzini et al. [4] with slight modifications. Triplicate sub-samples (50 mL) were distributed in 3 series of five 9.9 ml aliquots. Triolein solution (Sigma-Aldrich, typically 2 mg.mL^{-1} in isopropanol) was used to spike each tube (15 mL polyethylene tubes, VWR collection) with variables volumes (0 to 100 μL) to reach final concentrations from

0 to 20 mg.$mL-1$. Isopropanol (Sigma-Aldrich) was used (0 to 100 μL) to complete to a final volume of 10 mL. Triplicates of the supernatant (9.9 mL) of a centrifugated subsample (20 min, 1000 g, CR312 Jouan) topped up with 100 μL of isopropanol were used as blanks. Staining was performed with 100 μL of Nile red solution in DMSO (50 $\mu g.mL^{-1}$). Tubes were mixed by vortex after each addition. Fluorescence of each aliquots and blank was read at 582 nm with an excitation wavelength of 531 nm using a spectrofluorimeter PerkinElmer LS45 after an incubation period of 20 min at dark at ambient temperature. The average intensity of blanks fluorescence was substracted from the fluorescence intensity of each of the aliquots. The concentration in neutral lipids was calculated from the equation of the linear correlation among the corrected fluorescence intensity and the triolein equivalents. This equation is written as follow :

$$F = q.C_{triolein} + b \tag{4.10}$$

Where F is the fluorescence intensity corrected from blank value, $C_{triolein}$ is the triolein equivalent in the spiked samples, q is the slope and b is the y-axis intercept. The concentration of neutral lipids in the sample, C_s, corresponds to the absolute value of the x-axis intercept (i.e. the ratio of the y-axis intercept over the slope) and is expressed in mg equivalents of triolein.L^{-1} following the relation:

$$C_s = \frac{b}{q} \tag{4.11}$$

Optical microscope counting and size determination

The culture samples of *Isochrysis sp.* and *Phaedactylum sp.* were taken at the beginning, exponential and stationary growth phase of the 2 microalgaes (30mL) and then fixed in buffered formaldehyde (2% final concentration). The cells were directly counted with a Malassez cell and organisms abundance expressed as number of cells / L. Biovolumes of each species (μm^3) were estimated by microscopic measurement of length and width, assuming simple geometric shapes, based on indications Smayda[37], Hillebrand et al. [16] and Sun et al. [42]. These analyzes were performed using an upright microscope (Olympus BX60) equipped with a digital camera Jenoptik Progres CapturePro. From the mean dimensions of the cells, the equivalent spherical diameter (ESD) was calculated for each sample [18]. For a particle, the ESD is the diameter of a sphere of same volume. It is usually used in order to compare the dimensions of non-spherical particles to spherical ones.

Pigment concentration and composition

For pigment analysis, triplicates aliquots samples (15 to 50 mL depending on the algal density) were filtrated on glass-fiber filters (25 mm, 0.7-mm nominal pore size, Whatman

GF/F) at low vacuum (200 mm Hg), and stored at -80°C until analysis. Pigments were extracted in 3 mL of 95% methanol using the protocol described in Vidussi et al. [44]. Pigments were analyzed by high-performance liquid chromatography (HPLC), following the method of Zapata et al. [46], with some adaptations for the HPLC system used as described in Vidussi et al. [44]. Pigments were identified based on retention time and the absorbance spectra obtained with the photodiode array and the HPLC was calibrated with commercial standards (DHI and Sigma).

Total transmittance measurements on bulk algal media

Total transmitted signal $I_{T,tot}$ was collected with an integrating sphere (see figure 4.5) in contact with one side of the sample. The illumination beam reached the other side of the sample quartz cell with a 8° angle as presented in Chapter 1. $I_{T,tot}$ included both regular (1) and diffuse (2) transmitted light. Total transmittance $M_{T,measured}$ was calculated such that:

$$M_{T,measured} = \frac{I_{T,tot} - I_{T,dark}}{I_{T,0,tot} - I_{T,dark}} \tag{4.12}$$

Where $I_{T,0,tot}$ is the signal measured in the transmittance sphere when the input beam directly reaches the transmittance sphere (sample removed). $I_{T,dark}$ was the signal measured in transmittance spheres when the input light beam I_0 was stopped. The signals were corrected beforehand from the effects due to the spheres different appertures with the correction method presented in Chapter 1.

The sample cell was positioned outside of the sphere: in practice, and as already discussed in Chapter 1, this meant that the actual solid angle where the transmitted light was collected was smaller than 2π sr. In order to limit at best the light leaks, the sample cell thickness, the sample cell position, the incident light beam size upon the sample and the diameters of the spheres ports were adapted at best. In the case of this study, the solid angle detected by one sphere could be optimized to reach approximately 1.8π sr.

Six measurements of $M_{T,measured}$ were collected and averaged for each sample, what made possible to limit the effects of the experimental conditions. The measurements were conducted using 83mm-diameter transmittance sphere (3P-GPS-033-SL, Labsphere) fibered with 1mm-core low OH optical fibers (Ocean Optics). Normal illumination was provided by a mercury-xenon arc lamp (67005, Newport) and the spectral acquisition was carried out using a spectrometer (MMS1, Zeiss). The temperature fluctuations of the light source were limited by turning on the lamp at least one hour before beginning the measurements. The integration time varied between 700 and 5000ms depending on the signal measured. Liquid algal samples were put in quartz cells (100-OS, Hellma) with a 4mm-optical thickness d. The measurements were made in the spectral region between 400 and 750nm with 10nm resolution intervals and 3nm step intervals.

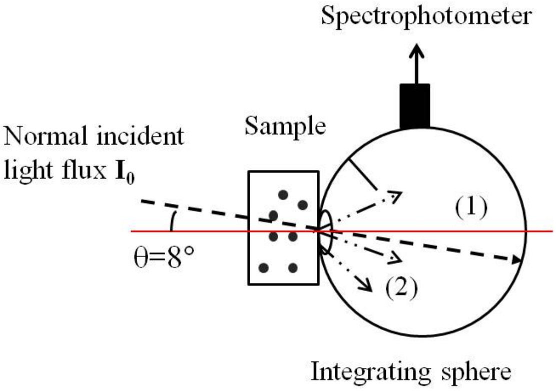

Figure 4.5: Description of the integrating sphere setup used for the measurement of the total transmittance of the bulk algal samples put in a 4mm-wide quartz cell. Both the regularly transmitted light (1) and diffusely transmitted light (2) are collected in the integrating sphere.

Implementation of the direct method

The direct method was implemented by using the mean physical and chemical data measured on the algal samples with the sandard methods as entry parameters of the *AlgaSim* program. The mean absorption, scattering and extinction cross sections C_{abs}, C_{sca}, C_{ext} and the mean anisotropy factor g were thus simulated over the [400-750nm] spectral range. They correspond to the spectral properties of one algal cell representing a mean individual among the algal population of the sample.

The algal suspension was chosen to be modeled as a monodispersion. Indeed, no granulometric measurements were implemented on the algal samples and consequently no histogram was available. Only a mean size, averaged over the whole algal population was measured. This assumption may introduce some approximations about the actual cell size: regarding the results of the sensitivity of *AlgaSim* to the cell radius analyzed in Chapter 3, it may be expected that the assumption of monodispersion may have an influence on the simulated cross sections, and in particular on the scattering cross sections. In this thesis we did not have time to explore more thouroughly this issue. That is why when discussing the results of our study we kept in mind the unknown factor introduced by the assumption of monodispersion.

In the case of a monodispersion, the spectral coefficients of the algal suspensions, μ_{abs}, μ_{sca} and μ_{ext} can be deduced from the cross sections with equations (6.15) to (6.17). The albedo a and the optical thickness τ of a slab of this algal distribution of width l can thus be calculated with relations (4.6) and (4.7). In the case of this study, $l = 4mm$.

The albedo a, the optical thickness τ and the anisotropy factor g characterizing each sample were thus calculated over the [400-750 nm] spectral range, and used as entry parameters for the Adding-Doubling program from Scott Prahl [33] run with MatLab (R2009a). All the details about the Adding-Doubling program can be found in Chapter 2. For this particular example, the number of quadratic points was set to 4. The refractive index of the quartz cell containing the algal aliquot was assumed to be constant over the considered spectrum and equal to 1.46. Normal incident light beam was considered. The total transmittance measurements M_T were thus simulated over the [400-750 nm] spectral range for all the algal samples.

Implementation of the inverse method

In this primary study we chose to test the retrieval of only three main characteristics of the cells from the total transmittance spectra measured over the [400-750 nm]spectral range, for each sample: the density N_{cell}, mean size R_{cell} and the pigment properties (composition and quantity). The other parameters such as the neutral lipids, carbohydrates and proteins quantities as well as the mean cell dry weight were thus fixed and were not varied during the optimization process. This choice was made in particular to limit the optimization time. The fixed parameters were set to mean representative values observed for the considered algal strains in other studies [7]. The cell density N_{cell}, and mean size R_{cell} were retrieved simultaneously. The pigment quantity and composition (respective proportion of each different photopigments) were retrieved afterward, in a separate optimization session.

In the present study, the ant colony algorithm presented previously was implemented and run with MatLab (R2009a). The variables were allowed to vary within ranges found as plausible in the literature [1, 7] i.e. between 0.5 and 7 μm for R_{cell} , 10^{11} and 10^{13}cell.m^{-3} for N_{cell}, 0 to 60 for the values %Chla, %Chlc, %PPC and %PSC, and 3 to 15 for the percentage of the total pigment weight compared to the cell dry mass. The quantity of Chlb was fixed to 0 as the two algal strains tested were known to have no Chlb among their photopigments [35]. In order to limit the optimization time, the ant colony algorithm was chosen to use a maximum of 100 iterations with 20 ants released at each iteration. The convergence criteria was set at $\delta < 5.10^{-3}$.

4.2.3 Results and discussion: characteristics of the algal samples

Primary microscope observations

Optical microscope images of the two strains at day 14 after the beginning of the culture are shown on figure 4.6. Primary rough observations reveal that *Isochrysis galbana* (figure 4.6 (a)) presents quasi-spherical cells with diameter close to 4 μm. The cells seem to be almost evenly pigmented as the whole cell volume appears green. However, *Phaeodactylum tricornutum* (figure 4.6 (b)) shows elongated thin cells with length up to 15 μm. The shape of those latter cells derives a lot from the spherical. Moreover, the cell volume appears to be non-evenly colored: the pigments seem to be only concentrated in a reduced zone at the center of the cells.

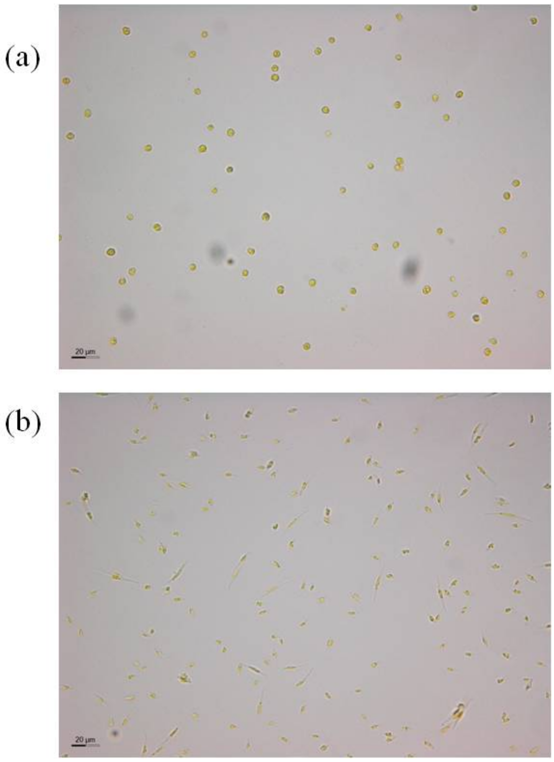

Figure 4.6: Optical microscope images of the algal populations studied: *Isochrysis galbana* (a) and *Phaeodactylum tricornutum* (b) at day 14 after the beginning of the culture.

Chemical composition, mean size and density of the cells at the different growth stages

Table 4.1 summarizes the chemical and physical characteristics measured on the algal cells of the two strains at the different growth stages.

Table 4.1: Chemical and physical data obtained by the reference measurement methods for each sample of the two studied species.

Day	Pigments mass proportions (% of the total pigments mass)					Mass proportions (% of the total dry mass)				$M_{dry,cell}$ (pg)	R_{cell} (ESD/2) (μm)	N_{cell} (10^{12}.cell.m^{-3})
	Chla	Chlb	Chlc	PSC	PPC	Lipids (neutral)	Carbo.	Proteins	Total pigments			
						Isochrysis galbana						
D7	44.2	0	12.7	15.5	27.7	21	27.5	26.5	14.6	10.0	2.13	4.89
D14	43.3	0	12.8	28.0	15.8	5	13.9	13.5	7.9	23.0	2.08	6.09
D34	42.0	0	11.8	28.1	18.1	9	21.9	25.5	8.5	22.7	2.21	7.73
						Phaeodactylum tricornutum						
D7	42.3	0	11.5	38.3	7.9	9	19.8	33.3	9.8	10.7	5.05	8.40
D14	35.1	0	11.5	40.5	13.0	2	26.3	12.4	3.7	11.4	4.8	26.1
D34	15.9	0	11.4	42.3	30.4	2	37.2	3.9	1.1	19.1	4.55	16.3

The cell abundance N_{cell} is expressed as a number of cells per cubic meter of culture medium. For *Isochrysis* the number of cells keeps increasing at each sample date. For *Phaeodactylum* however, a maximum abundance appears to be reached at day 14, and the algal population then decreases.

The mean radius of the cell population R_{cell} is calculated as half the mean equivalent spherical diameter (ESD) and is expressed in μm. For *Isochrysis* the cell size remains quite stable around 2.1 μm over the three sample dates. *Phaeodactylum* cell size slowly decreases as the culture gets older, passing from 5.05 μm to 4.55 μm between day 7 and 34. The mean total dry mass per cell $M_{dry,cell}$ is given in pg. *Isochrysis* cells get heavier between day 7 and day 14 and seem to remain stable until day 34. For *Phaeodactylum*, the cells seem to keep getting matter all along the cultivation process as the mean dry weight keeps increasing.

The chemical composition is described by giving the respective mass proportions of the neutral lipids, carbohydrates, proteins and total pigments expressed in percentage of the cell total dry weight $M_{dry,cell}$. The proportions of the different organic materials appear to vary quite significantly for the two strains all along the cultivation time: *Isochrysis* cells seem to have balanced proportions of carbohydrates and proteins at the three sample dates, with less important values at day 14. The proportion of neutral lipids has been measured to decrease between day 7 and day 14, and to increase again between day 14 and day 34. The total pigments are proportionally more important at day 7, reaching 14.6% of the total dry weight, and then become less present with a proportion varying around 8% of the total dry weight at day 14 and day 34. *Phaeodactylum* cells have proteins proportions that vary significantly with time, decreasing from 33.3% of the total dry weight at day 7 to only 3.9% at day 34. Meanwhile the mass proportion of carbohydrates increases, from 19.8% of the total dry weight at day 7 to 37.2% at day 34. The total pigment proportion keeps decreasing all along the three sample dates, from 9.8% of the total dry weight at day 7 to 1.1% at day 34. The same trend is observed with the proportion of neutral lipids, passing from 9% to 1% of the total dry weight between day 7 and day 34.

The pigment composition is detailed by giving the relative mass proportion of each pigment compared to the total pigment weight. *Isochrysis* cells appear to have a pigment composition that does not vary significantly along the cultivation process: the proportion of Chlorophyll a remains important, varying around 43% of the total pigment mass. The proportion of Chlc also remains stable, around 12% of the total pigment weight. PSC proportion increases between day 7 and day 14, passing from 15 to 28% of the total pigment weight, and remains stable at day 34. On the contrary, the PPC proportion decreases from 28% to 16% of the total pigment weight between day 7 and day 14 and slightly increases to day 34. No Chlb was measured for this strain, what was expected [35]. *Phaeodactylum* cells show more variations in their pigment composition: the Chla proportion in particular significantly decreases, from 42% of the total pigment weight at day 7 to only 16% at day 34. Meanwhile, the photoprotective carotenoids proportion increases, from 8% of the total pigment weight at day 7 to 30.4% at day 34. The PSC proportion slightly increases between day 7 and day 34, passing from 38.3% to 42% of the total pigment weight. The Chlc proportion remains stable all along the sampling period, around 11.5% of the total pigment weight. As for *Isochrysis*, no Chlb was present in the algal cells.

4.2.4 Results and discussion: test of the direct method

Spectra of the simulated cross sections and anisotropy factor

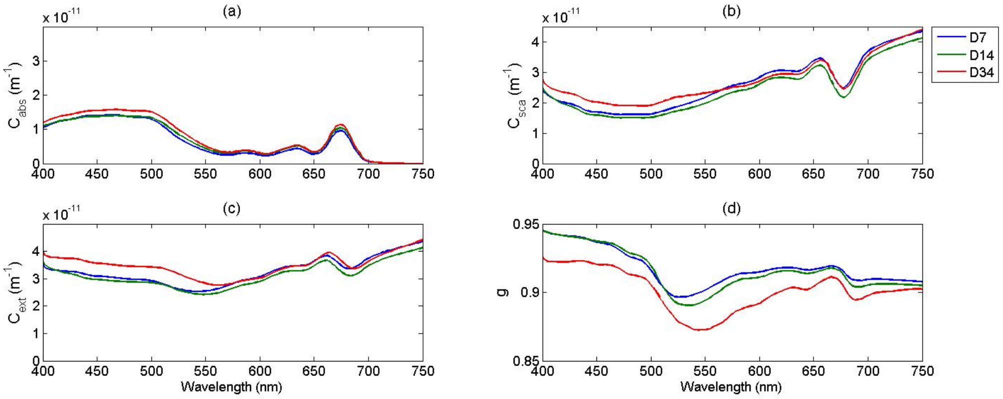

Figure 4.7: Absorption (a), scattering (b), extinction (c) cross sections and anisotropy factor (d) obtained for the three samples of *Isochrysis galbana*: D7 (blue line), D14 (green line) and D34 (red line).

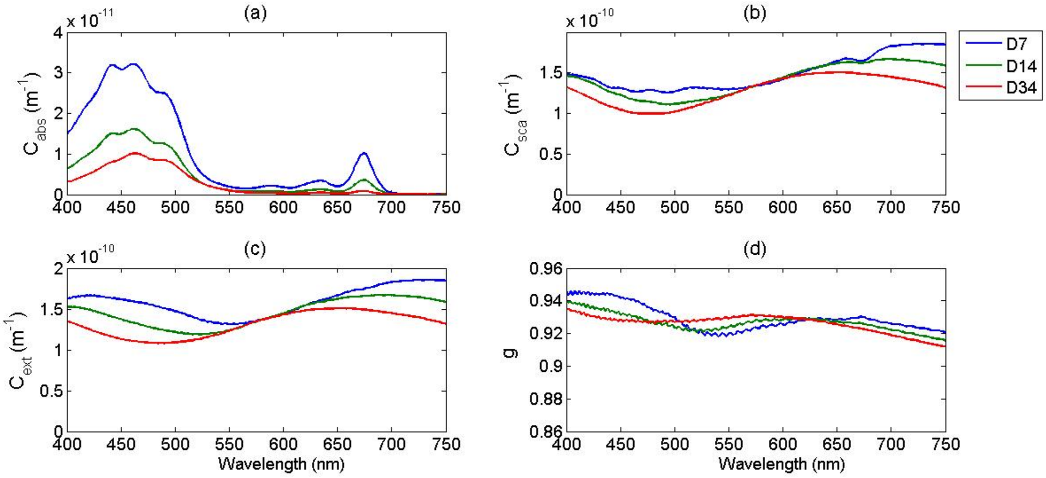

Figure 4.8: Absorption (a), scattering (b), extinction (c) cross sections and anisotropy factor (d) obtained for the three samples of *Phaeodactylum tricornutum*: D7 (blue line), D14 (green line) and D34 (red line).

Figures 4.7 and 4.8 show the absorption, scattering and extinction cross sections as well as the anisotropy factor spectra that were obtained on the [400-750 nm] spectral range by entering the measured chemical and physical data of table 4.1 as entry parameters in *AlgaSim*, for each strain at the three sampling dates.

The simulated spectra show orders of magnitude for the optical cross sections around 10^{-11} - 10^{-10} m^2, which concurs with other works [23]. For both strains the scattering cross section is higher than the absorption cross section, which is also commonly observed on real algal cells [19, 23]. It can also be noted that the anisotropy factor g shows values that are very close to 1, varying from 0.88 to 0.95 for the two strains on the [400-750nm] spectral range. This means that algal cells mainly scatter light in the forward direction, and that the transmitted light flux is expected to be high. This explains in particular why the total transmittance could be obtained with a good SNR.

We can note some high frequency patterns on the C_{sca}, C_{ext} and g spectra simulated for *Phaeodactylum*. They were not expected and are thought to originate in numerical artifacts due to Mie calculations. After testing the *Scattnlay* program for spheres simpler than complete algal cells, it appeared indeed that those artifacts were also observed for big spheres with radius > 5 μm. That is why we considered those patterns as numerical artifacts.

For both strains, the absorption cross section spectra reflect the pigment total quantity and composition. The difference in the pigmentation between the two species is clearly visible when comparing the absorption spectra shapes: the absorption peaks at 680nm and 430nm, corresponding to Chla are indeed higher for *Isochrysis*, whereas the absorption on the [450-550nm] spectral range, mainly due to the carotenoids is clearly more important for the *Phaeodactylum samples.* The absorption cross section magnitude is also directly linked to the total pigment quantities: for both strains, the magnitude of the absorption cross section increases with increasing total pigment quantity and inversely, which illustrates the evolution of the pigment concentration at each sampling date.

The magnitude of the scattering cross section varies a lot with the strain: on the considered spectral range, the simulated scattering cross sections for *Phaeodactylum* were found to be approximately three times higher than the ones obtained for *Isochrysis*. This interspecific variability has been observed by previous works, [6] and is influenced at the first order by the cell size. It is in particular visible that for each strain, the mean magnitude of the scattering cross section over the considered spectral range increases with increasing cell size: it is thus possible to deduce the evolution of the cell size between two sampling dates from the relative position of the spectra. The scattering cross sections spectra also show variations that are approximately inverse to those of absorption, especially in the vicinity of the strong absorption bands. These features are also in accordance with observations of previous works [6, 19, 23].

The extinction cross section is defined as the sum of the absorption and scattering cross sections. The spectra shape and magnitude are thus mainly influenced by those of the scattering cross section as the albedo (not shown here) is close to 1, in particular for the highly scattering *Phaeodactylum* cells. The spectral patterns in the vicinity of the strong absorption bands are also less visible than they are on the scattering cross section spectra, due to a compensation effect between absorption and scattering, as already observed in the analysis of Chapter 3. These are also classical observations that have been reported in previous works [6].

The simulated spectra show orders of magnitude and spectral patterns that are in accordance with other works,[6, 19, 23]. This gives a primary validation of the first step of the direct method.

Comparison of the measured and simulated transmittance spectra for both species

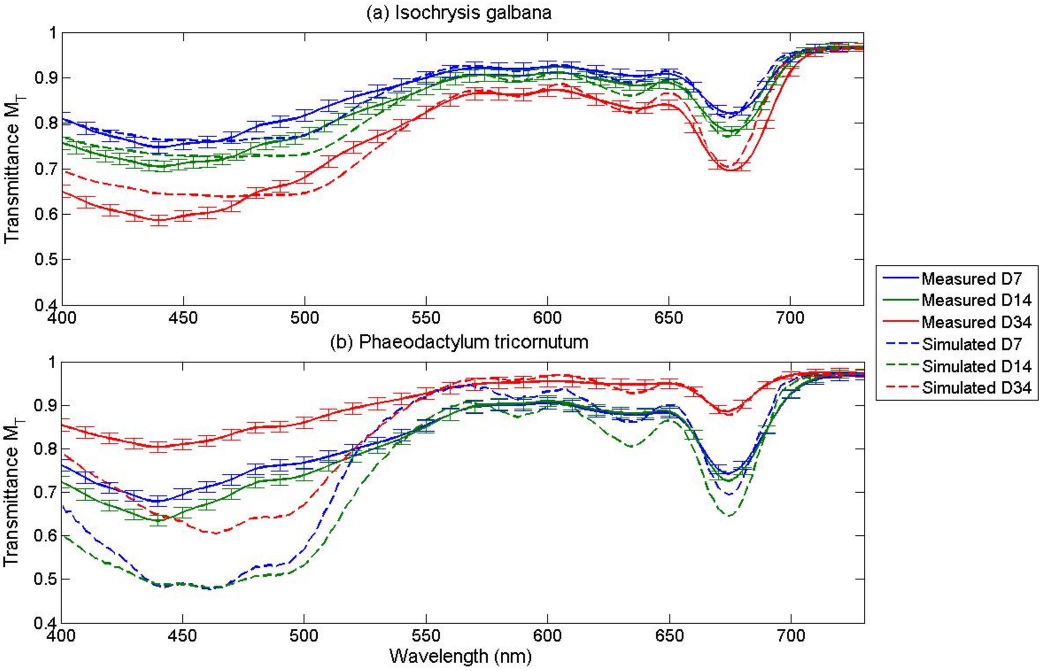

Figure 4.9: Comparison of the experimentally measured total transmittance (solid lines) and that simulated using *AlgaSim* and Adding-Doubling (dotted lines), at the three sampling dates for the two strains: (a) *Isochrysis galbana* and (b) *Phaeodactylum tricornutum*. The errorbars on the measured spectra are set to ± 2σ with σ the standard deviation.

Figure 4.9 shows the total transmittance spectra respectively measured (solid lines) and simulated (dotted lines) at the three sampling dates for *Isochrysis* (figure 4.9 (a)) and *Phaeodactylum* (figure 4.9 (b)). The measurements uncertainty on M_T has been estimated with a method similar as the one presented in Chapter 2. The errorbars are set to ± 2σ with σ the standard deviation.

The corresponding optical thickness (not shown here) for the different samples and the two strains could be calculated from the absorption and scattering cross sections, the cell density N_{cell} and the width d of the slab of algal medium considered. They were found to present high values, with $0.5 < \tau < 1.35$ for *Isochrysis* samples, and $5 < \tau < 16$ for *Phaeodactylum*. In our case, the optical thickness of the sample is far higher than 0.3 [43], [9]. This confirms that the considered algal samples present significant multi-scattering phenomena, which is in the framework of the present study.

Two main parts can be clearly distinguished on the spectra: the [400-550nm] range, corresponding to the blue part of the visible spectrum, and the [550-750nm] range that corresponds to the red part of the visible spectrum. It can be seen on figure 4.9 (a) and (b) that the simulation seems to be in better agreement with the measurement on the red part of the spectrum.

For *Isochrysis* (figure 4.9 (a)), the absorption peak at 680nm due to Chla, and the peaks at 630nm and 590nm corresponding to the absorption of Chlc are clearly visible on both the simulated and measured spectra. Over the [550-750 nm] spectral range the simulated spectra show good agreement with the measurements with a relative error of less than 5% for the three sampling dates, remaining within the measurement uncertainty zone. The measured total transmittance decreases with increasing age of the culture: this could be expected regarding table 4.1 as the number of cells and biomass increase, resulting in less light transmitted throughout the algal medium. This phenomenon is correctly taken into account by the simulation method. Over the blue part of the spectrum, i.e. on the [400-550 nm] spectral range, the simulated spectra show more discrepancies with the measured ones, with a relative error that can reach 10% for some wavelengths. Two main discrepancies can be identified: the simulated transmittance appears to be underestimated compared to the measurement in the vicinity of 500 nm, and overestimated on the wavelengths below 450 nm. The first observation may correspond to the influence of the absorption by the photoprotective carotenoids (PPC): it seems that it is overestimated by the model compared to reality, what resulted in a artificially lowered transmittance. This may be explained by the fact that a reduced set of photopigments were considered in this study, and that their respective quantity was expressed in *AlgaSim* as proportions of the total pigment weight. The relative proportion of each pigment would therefore be reduced if more pigments were considered. It seems that in our case, the PPC which present a high absorption peak at 500 nm are particularly sensitive to this phenomenon. The low values of the measured transmittance below 450 nm are due to the absorption of the pigments (mainly Chla and PPC) as well as the scattering by the algal particles. The fact that the simulated transmittance spectra show values higher than the measurements over this spectral range means that the model either underestimates absorption, scattering or both of them. Given the previous remark concerning the overestimation of the PPC absorption, it rather seems that the discrepancies between the measurements and the model are due to a slight underestimation of the scattering influence on this spectral range. This may be due to the choice of the structure of the model cell described in Chapter 3: further investigations on the influence of the order and number of organic layers could be made to validate this explanation. We could also wonder which portion of those discrepancies could be attributable to the assumption of monodispersion, which was expected to introduce some approximation effects on the simulated spectra, and in particular on the scattering cross sections.

For *Phaeodactylum* (figure 4.9 (b)) we observe more discrepancies between the simulation and the measurement. On the [550-750nm] spectral range, the relative error remains low and does not exceed 11%, obtained for day 14 at the Chla absorption peak at 680nm. The simulated total transmittance appears to be slightly underestimated by the simulation model. However this phenomenon is more important on the blue part of the spectra: the relative error at 450nm between the simulated and measured transmittance at day 14 reaches 25%, and 30% at 482nm. These discrepancies are surely explained by the fact that the scattering cross sections of the model algal cells are far higher than the ones of the real cells. This could be explained by the difference in shape between the elongated real cells and the spherical model ones, which introduces a difference in the scattering properties of the cells. This indicates that the shape of the cell was too far from the spherical to have no significant influence on its scattering properties [5]. This could be taken into account in the model method by using other Mie calculations adapted to spheroid particles that would be closer to in shape to *Phaeodactylum* cells. Some Mie calculations algorithms have been proposed to address such an issue [11], however no multi-layered models already exist in that case. Another solution would be to study the discrepancies in the scattering spectra between spherical and real cells and to propose a correction method making it possible to retrieve the second from the already existing model. Another phenomenon which could explain those discrepancies is the assumption of monodispersion, which is expected to influence the simulated scattering cross section. Despite the discrepancies in the order of magnitude, the simulated and measured spectra show the same relative positioning between the three samples, directly due to the change in biomass throughout the cultivation process.

Conclusion on the potential of the direct method

The complete method was tested in the forward running by simulating the individual spectral absorption, scattering and extinction cross sections as well as the spectral anisotropy factor of real algal cells cultivated in batch, at three sampling dates during the cultivation process. Two strains were studied in this work: the quasi-spherical *Isochrysis galbana* and the elongated *Phaeodactylum tricornutum*. The corresponding simulated total transmittance of the algal media was deduced from the simulated optical properties of the constitutive cells, and compared to spectrophotometric measurements on the real algal samples. The spectral optical cross sections simulated show orders of magnitude and spectral patterns that seem to be in accordance with literature [6, 19, 23], which gives a primary validation of the first part of the method. The simulated total transmittance obtained for *Isochrysis* at the three sample dates was demonstrated to be in great accordance with the spectrophotometric measurements implemented on the real samples. The relative error between the simulations and the measurements remains below 10% over the considered spectral range, which indicates that the absorption and scattering phenomena at stakes were globally correctly modeled. This indicates that the modeling method implemented in this study is successful in miming the optical behavior of dense algal media where multi-scattering occurs, with optical thickness $\tau>0.3$ for samples of quasi-spherical algal strains. The simulated total transmittance obtained for the elongated strain *Phaeodactylum* show good accordance with the measurements for the higher wavelengths above 550nm. However they show more discrepancies in the blue part of the spectrum below 550nm, where the scattering phenomena do not seem to be adequately modeled: this is surely due to the influence of the shape of the algal cells, differing a lot from the spherical [5], and probably to the assumption of monodispersion. The cell shape is surely a limit of the method presented in its first version. Further investigations could be implemented in future works in order to adapt the method principle to other cell shapes, and to test the influence of including the information of polydispersion.

4.2.5 Results and discussion: test of the inverse method

The results of the inverse method are presented: first we show the retrieval of the cell mean size and density, and second the retrieval of pigment quantity and composition.

Cell mean size and density

Table 4.2: Results of the inversion of the method for the retrieval of the cell mean equivalent spherical diameter (ESD) and cell density for the total transmittance measurements: comparison of the measured and predicted quantities for the two strains at each sample date.

Sample day	Mean equivalent spherical diameter (ESD) (μm)			Cell density (10^{12} cell.m^{-3})		
	Measured	Predicted	Relative error	Measured	Predicted	Relative error
			Isochrysis galbana			
D7	4.25±0.08	4.28	0.71%	4.89	5.13	4.9%
D14	4.15±0.08	3.76	9.4%	6.09	6.02	1.1%
D34	4.42±0.08	4.28	3.2%	7.73	7.19	7.0%
			Phaeodactylum tricornutum			
D7	10.1±0.2	10.14	0.40%	8.4	10.2	21.4%
D14	9.6±0.2	9.46	1.5%	26.1	22	15.7%
D34	9.1±0.2	9.6	5.5%	16.3	20.6	26.4%

Table 4.2 shows the results obtained when inverting the method as explained previously for the retrieval of the cell mean equivalent diameter (ESD) and cell density inside the culture medium from the measured total transmittance spectra, for both strains at each sample date. The mean ESD could be retrieved for both strains and at each sampling date with a relative error below 10%, which is a very satisfying result. The cell density was satisfyingly predicted for *Isochrysis* at each sampling date, with a relative error below 7%., which makes it possible to predict the trends in the cell population growth. However, more discrepancies are observed for *Phaeodactylum*, for which the cell density could be predicted with a higher relative error, up to 27% at day 34. These discrepancies could be expected, as the cell density mainly influences the transmittance spectra magnitude. However, as presented previously, the non-spherical shape [5] of the *Phaeodactylum* cells, and the assumption of monodispersion introduce discrepancies in the magnitude between the simulated and measured transmittance in the blue part of the spectrum in particular. However the error between the predicted and measured spectra was calculated in the inversion process as one minus the cosine of the SAM [22] between the two spectra, which takes into account all the wavelengths, including the blue part of the spectrum. This may explain why no better results could be obtained with the inversion process.

Pigments quantity and composition

Table 4.3: Results obtained by inverting the method to retrieve the pigments quantity and composition from the measured total transmittance spectra: comparison of the predictions to the reference measurements for the two strains at each sample date.

Sample day		***Isochrysis galbana***					
		Relative pigment proportions				Carotenoids/Chl	Pigment total quantity (pg)
		%Chla	%Chlc	%PPC	%PSC		
D7	Measured	44.2	12.7	27.7	15.5	0,76	1.46
	Predicted	45	13	26	16	0,72	1
	Relative error	1.8%	2.4%	6%	3.2%	4.6%	32%
D14	Measured	43.3	12.8	28.1	15.8	0,78	1.81
	Predicted	45	13	26	16	0,72	1.84
	Relative error	3.9%	1.6%	7.5%	1.3%	7.5%	1.7%
D34	Measured	42.0	11.8	28.1	18.1	0,86	1.94
	Predicted	42	11	28	19	0,89	1.93
	Relative error	0%	6.8%	0.4%	5%	3.3%	0.52%

Sample day		***Phaeodactylum tricornutum***					
		Relative pigment proportions				Carotenoids/Chl	Pigment total quantity (pg)
		%Chla	%Chlc	%PPC	%PSC		
D7	Measured	42.3	11.5	38.3	7.9	0.86	1.05
	Predicted	54	13	30	8	0.57	0.55
	Relative error	27.7%	13%	21.7%	1.3%	34%	48%
D14	Measured	35.1	11.5	40.5	13	1.15	0.43
	Predicted	40	12	30	18	0.92	0.23
	Relative error	14%	4.3%	25.9%	38.5%	19.6%	47%
D34	Measured	15.9	11.5	42.3	30.4	2,7	0.22
	Predicted	30	12	40	18	1.4	0.095
	Relative error	88.6%	4.3%	5.4%	40.8%	48%	57%

Table 4.3 summarizes the results obtained with the inversion of the method to retrieve the pigments quantity and composition from the measured total transmittance spectra for the two strains, at each sampling date. The pigment characteristics of an algal cell population have been shown to be a good strain marker [2] as well as an important indicator of the health of the algal population [38]. The relative proportion of carotenoids compared to chlorophylls in particular is commonly evoked as an indicator of the algal culture stress [38]. This is why the ratio of the quantity of the total quantity of carotenoids (PPC+PSC) and total chlorophylls (Chla+Chlc) is also presented in table 4.3.

For *Isochrysis*, table 4.3 shows that the pigment total quantity could be generally well predicted: for day 14 and day 34 with a relative error below 2%, and at day 7 with a higher relative error which remains however below 35%. The prediction of the relative proportions of the different pigments also gives values that are remarkably in accordance with the HLPC measurements, with relative errors that do not exceed 9%. As a consequence the evolution of the ratio carotenoids/Chl could also be predicted with low relative errors.

For *Phaeodactylum* the predicted values generally show more discrepancies with the measurements than what is obtained for *Isochrysis*. This is surely also explained by the shape effect that has already been evoked in the previous sections, and maybe also by the fact that the pigments are not evenly distributed in the algal cells, as observed on figure 4.6 (b). The total pigment quantity thus seems to be underestimated by the predictions up to 50% compared to the measurements. Nevertheless the general decreasing trend of the total pigment quantity with the culture age could be retrieved. The relative proportions of the different pigments could be predicted more or less satisfyingly depending on the pigment considered: the Chlc proportions were well predicted with relative errors below 15% at each sampling date. The PPC show also quite well predictions with relative errors below 25%. More discrepancies are observed for Chla and the PSC, more particularly at day 34. This may originate from the fact that those two pigments present high absorption in the blue part of the spectrum, where we have already observed that the simulated and measured transmittance spectra were very different. The carotenoids/Chl ratio is predicted with quite high relative errors: however the simulations reproduce the trend observed with the measurement, i.e. a progressive increase of the carotenoids/Chl ratio, what gives relative information about the evolution of the algal population health in time.

Conclusion on the potential of the inverse method

The test of the inversion method shows that the mean cell size could be satisfyingly predicted from total transmittance spectra for the two tested algal strains: this suggests that the non-spherical shape of *Phaeodactylum* does not influence the retrieving of the cell mean diameter. This means that the mean cell diameter may be obtained with a good approximation from fast spectral measurements which could be adapted to be implemented in-line: this offers very interesting prospects for industrial or research applications that would require a daily screening of the cell size. For *Isochrysis* the inversion also gives cell densities, pigment total quantity and relative composition that are remarkably in accordance with the reference measurements, which is a promising result for applications to culture monitoring. The results predicted for *Phaeodactylum* are less close to the measurements, which may be due to the influence of the non-spherical shape of the algal cells. However the method could be adapted to produce a first qualitative approximation of the culture sate and evolution in time, in particular by giving the trends in the evolution of the carotenoids/Chl ratio [38].

4.3 Conclusion

This Chapter aims at proposing a complete method linking the paradigms developed in Chapter 1, Chapter 2 and in Chapter 3: more precisely, we investigated the means to link the description of the spectral apparent properties at the global scale of the dense algal aliquot to the description at the scale of an individual algal cell, characterized by its physico-chemical properties. To the state of our knowledge, our study is the first one attempting to link directly the apparent spectral properties of a dense algal medium with optical thickness much higher than 0.3 to the physical and chemical data characterizing the constitutive cells.

For this purpose, an original modeling method using both extended Mie theory [45] and the RTE [17] paradigm has been implemented. The direct method allows to simulate the reflectance and transmittance spectra of dense algal aliquots from the physiological parameters describing the constitutive algal cells. The inverse method makes it possible to retrieve a set of physico-chemical data characterizing the cells from spectral measurements of the reflectance and/or transmittance of a dense algal sample.

The principle of the method has been tested as a first step with the data of a measurement campaign implemented on two different algal cultures sampled at three different growth stages. In order to test the influence of the shape of the cells, a quasi-spherical strain, *Isochrysis galbana* and a stick shaped one, *Phaeodactylum tricornutum* were chosen. In the context of the primary study implemented during this thesis, the complete method was simplified: only the total transmittance M_T was considered for the direct, and inverse method. For the inverse method, the set of variables was reduced to only the cell size and density, and pigment quantity and composition. Those choices were made in particular in order to limit the convergence time. The algal suspensions were assumed to be monodisperse, which simplifies the calculation of the linear optical properties.

The direct method seems adapted to model dense algal media total transmittance spectra over the [400-750nm] spectral range for the quasi-spherical strain *Isochrysis galbana*. Indeed, the relative error between the simulations and the measurements was shown to remain below 10% over the considered spectral range. However for the elongated *Phaeodactylum tricornutum*, more discrepancies have been found between the simulations and the measurements in particular in the blue part of the spectrum where the scattering phenomena are expected to be high. This is probably due to an oversestimation of the scattering cross section of the cells by the *AlgaSim* program, originating in the non-spherical shape of the real algal cells [5], and/or in the assumption of monodispersion. This indicates that the assumption of the spherical shape of the cells is a limit of the present version of our method. In practice this could be oversteped by using another Mie model, adapted to spheroidal particles for example [11]. However the presently available solutions adapted to non-spherical particle shapes cannot model a multilayered structure. Another solution would be to model the influence of the cell shape on the spectra and to apply an empirical correction.

The inverse method shows promising results for *Isochrysis galbana*, for which the cell mean size and density as well as the pigment quantity and composition were retrieved with relative error below 10% from the total transmittance spectra. For *Phaeodactylum tricornutum* only the cell mean equivalent diameter could be determined with such a low relative error. More quantitative discrepancies are found between the predicted values and the measurements for the cell density and pigment composition. Those may be explained also by the non-spherical shape of the real cells. However the predicted values seem to be qualitatively informative about the culture physiological evolution, as they reproduce correct relative trends in particular for the carotenoids/Chl ratio [38]. Those first results are promising, in particular for practical applications to the monitoring of the culture of dense algal media. Future works would be to test the method while introducing more variables in the inverse method, and using also the measurements of the total reflectance and regular transmittance. The influence of the assumption of poly/monodisperse suspension should also be investigated.

Bibliography

[1] E. Aas. Refractive index of phytoplankton derived from its metabolite composition. *Journal of Plankton Research*, 18(12), 1996.

[2] R. Aguirre-Gomez, S. R. Boxall, and A. R. Weeks. Identification of algal pigments using high order derivatives. *IEEE*, 1995.

[3] H. Berberoglu, P.S. Gomez, and L. Pilon. Radiation characteristics of botryococcus braunii, chlorococcum littorale, and chlorella sp. used for co2 fixation and biofuel production. *Journal of Quantitative Spectroscopy and Radiative Transfer*, 110(17), 2009.

[4] E. Bertozzini, L. Galluzzi, A. Penna, and M. Magnani. Application of the standard addition method for the absolute quantification of neutral lipids in microalgae using nile red. *Journal of microbiological methods*, 87(1), 2011.

[5] A. Bricaud, A. L. Bédhomme, and A. Morel. Optical properties of diverse phytoplanktonic species: experimental results and theoretical interpretation. *Journal of plankton research*, 10(5), 1988.

[6] A. Bricaud, A. Morel, and L. Prieur. Optical efficiency factors of some phytoplankters. *Journal of limnology and oceanography*, 1983.

[7] M. R. Brown and S. W. Jeffrey. Biochemical composition of microalgae from the green algal classes chlorophyceae and prasinophyceae. 1. amino acids, sugars and pigments. *Journal of experimental marine biology and ecology*, 161, 1992.

[8] O.B. Brown and H.R. Gordon. The size-refractive index distribution of clear coastal water particulates from light scattering. *Applied Optics*, 13, 1974.

[9] D.S. Bugnolo. On the question of multiple scattering in the troposphere. *Journal of geophysical research*, 65, 1960.

[10] A. M. Ciotti, M. R. Lewis, and J. J. Cullen. Assessment of the relationships between dominant cell size in natural phytoplankton communities and the spectral shape of the absorption coefficient. *Journal of limnology and oceanography*, 47, 2002.

[11] W.R. Clavano, E. Boss, and L. Krap-Boss. Inherent optical properties of non-spherical marine-like particles - from theory to observation. *Oceanography and Marine Biology*, 45, 2007.

[12] M. Dorigo, M. Birattari, and T. Stützle. Ant colony optimization. Technical report, Institut de Recherches Interdisciplinaires et de Développements en Intelligence Artificielle, Université libre de Bruxelles, 2006.

[13] Q. Dortch, J.R. Jr. Clayton, S.S. Thoresen, and S.I. Ahmed. Species differences in accumulation of nitrogen pools in phytoplankton. *Marine biology*, 81, 1984.

[14] M. Dubois, K.A. Gillies, J.K. Hamilton, P.A. Rebers, and F. Smith. Colorimetric method for the determination of sugars and related substances. *Analytical chemistry*, 28, 1956.

[15] E. Le Floc'h, G. Malara, and A. Sciandra. An automatic device for in vivo absorption spectra acquisition and chlorophyll estimation in phytoplankton cultures. *Journal of Applied Phycology*, 14, 2002.

[16] H. Hillebrand, C.D. Düreselen, D. Kischtel, U. Pollingher, and T. Zohary. Biovolume calculation for pelagic and benthic microalgae. *Journal of phycology*, 35, 1999.

[17] A. Ishimaru. *Wave propagation and scattering in random media.* IEEE press: New York, 1997.

[18] B.R. Jennings and K. Parslow. Particle size measurement: The equivalent spherical diameter. *Proceedings of the Royal Society of London, Series A*, 419, 1988.

[19] R. Kandilian, E. Lee, and L. Pilon. Radiation and optical properties of nannochloropsis oculata grown under different irradiances and spectra. *Bioresource Technology*, 2013.

[20] M. Kerker, editor. *Light scattering by non-spherical particles: theory, measurements and applications.* Academic press, New York, 1969.

[21] J. C. Kitchen and J. R. V. Zaneveld. A three-layered sphere model of the optical properties of phytoplankton. *Journal of limnology and oceanography*, 37, 1992.

[22] F.A. Kruse, A.B. Lefkoff, J.W. Boardman, K.B. Heiedbrecht, A.T. Shapiro, P.J. Barloon, and A.F.H. Goetz. The spectral image processing system (sips) - interactive visualization and analysis of imaging spectrometer data. *Remote sensing of environment*, 44(2-3), 1993.

[23] E. Lee, R. L. Heng, and L. Pilon. Spectral optical properties of selected photosynthetic microalgae producing biofuels. *Journal of Quantitative Spectroscopy and Radiative Transfer*, 114, 2013.

[24] O.H. Lowry, N.J. Rosebrough, A.L. Farr, and R.J. Randall. Protein measurement with folin-phenol reagent. *Journal of biological chemistry*, 193, 1951.

[25] G. Mie. Beitrage zur optik trüber medien, speziell kolloidaler metallösungen. *Annalen der physik*, 25(3), 1908.

[26] C. Mobley. Ocean optics web book. http://www.oceanopticsbook.info. (accessed August 2014).

[27] A. Morel and A. Bricaud. Theoretical results concerning light absorption in a discrete medium, and application to specific absorption of phytoplankton. *Deep sea research*, 28, 1981.

[28] J. L. Mueller. *The influence of phytoplankton on ocean color spectra.* PhD thesis, Oregon state university, 1973.

[29] T.T. Packard, T.M. Moore, and D.A. Harmon. *Phytoplankton growth dynamics*, volume I, chapter Biochemical assays, pages 119–130. Seattle, WA : University of Washington Special Report, 1972.

[30] O. Peña and U. Pal. Scattering of electromagnetic radiation by a multilayered sphere. *Computer Physics Communications*, 180, 2009.

[31] T. Platt and A.D. Jassby. The relationship between photosynthesis and light for natural assemblages of coastal marine phytoplankton. *Journal of Phycology*, 12, 1976.

[32] L. Pottier, J. Pruvost, J. Deremetz, J. F. Cornet, J. Legrand, and C. G. Dussap. A fully predictive model for one-dimensional light attenuation by chlamydomonas reinhardtii in torus photobioreactor. *Wiley InterScience*, 2005.

[33] S. A. Prahl. *Optical-Thermal Response of Laser Irradiated Tissue.* 1995.

[34] A. Quirantes and S. Bernard. Light scattering by marine algae: two-layer spherical and non-spherical models. *Journal of Quantitative Spectroscopy and Radiative Transfer*, 89, 2004.

[35] K.S. Rowan. *Photosynthetic pigments of algae.* Cambridge university press, 1989.

[36] S. Roy, S. Sathyendranath, and T. Platt. Retrieval of phytoplankton size from bio-optical measurements: theory and applications. *Journal of the royal society Interface*, 8, 2011.

[37] T.J. Smayda. *Phytoplankton manual*, chapter From phytoplankton to biomass, pages 273–279. UNESCO, Paris, 1978.

[38] A.E. Solovchenko, I. Khozin-Goldberg, and M.N. Merzlyak Z. Cohen. Carotenoid-to-chlorophyll ratio as a proxy for assay of total fatty acids and arachidonic acid content in the green microalga parietochloris incise. *Journal of applied phycology*, 21, 2009.

[39] R. Steponavicius and S. N. Thennadil. Extraction of chemical information of suspensions using radiative transfer theory to remove multiple scattering effects: application to a model two-component system. *Analytical Chemistry*, 18, 2009.

[40] R. Steponavicius and S. N. Thennadil. Extraction of chemical information of suspensions using radiative transfer theory to remove multiple scattering effects: application to a model multicomponent system. *American Chemical Society*, 83, 2011.

[41] D. Stramsky, A. Morel, and A. Bricaud. Modeling the light attenuation and scattering by spherical phytoplanktonic cells: a retrieval of the bulk refractive index. *Applied Optics*, 27(19), 1988.

[42] J. Sun and D. Liu. Geometric models for calculating cell biovolume and area for phytoplankton. *Journal of phytoplankton research*, 25(11), 2003.

[43] H. C. van de Hulst. *Light scattering by small particles.* Wiley, 1957.

[44] F. Vidussi, B. Mostajir, E. Fouilland, E. Le Floch, J. Nouguier, C. Roques, P. Got, D. Thibault-Botha, T. Bouvier, and M. Trousselliera. Effects of experimental warming and increased ultraviolet b radiation on the mediterranean plankton food web. *Limnology and oceanography*, 56(1), 2011.

[45] Z.S. Wu and Y.P. Wang. Electromagnetic scattering for multilayered sphere: recursive algorithms. *Radio Science*, 26(6), 1991.

[46] M. Zapata, F. Rodríguez, and J.L. Garrido. Separation of chlorophylls and carotenoids from marine phytoplankton: a new hplc method using a reversed phase c8 column and pyridine-containing mobile phases. *Marine ecology progress series*, 195, 2000.

[47] C.J. Zhu and Y.K. Lee. Determination of biomass dry weigh of marine microalgae. *Journal of applied phycology*, 9, 1997.

Chapter 5

Conclusion

Contents

5.1 Summary of the thesis

Aims

This thesis is a primary investigation of the potential of characterizing dense algal cultures with their spectral absorption and scattering properties by VIS-NIR spectroscopy. It addresses in particular the operational issue of the monitoring of the mass cultivation process, originating in a lack of specific measurement instrumentation currently available [12, 17]. Among the scientific issues at stake we can cite first the theoretical modelling of light variations in highly scattering media. The modelling of the spectral properties of the algal cells which are living organisms with a complex structure is also adressed.

To address those issues, the proposed work includes different guidelines corresponding to the different scales of description of the problem. In a first time, the scale of the bulk aliquot of culture medium was considered. We thus aimed at investigating how to characterize the apparent spectral properties of this given aliquot of dense algal culture medium. The apparent spectral properties depend on the intrinsic properties of the medium itsef, but also on the experimental conditions with which they are actually measured. That is why we first defined precisely the notions of apparent spectral reflectance and transmittance, and proposed a practical measurement setup and the associated protocol for their sensible measurement.

In a second time we investigated the links between the apparent properties of the aliquot and the intrinsic linear properties of the medium itself. For this purpose, solving the radiative transport equation which rigorously formulates the light variation within a defined complex sample from its intrinsic optical characteristics was explored.

In a third time our work aimed at studying the scale of the individual algal cell. More precisely, the links between the physical and chemical properties of an algal cell and its resulting spectral absorption and scattering characteristics were investigated.

In a final step, our work aimed at linking the description of the individual constitutive cells to the apparent spectral properties measurable on a sample aliquot. The goal was in particular to propose a complete method making it possible to translate the apparent spectral properties in terms of information on the chemical and physical states of the algal cells, and vice versa.

Method and results

In the first Chapter we gave the precise definition of what we call the apparent spectral properties. For a sample illuminated by an incident beam, the total reflectance is defined as the ratio of the light flux reflected back in the whole half space containing the incident beam, and the incident flux. Similarly, the total transmittance is the ratio of the light flux transmitted throughout the sample in the second half space and the incident light flux. We also defined the regular transmittance as the ratio of the transmitted light flux in the direction of the incident beam and the incident flux. In practice, different setups can be implemented to measure those quantities. However for highly turbid media such as dense algal cultures, the Double Integrating Sphere setup [13] is looked as an interesting solution: as the spheres are designed to collect light in a wide solid angle, they make it possible to have more signal even for highly absorbing and scattering samples. Yet several technical keypoints must be taken into account when designing a DIS setup in order to perform the correct measurement of the apparent properties. Photometrical considerations constrain the spheres dimensions, the injection in the detection system as well as the positionning and geometry of the sample. In this thesis we presented a model DIS setup specially designed for the applications on dense algal samples, and tested it on phantom solutions of dyed polystyrene microspheres. This primary test was performed as a first step at one single wavelength (632.8 nm), and made it possible to observe the evolution of M_R, M_T and M_U as functions of the particulate concentration and of the sample thickness.

In the second Chapter the linear spectral coefficients were defined as optical properties intrinsic to the medium under study. They can be seen as statistical quantities representing the spectral probability to undergo absorption and scattering events for a photon traveling through a unit length of medium. We saw that the radiative transport equation [7] is one of the rigorous paradigms describing the light variations inside a sample defined by its intrinsic optical properties and its geometry: it thus allows to link the intrinsic properties to the apparent properties described previously. However, in the general case of suspensions with an occupied volume ranging between 0.1 and 1% the RTE cannot be analytically solved, nore simplified with an approximation theory such as simple scattering model or the diffusion approximation [7]. Among the alternative methods to solve the RTE are the numerical resolution methods, and more precisely the Adding-Doubling method [14]. The AD method discretizes the RTE by considering a slab geometry. The sample under study is thus seen as a set of infinitely thin homogeneous slabs for which the RTE can be solved. The Adding and Doubling operations are matrix calculations making it possible to compute the resulting light variations inside a set of different slabs from the light variations in each slab. The direct method makes it possible to obtain the apparent properties of the sample from the description of its intrinsic properties and its geometry. With the inverse method, the intrinsic spectral properties of a medium can be retrieved from the apparent properties measured on a given aliquot. A comprehensive program coding the AD and IAD computations was developed by Scott Prahl [15] for his own work on biological tissues, and used for our own applications. We tested in particular the IAD method on real dense algal samples. From the measurements of M_R and M_T implemented with a Double Integrating Sphere setup, we investigated the retrieval of the intrinsic linear properties of four algal samples over the [400-1020 nm] spectral range. Due to operational constraints, the DIS setup implemented could not be designed as the model setup presented previously: smaller spheres and a multispectral detection system with a smaller active area had to be used. The first results obtained showed that the retrieved linear spectral coefficients seem to be qualitatively and quantitatively in accordance with the observations commonly described in litterature [18, 1, 6]. Nevertheless, the significant influence of the experimental errors made on the measurement of M_R and M_T on the quantitative values of the retrieved intrinsic properties was observed on certain spectral ranges. Indeed, the light losses in the DIS setup can introduce significant misestimations of the linear coefficients [4]: by interpreting the light loss as absorption, this lead in particular to an oversestimation of the absorption coefficient and an underestimation of the scattering coefficient. This issue illustrates the great influence of the operational measurement setup on the interpretation of the spectra, and should be kept in mind at each stage of the work.

In the third Chapter the individual algal cells are considered. Our work aimed in particular at studying the influence of the cell physiology, described by chemical and physical parameters, on its individual spectral properties, i.e. its absorption and scattering cross sections. For this purpose a simulation program called AlgaSim was developed: it made it possible to simulate the spectra of the absorption and scattering cross section of one algal cell modeled as a three-layered sphere, and defined by a set of physiological data such as its size, dry weight, the proportions of the different cell materials (carbohydrates, proteins and neutral lipids) as well as the total pigment quantity and the respective proportions of the different pigments. The AlgaSim program was based on the extended Mie theory, and more precisely on the solution of Kerker [9] for multilayered spheres. Indeed, formulating the links between the spectral properties of algal cells and their physical and chemical characteristics is a complex issue, as the relations have been observed to be non linear and multivariate. As no explicit relations can be formulated between on the one hand the spectral absorption and scattering properties, and on the other hand the physico-chemical parameters of the cell, it is necessary to use an implicit modelling. Simple and extended Mie theory have been investigated by previous works, in particular in oceanography, to adress this issue. The solution of Kerker for multilayered spheres in particular has been proved to adequately model the structure of a cell of shape not significantly different from a sphere [16]. That is why it was chosen and implemented in our work. To the state of our knowledge our approach is the first one to use such a simulation tool to investigate as throuroughly the influence of the cell physiology on its spectral properties. The AlgaSim program was thus specially designed to integrate a wide range of different variable parameters. However our model included assumptions that must be kept in mind while observing the results: the cell shape is supposed to be spherical, and even if taken as wide as possible, the number of pigments and materials had to be reduced compared to the real case.

The general running was first tested by reproducing the case of a 5-μm algal cell with a determined pigment composition presented by Mueller in his PhD thesis [11]. The simulated optical cross section spectra obtained with *AlgaSim* show good qualitative and quantitative agreement with the ones of Mueller, which validates the general running of the program. A second investigation of *AlgaSim* running was achieved by simulating and analysing large databases of optical cross section spectra. Thousands of different individual cells with chemical and physical characteristics ranging between plausible values were created. Their absorption and scattering spectra were thus simulated with the *AlgaSim* program, and analyzed with the method of the Principal Component Analysis (PCA) [8]. This made it possible to determine the links between the spectra variations and the cell characteristics. The trends observed on the optical cross section spectra appear to be consistent with previous observations reported in litterature [1, 10]: absorption spectra are influenced by the pigment composition and quantity as well as by the cell size, following Ciotti et al. findings [1]. The scattering spectra are mainly dependant on the size of the algal cell: an important observation though is that the scattering spectra also brings information about the chemical state of the cell, in particular about the pigments. This second analyze validates *AlgaSim* ability to simulate adequately the optical properties of single algal cells by taking into account the influence of the cell physiology.

In the last Chapter, a complete method was proprosed to organize together all the scales of description prevously considered, making it possible in particular to link the physiological description of algal cells to the apparent spectral properties measured on dense aliquots from the culture medium. For this purpose, a complete method using both extended Mie theory [20] and the RTE [7] paradigms was implemented. The direct method allows to simulate the reflectance and transmittance spectra of dense algal aliquots from the physiological parameters describing the constitutive algal cells. The inverse method makes it possible to retrieve a set of physico-chemical data characterizing the cells from spectral measurements of the reflectance and/or transmittance of a dense algal sample.

It was also necessary to define how to switch from the individual cell cross sections to the instrinsic properties of an algal suspension made of thousands of cells. In theory the resulting linear instrinsic properties of a cell population are the weighted sum of each individual cross sections: the rigorous modelling of a real population would require to model each individual cell with its own physical and chemical properties. This solution can be hard to implement in practice: in standard characterization methods such as microscopy observation, chemical extraction and analysis, quantities are measured not only for single cells, but they are averaged on thousands of cells. To the state of the current techniques, it is only possible to measure size distribution frequency with some particle counters. If the size distribution frequency is known it would thus be possible to calculate the resulting spectral properties of a population by implementing a weighted sum of the cross sections corresponding to the different cell sizes. If only a mean cell size is known, the case of a monodisperse algal suspension is assumed which simplifies the expression of the resulting linear properties, expressed as a simple sum of cross sections.

The complete method was tested with two different algal cultures: a quasi-spherical strain, *Isochrysis galbana* and a elongated one, *Phaeodactylum tricornutum*, chosen in order to test the influence of the shape on the modelling implemented. This experimental work was a primary practical study of the complete method, and some assumptions were made to simplify the test: only the total transmittance M_T was considered for the direct, and inverse method. For the inverse method, the set of variables was reduced to only the cell size and density, and pigment quantity and composition. Those choices were made in particular in order to limit the convergence time. The algal suspensions were assumed to be monodisperse, which simplifies the calculation of the linear optical properties.

Over the [400-750nm] spectral range, the direct method was shown to simulate total transmittance spectra that were in good agreement with the measurements for the quasi-spherical strain *Isochrysis galbana*, the relative error between the simulations and the measurements was shown to remain below 10% over the considered spectral range. More discrepancies were observed for the elongated *Phaeodactylum tricornutum*, especially in the blue part of the spectrum. Possible explanation is an overestimation of the scattering cross sections of the cells by the AlgaSim program, due to the non-spherical shape of the cells. Moreover, the assumption of monodispersion might have introduced supplementary approximations in the estimation of the algal suspension resulting spectral properties. This reveals that the assumption of the spherical shape of the cells, and of the monodispersion are limits of the persent version of our method. In practice the shape issue could be oversteped by using another Mie model, adapted to spheroidal particles for example [2]. However the presently available solutions adapted to non-spherical particle shapes cannot model a multilayered structure. Another solution would be to model the influence of the cell shape on the spectra and to apply an empirical correction. The monodispersion issue could be explored by comparing the results obtained with different profiles of size distributions which could make possible to characterize the actual impacts on the simulated spectra.

As for the inverse method, excellent results were obtained for *Isochrysis galbana*. The cell mean size and density as well as the pigment quantity and composition were retrieved with relative error below 10% from the total transmittance spectra. The mean cell equivalent spherical diameter could also be predicted with such a low relative error for *Phaeodactylum tricornutum*. However, more quantitative discrepancies were observed between the predictions and the measurements for the cell density and pigment composition. This was expected regarding the previous observations with the direct method, and might also originate in the non-spherical shape of the real cells, as well as in the monodispersion assumption. Nevertheless, one could note that the predicted values seem to be at least qualitatively informative about the culture physiological evolution, as they reproduce correct relative trends in particular for the carotenoids/Chl ratio [19], which is known to be an important indicator of the culture stress. Those first results are promising, in particular for practical applications to the monitoring of the culture of dense algal media.

5.2 Prospects and future work

5.2.1 Prospects of the work developed in this thesis

The results presented in this thesis suggest that the VIS-NIR spectroscopy shows great potential for the aimed application in microalgal cultivation process monitoring. The complete method presented in Chapter 4 in particular can be seen as the principle of a future operational system designed for the fast diagnosis of the dense algal culture state. Obviously, some supplementary studies for the optimization of the computational inversion as well as for the exact configuration of the measurement setup are necessary before proposing a practical solution more advanced than the bench scale. However we believe that the results of this thesis are promising.

The general principle developed in our work, i.e. coupling a thourough optical modelling to spectroscopy measurements, could also be seen as an interesting approach for other application domains. The approach has been proved to be consistent for microalgal cells, yet we believe it could be extended to other biological suspensions, e.g. bacteria, blood, juices. Due to their extreme specificity, a thourough study must be obviously implemented for each medium, and the very practical results found in this thesis do not apply to any other material than dense algal suspensions. Yet the principle of our work remains generic and interesting for any particle suspensions.

5.2.2 Proposition of future investigations following this thesis

About the measurement setup

The model DIS setup presented in Chapter 1 was designed specifically to maximize the collection solid angles of the spheres. This was surely a crucial point to take into account in order to implement a bench photometrically rigorous. Consequently, the spheres were chosen with a wide inner diameter. And as another consequence, the bigger the spheres, the less signal inside of them, according to the law of integrating spheres. In an ideal setup, this small loss of signal should not trouble the measurements provided that the detection chain is adapted, i.e. that the detector active area is big, and the detector sensitive. Unfortunately, during this thesis we experienced operational constraints and limited available multispectral detection devices when implementing our campaigns. That is why a poorly adapted detection system, with a too small detection area, had to be used. This obviously deteriorated the actual signal to noise ratio of our measurements, which introduced experimental errors and their consequences on the simulations already described.

Optimizing the light injection in the detection system is surely the first step to implement in order to greatly improve the measurement setup. For this purpose, we would suggest to use a non-fibered photodetector with a wide active area, such as the $100mm^2$-active area, amplified, switchable-gain, silicon detector from Thorlabs (PDA100A) for example. This model is designed for detection over all the visible range [400-1100nm]. As the photodetector detects light flux without wavelength distinction, this solution would require to use a monochromator, and to perform the measurements wavelength by wavelength. Such technical solutions have been tested by other research teams and have been shown to be functional [21].

About the assumptions linked to the modelling

The modelling of the algal cells, and of the algal populations presented in this thesis were based on several assumptions: future prospects of this work would be to further investigate those primary hypothesis and to test other configurations.

About the algal culture medium itself, we assumed as a first step that only algal cells were present. As presented in the introduction, there are many other particles in a real culture. Bacteria in particular can be really numerous, with concentrations comparable or even greater than the algal cells themselves. Bacteria are usually smaller than algal cells and are not pigmented, which explains that are expected to be mainly scattering and not significantly absorbing. Many studies have investigated the role of bacteria in aquatic ecosystems [3, 5], and have proved that bacterial and algal growth were closely linked. Including the bacteria in the optical modelling proposed in this thesis would surely offer new interesting prospects, and that is why we strongly suggest to implement it as a futur development of our work. The same principle than the one presented in this thesis to model the algal cells could be tested in particular.

In the framework of this thesis, we chose to model the algal cells as spherical, with three concentric layers of organic materials put in a given order. Many further tests of different configurations could be implemented. We have seen in our work that the cell shape in particular could have great influence on the scattering cross section in particular when it is too far from the spherical. One of the pathways to development of our work would be to investigate how to include the influence of the cell shape in the modelling. A second study would be to investigate the influence of the order of the successive layers on the simulated cross sections spectra. We could also consider modelling more specific microalgae strains, such as Coccolithophycae for example, which are known to present an external calcium carbonate shell. This would make it possible to add a supplementary reflective layer on the model cell and to check if the simulations show expected trends.

As far as the algal population is concerned, we made the choice in this work to model it as a monodispersion of identical cells characterized by averaged chemical and physical characteristics. This first step has already shown promising results, yet we believe that even better simulations could be obtained by bringing more complexity in the modelling. For this purpose, we would suggest to analyze as a first step the influence of the size distribution on the simulated absorption and scattering spectra as well as on the anisotropy factor: indeed, we expect the resulting linear scattering coefficient in particular to be highly dependent on the size distribution. Moreover, we have observed during this thesis that classical size distributions were linked to the cell division, and that two main dominant diameters could be recognized: diameter d corresponding to a mature cell, and diameter $d/2$ corresponding to daughter cells. Modelling a cell population with diameter distrubution centered on two values at d and $d/2$ would thus be a first suggestion of investigation. As a second step, supplementary studies could investigate the influence of the distribution within the population of other parameters such as the total pigment quantity or the neutral lipids. The idea would be to determine whether the distribution plays an influent role in the modelling, and if typical distribution forms could be recognized. Finally, the case of polyspecific algal populations could be investigated: in practice, and in particular in open pounds, real "algal meadows" are cultivated with various strains living together, which optimizes the biomass production all year long despite the changes in environmental conditions.

Bibliography

[1] A. M. Ciotti, M. R. Lewis, and J. J. Cullen. Assessment of the relationships between dominant cell size in natural phytoplankton communities and the spectral shape of the absorption coefficient. *Journal of limnology and oceanography*, 47, 2002.

[2] W.R. Clavano, E. Boss, and L. Krap-Boss. Inherent optical properties of non-spherical marine-like particles - from theory to observation. *Oceanography and Marine Biology*, 45, 2007.

[3] J.J. Cole. Interaction between bacteria and algae in aquatic ecosystems. *Anual review of ecology and systematics*, 13, 1982.

[4] G. de Vries, J. F. Beek, G. W. Lucassen, and M. J. C. van Gemert. The effects of light losses in double integrating spheres on optical properties estimation. *IEEE journal of selected topics in quantum electronics*, 5(4), 1999.

[5] E. Fouilland and B. Mostajir. Revisited phytoplanktonic carbon dependency of heterotrophic bacteria in freshwaters, transitional, coastal and oceanic waters. *FEMS Microbiology Ecology*, 73(3), 2010.

[6] C. Frankovitch, O. Reich, and H.G. Löhmannsröben. Investigation of microalgae with photon density waves. *Proceedings SPIE 6761, Optics for Natural Resources, Agriculture, and Foods II*, 2007.

[7] A. Ishimaru. *Wave propagation and scattering in random media.* IEEE press: New York, 1997.

[8] I.T. Jolliffe. *Principal Component Analysis, second edition.* Springer, 2002.

[9] M. Kerker, editor. *Light scattering by non-spherical particles: theory, measurements and applications.* Academic press, New York, 1969.

[10] A. Morel and A. Bricaud. Theoretical results concerning light absorption in a discrete medium, and application to specific absorption of phytoplankton. *Deep sea research*, 28, 1981.

[11] J. L. Mueller. *The influence of phytoplankton on ocean color spectra.* PhD thesis, Oregon state university, 1973.

[12] A. Nair, S. Sathyendranath, T. Platt, J. Morales, V. Stuart, M. Forget, E. Devred, and H. Bouman. Remote sensing phytoplankton functional types. *Remote sensing of environment*, 112, 2008.

[13] J. W. Pickering, C. J. M. Moes, H. J. C. M. Sterenborg, S. A. Prahl, and M. J. C. van Gemert. Two integrating spheres with an intervening scattering sample. *Journal of Optical society of America*, 9(4), 1992.

[14] S. A. Prahl. *Optical-Thermal Response of Laser Irradiated Tissue.* 1995.

[15] S. A. Prahl. *Everything I think you should know about Inverse Adding-Doubling.* Oregon Medical Laser Center, 2011.

[16] A. Quirantes and S. Bernard. Light scattering by marine algae: two-layer spherical and non-spherical models. *Journal of Quantitative Spectroscopy and Radiative Transfer*, 89, 2004.

[17] S. Roy, S. Sathyendranath, and T. Platt. Retrieval of phytoplankton size from bio-optical measurements: theory and applications. *Journal of the royal society Interface*, 8, 2011.

[18] S. Sathyendranath, L. Lazzara, and L. Prieur. Variations in the spectral values of specific absorption of phytoplankton. *Limnology and Oceanography*, 32(2), 1987.

[19] A.E. Solovchenko, I. Khozin-Goldberg, and M.N. Merzlyak Z. Cohen. Carotenoid-to-chlorophyll ratio as a proxy for assay of total fatty acids and arachidonic acid content in the green microalga parietochloris incise. *Journal of applied phycology*, 21, 2009.

[20] Z.S. Wu and Y.P. Wang. Electromagnetic scattering for multilayered sphere: recursive algorithms. *Radio Science*, 26(6), 1991.

[21] E. Zamora-Rojas, B. Aernouts, A. Garrido-Varo, D. Perez-Marin, J. E. Guerrero-Ginel, and W. Saeys. Double integrating sphere measurements for estimating optical properties of pig subcutaneous adipose tissue. *Innovative Food Science and Emerging Technologies*, 2013.

Chapter 6

Résumé de la thèse en Français

Contents

6.1 Introduction

Les microalgues autotrophes sont des organismes unicellulaires photosynthétiques capables de produire de la biomasse à partir de dioxyde de carbone et d'énergie lumineuse. Leur cycle de division très court, de l'ordre de quelques heures, en font une source de biomasse extrêment intéressante pour de multiples applications à l'échelle industrielle, telles que l'extraction de molécules d'intérêt [39], l'alimentation animale et humaine [20, 16], l'aquaculture [48, 45] ou encore la chimie verte. Les microalgues sont aussi considérées comme une source d'énergie verte majeure, pour la production de biogaz ou de biofuel [10, 9] ou encore comme une solution d'avenir pour la décontamination des eaux usées [45], des fumées d'usines [5], pour la fixation du dioxyde de carbone atmosphérique [13] ou encore la biosorption des métaux lourds [30]. En conséquence la production mondiale de microalgues a considérablement augmentée au cours des dernières décennies [10].

Des systèmes de cultures ouverts, comme les bassins, et fermés, comme les photobioréacteurs [67], ont été developpés pour optimiser la production de microalgues, de la culture à la récolte. De tels systèmes sont conçus pour piloter le procédé en contrôlant les conditions de culture (qualité de l'eau, pH et température, concentration en nutriments, illumination, taux de CO2 dissous et agitation du milieu). La prise d'information sur le milieu de culture se fait via des sondes et contrôleurs commerciaux [3]. Cependant pour optimiser le pilotage, des informations concernant les cellules d'algue elles-mêmes, et non plus seulement le milieu sont nécessaires. Dans l'état actuel de la discipline, l'analyse des cellules algales est réalisée via plusieurs mesures standards pour la plupart inadaptées à une mesure en ligne [49, 60]. La densité et la taille des cellules est déterminée par microscopie optique [3], la cytometrie en flux [25] ou avec des compteurs de particules [6]. La biomasse peut être déduite de la mesure de la masse sèche [3], ou en corrélation avec la turbidité du milieu mesurée par néphélométrie par exemple [5]. La quantité et la composition de pigments est habituellement déterminée par HPLC [72]. Ces méthodes standards sont coûteuses en temps humain et en matériel, et impliquent des étapes de préparation des échantillons importantes. Elles paraissent difficilement adaptables à une prise d'information en routine. De nouvelles méthodes de mesure pour la caractérisation de l'état des cellules algales dans une culture dense doivent être développées.

La thèse propose de répondre à cette problématique opérationnelle en étudiant les potentialités offertes par la spectrométrie visible et proche infrarouge (VIS-NIR) pour caractériser l'état physiologique des cellules de microalgues dans un milieu de culture dense. La spectrométrie est basée sur l'étude qualitative et quantitative de spectres issus de l'intéraction entre un échantillon et les radiations incidentes. Deux raisons principales ont motivé le choix de cette technologie de mesure: tout d'abord, la spectrométrie est un outils de diagnostic largement utilisé dans des domaines aussi variés que l'agroalimentaire [69], l'industrie pharmaceutique [41] ou le pilotage de bioprocédés liés à la culture cellulaire [12, 4]. L'avantage de la spectrométrie est que les mesures sont non-desctructives et peuvent être faites sans préparation de l'échantillon, ce qui en fait une technologie d'analyse de procédés (PAT) de premier choix [41]. D'autre part, de nombreux travaux ont démontrés que les propriétés spectrales dans le VIS-NIR des cellules microalgales étaient fortement liées à leurs caractéristiques chimiques [46, 7] (principalement les pigments) et physiques [7, 71, 1, 15, 46, 58, 33, 32, 34] (taille, forme, densité de cellules). Cette thèse a pour but de proposer une méthode complète permettant d'extraire des informations sur les caractéristiques physiologiques des cellules algales issues de milieux de culture denses à partir de mesures spectrales réalisées sur un échantillon brut du milieu de culture.

Le travail de thèse s'articule autour de quatre chapitres correspondant à quatre échelles de description du problème. En effet, deux problématiques scientifiques principales soustendent notre réflexion: la première relève de la spectrométrie dans un milieu particulièrement turbide. Les méthodes de mesures [52, 64] et d'analyse [59, 40] de la spectrométrie classique, historiquement developpées pour des solutions diluées, sont mises en échec dans un milieu très diffusant, comme la loi de Beer-Lambert n'est plus valide [18]. Dans un premier Chapitre nous aborderons le problème de la mesure spectrale pour des suspensions denses en proposant une structure de banc modèle. Nous définirons aussi les propriétés spectrales apparentes qui sont celles mesurables avec un tel banc, dépendantes à la fois des conditions expériementales et des propriétés intrinsèques du milieu étudié. Dans le second Chapitre, nous ferons le lien entre les propriétés apparentes et les propriétés spectrales intrinsèques de l'échantillon, en utilisant une modélisation rigoureuse du transport radiatif dans un milieu très diffusant et très absorbant. La seconde problématique scientifique principale relève de la modélisation de l'influence des propriétés physico-chimiques d'une cellule d'algue sur ses propriétés spectrales d'absorption et de diffusion. De précédentes études [22, 7, 53, 60, 15, 21, 32] ont démontré que les relations entre les caractéristiques structurelles des cellules et leur propriétés spectrales sont hautement non-linéaires. Comme il apparaît difficile de trouver des relations explicites entre d'une part les propriétés structurelles de la cellules et d'autre part ses propriétés spectrales, le Chapitre 3 de notre thèse propose une modélisation implicite basée sur l'utilisation de la théorie de Mie étendue, et notamment de la solution de Kerker pour des particules vues comme des sphères multicouches [31]. Afin de relier la description à l'échelle de l'échantillon brut étudiée dans les Chapitres 1 et 2 à celle de la cellule individuelle exposée dans le Chapitre 3, nous proposons une méthode complète dans le Chapitre 4. Les paradigmes développés aux différentes échelles sont articulés entre eux, afin de proposer des liens directs entre propriétés spectrales apparentes d'un milieu de culture dense et caractéristiques physico-chimiques des cellules algales constitutives.

6.2 Chapitre 1: Comment mesurer les propriétés de réflectance et de transmittance d'un milieu dense de particules?

6.2.1 Définitions générales: les propriétés spectrales apparentes

La spéctrométrie VIS-NIR manie des grandeurs spectrales appelées propriétés apparentes d'un échantillon: elles dépendent tout d'abord des propriétés intrinsèques du milieu étudié,

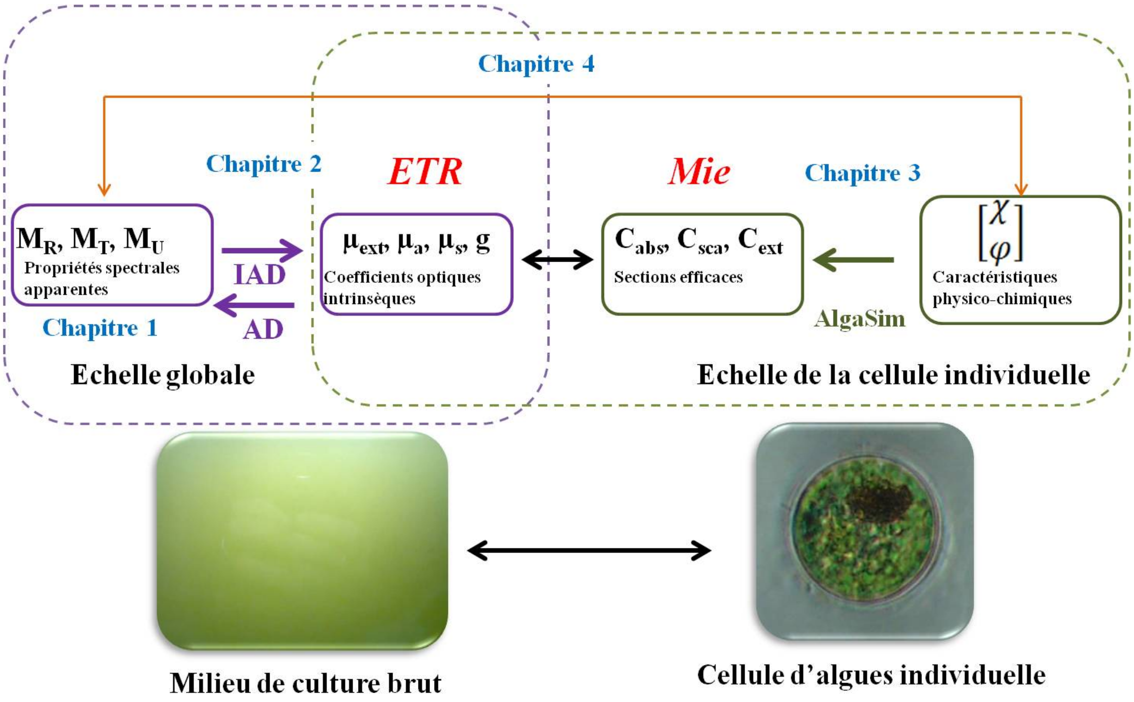

Figure 6.1: Schéma fonctionnel de la proposition de thèse. Chapitre 1: "Comment mesurer les propriétés de réflectance et de transmittance d'un milieu dense de particules?" Chapitre 2: "Comment décrire les propriétés optiques intrinsèques d'un milieu dense constitué de particules à partir de la mesure de ses propriétés de réflectance et de transmittance?" Chapitre 3: "Comment décrire les propriétés optique d'une cellule d'algue individuelle à partir de ses caractéristiques physico-chimiques?" Chapitre 4: "Comment relier les propriétés physico-chimiques d'une cellule individuelle aux propriétés spectrales apparentes mesurées sur un échantillon de milieu de culture algal dense?"

mais aussi des conditions expérimentales dans lesquelles elles sont mesurées en pratique sur l'échantillon. On distingue les propriétés de réflectance et de transmittance, caractérisant respectivement les capacités d'un échantillon à réfléchir et à transmettre la lumière incidente. Ces propriétés sont spectrales, c'est à dire dépendantes de la longueur d'onde considérée. Il existe un grand nombre de définitions de ces grandeurs en fonction des expérimentateurs et des applications, les angles solides considérés notamment pouvant être différents. Dans le cadre de la thèse nous définissons la reflectance totale, la transmittance totale et la transmittance régulière de la manière suivante: si l'on considère un faisceau de lumière monochromatique incident sur l'échantillon avec un angle θ, on appelle $\Phi_R(\lambda,\theta)$ le flux réfléchi par l'échantillon dans tout le demi-espace d'où provient la lumière incidente. Il est la somme du flux rétrodiffusé dans la même direction θ que le faisceau incident, du flux spéculairement réfléchi et du flux réfléchi diffus. La réflectance totale $M_R(\lambda,\theta)$ est le ratio sans dimension du flux réfléchi $\Phi_R(\lambda,\theta)$ et du flux incident $\Phi_i(\lambda,\theta)$:

$$M_R(\lambda,\theta) = \frac{\Phi_R(\lambda,\theta)}{\Phi_i(\lambda,\theta)} \tag{6.1}$$

Le flux transmis $\Phi_T(\lambda, \theta)$ est le flux qui traverse le milieu et qui atteint l'autre demi-espace. Il est la somme du flux transmis régulier dans la même direction θ que le faisceau incident et du flux transmis diffus. De même, on définit la transmittance totale $M_T(\lambda, \theta)$ comme le ratio de $\Phi_T(\lambda, \theta)$ et du flux incident $\Phi_i(\lambda, \theta)$:

$$M_T(\lambda, \theta) = \frac{\Phi_T(\lambda, \theta)}{\Phi_i(\lambda, \theta)} \tag{6.2}$$

La transmittance régulière $M_U(\lambda, \theta)$ est le ratio du flux transmis régulier $\Phi_{T,regular}(\lambda, \theta)$ et du flux total $\Phi_i(\lambda, \theta)$:

$$M_U(\lambda, \theta) = \frac{\Phi_{T,regular}(\lambda, \theta)}{\Phi_i(\lambda, \theta)} \tag{6.3}$$

Pour définir la répartition angulaire de la lumière réémise par un échantillon, on définit aussi sa fontion de phase p: pour un échantillon illuminé par un faisceau selon la direction $\vec{u_i}$, la fonction de phase $p(\vec{u}, \vec{u_i})$ donne la fraction du flux incident qui est envoyée dans la direction $\vec{u}$. La fonction de phase est normalisée telle que:

$$\int p(\vec{u}, \vec{u_i}) d\Omega = 4\pi \tag{6.4}$$

On utilise en pratique le facteur d'anisotropie g, la moyenne du cosinus de l'angle entre les vecteurs $\vec{u}$ and $\vec{u_i}$ [11]:

$$g = \frac{1}{4\pi} \int_{4\pi} \vec{u}.\vec{u_i} p(\vec{u}, \vec{u_i}) d\Omega \tag{6.5}$$

6.2.2 Aspect de la mesure en pratique: le banc à double sphères (DIS) développé

En pratique il existe diverses techniques pour mesurer les propriétés spectrales apparentes, celles-ci étant adaptées à la nature des échantillons ainsi qu'au domaine d'application qui sont très variés pour la spectrométrie VIS-NIR. Parmi les techniques les plus classiques on trouve notamment les spectromètres à simple ou double faisceaux ou encore la gonio-photométrie. Pour des échantillons particulièrement complexes présentant des propriétés d'absorption et de diffusion importantes, le montage à double sphères d'intégration (DIS) se révèle être particulièrement performant. En effet, la sphère d'intégration est un dispositif optique permettant de collecter des photons dans une grande partie de l'espace, ce qui augmente le rapport signal sur bruit (SNR).

Les figures 6.2 et 6.3 présentent la configuration du banc DIS proposé dans la thèse. Le principe est de mesurer avec le même banc la réflectance, transmittance totale et régulière d'un échantillon turbide. L'échantillon est placé entre les sphères de réflectance et de transmittance, et illuminé par un faisceau incident incliné d'un angle θ par rapport à l'axe optique. Cet angle permet de s'assurer que la réflection spéculaire est bien collectée dans la sphère de réflectance. La sphere de transmittance est équippée d'un trou escamotable dans la direction du faisceau incident: en position fermée, le flux transmis régulier et le flux transmis diffus sont collectés dans la sphère. En position ouverte, le flux transmis régulier s'échappe, et seul le flux transmis diffus est mesuré. Le niveau de flux collecté est mesuré à l'aide de photodétecteurs placés directement au niveau des ports de détection de la sphère.

En pratique, optimiser les performances du montage DIS requiert de considérer un certain nombres de points techniques. Dans la théorie de la sphère d'intégration [27, 24, 37], un équilibre doit être trouvé entre l'optimisation du gain, d'autant plus grand que la sphère a un petit diamètre, et celle de l'angle de collection effectif, d'autant plus grand que les ports d'entrée sont ouverts. Ceci contraint donc les dimensions des sphères. Le système de détection doit également être adapté, afin notamment d'avoir une injection convenable de la lumière ambiante de la sphère collectrice: cela impose d'avoir en pratique une surface active la plus grande possible pour le photodétecteur. Les dimenions de l'échantillon et du faisceau lumineux incident sont également importantes: l'échantillon doit être le plus fin possible et le faisceau le moins large possible, afin de réduire les pertes de lumière non linéaires.

Un protocole précis a été établi dans la thèse afin de réaliser les mesures de réflectance et de transmittance avec le DIS présenté, et d'appliquer les corrections nécessaires aux signaux bruts pour prendre en compte les effets des conditions expérimentales. Le montage DIS et le protocole associé ont été testés sur des échantillons fantômes de microsphères colorées de polystyrène présentant des concentrations variables. Plusieures tailles de cuves ont aussi été testées. Dans un premier temps les tests ont été réalisés pour une seule longueur d'onde à 632.8 nm. M_R, M_T et M_U ont put être obtenus: différents régimes de diffusion ont put être distingués en fonction de la concentration de particules. Pour des faibles densités, on observe que la diffusin reste très réduite, comme la plupart de la lumière est transmise, avec peu de divergence par rapport à la direction régulière. M_U décroît ensuite rapidement avec l'augmentation de la concentration de particules, tandis que la part de la transmission diffuse augmente: le régime de simple diffusion est atteint. Pour de très fortes concentrations, la part de lumière transmise devient de plus en plus faible tandis que la part réfléchie augmente: le régime de multi-diffusion est atteint. On observe que M_R varie non linéairement avec la taille de la cuve, du fait d'une compétition entre phénomènes d'absorption et phénomènes de diffusion. La relation est linéaire pour M_T et M_U, à part pour de très fortes densités de particules où la multi-diffusion domine.

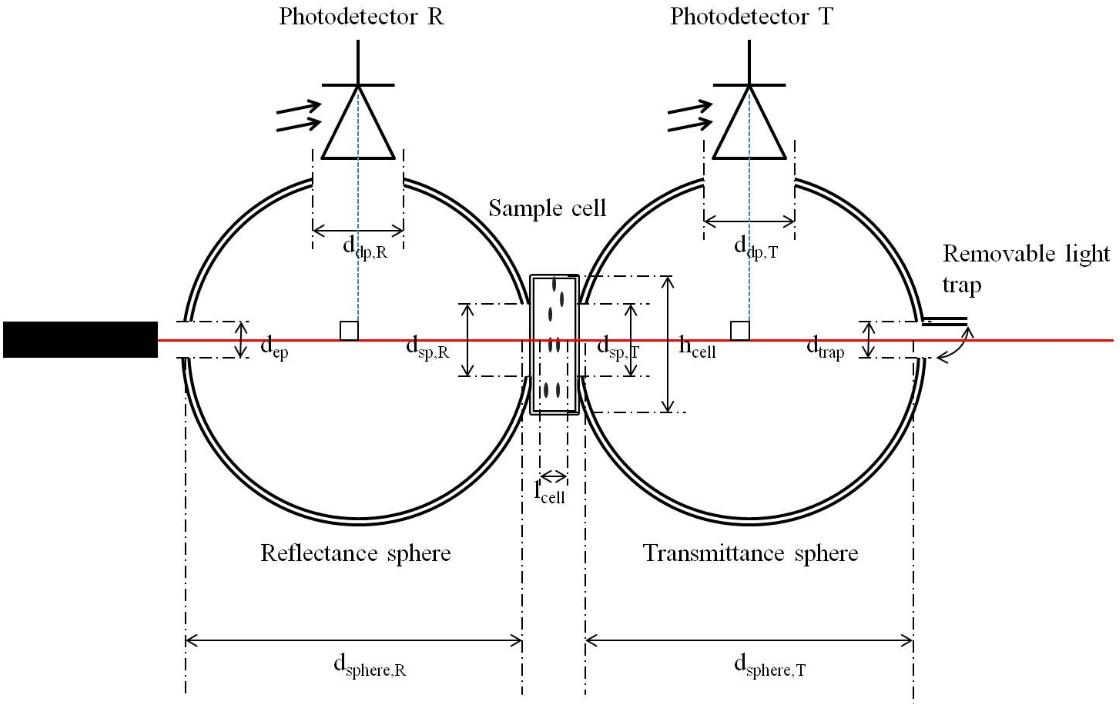

Figure 6.2: Side view of the double integrating sphere setup

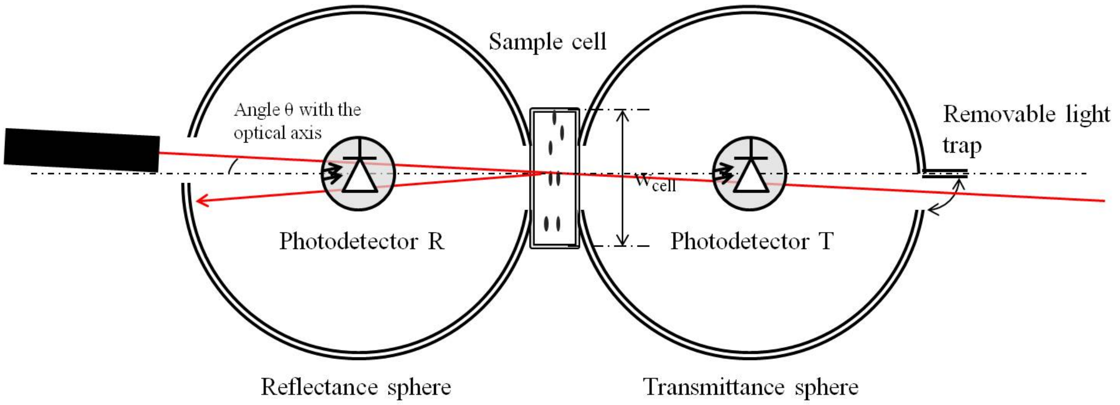

Figure 6.3: Upper view of the double integrating sphere setup

6.3 Chapitre 2: Comment décrire les propriétés optiques intrinsèques d'un milieu dense constitué de particules à partir de la mesure de ses propriétés de réflectance et de transmittance?

6.3.1 Modéliser les propriétés spectrales intrinsèques d'un milieu dense de particules

Les propriétés optiques intrinsèques d'un milieu sont caractérisées par ses coefficients linéaires d'absorption, de diffusion et d'extinction, respectivement notés μ_{abs}, μ_{sca} et μ_{ext} exprimés en m^{-1}. Ceux-ci peuvent être vus comme des grandeurs statistiques exprimant la probabilité pour un photon de subir un évènement d'absorption ou de diffusion en parcourant une distance unité dans le milieu. Considérons une tranche infinie de milieu de longueur finie l comme montrée dans la figure 6.4 avec $\Phi_i(\lambda, z)$ le flux lumineux incident dans la direction z. $\Phi_{abs}(\lambda, z)$ et $\Phi_{sca}(\lambda, z)$ sont les flux respectivement absorbés et diffusés par le milieu. On définit μ_{abs}, μ_{sca} et μ_{ext} tels que:

$$\mu_{abs} = \frac{\Phi_{abs}(\lambda, z)}{l\Phi_i(\lambda, z)} \tag{6.6}$$

$$\mu_{sca} = \frac{\Phi_{sca}(\lambda, z)}{l\Phi_i(\lambda, z)} \tag{6.7}$$

$$\mu_{ext} = \mu_{abs} + \mu_{sca} \tag{6.8}$$

On définit aussi le coefficient de diffusion réduit comme suit:

$$\mu'_{sca} = \mu_{sca}(1 - g) \tag{6.9}$$

Avec g le facteur d'anisotropie défini précédemment.

6.3.2 L'équation de transport radiatif

L'équation de transport radiatif (ETR) est une formulation heuristique du transport d'énergie à travers un milieu [14, 62, 57, 43]. Elle permet notamment de formuler rigoureusement les variations de la luminance dans un milieu, quelques soient les ordres de grandeurs de ses coefficients d'absorption et de diffusion. Elle exprime un bilan d'énergie effectué pour un volume unité de milieu, et son expression est la suivante [26]:

$$\frac{dL(r, \vec{u})}{ds} = -\mu_{ext}L(r, \vec{u}) + \frac{\mu_{sca}}{4\pi}\int_{4\pi} p(\vec{u'}, \vec{u})L(r, \vec{u'})d\omega' + \epsilon(r, \vec{u}) \tag{6.10}$$

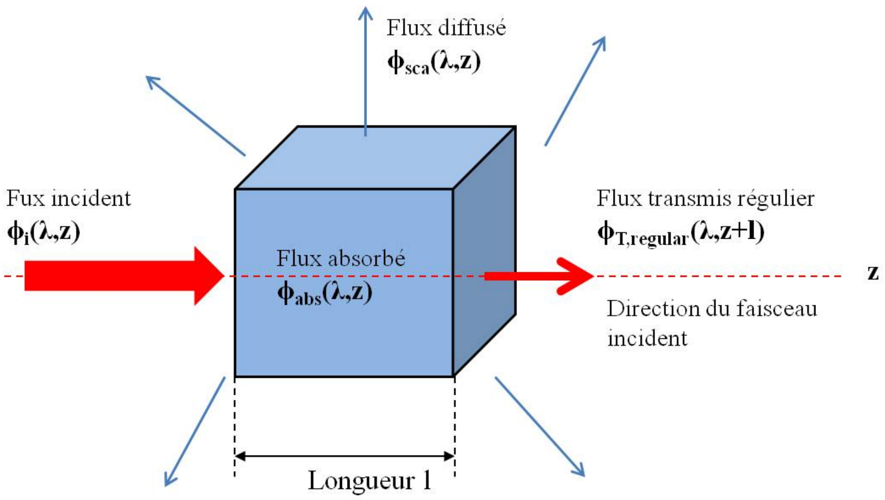

Figure 6.4: Scheme of the interaction of an incident light flux with a volume of bulk medium [44].

Avec $L(r, \vec{u})$ la radiance spectrale au point r du milieu dans la direction $\vec{u}$, $p(\vec{u'}, \vec{u})$ la fonction de phase décrite précédemment, et $\epsilon(r, \vec{u}$ un terme d'émission. μ_{ext} et μ_{sca} sont les coefficients linéaires d'extinction et de diffusion décrits précédemment. Un nombre limité de cas particuliers comme le problème plan-parallèle ou le cas de diffusion isotrope admettent une solution exacte explicite de l'ETR [26]. Cependant dans la majorité des cas pratiques l'ETR ne peut être résolue analytiquement. Il est donc nécessaire d'approximer la solution [51]. Parmi les méthodes existantes on compte la résolution numérique avec la méthode des ordonnées discrètes [26] ou Adding-Doubling (AD) [56]. Pour la première, le principe est de discrétiser l'ETR en décomposant l'espace en directions discrètes selon la quadrature de Gauss-Legendre [66]. Pour la méthode d'Adding-Doubling, l'ETR est discrétisée en modélisant le milieu de propagation comme un assemblage de tranches infiniment fines. Dans le cadre de la thèse, la méthode Adding-Doubling a été mise en oeuvre pour résoudre l'ETR.

6.3.3 La méthode Adding-Doubling

La méthode AD a été introduite par Van de Hulst [68] pour la résolution de l'ETR dans le cas d'une géométrie en couches: le milieu de propagation étudié est alors représenté comme un assemblage de couches infiniment fines ayant chacune des coefficients d'absorption et de diffusion homogènes. Le principe de la résolution numérique est basée sur l'expression matricielle des propriétés de réflection et de transmission de chaque couche, décomposées dans un nombre fini d'angles solides. La technique de "Adding" permet de calculer matriciellement les propriétés de réflection et de transmission d'une couche résultant de l'assemblage de deux couches unités de nature différentes. La technique de "Doubing" permet de calculer les matrices de transmission et de réflection d'une couche résultant du doublement d'une couche unité. La méthode directe permet de retrouver les propriétés optiques apparentes, réflectance et transmittance d'un échantillon à partir de ses coefficients linéaires intrinsèques et de la description de sa géométrie (épaisseur et nature des couches). La méthode inverse (IAD) permet d'obtenir les propriétés optiques intrinsèques d'un milieu à partir des grandeurs apparents mesurées sur un échantillon.

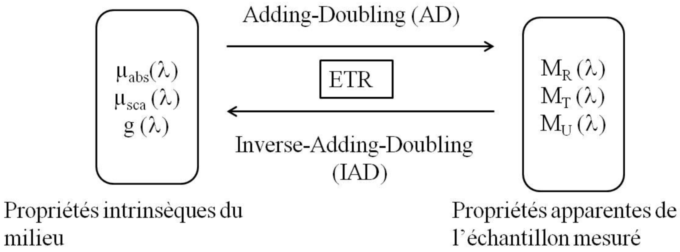

Figure 6.5: Schéma illustrant le principe de la méthode Adding-Doubling et Inverse-Adding-Doubling permettant la résolution numérique de l'ETR.

Dans le cadre de la thèse nous avons utilisé le programme codant Adding-Doubling développé par Scott Prahl [55] et disponible sur le site internet http://omlc.ogi.edu/software/. Nous avons testé la méthode IAD sur des échantillons de milieux denses de culture algale réels.

6.3.4 Application à des milieux algaux réels

Nous avons testé les potentialités de la méthode IAD pour le cas concret d'échantillons denses de milieux algal issus de quatre bassins ouverts du Laboratoire de Biotechnologie de l'Environnement (LBE, Narbonne), constitués de populations mixtes de *Scenedesmus* et de *Chlorella*. Les échantillons ont été caractérisés par des méthodes standards: détermination du nombre et de la taille des cellules par un compteur de particules (Z2 Coulter Counter, Beckman), mesure de la chlorophylle a et b après extraction et mesures colorimétriques. En parallèles, la réflectance et la transmittance totales des échantillons non dilués ont été mesurées avec un dispositif DIS comme décrit précédemment. Pour des contraintes de transport du banc, les dimensions des sphères ont cependant dûes être réduites. Le système de détection a aussi dû être fibré, ce qui a réduit la surface active du détecteur et dégradé l'injection. A partir des réflectances et tansmittances mesurées, la méthode IAD a permit de simuler les coefficients d'absorption et de diffusion réduit pour chaque échantillons sur le domaine spectral [400-1020 nm].

Nous avons constaté que les erreurs expérimentales de mesure des propriétés apparentes, liées principalement aux pertes de lumière dans le montage DIS avaient une influence non négligeable sur la convergence du program d'IAD. Ceci a pu introduire notamment des erreurs quantitatives dans l'estimation du μ_{abs}, comme les pertes de lumière sont interprétées par l'algorithme comme de l'absorption [17]. Au-delà de ces difficultés, les coefficients d'absorption et de diffusion obtenus ont put être comparés aux résultats attendus au regard de la littérature. Les coefficients d'absorption obtenus représentent qualitativement les différences de pigmentation entre les quatre échantillons. Malgré les incertitudes dues aux erreurs expérimentales de mesure, les spectres obtenus présentent des ordres de grandeurs comparables à ceux observés dans la littérature [61]. Quant aux spectres des coefficients de diffusions obtenus, ils se révèlent fortement corrélés à la distribution de taille des cellules algales: cette conclusion est cohérente avec celles d'autres travaux [15, 23]. De plus, la forme des spectres, notamment dans les zones de fortes absorption, est en accord avec les tendances prédites par la théorie de Mie. Cette étude préliminaire montre donc que la méthode proposée est adéquate pour estimer les coefficients linéaires d'absorption et de diffusion d'un milieu algal dense à partir de la mesure des propriétés spectrales apparentes avec un montage DIS, à condition toutefois que les erreurs expérimentales soient minimes. Ceci impose d'utiliser un banc à double sphères dont les dimensions et la géométrie ont été adaptés scrupuleusement, d'après les principes présentés dans le Chapitre 1.

6.4 Chapitre 3: Comment décrire les propriétés optique d'une cellule d'algue individuelle à partir de ses caractéristiques physico-chimiques?

6.4.1 Modéliser les propriétés spectrales d'une cellule individuelle

Dans ce Chapitre, les propriétés spectrales d'une cellule individuelle sont étudiées. Celles-ci sont décrites à l'échelle de la particule par les notions de sections efficaces d'absorption, de diffusion et d'extinction respectivement notées C_{abs}, C_{sca} et C_{ext} et exprimées en m^2. La configuration considérée est présentée par la figure 6.6.

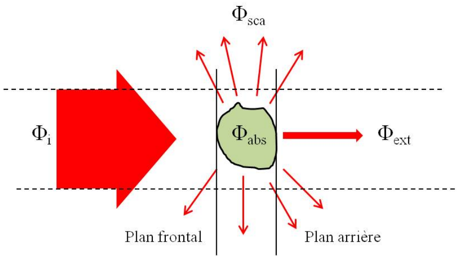

Figure 6.6: Représentation schématique de l'intéraction de la lumière avec une particule.

C_{abs} est définie comme le ratio du flux total absorbé par la particule Φ_{abs} et de l'éclairement E_i au niveau du plan frontal [44]:

$$C_{abs} = \frac{\Phi_{abs}}{E_i} \tag{6.11}$$

De même, C_{sca} est le ratio du flux total diffusé par la particule Φ_{sca} et de E_i:

$$C_{sca} = \frac{\Phi_{sca}}{E_i} \tag{6.12}$$

C_{ext} décrit l'extinction de la lumière dans la direction du faisceau incident: elle s'exprime comme la somme des sections efficaces d'absorption et de diffusion:

$$C_{ext} = C_{sca} + C_{abs} \tag{6.13}$$

Comme expliqué dans l'introduction, il n'existe pas de formules explicites permettant de déduire les propriétés optiques d'une cellule d'algue à partir de toutes ses caractéristiques physico-chimiques, du fait des influences non-linéaires de celles-ci sur les spectres. Historiquement, différents modèles implicites ont été testés pour le cas des cellules algales. En océanographie en particulier, la théorie de Mie simple a été largement utilisée [65]. Les cellules d'algues sont alors modélisées comme des sphère homogènes d'indice de réfraction donné. Cependant cette modélisation présente des limites comme elle ne prend pas en compte notamment les effets de la structure interne des cellules, composées en réalité de différents organelles. Pour prendre en compte ces hétérogénéités internes, la solution de Kerker peut être utilisée [31]: elle permet de représenter les cellules comme des sphères formées de couches concentriques [47, 35, 58]. Cette modélisation est celle qui a été choisie dans la thèse: elle a servit de base au développement d'un programe de simulation appelé AlgaSim.

6.4.2 Principe de fonctionnement d'AlgaSim

Le programme AlgaSim a été développé au cours de cette thèse afin de simuler les spectres des sections efficaces d'absorption, de diffusion et du coefficient d'anisotropie d'une cellule algale décrite par ses caractéristiques physiques (taille, poids sec, proportions des différents matéraux organiques) et chimiques (quantité totale et composition des pigments). Il a été specialement conçu afin de fonctionner avec de nombreuses variables pouvant avoir chacune de larges gammes afin d'étudier un large panel d'individus possibles. Cette originalité le distingue de précédentes simulations de cellules d'algues par des sphères multicouches [47].

Dans AlgaSim, les cellules algales sont représentées selon le schéma montré par la figure 6.7.

Elles sont repésentées comme des sphères composées de trois couches concentriques correspondant à différentes substances organiques principalement rencontrées dans les cellules d'algues [2, 8]: la couche interne, composée de pigments dissous dans l'eau, mime les chloroplastes. La seconde couche correspondrait aux lipides neutres, accumulés par la cellule en cas de stress, particulièrement étudiés car potentiellement utilisables pour la fabrication de biocarburants [70]. La dernière couche, composée de glucides et de protéines, représente une structure proche de la membrane externe d'une cellule réelle.

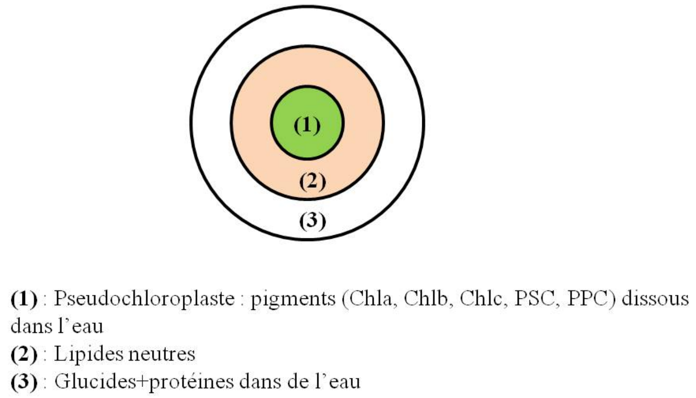

Figure 6.7: Structure de la cellule d'algue virtuelle simulée dans AlgaSim.

Le programme AlgaSim lui-même s'organise de la façon suivante: il déduit des paramètres physiques donnés en entrée les rayons de chaque couche. Par ailleurs, les indices optiques de chaque couche successive sont calculés en fonction de la quantité des différentes substances, absorbantes (pigments) ou non (protéines, glucides et lipides). Les rayons et indices optiques de chaque couche servent ensuite d'entrée au programme de calcul des coefficients de Mie. Le programme utilisé dans cette thèse a été développé par Peña et al. [50], et est adapté à de larges gammes de rayons et d'indices. Il permet de calculer les sections efficaces d'absorption, de diffusion et le facteur d'anisotropie des sphères multicouches ainsi simulées, ceci pour chaque longueur d'onde désirée.

6.4.3 Test d'AlgaSim et étude de l'infuence des paramètres physico-chimiques de la cellule sur ses propriétés spectrales

Le fonctionnement général d'AlgaSim a d'abord été testé sur le cas exemple d'une cellule d'algue de 5 μm de rayon décrite dans la thèse de Mueller [47]. Les spectres des sections efficaces d'absorption, de diffusion et d'extinction simulés avec AlgaSim sur la plage [400-750 nm] ont donc put être comparés avec les résultats de Mueller. Les deux simulations coïcident qualitativement et quantitativement de manière très satisfaisante, ce qui apporte une première validation du fonctionnement général d'AlgaSim.

Afin d'étudier plus en profondeur les simulations d'AlgaSim, une étude supplémentaire a été réalisée en analysant de larges collections de spectres simulés: de grandes bases de données d'individus différents ont été tout d'abord construites en faisant varier les paramètres physiques et chimiques à l'intérieur de gammes étendues. AlgaSim a ensuite été utilisé pour simuler les spectres des sections efficaces correspondants à chacun de ces individus. Une méthode d'analyse de données, l'Analyse en Composantes Principales (ACP) [28, 42] a été utilisée afin d'extraire des informations concernant les corrélations entre les caractéristiques des spectres simulés et les paramètres d'entrée. Les tendances observées se révèlent être en accord avec les observations reportées dans la littérature [15, 46]. Le spectre de la section efficace d'absorption est influencé par la composition pigmentaire, la quantité totale de pigments ainsi que par la taille de la cellule, corroborant les observations de Ciotti et al. [15]. Les spectres de diffusion dépendent principalement de la taille des cellules, comme attendus. Une observation intéressante et peu mentionnée cependant est que le coefficient de diffusion porte aussi des informations sur les pigments présents. Cette étude donne une seconde validation de la capacité de la méthode développée et d'AlgaSim à modéliser les propriétés spectrales des cellules algales en fonction de leurs caractéristiques structurelles.

6.5 Chapitre 4: Comment relier les propriétés physico-chimiques d'une cellule individuelle aux propriétés spectrales apparentes mesurées sur un échantillon de milieu de culture algal dense?

6.5.1 Principe de la méthode complète

Dans la dernière phase de la thèse, une méthode complète est proposée pour relier les différentes échelles de description étudiées dans les chapitres précédents. Dans l'état de nos connaissances bibliographiques, nous pensons que nos travaux sont les premiers à proposer une méthode permettant de relier la description physiologique détaillée des cellules algales à des grandeurs spectrométriques apparentes.

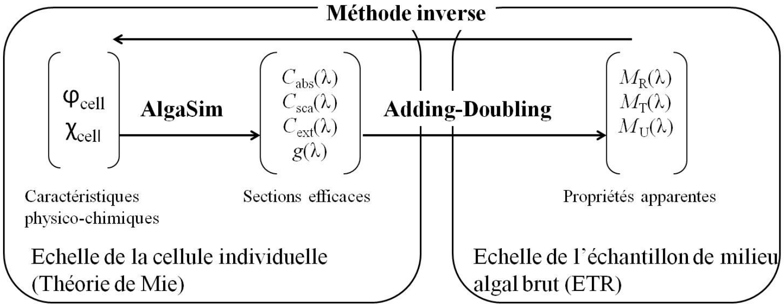

Figure 6.8: Schéma illustrant le principe de la méthode complète développée dans la thèse pour simuler les propriétés spectrales apparentes d'un échantillon de milieu algal dense à partir des caractéristiques physiques et chimiques des cellules constitutives.

La méthode directe

En particulier, comme illustré par la figure 6.8, la méthode directe vise à relier la description des caractères physiologiques des cellules d'algues aux propriétés spectrales apparentes mesurables sur un échantillon brute de milieu algal dense. Pour cela, différentes étapes sont mises en oeuvre: à l'échelle de la cellule individuelle, la solution de Kerker [31] de la théorie de Mie étendue est utilisée pour lier propriétés structurelles de la cellule et sections efficaces, d'après la modélisation décrite dans le Chapitre 3. Le programme AlgaSim est utilisé.

Une étape est ensuite nécessaire pour décrire les coefficients linéaires d'une population d'algue donnée à partir des sections efficaces individuelles. Les coefficients linéaires s'expriment comme la somme des sections efficaces de toutes les cellules algales présentes dans un volume unité de milieu. En théorie, l'expression rigoureuse de μ_{abs} et de μ_{sca} exigerait donc de connaître exactement les sections efficaces de chaque cellule. En pratique il est cependant impossible de déterminer par la mesure toutes les propriétés d'une seule cellule. Pour la quantité de pigments, la masse sèche et les proportions des différents matériaux organiques, seules sont accessibles des grandeurs moyennées sur l'ensemble de la population. Il peut être possible éventuellement d'obtenir un diagramme de répartition des tailles d'une population cellulaire avec un compteur de particules [29, 5, 38]: dans ce cas-là, les coefficients linéaires sont obtenus de la façon suivante:

$$\mu_i = \int_0^\infty N(r_{cell}) C_i(r_{cell}) dr_{cell} \tag{6.14}$$

Avec $i = abs, sca, ext$, $C_i(r_{cell})$ la section efficace d'une cellule seule de rayon r_{cell} et $N(r_{cell})$ le nombre de cellules par unité de volume de la suspension ayant un rayon compris entre r_{cell} et $r_{cell} + dr_{cell}$.

Dans le cas où seule une taille moyenne est connue pour la population, on fait l'hypothèse que celle-ci est monodisperse [46]: l'expression des coefficients linéaires est alors simplifiée:

$$\mu_{abs} = N_{cell}.C_{abs} \tag{6.15}$$

$$\mu_{sca} = N_{cell}.C_{sca} \tag{6.16}$$

$$\mu_{ext} = N_{cell}.C_{ext} \tag{6.17}$$

Avec N_{cell} la concentration de cellules dans la population considérée.

Une fois les coefficients linéaires déterminés, une dernière étape consiste à les intégrer dans l'ETR pour en déduire les propriétés spectrales apparentes. Pour cela, la méthode Adding-Doubling [54], présentée dans le Chapitre 2 est utilisée.

La méthode inverse

La méthode inverse consiste à prévoir les caractéristiques physico-chimiques des cellules algales à partir des grandeurs spectrales apparentes mesurées sur un échantillon de milieu brut. Pour cela, une inversion de la chaine directe précédemment décrite a été réalisée. Le principe est d'utiliser la méthode en direct pour simuler des spectres de M_R, M_T et M_U correspondant à une population de cellules algales décrite par un ensemble de paramètres physiologiques initiaux. Les spectres ainsi simulés sont ensuite comparés avec les spectres réellement mesurés. L'erreur résultante entre mesure et simulation est alors calculée comme le Spectral Angle Mapper (SAM) [36] entre les deux spectres. Un algorithme d'optimisation numérique, en l'ocurrence un algorithme de colonie de fourmis [19] est ensuite utilisé pour minimiser l'erreur entre mesure et simulation, en faisant varier les paramètres décrivant la population de cellules algales. Il est ainsi possible d'obtenir un ensemble de paramètres finaux décrivant au mieux les caractéristiques physiologiques des cellules constitutives.

6.5.2 Application à des échantillons de milieux algaux denses

Un premier test de la méthode complète et de son inverse a été réalisé au cours des travaux de thèse, à partir des données issues d'une campagne de mesures réalisée sur deux cultures monospécifiques à trois différents stades de croissance. Pour jauger l'influence de la forme des cellules d'algue, une espèce présentant des cellules quasi-sphériques, *Isochrysis galbana*, et une espèce présentant des cellules en forme de bâtonnets, *Phaeodactylum tricornutum* ont été choisies. Dans le contexte du test préliminaire réalisé dans la thèse, la méthode complète a été simplifiée: dans un premier temps, seule la transmittance totale M_T a été considérée. Pour le test de la méthode inverse, l'ensemble des variables a été réduit pour ne garder que la taille et densité de cellules ainsi que la quantité et la composition des pigments. Ceci a été fait notamment afin de maintenir le temps de convergence de l'algorithme inverse à un temps raisonnable. Les populations algales ont été supposées monodisperses.

la méthode directe se montre adaptée pour modéliser la transmittance totale d'un milieu algal dense dans le domaine spectral [400-750 nm] pour les cellules quasi-sphériques d'*Isochrysis galbana*. L'erreur relative entre les spectres de M_T simulés et ceux mesurés avec un montage DIS sur des échantillons réels ne dépasse pas 10% sur toute la gamme spectrale, et ceci pour chacune des trois dates de mesure. Plus de divergence entre simulations et mesures ont été constatées pour *Phaeodactylum tricornutum*, en particulier pour les basses longueurs d'onde. Ceci a sans doute pour origine une surestimation de la section efficace de diffusion par AlgaSim venant de la forme non-spérique des cellules réelles, et/ou de l'hypothèse de monodispersion.

Des résultats très prometteurs ont été obtenus avec la méthode inverse appliquée à *Isochrysis galbana*: la taille et la densité moyenne des cellules ainsi que la quantité et composition des différents pigments ont put être prédites à partir des spectres mesurés de

M_T avec une erreur relative inférieure à 10%. Pour les cellules allongées de *Phaeodactylum tricornutum*, seuls le diamètre sphérique équivalent moyen a pu être prédit avec une erreur relative aussi basse. Plus d'erreurs quantitatives ont été observées pour les prédictions de la densité et des pigments, probablement dûes à l'influence de la forme non-sphérique des cellules et de l'hypothèse de monodispersion. Cependant, les grandeurs prédites suivent des tendances relatives correctes, notamment pour le rapport caroténoïdes/chlorophylle connu pour être un indicateur de premier ordre du stress de la culture [63]. Ces résultats préliminaire sont prometteurs, notamment dans le cadre d'applications pratiques au pilotage de culture de milieux algaux denses.

6.6 Conclusion

La thèse est une première étude des potentialités offertes par la spectroscopie VIS-NIR pour des applications au suivi de milieux de culture denses de microalgues. Pour cela, une étude structurée a été menée à différentes échelles de description du problème afin de modéliser pas à pas les phénomènes d'intéraction entre la lumière et le milieu. Dans un premier temps, les propriétés spectrales apparentes mesurables en pratique sur un échantillon de milieu brut ont été définies, et un protocole de mesure associé à une configuration de banc à double sphères d'intégration a été décrit. Dans un second temps, les liens entre les propriétés optiques intrinsèques du milieu et les propriétés apparentes d'un échantillon donné ont été établis, en utilisant le formalisme de l'ETR et en proposant la méthode Adding-Doubling pour la résolution. Dans un troisième temps, les propriétés spectrales d'une cellule d'algue individuelle ont été modélisées à partir de la description de celle-ci en termes de caractéristiques physiques et chimiques. Enfin, une méthode complète permettant le passage de l'échelle physiologique à l'échelle des propriétés spectrales apparentes a été proposée, utilisant l'ensemble des paradigmes successivement décrits. Des résultats prometteurs ont été obtenus aux tests préliminaires menés avec des échantillons de milieux algaux réels, ce qui valide l'ensemble de la démarche de thèse, et appelle à des développements futurs.

Bibliography

[1] E. Aas. Influence of shape and structure on light scattering by marine particles. Technical report, University of Oslo, 1984.

[2] E. Aas. Refractive index of phytoplankton derived from its metabolite composition. *Journal of Plankton Research*, 18(12), 1996.

[3] R. A. Anderson. *Algal culturing techniques.* R.A. Anderson, 2005.

[4] S.A. Arnold, J. Crowley, N. Woods, L.M. Harvey, and B. McNeil. In-situ near infrared spectroscopy to monitor key analytes in mammalian cell cultivation. *Biotechnology and bioengineering*, 84, 2003.

[5] H. Berberoglu, P.S. Gomez, and L. Pilon. Radiation characteristics of botryococcus braunii, chlorococcum littorale, and chlorella sp. used for co2 fixation and biofuel production. *Journal of Quantitative Spectroscopy and Radiative Transfer*, 110(17), 2009.

[6] O. Bernard, G. Malara, and A. Sciandra. The effects of a controlled fluctuating nutrient environment on continuous cultures of phytoplankton monitored by a computer. *Journal of experimental marine biology and ecology*, 197(2), 1996.

[7] A. Bricaud, A. Morel, and L. Prieur. Optical efficiency factors of some phytoplankters. *Journal of limnology and oceanography*, 1983.

[8] M. R. Brown and S. W. Jeffrey. Biochemical composition of microalgae from the green algal classes chlorophyceae and prasinophyceae. 1. amino acids, sugars and pigments. *Journal of experimental marine biology and ecology*, 161, 1992.

[9] J.S. Burlew. Algal culture from laboratory to pilot plant. *Aquatic Living Resources*, 23(2), 1953.

[10] J. P. Cadoret and O. Bernard. La production de biocarburant lipidique avec des microalgues: promesses et défis. *Société de biologie*, 202(3), 2008.

[11] R. Carminati. Optique des milieux complexes. cours de 3ème année, Institut d'Optique Graduate School, 2009.

[12] A. Cervera and N. Petersen. Application of near-infrared spectroscopy for monitoring and control of cell culture and fermentation. *Biotechnology Progress*, 25, 2009.

[13] S.R. Chae, E.J. Hwang, and H.S. Shin. Single cell protein production of euglena gracilis and carbon dioxide fixation in an innovative photobioreactor. *Bioresource technology*, 97, 2006.

[14] S. Chandrasekhar. *Radiative transfer.* Oxford University Press, London, 1950.

[15] A. M. Ciotti, M. R. Lewis, and J. J. Cullen. Assessment of the relationships between dominant cell size in natural phytoplankton communities and the spectral shape of the absorption coefficient. *Journal of limnology and oceanography*, 47, 2002.

[16] V. Dallaire, P. Lessard, G. Vanderberg, and J. de la Noüe. Effect of algal incorporation on growth, survival and carcass composition of rainbow trout (oncorhynchus mykiss) fry. *Bioresource technology*, 98, 2007.

[17] G. de Vries, J. F. Beek, G. W. Lucassen, and M. J. C. van Gemert. The effects of light losses in double integrating spheres on optical properties estimation. *IEEE journal of selected topics in quantum electronics*, 5(4), 1999.

[18] V.P. Dick. Applicability limits of beer's law for dispersion media with a high concentration of particles. *Applied optics*, 37(21), 1998.

[19] M. Dorigo, M. Birattari, and T. Stützle. Ant colony optimization. 2006.

[20] L. Dufossé, P. Galaup, A. Yaron, S. Malis Arad, P. Blanc, K. N. Chidambara Murthy, and G. A. Ravishankar. Microorganisms and microalgae as sources of pigments for food use: a scientific oddity or an industrial reality? *Trends in food science and technology*, 16, 2005.

[21] L. N. M. Duysens. Flattening of the absorption spectrum of suspensions, as compared to that of solutions. *Biochimica and Biophysica acta*, (19), 1956.

[22] E. Le Floc'h, G. Malara, and A. Sciandra. An automatic device for in vivo absorption spectra acquisition and chlorophyll estimation in phytoplankton cultures. *Journal of Applied Phycology*, 14, 2002.

[23] C. Frankovitch, O. Reich, and H.G. Löhmannsröben. Investigation of microalgae with photon density waves. *Proceedings SPIE 6761, Optics for Natural Resources, Agriculture, and Foods II*, 2007.

[24] D.G. Goebel. Generalized integrating sphere theory. *Applied Optics*, 6, 1967.

[25] P. Hyka, S. Lickova, P. Pribyl, K. Melzoch, and K. Kovar. Flow cytometry for the development of biotechnological process with microalgae. *Biotechnology advances*, 2012.

[26] A. Ishimaru. *Wave propagation and scattering in random media.* IEEE press: New York, 1997.

[27] J.A.J. Jacquez and H.F. Kuppenheim. Theory of the integrating sphere. *Optical Society of America*, 45, 1955.

[28] I.T. Jolliffe. *Principal Component Analysis, second edition.* Springer, 2002.

[29] R. Kandilian, E. Lee, and L. Pilon. Radiation and optical properties of nannochloropsis oculata grown under different irradiances and spectra. *Bioresource Technology*, 2013.

[30] S. Karthikeyan, R. Balasubramanian, and C.S.P. Iyer. Evaluation of the marine algae ulva fasciata and sargassum sp. for the biosorption of cu(ii) from aqueous solutions. *Bioresource technology*, 98, 2007.

[31] M. Kerker, editor. *Light scattering by non-spherical particles: theory, measurements and applications.* Academic press, New York, 1969.

[32] J. T. O. Kirk. A theoretical analysis of the contribution of algal cells to the attenuation of light within natural waters. 1. general treatment of suspensions of pigmented cells. *New phytologist*, 75, 1975.

[33] J. T. O. Kirk. A theoretical analysis of the contribution of algal cells to the attenuation of light within natural waters. ii. spherical cells. *New phytologist*, 75, 1975.

[34] J. T. O. Kirk. A theoretical analysis of the contribution of algal cells to the attenuation of light within natural waters. iii. cylinfrical and spheroidal cells. *New phytologist*, 77, 1976.

[35] J. C. Kitchen and J. R. V. Zaneveld. A three-layered sphere model of the optical properties of phytoplankton. *Journal of limnology and oceanography*, 37, 1992.

[36] F.A. Kruse, A.B. Lefkoff, J.W. Boardman, K.B. Heiedbrecht, A.T. Shapiro, P.J. Barloon, and A.F.H. Goetz. The spectral image processing system (sips) - interactive visualization and analysis of imaging spectrometer data. *Remote sensing of environment*, 44(2-3), 1993.

[37] Labsphere. *Integrating sphere theory and applications.*

[38] E. Lee, R. L. Heng, and L. Pilon. Spectral optical properties of selected photosynthetic microalgae producing biofuels. *Journal of Quantitative Spectroscopy and Radiative Transfer*, 114, 2013.

[39] R.T. Lorenz and G.R. Cysewski. Commercial potential for haematococcus microalgae as a natural source of astaxanthin. *TIBTECH*, 18, 2000.

[40] B. Lu, S.P. Morgan, J.A. Crowe, and I.M. Stockford. Comparison of methods for reducing the effects of scattering in spectrophotometry. *Applied spectroscopy*, 60(10), 2006.

[41] J. Luypaert, D.L. Massart, and Y. Vander Heyden. Near-infrared spectroscopy applications in pharmaceutical analysis. *Talenta*, 72(3), 2007.

[42] H. Martens and T. Naes. *Multivariate Calibration.* Wiley, 1989.

[43] D.H. Menzel, editor. *Selected papers on the transfer of radiations.* Dover, New York, 1966.

[44] J-L. Meyzonnette. Radiometry and detection systems. Institut d'Optique Graduate School courses, 2009.

[45] I. Mladineo, I. Bocina, C. Przybyla, J. Fievet, and J-P. Blancheton. Fish growth and health aspects of sea bass (dicentrarchus labrax) reared in standard vs. high rate algal pond recirculation systems. *Aquatic Living Resources*, 23(2), 2010.

[46] A. Morel and A. Bricaud. Theoretical results concerning light absorption in a discrete medium, and application to specific absorption of phytoplankton. *Deep sea research*, 28, 1981.

[47] J. L. Mueller. *The influence of phytoplankton on ocean color spectra.* PhD thesis, Oregon state university, 1973.

[48] A. Muller-Feuga. The role of microalgae in aquaculture: situation and trends. *Journal of applied phycology*, 12, 2000.

[49] A. Nair, S. Sathyendranath, T. Platt, J. Morales, V. Stuart, M. Forget, E. Devred, and H. Bouman. Remote sensing phytoplankton functional types. *Remote sensing of environment*, 112, 2008.

[50] O. Peña and U. Pal. Scattering of electromagnetic radiation by a multilayered sphere. *Computer Physics Communications*, 180, 2009.

[51] B. Philips-Invernizzi, D. Dupont, and C. Cazé. Bibliographical review for reflectance of diffusing media. *Optical Engineering*, 40(6), 2001.

[52] J. W. Pickering, C. J. M. Moes, H. J. C. M. Sterenborg, S. A. Prahl, and M. J. C. van Gemert. Two integrating spheres with an intervening scattering sample. *Journal of Optical society of America*, 9(4), 1992.

[53] T. Platt and A.D. Jassby. The relationship between photosynthesis and light for natural assemblages of coastal marine phytoplankton. *Journal of Phycology*, 12, 1976.

[54] S. A. Prahl. *Optical-Thermal Response of Laser Irradiated Tissue.* 1995.

[55] S. A. Prahl. *Everything I think you should know about Inverse Adding-Doubling.* Oregon Medical Laser Center, 2011.

[56] S. A. Prahl, M. J. C. van Gemert, and A. J. Welch. Determining the optical properties of turbid media using adding-doubling method. *Applied optics*, 32(4), 1993.

[57] R. W. Preisendorfer. *Radiative transfer on discrete spaces.* Oxford University Press, London and New York, 1965.

[58] A. Quirantes and S. Bernard. Light scattering by marine algae: two-layer spherical and non-spherical models. *Journal of Quantitative Spectroscopy and Radiative Transfer*, 89, 2004.

[59] M.M. Reis, P.H.H. Araújo, C. Sayer, and R. Giudici. Spectroscopic on-line monitoring of reactions in dispersed medium: Chemometric challenges. *Analytical and Chemical acta*, 595(1-2), 2007.

[60] S. Roy, S. Sathyendranath, and T. Platt. Retrieval of phytoplankton size from bio-optical measurements: theory and applications. *Journal of the royal society Interface*, 8, 2011.

[61] S. Sathyendranath, L. Lazzara, and L. Prieur. Variations in the spectral values of specific absorption of phytoplankton. *Limnology and Oceanography*, 32(2), 1987.

[62] V.V. Soblev. *A treatise on radiative transfer.* Van Nostrand-Reinhold, Princeton, New Jersey, 1963.

[63] A.E. Solovchenko, I. Khozin-Goldberg, and M.N. Merzlyak Z. Cohen. Carotenoid-to-chlorophyll ratio as a proxy for assay of total fatty acids and arachidonic acid content in the green microalga parietochloris incise. *Journal of applied phycology*, 21, 2009.

[64] R. Steponavicius and S. N. Thennadil. Extraction of chemical information of suspensions using radiative transfer theory to remove multiple scattering effects: application to a model two-component system. *Analytical Chemistry*, 18, 2009.

[65] D. Stramski, A. Morel, and A. Bricaud. Modeling the inherent optical properties of the ocean based on the detailed comparison of the planktonic community. *Applied Optics*, 40, 2001.

[66] S.T. Thynell. Discrete-ordinates method in radiative heat transfer. *International Journal of Engineering Science*, 36, 1998.

[67] C. U. Ugwu, H. Aoyagi, and H. Uchiyama. Photobioreactors for mass cultivation of algae. *Bioresource Technology*, 99, 2008.

[68] H. C. van de Hulst. *Light scattering by small particles.* Wiley, 1957.

[69] P. Williams and K. Norris. *Near-Infrared Technology in the Agricultural and Food Industries.* American association of cereal chemists, Saint Paul, Minnesota, 2001.

[70] Y.Gong and M. Jiang. Biodiesel production with microalgae as feedstock: from strains to biodiesel. *Biotechnology letters*, 33(7), 2011.

[71] J. R. V. Zaneveld and J. C. Kitchen. The variation in the inherent optical properties of phytoplankton near an absorption peak as determined by various models of cell structure. *Journal of geophysical research*, 100, 1995.

[72] M. Zapata, F. Rodriguez, and J. Garrido. Separation of chlorophylls and carotenoids from marine phytoplankton: A new hplc method using a reversed phase c-8 column and pyridine-containing mobile phases. *Marine ecology progress series*, 195, 2000.

Appendix A

Supplementary measurements of Chapter 1

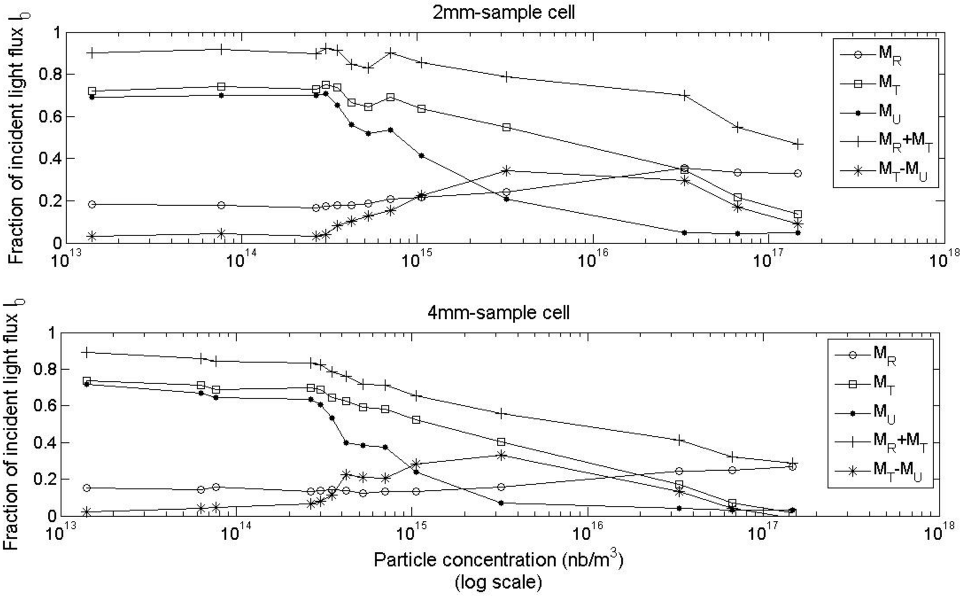

Figure A.1: M_R, M_T, M_U, $M_R + M_T$ and $M_T - M_U$ measured for the samples put in sample cells with different width, namely 2mm and 4mm.

Appendix B

Complex refractive index of a medium

The book of Lucarini et al. excellently details the rigorous constitutive laws of linear optics in materials: in this section we quote their work in order to recall some basic definitions, and more particularly the one of the refractive index of a material.

The complex refractive index N of a given material is defined by its dielectric properties: it is expressed as the square root of the dielectric permittivity $\epsilon(|\vec{k}|, \omega)$, which accounts for the relation between the electric displacement and the electric field.

$$\begin{aligned} N(|\vec{k}|, \omega) &= \sqrt{\epsilon(|\vec{k}|, \omega)} \\ &= Re(\sqrt{\epsilon(|\vec{k}|, \omega)}) + iIm(\sqrt{\epsilon(|\vec{k}|, \omega)}) \\ &= n(|\vec{k}|, \omega) + im(|\vec{k}|, \omega) \end{aligned} \tag{B.1}$$

Where $\vec{k}$ and ω are respectively the wave vector and the angular frequency of the electromagnetic field and c the celerity. ω is directly linked to the wavelength λ by the simple relation: $\omega = 2\pi c/\lambda$. Re and Im stand for the real and imaginary part respectively. It is important to note that the real and imaginary part of the refractive index are wavelength dependant, which is particularly important to take into account in the regions of anomalous dispersion. The complex refractive index of a medium describes the behavior of light incident on it: when low radiation intensities are considered, linear optics provides an extensive description of light-matter interaction phenomena.

For an incident electromagnetic field on an isotropic medium in which no sources are present, the following dispersion relation can be written:

$$|\vec{k}|^2 = \epsilon(|\vec{k}|, \omega)\frac{\omega^2}{c^2} \tag{B.2}$$

Each monochromatic component of the electric field of the radiation at time t and point r can be expressed as:

$$\vec{E}_\omega(\vec{r},t) = \hat{e}E_\omega exp[i\frac{\omega}{c}(\frac{c|\vec{k}|}{\omega}\hat{k}.\vec{r} - ct)] + c.c \tag{B.3}$$

Where $\hat{e}$ is the unit vector giving the polarization of light, $\hat{k}$ is the unit vector in the direction of $\vec{k}$, E_ω is a constant amplitude and $c.c$ a component depending on the initial conditions. By replacing the modulus of the wave vector $\vec{k}$ using the dispersion relation B.2 we obtain:

$$\begin{aligned}
\vec{E}_\omega(\vec{r},t) &= \hat{e}E_\omega exp[i\frac{\omega}{c}(\sqrt{\epsilon(|\vec{k}|,\omega)}\hat{k}.\vec{r} - ct)] + c.c \\
&= \hat{e}E_\omega exp[i\frac{\omega}{c}(N(|\vec{k}|,\omega)\hat{k}.\vec{r} - ct)] + c.c \\
&= \hat{e}E_\omega exp[i\frac{\omega}{c}(n(|\vec{k}|,\omega)\hat{k}.\vec{r} - ct)]exp[-\frac{\omega}{c}m(|\vec{k}|,\omega)\hat{k}.\vec{r}] + c.c
\end{aligned} \tag{B.4}$$

Relation B.4 shows that in the case of an electromagnetic wave traveling in an isotropic medium, the real part of the refractive index of the medium $n(|\vec{k}|,\omega)$ is responsible for dispersive optical phenomena as it influences the phase of the traveling wave. The imaginary part $m(|\vec{k}|,\omega)$ introduces a decreasing non oscillatory real exponential that describes an extinction phenomenon: it is then related to light absorption.

When expressing the light intensity, the absorption term of equation B.4 becomes:

$$\begin{aligned}
I_{abs}(\vec{r},t) &= |E_{\overrightarrow{abs}},\omega(\vec{r},t)|^2 \\
&= exp[-2\frac{\omega}{c}m(|\vec{k}|,\omega)\hat{k}.\vec{r}]
\end{aligned} \tag{B.5}$$

Beer law is the direct consequence of relation B.5 for absorbing media which scattering properties are negligible. In the case of heterogeneous media, additional dispersion phenomena of the incident light at each interface between two different materials intervene. Those phenomena are described entirely by Snell-Descartes refraction laws and by Fresnel coefficients. At a boundary between two media of complex refractive indices N_1 and N_2, the behavior of the incident electromagnetic wave is determined by relationships that depend on the values of N_1 and N_2. The angular behavior of the refracted wave is determined by the Snell-Descartes relationships. The changes of amplitude of the electric and magnetic fields are given, for all the direction of polarization, by the Fresnel relationships and the transmission and refraction coefficients. The complex value of N_1 and N_2 directly intervene in both relationships.

The complex refractive index of a medium makes it possible to describe the behavior of an incident light on the medium. However it is important to know that the real and imaginary parts of the refractive index are interdependent, and linked by the Kramers-Kronig relations (see section 3.2.4 for more details).

RESUME

Dans le contexte actuel de diversification des ressources en biomasse pour des applications comme la production énergétique, la culture des micro-algues est un domaine en pleine expansion. Photosynthétiques, les micro-algues se développent en eaux douces ou marines en convertissant lumière et CO2 en O2 et chaînes carbonées. Les procédés de conduite de culture en photobioréacteurs ou en bassins extérieurs restent rudimentaires : le manque d'instrumentation dédiée est un verrou pour la mise en place de suivis de cultures en ligne automatisés. La thèse étudie la potentialité d'une mesure optique multispectrale comme outil de caractérisation de l'état physico-chimique des suspensions de microalgues dans un contexte de culture dense. Les questions scientifiques posées relèvent à la fois de l'étude théorique de l'optique en milieux complexes, de la métrologie, et de la modélisation pour interpréter des spectres mesurés en terme de données sur l'état physiologique des cellules algales.

Mots clés : Optique dans les milieux complexes - Microalgues - Transport radiatif - Mie -

ABSTRACT

Current environmental and energy issues such as biofuel production require new source of biomass. Microalgae are seen as a promising solution, and the global mass production has largely increased over the last decade. Microalgae are photosynthetic organisms growing in freshwaters or oceans. They absorb light and carbon dioxide and produce oxygen and carbon chains. Nowadays, the monitoring of the cultivation process in closed or open systems still remains limited. This is due in particular to a lack of specific measuring instrumentation, fully adapted to the constraints of in-line monitoring. This thesis investigates the potential of a multispectral optical method as a tool to characterize the physicochemical state of dense algal cultures. The theoretical formulation of the optical phenomena in complex media is addressed. The metrological issue is also investigated. Finally, the modeling of the spectral information and the interpretation in terms of physiological data are studied.

Keywords : Optics in complex media - Microalgae - Radiative transport - Mie theory -

Sarah BELLINI
Irstea - UMR ITAP - COMiC - Capteurs Optiques pour les Milieux Complexes
351 rue Jean François Breton - 34196 Montpellier Cedex 5 (France).